

TECHNISCHE UNIVERSITÄT MÜNCHEN
Lehrstuhl für Biofunktionalität der Lebensmittel

Identification of metabolic markers for the development of chronic intestinal inflammation

Pia Magdalena Lichti

Vollständiger Abdruck der von der Fakultät Wissenschaftszentrum Weihenstephan für Ernährung, Landnutzung und Umwelt der Technischen Universität München zur Erlangung des akademischen Grades eines

Doktors der Naturwissenschaften

genehmigten Dissertation.

Vorsitzender: Univ.-Prof. Dr. M. Rychlik

Prüfer der Dissertation: 1. Univ.-Prof. Dr. D. Haller
2. Univ.-Prof. Dr. H. Daniel

Die Dissertation wurde am 10.05.2012 bei der Technischen Universität München eingereicht und durch die Fakultät Wissenschaftszentrum Weihenstephan für Ernährung, Landnutzung und Umwelt am 07.08.2012 angenommen.

ABSTRACT

Inflammatory bowel diseases (IBD) with ulcerative colitis (UC) and Crohn's disease (CD) as the two main idiopathic pathologies are chronically remittent and immunological mediated disorders of the gastrointestinal tract of unknown etiology. The biochemical consequences of IBD on the systemic and gastrointestinal metabolism have not yet been fully elucidated, but could help to better understand the disease pathogenesis. As a result, the identification of specific metabolic markers associated with the different disease stages could improve the IBD diagnosis and therapy.

In the current study, metabolic variations during the development of chronic intestinal inflammation were investigated through the use of metabolic profiling of two different animal models of IBD. IL-10^{-/-} and TNF^{ΔARE/WT} mice exhibit intestinal compartment specific inflammation in the colon and the distal ileum, respectively. Moreover, WT and non-inflamed IL-10^{-/-} mice were used to characterize the physiological impact of a genetic predisposed but disease-free phenotype on the host's metabolism. The metabolite profiling approach included holistic proton nuclear magnetic resonance (¹H NMR) spectroscopy and targeted liquid chromatography coupled to mass spectrometry (LC-MS) of blood plasma and intestinal tissue extracts at different time points. Different data integration techniques using chemometric tools were applied to map the metabolic effects associated with the development of UC and CD-like ileitis in the two animal models. These measurements were further combined with histopathological scoring of intestinal tissue sections, evaluation of body weight and body composition, and assessment of the nutritional energy utilization, adipocyte sizes, and plasma inflammatory biomarkers to characterize site specific and systemic metabolic phenotypes in these animals. This integrated metabolomic approach provided evidence for increased fatty acid oxidation and glycolysis, an impaired metabolism of lipoproteins and glycosylated proteins, and the generation of pro-inflammatory signaling lipids in the plasma profiles of inflamed animals. Moreover, it highlighted shifts in the intestinal lipid metabolism concomitant to the histopathological onset of inflammation. These results described different biological processes associated with the disease onset, including modifications of the cell membrane composition, increase of fat oxidation, and finally the generation of pro-inflammatory signaling mediators. Detection of early metabolite changes in non-inflamed IL-10^{-/-} animals demonstrated that already a genetic susceptibility, here in form of the IL-10 gene knock-out, can lead to events detectable *via* ¹H NMR-based metabolic profiling.

Taken together, these results provide novel insights into IBD-related metabolite alterations, especially of specific lipid-dependent processes, during inflammatory states. This integrated system investigation demonstrates the potential of metabolomics for investigating the mechanistic basis of IBD and will provide novel avenues for management and therapy of IBD.

ZUSAMMENFASSUNG

Colitis ulcerosa (CU) und Morbus Crohn (MC) sind die beiden bedeutendsten Krankheitsverlaufsformen von chronisch entzündlichen Darmerkrankungen (CED). Sie werden als chronisch remittierende und immunologisch vermittelte Erkrankungen des Gastrointestinaltrakts mit unbekannter Ätiologie beschrieben. Bis heute konnten die Auswirkungen von CED auf den systemischen und intestinalen Stoffwechsel noch nicht vollständig aufgeklärt werden. Dies könnte aber für ein besseres Verständnis der zu Grunde liegenden Pathogenese sorgen und zum anderen helfen, spezifische Stoffwechselmarker für die unterschiedlichen Krankheitsstadien zu identifizieren. Des Weiteren könnte dadurch auch die Diagnose und Therapie von CED erheblich verbessert werden.

In der vorliegenden Studie wurden Stoffwechselveränderungen, die während der Entstehung und des Krankheitsverlaufs von CED auftreten, mit Hilfe von „Metaboliten Profiling“ in zwei unterschiedlichen CED-Tiermodellen untersucht. Die verwendeten IL-10^{-/-} Mäuse entwickeln eine chronische Entzündung des Colons, wohingegen TNF^{ΔARE/WT} Mäuse an einer starken, chronischen Entzündung des distalen Ileums leiden. Zusätzlich wurden WT und nicht-entzündete IL-10^{-/-} Mäuse benutzt, um den Einfluss einer genetischen Prädisposition für CED mit symptomfreiem Phänotyp auf den Stoffwechsel zu charakterisieren. Der hierbei verwendete metabolische Ansatz beruht auf dem Einsatz von Protonen-Kernspinresonanz-Spektroskopie und Flüssigchromatographie mit Massenspektrometrie-Kopplung, um Blutplasma- und Darmgewebe-Proben zu verschiedenen Zeitpunkten während des Krankheitsverlaufs von CED zu untersuchen. Mit Hilfe von verschiedenen Datenverarbeitungstechniken wurden anschließend die nachgewiesenen Stoffwechselveränderungen der Entstehung von CU und MC zugeschrieben. Für eine bessere Beschreibung der Stoffwechsel-Phänotypen der untersuchten Tiere wurden die genannten Messungen zusätzlich mit folgenden Analysen kombiniert: (I) Histopathologische Bewertung von Darmabschnitten, (II) Messungen von Körpergewicht, Körperzusammensetzung und Adipozytengröße, (III) Bestimmung der Nahrungsenergienutzung und (IV) Quantifizierung von Entzündungsmarkern im Blutplasma. Die Ergebnisse der Metabolitenuntersuchung im Plasma wies auf eine reduzierte Fettsäureoxidation und verminderte Glykolyserate, einen gestörten Stoffwechsel von Lipoproteinen und glykosylierten Proteinen und auf die Erzeugung von entzündungsfördernden Signalmolekülen in den erkrankten Tieren hin. Darüber hinaus konnten Verschiebungen des intestinalen Fettstoffwechsels zeitgleich zum histopathologischen Auftreten der Entzündung festgestellt werden. Diese Ergebnisse beschreiben unterschiedliche biologische Prozesse, die mit dem Auftreten von CED in Verbindung stehen, einschließlich der Modifizierung der Zellmembranzusammensetzung des Darmgewebes, Veränderungen des Fettstoffwechsels und schließlich die Entstehung von Entzündungsmediatoren. Der Nachweis von frühen Stoffwechselveränderungen in nicht-entzündeten IL-10^{-/-} Tieren zeigt zusätzlich, dass bereits

eine genetische Prädisposition für CED, hier in Form eines Gen-Knockouts des IL-10 Gens, durch Metaboliten Profiling nachgewiesen werden kann.

Zusammengefasst gewährt die folgende Arbeit neue Einblicke in CED-abhängige Stoffwechselveränderungen, vor allem in spezifische Fettstoffwechsel-abhängige Prozesse. Diese Ergebnisse unterstreichen somit das Potential von Metaboliten Profiling-Techniken in der Aufklärung von verschiedenen krankheitsabhängigen Fragestellungen, welche zukünftig dazu beitragen können neue Wege für die Behandlung und Therapie von CED zu liefern.

TABLE OF CONTENTS

1	Introduction	8
1.1	Inflammatory Bowel Disease	8
1.1.1	Host-Microbiota Interactions in Inflammatory Bowel Disease	9
1.1.2	Loss of Intestinal Epithelial Cell Homeostasis in Inflammatory Bowel Disease	10
1.2	Animal Models of Inflammatory Bowel Disease	11
1.2.1	IL-10 ^{-/-} Mouse Model	13
1.2.2	TNF ^{ΔARE/WT} Mouse Model	14
1.3	Metabonomics	16
1.3.1	Analytical Techniques Used in Metabonomics	17
1.3.1.1	Nuclear Magnetic Resonance Spectroscopy	18
1.3.1.2	Mass Spectrometry	19
1.3.2	Chemometrics in Metabonomics	20
1.4	Application of Metabonomics in Inflammatory Bowel Disease Research	21
1.5	Aim of the Current Work	27
2	Material and Methods	28
2.1	General Work Flow for Metabonomic Analysis	28
2.2	Animal Experiments	30
2.2.1	IL-10 ^{-/-} Mouse Model	30
2.2.2	TNF ^{ΔARE/WT} Mouse Model	30
2.2.3	Histopathological Scoring	32
2.3	¹H NMR Spectroscopy	32
2.3.1	NMR Spectroscopy Approaches: 1D and 2D Spectroscopy	32
2.3.2	Sample Preparation and ¹ H NMR Spectroscopic Analysis	33
2.3.2.1	Plasma Samples	33
2.3.2.2	Intestinal Tissue Extracts	34
2.3.3	¹ H NMR Spectroscopic Assignment	35
2.3.3.1	JRES ¹ H NMR Spectroscopy	35
2.3.3.2	¹ H- ¹ H COSY and ¹ H- ¹ H TOCSY	35
2.3.4	¹ H NMR Data Processing	35
2.3.5	¹ H NMR Data Preparation for Statistical Analysis	36
2.4	LC-MS Analysis	36
2.4.1	Sample Preparation and Biocrates Life Sciences AbsoluteIDQ™ kit Analysis	36
2.4.2	Sample Preparation and Inflammation Marker Quantification by UPLC-ESI-MS/MS Using Isotope Dilution Technique	37
2.5	Chemometrics	38
2.5.1	Data Preparation	38
2.5.2	Principal Component Analysis	39
2.5.3	Projections to Latent Structures (PLS) and Orthogonal-Projection to Latent Structures (O-PLS) Discriminant Analyses	41

3	Results	44
3.1	Metabolic Characterization of the IL-10^{-/-} Mouse Model	44
3.1.1	Gradual Development of Body Weight and Inflammation Status in c-IL-10 ^{-/-} Mice	44
3.1.2	Analysis of ¹ H NMR Spectroscopic Profiles of Blood Plasma	45
3.1.3	Time-Dependent Metabolic Changes in Blood Plasma Associated with Colitis	45
3.1.4	Gradual Development of Body Weight and Inflammation Status in s-IL-10 ^{-/-} Mice	51
3.1.5	Time-Dependent Metabolic Changes in Blood Plasma Associated with Colitis Susceptibility	51
3.1.6	Time-Dependent Metabolic Changes in the Colon Associated with Colitis Susceptibility	56
3.2	Metabolic Characterization of the TNF^{ΔARE/WT} Mouse Model	61
3.2.1	Gradual Development of Ileal Inflammation and Body Fat Composition in TNF ^{ΔARE/WT} mice	61
3.2.2	Time-Dependent Metabolic Changes in Blood Plasma Associated with Ileitis	63
3.2.3	Time-Dependent Metabolic Changes in the Intestine Associated with Ileitis	68
4	Discussion	74
4.1	Effect of Inflammation on Plasma Lipids and Lipoprotein Metabolism	74
4.2	Metabolic Assessment of Experimental Colitis in IL-10^{-/-} mice	77
4.2.1	Histopathological Scoring, Body Weight, and Inflammatory Biomarkers Describe the Gradual Development of Colitis	77
4.2.2	Association of Plasma Metabolic Changes with the Gradual Development of Colitis	78
4.2.3	Association of Plasma Metabolic Changes with Colitis Susceptibility	79
4.2.4	Association of Colonic Metabolic Changes with Colitis Susceptibility	80
4.3	Metabolic Phenotyping of Crohn's Disease-like IBD in TNF^{ΔARE/WT} Mice	81
4.3.1	Body Compositional Changes Describe Ileal Inflammation in TNF ^{ΔARE/WT} Mice	81
4.3.2	Association of Plasma Metabolic Changes with the Gradual Development of Ileitis	81
4.3.3	Association of Colonic Lipid Alterations with the Gradual Development of Ileitis	83
4.3.3.1	Inflammation-Related Changes in the Cell Membrane Composition	83
4.3.3.2	Inflammation-Related Changes in the Energy Supply Machinery	84
4.3.3.3	Inflammation-Related Changes in Lipid Signaling	85
5	Conclusion and Perspectives	87
5.1	Comparison of the Results and Subsequent Implications	87
5.2	Implications and Potential Future Studies	89
6	Appendix	91
	Abbreviations	105
	References	107
	Curriculum Vitae	<i>Fehler! Textmarke nicht definiert.</i>
	Eidesstattliche Erklärung	117

1 INTRODUCTION

Chronic diseases comprise metabolically-driven pathologies such as obesity, insulin resistance, type 2 diabetes, and cardiovascular diseases, but also immunologically mediated disorders like allergies or inflammatory bowel disease. The incidence and prevalence of chronic diseases have been rising dramatically over the last decades in western societies,^{1, 2} leading to a horrendous increase of healthcare expenditures in the affected countries.^{2, 3} As a result, the holistic understanding of the individual disease etiopathologies, the formation of prevention strategies, including nutritional interventions, and the development of early prognostic diagnosis tools could help to optimize the clinical therapy and management of these chronic diseases.

1.1 Inflammatory Bowel Disease

The clinically defined and idiopathic forms of inflammatory bowel disease (IBD), encompassing ulcerative colitis (UC) and Crohn's disease (CD), are spontaneously relapsing and immunologically-mediated chronic disorders of the gastrointestinal (GI) tract.⁴⁻⁶ Both disorders affect people in approximately equal female/male proportion with incidences ranging from 37 to 246 cases per 100.000 people for UC and from 26 to 199 cases per 100.000 people for CD depending on investigated populations, with the incidence being at the higher end of the scale in developed countries.^{1, 7}

The clinical appearance of human IBD is highly heterogeneous across populations. CD can generally affect the entire GI tract in a segmental or discontinuous manner, predominantly involving the terminal ileum, followed by the colon. The inflammatory process is frequently transmural and associated with intestinal granulomas, strictures, and fistulas and the clinical features include diarrhea, fever, abdominal pain, and obstructions. On the other hand, UC displays a non-transmural, continuous inflammatory pathology generally starting at the rectum and then spreading across the entire colon in an uninterrupted pattern, with inflammation being typically restricted to the mucosa.⁴⁻⁶ CD was thought to majorly display a T helper cell (Th) 1-type mediated immune response associated with excess interferon gamma (IFN γ) as predominantly secreted cytokine under the stimulus of interleukin (IL)-12.^{8, 9} But current research sheds also new light on the role of Th17 cell responses during the pathogenesis of CD.^{10, 11} Several studies demonstrated increased levels of Th17-derived IL-17 in the mucosa of UC and CD patients,¹² and showed that several cytokines, including IL-21 and IL-23, are involved in regulating Th17 cell activation and differentiation in IBD.¹⁰ Moreover, genome-wide association studies (GWAS) indicated that genes involved in the differentiation of Th17 cells, including the IL-23 receptor, IL-12 beta, and the signal transducer and activator of transcription protein 3 (STAT3), are associated with susceptibility to CD.^{13, 14} Contrary to that, UC

is predominantly referred to a Th2-type mediated disease with IL-4 as main secreted cytokine.¹⁵

Both manifestations, UC and CD, are discussed to be mediated by common and distinct mechanisms.⁴⁻⁶ Although many aspects are still unknown, the current paradigm for the pathogenesis of IBD is characterized by alterations of the luminal and mucosa associated microbiota, the epithelial function, as well as the innate and adaptive immune system in genetically susceptible individuals, whereby onset and recurrence of disease are most likely triggered by unknown environmental agents (Figure 1).^{4, 16} A genetic contribution to the development of IBD was clearly evident from twin studies showing a higher concordance rate in monozygotic versus dizygotic twins (37-58% for CD and 6-17% for UC versus 3.6-12% and 0-5%, respectively^{17, 18}). Moreover, GWAS identified more than 100 susceptibility loci for IBD, mostly affecting genes that are responsible for bacterial recognition and clearance (e.g. nucleotide oligomerization domain (NOD) 2 / caspase recruitment domain-containing protein (CARD) 15), epithelial cell function (e.g. ATP-binding cassette (ABC) subtype B1), immune regulation (e.g. IL-12R), and autophagy (e.g. autophagy-related protein (ATG) 16 like 1).^{19, 20} In addition, the relatively low overall concordance rates in dizygotic twins together with the rapid increase in the IBD prevalence in countries experiencing rapid Westernization indicated a strong environmental impact on the IBD pathogenesis.^{18, 21} Among the environmental factors implicated are diet, food storage in refrigerators, smoking, non-steroidal anti-inflammatory drugs (NSAIDs), and infections.²¹

1.1.1 Host-Microbiota Interactions in Inflammatory Bowel Disease

In general, host-microbiota interactions can be mutually beneficial or deleterious *via* initiating intestinal inflammation as bacteria profoundly affect the host's immune composition already under physiologic conditions. The intestinal microbiota is therefore likely the most important driver in the initiation of IBD. In healthy hosts, commensal bacteria activate homeostatic responses by epithelial cells and the intestinal immune system that permit coexistence with potentially toxic microbial products.^{16, 22, 23} Observations in animal models and IBD patients point also towards an important role of bacteria during the inflammation process, as antibiotics are partially effective in the treatment of IBD patients²⁴ and most mouse models of colitis require intestinal bacteria for the initiation of inflammation.^{25, 26} Moreover, an altered microbial composition²⁷ and an increased amount of mucosa-associated²⁸ and pathogenic²⁹ bacteria were observed in IBD patients. This can result in a loss of the described tolerance and subsequently in a constant immune stimulation followed by intestinal inflammation and mucosal tissue damage (Figure 1).^{16, 22, 23} In addition, these defects are abetted by genetically determined alterations in the gut epithelial barrier function which enhances the exposure of the mucosal immune system to bacterial components. As a consequence, penetration of im-

mune-activating antigens and pathogens into the host tissue is facilitated inducing further progression of the inflammatory response.¹⁵

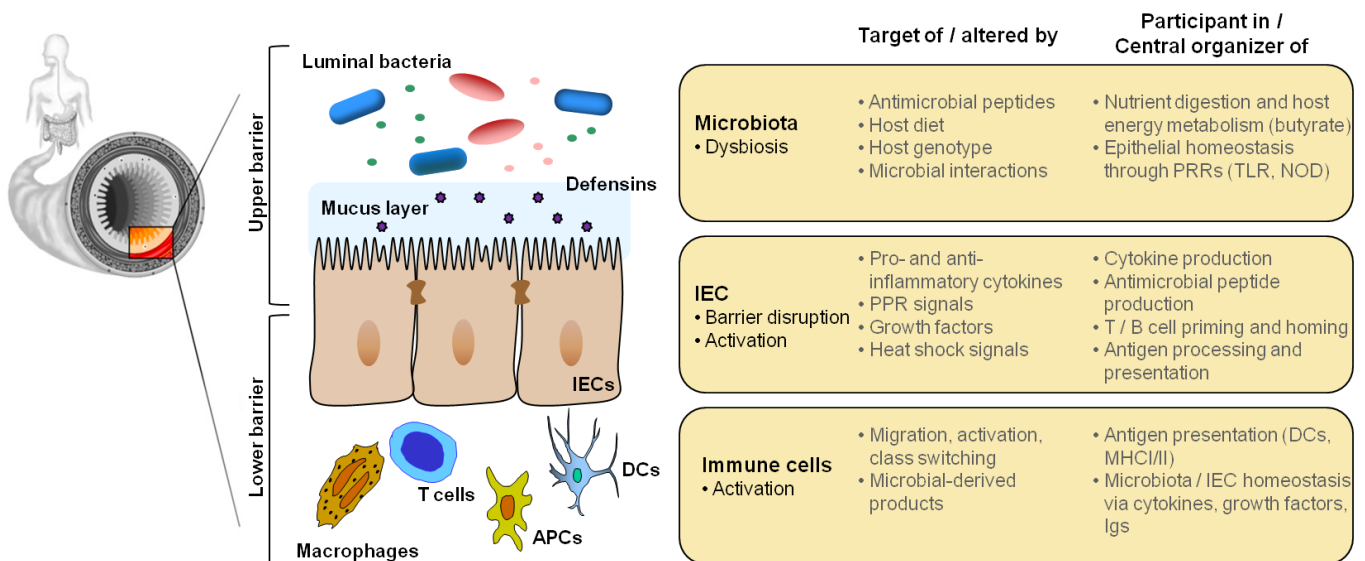


Figure 1: Loss of intestinal homeostasis results in chronic intestinal inflammation: Microbiota, intestinal epithelial cells, and lamina propria immune cells as targets, participants, and central organizers in intestinal immune responses (modified from⁴)

Abbreviations: APC: antigen presenting cell; DC: dendritic cell; Ig: immunoglobulin; IEC: intestinal epithelial cell; MHC: major histocompatibility complex; PRR: pattern recognition receptor; TLR: toll-like receptor.

1.1.2 Loss of Intestinal Epithelial Cell Homeostasis in Inflammatory Bowel Disease

Intestinal epithelial cells (IECs), as the interface between the gut microbiota and the gut-associated immune system (GALT), are crucial for maintaining the intestinal homeostasis and need to adapt constantly to changes in their environment by processing both bacterial and host-derived immune signals. In a healthy subject, IECs form an intestinal barrier by separating intestinal contents from the host tissues, regulating nutrient absorption, and allowance of interactions between the resident microbiota and the mucosal immune system.³⁰ Alterations of IEC key functions, including alterations and thinning of the mucus layer,³¹ disabled epithelial junctions,³² increased intestinal permeability,³³ and a defective production of antimicrobial peptides, called defensins,³⁴ play a key role in the pathogenesis of CD and UC. Recent advantages also assign IECs an active role within the mucosal immune system. IECs are able to protect the host against invasion by pathogenic bacteria *via* sensing of intestinal microbiota through pattern recognition receptors (PRR; toll-like receptors (TLR), NOD). Moreover, they are capable of cytokine and chemokine secretion to attract innate and adaptive immune effector cells and can action as non-professional antigen presenting cells (APCs) activating subsets of T-cells with regulatory function.³⁵

1.2 Animal Models of Inflammatory Bowel Disease

Human IBD studies are limited by many ethical and practical considerations:^{36, 37} (I) repeated surgical or endoscopic procedures to monitor the disease; (II) difficulties in controlling patient specific variables (individual genetic variation, environmental factors, diet); and (III) difficulties in studying the early steps of disease development.^{36, 37} Therefore, animal models offer an invaluable tool to study the pathogenesis and possible etiology of IBD.

Even though one single animal model cannot fully reflect the complex picture of the human disease, they provide important opportunities and tools to more closely examine the mechanisms underlying the pathology of IBD. Several animal models that recapitulate aspects of human IBD have been developed based on triggering gut associated inflammation *via* chemical induction or exogenous agents, *via* immune cell transfer, or *via* genetic modification (Table 1-1).^{36, 37} In many animal models the functionality of important cell types for the regulation of mucosal homeostasis is modified. This includes the infiltration of CD4⁺ T cells into the lamina propria (e.g. scid and Tgε26 transfer models, IL-10^{-/-}, IL-2^{-/-}, TCRα^{-/-}, TNBS) and the recruitment and activation of macrophages (myeloid-specific STAT3^{-/-}).³⁸ Moreover, various models remarkably depend on the presence of symbiotic and non-pathogenic microbiota. This is clearly demonstrated as none of these mouse models develops mucosal inflammation under germ-free conditions (e.g. IL-10^{-/-}, TCRα^{-/-}, IL-2^{-/-}, SAMP1/Yit, HLA-B27 tg).^{25, 26} Interestingly, the majority of the experimental IBD models show a Th1-dominant immune response, mimicking CD with regard to their effector mechanisms, whereas the disease location is almost exclusively the colon. In contrast, mouse models developing Th2-mediated colitis for the study of UC are strongly limited (TCRα^{-/-}, oxazalone, WASP^{-/-}).³⁷ In addition, administration of chemical agents such as dextran sodium sulfate (DSS) to knockout mice strains which do not give rise to intestinal abnormalities by themselves, is particularly valuable in the dissection of specific aspects or events on the overall background of intestinal inflammation.³⁸ Recent advances in genetic engineering technologies have also allowed the discovery of previously unrecognized functions of important molecules in IBD, such as the X-box binding protein (XBP) 1 and autophagy genes (Atg). Consequently, this led to the generation of new IBD animal models.³⁷

Nevertheless, the most suitable animal model of UC and CD is, however, still under debate. For the current work, two particular animal models of IBD were chosen: IL-10^{-/-} and TNF^{ΔARE/WT} mice. The IL-10^{-/-} animal model lacks one of the most important immunoregulators in the intestinal tract. The cytokine IL-10 is responsible for the induction of tolerance mechanisms stimulated by enteric antigens that are mediated by regulatory T cells. As a result, these mice exhibit intestinal compartment specific inflammation in the colon when housed in presence of normal and non-pathogenic microbiota.³⁹ Contrary, TNF^{ΔARE/WT} mice are genetically engineered to over-produce the essential pro-inflammatory cytokine tu-

mor necrosis factor (TNF). These mice develop ileitis closely resembling the immune and tissue-related phenotype of human CD with ileal involvement.⁴⁰ Both models are immunologically well characterized and therefore constitute ideal models to investigate metabolic alterations during the development of UC and CD.

Table 1-1: Animal models of inflammatory bowel disease (modified from³⁸)

Spontaneous	Induced		
	Administration of exogenous agents	Gene targeting: knockout or transgenic	Transfer of cells into immunodeficient animals
Cotton top tamarin C3H-HeJBir inbred SAMP1/Yit	Enema/intramural injection TNBS Oxazolone Acetic acid Peptidoglycan polysaccharide	Cytokine function IL-2 ^{-/-} IL-2R α ^{-/-} IL-10 ^{-/-} TGF- β ^{-/-} TGF- β RII dominant negative tg TNF ^{ΔARE/WT} IL-7 tg CRFB4 ^{-/-} STAT3 Stat4 tg NEMO A20	CD4 ⁺ CD45RB ^{hi} into scid mice CD4 ⁺ CD45RB ^{hi} into Rag ^{-/-} mice Bone marrow into Tg ϵ 26 mice
	Oral Indomethacin Carageenan Dextran sodium sulfate		
	Subcutaneous Cyclosporin A		
		T cell function Gai2 ^{-/-} TCR α ^{-/-} TCR β ^{-/-} MHC class II ^{-/-} Tg ϵ 26 WASP HLA-B27 tg rat	
		IEC barrier function Trefoil factor ^{-/-} NCAD mdr1a ^{-/-}	
		Host defense Muc2 ^{-/-} Nod2 ^{-/-} TLR	
		Others XBP-1 ^{-/-} t-bet ^{-/-} Atg5 ^{-/-}	

Key: A20: tumor necrosis factor induced protein 3; Atg: autophagy gene; CRFB: IL-10 receptor β ; Gai2: G protein α 2; HLA-B27: human β 2 microglobulin transgenic; IL: interleukin; Mdr: multiple drug resistance; MHC: major histocompatibility complex; Muc: mucin; NCAD: N-cadherin; NEMO: NF κ B essential modulator; Nod: Nucleotide Oligomerization Domain; Rag: recombinase activating gene; scid: severe combined immunodeficiency; STAT: signal transducer and activator of transcription; T-bet: T-box transcription factor; TCR: T cell receptor; Tg ϵ 26: All transgenic epsilon, TGF: tumor growth factor; TNBS, trinitrobenzene sulfonic acid; TLR: toll-like receptor; TNF: tumor necrosis factor; WASP: Wiskott–Aldrich syndrome protein; XBP: X-box binding protein.

1.2.1 IL-10^{-/-} Mouse Model

Interleukin-10 (IL-10) was first identified in 1989 by Fiorentino *et al.*⁴¹ as a cytokine secreted by CD4⁺ Th2-cells that inhibits cytokine production of APCs. Moreover, it was the founding member of the type II cytokine family that also includes IL-19, IL-20, IL-22, IL-24, IL-26, IL-28, and IL-29.⁴² IL-10 can modulate both, innate and adoptive immune responses, and is expressed by various immune cells such as macrophages, dendritic cells, and T-cells.^{43, 44} It functions in a pleiotropic fashion, predominantly limiting and ultimately terminating immune responses. These immunosuppressive functions of IL-10 include the suppression of pro-inflammatory cytokine production by immune cells, down-regulation of major histocompatibility complex (MHC) class II and co-stimulatory molecules on APCs, inhibition of T-cell proliferation, and formation of antigen-specific regulatory T cells.^{43, 44}

Despite the demonstrated role of IL-10 in the intestinal mucosal immunity, the association between IL-10 gene variants and IBD is weak.⁴⁵ Several GWAS have been performed identifying genetic risk loci for IBD, including genes involved in sensing and handling microbiota in the gut (NOD2) and genes involved in autophagy (ATG16L1 and immunity-related GTPase family M protein (IRGM)).^{19, 20} Thereby, the single nucleotide polymorphism (SNP) rs3024505 flanking the IL-10 gene was discovered as a risk factor solely found in UC patients.⁴⁶ However, IL-10 is likely to be also involved in CD as peripheral and mucosal immune cells from CD patients produce lower amounts of IL-10 than healthy controls.⁴⁷ This suggests a possible disease mechanism in CD patients with this mutation. Furthermore, the NOD2 mutant protein (3020insC) associated with CD was identified to inhibit IL-10 transcription.⁴⁸ In addition, IL-10 receptor (IL-10R) signaling mediated by IL-10R1 and IL-10R2 is affected by SNPs in the encoding genes.⁴⁹ Recently, also loss-of-function mutations in subunits of the IL-10R were discovered in four patients with severe early onset enterocolitis.⁴⁹ Risk alleles have also been identified for STAT3, the key transducer molecule for the anti-inflammatory properties of IL-10,⁵⁰ demonstrating that loss of IL-10 signaling in humans can result in IBD. These findings strongly suggest that defective IL-10 function is central to the pathogenesis of IBD.⁴⁶ Interestingly, administration of recombinant IL-10 or the use of an IL-10 gene-based therapy proved therapeutic efficacy in several animal models of colitis.⁵¹ However, systemic injection of recombinant IL-10 showed only a modest potency in patients with active CD in phase III clinical trials.⁵² Surprisingly, at high doses, IL-10 even induced the production of the pro-inflammatory cytokine IFN γ .⁵³ It has been speculated that the lack of clinical efficacy may result from limited bioavailability of IL-10 at the intestinal mucosa.⁵⁴

Mice with targeted deletion of the IL-10 gene (IL-10^{-/-}) are growth retarded and anemic, and spontaneously develop chronic enterocolitis. This is associated with epithelial cell hyperplasia, abscesses, and transmural inflammation with massive infiltration of lymphocytes, activated macrophages, and neutrophils into the intestinal mucosa and submucosa.³⁹ The disease is

accompanied by a Th1-type cytokine response, which can be ameliorated by neutralizing antibodies to IL-12p40 and to a lesser extent by IFN γ or systemic administration of recombinant IL-10.^{55, 56} Similar disease pathologies are also present in mice deficient for CRF2-4, the IL-10R beta chain, and in mice with myeloid cell specific STAT3 deficiency that reveal a defect in IL-10 signaling.⁵⁷ The importance of IL-10 in the regulation of intestinal mucosal immunity toward intestinal microbiota is also demonstrated as animals raised under germfree conditions do not develop chronic inflammation. Moreover, intestinal inflammation is less severe when mice are raised in specific pathogen-free (SPF) conditions compared to normal housing conditions. This highlights that intestinal inflammation is driven by antigens of the mucosal microbiota.^{26, 39} Moreover, inheritable factors seem to strongly influence the disease susceptibility of IL-10^{-/-} mice, as the severity of the developed intestinal lesions varies with the genetic background of the mice.⁵⁵ Interestingly, the IL-10^{-/-} mouse model displays physiological and biochemical similarities to UC, including intermittent transmural inflammatory lesions⁵⁵ and an increased intestinal permeability prior to the development of established colitis.⁵⁸ Therefore, the use of the IL-10^{-/-} animal model for experimental studies may provide insights into the role of IL-10 in IBD, especially during UC.

1.2.2 TNF ^{Δ ARE/WT} Mouse Model

The tumor necrosis factor (TNF) is an important pleiotropic, pro-inflammatory cytokine that is involved in systemic inflammation and stimulates acute phase reactions.^{59, 60} TNF is produced in response to bacterial, inflammatory, and other stimuli primarily by cells of the immune system, such as macrophages and T and B lymphocytes, but also by additional cell types, including endothelial cells, mast cells, and neuronal tissues.⁶¹ Both, the soluble and transmembrane forms of TNF are biologically active⁶² and interact with their cognate membrane receptors TNFR1 and TNFR2.⁶⁰ The TNFRs can additionally be released from the cell surface by proteolysis to produce soluble forms which are suggested to neutralize the action of TNF.⁶³ Ligand binding of TNF to its TNFR leads to several downstream effects, including activation of the heterodimeric transcription factor and nuclear factor NF κ B.⁶⁰ In addition, TNF/TNFR interactions do not only play a pivotal role in the pathogenesis of inflammatory responses, but also cause programmed cell death (apoptosis), cell proliferation, and cell differentiation.⁶⁴ Deregulated TNF concentrations, especially TNF overexpression, have been implicated in a variety of symptoms associated with autoimmune disorders, such as chronic inflammatory arthritis, multiple sclerosis, and IBD, especially CD.⁶⁵

Already 20 years ago, several studies implicated TNF as a dominant player in a cytokine network that promotes inflammation in human IBD.^{66, 67} It has been shown that TNF significantly contributes to intestinal damage in CD by altering the integrity of epithelial and endothelial cell barriers, increasing the recruitment of inflammatory cells, and contributing to the

formation of granulomas.⁶⁸ Moreover, several SNPs in the TNF promoter region are known to affect the level of TNF gene expression and have previously been associated with susceptibility to a range of autoimmune disorders, including IBD.^{69, 70} For example the G-A polymorphism at position 238 in the TNF gene is associated with lower production of TNF in patients with UC.⁷¹ Conversely, the 308A polymorphism is associated with enhanced TNF production in cells *in vitro* and in CD patients *in vivo*.^{70, 71} In addition, the role of TNF has been shown directly in several animal models of IBD *via* the application of monoclonal anti-TNF antibodies which ameliorated the severity of inflammation.^{72, 73} Possibly van Dullemen *et al.*⁷⁴ provided the most compelling evidence for the central role of TNF in the pathogenesis of IBD. He was first to demonstrate that the treatment of IBD patients with anti-TNF antibodies provided marked clinical benefits in UC and CD patients. Still today, the treatment with anti-TNF antibodies, such as infliximab, adalimumab, and certolizumab pegol, are effectively used in clinical therapy of IBD.^{75, 76} However, at present it is unclear whether the beneficial effects of this therapy form results from the neutralization of soluble and membrane-associated TNF or by lysis of TNF-expressing cells, for example by antibody-dependent cellular cytotoxicity or complement fixation.⁷⁷

Kontoyiannis and co-workers⁴⁰ genetically impaired the regulation of TNF in C57BL/6 mice by deletion of a repeated octanucleotide AU-rich motif (ARE) in the 3'-untranslated region of the TNF encoding gene, referred as TNF^{ΔARE}. This genetic variation resulted in enhanced mRNA stability of TNF characterized by the persistent accumulation and decreased degree of decay of the mutant TNF mRNA. Homozygous TNF^{ΔARE/ΔARE} mice show a severely reduced weight gain and high mortality and succumb to disease between 5 and 12 weeks of age. These mice develop clinical evidence of chronic polyarthrititis, present with swelling of joints and distortion of front and rear paw morphology. Moreover, TNF^{ΔARE/ΔARE} mice suffer from chronic CD-like ileitis, where inflammatory infiltrates extend deep into the muscular layers of the bowel wall and a complete loss of villous structures as well as rudimental granulomata with multinucleated giant cells were observed. Mice heterozygous for the genetic modification (TNF^{ΔARE/WT}), develop a severe CD8⁺ T cell-dependent ileitis with an up-regulation of Th1-like cytokines closely resembling the immune and tissue-related phenotype of human CD with ileal involvement and arthritis.^{40, 78, 79} Disease onset of arthritis and ileitis is detectable after 4 and 8 weeks of age, respectively, and the inflammatory scores increase with age for both diseases.⁴⁰ TNF^{ΔARE/WT} mice are immunologically well characterized.^{78, 80, 81} Backcrossing of TNF^{ΔARE/WT} to recombinaise activating gene (RAG)-1^{-/-} mice showed that ileitis but not arthritis depends on the presence of lymphocytes and that the adoptive transfer of T cells from these mice can transfer disease to recipient mice. This emphasizes the importance of TNF production in T cells and not innate immune cells for disease development. Moreover, it was shown that already an epithelial specific over-expression of TNF is sufficient to cause full

development of CD-like pathology.⁸² Therefore, the TNF^{ΔARE/WT} mouse is an appropriate model to study metabolic changes associated with the gradual development of CD-like ileitis.

1.3 Metabonomics

The development and use of appropriate analytical tools that allow comprehensive and robust metabolic analyses is the key to understand the impact of IBD-related changes on the host's overall metabolic profile. Modifications in various biological functions and processes ultimately leading to the development of IBD do not appear isolated. Instead they are embedded in a large network of genetic, physiological, and pathophysiological interactions, and can be affected by environmental and dietary factors as well as by the symbiotic gut microbiota.³⁰ Functional studies have emphasized that unlike variations in gene transcription and protein levels, which might only indicate the potential for physiological changes, metabolites and their kinetic changes in concentration within cells, tissues, and organs represent the real end-points of physiological regulatory processes, therefore bridging the genotype-to-phenotype gap.^{83, 84} Metabolites are products and by-products of many complex biosynthetic and catabolic pathways existing in all living systems. Physiological as well as pathological processes can disrupt the established homeostatic metabolite conditions within single cells, for instance via the modification of individual enzyme quantities. As a result this can lead to concentration changes of numerous metabolites.^{85, 86} Consequently, all changes across cells and tissues are thus ultimately reflected in an altered metabolite composition of biofluids, including plasma and urine, as the organism tries to maintain the homeostatic control.^{86, 87} Therefore, measuring the 'metabolic fingerprint' of biochemical disturbances, both static and flux, is an excellent means to assess physiological changes which have actually occurred in a biological system.⁸⁴

Metabonomics has its roots in toxicology and the secondary plant metabolism research, but later on, also topics such as disease diagnosis and personalized medicine have been drawing the attention of many researchers.⁸⁸ It belongs to the rapidly progressing 'omic' technologies, including genomics, transcriptomics, proteomics, as well as metagenomics and metaproteomics, and has opened new perspectives in understanding molecular mechanisms at different levels of biological organizations. Metabolic profiling is a well-established and powerful tool used for the investigation of metabolic pathway regulations to gain insights into functional biology.⁸⁴ Metabonomics was first defined by Nicholson *et al.*⁸⁷ as 'the quantitative measurement of the dynamic multiparametric metabolic response of living systems to pathophysiological stimuli or genetic modification'. In contrast to that, metabolomics is referred to 'the analysis of the entire complement of all the small molecular weight metabolites inside a cell suspension to reveal aspects of cellular metabolism and global regulation'.⁸⁹ But the dis-

inction is mainly philosophical, rather than technical, as the analytical and modeling procedures are the same and therefore both words are often used interchangeably.⁹⁰ Generally, the study of the metabolome can be applied either in isolation or in combination with other profiling techniques (including, genomics, transcriptomics, proteomics) as an integrative science applying high throughput experiments (systems biology).⁹⁰ Here, the role of metabonomics within systems biology is to define qualitatively or quantitatively the interactions of metabolites (and their associated changes) in biological networks. From a technical point of view, one can distinguish in systems biology so-called 'top-down' from 'bottom-up' approaches. Here, 'top-down' studies take a holistic view on the system, where no a priori selection of any metabolites is made, aiming to study the components and interactions of the complete system, generally by a semi-quantitative approach. By contrast, 'bottom-up' systems biology performs a targeted and quantitative study of specific components or sub-profiling of molecular families and interactions within the system, i.e. lipids, amino acids, bile acids, organic acids.⁸⁶

Most of the work in the field of metabonomics was performed investigating the metabolic effects of various toxins, xenobiotics, and drugs.^{91, 92} But, metabonomics can also provide novel diagnostic biomarker information in clinical research settings such as for example for rheumatoid arthritis⁹³, obesity⁹⁴, and diabetes.⁹⁵ Moreover, application of metabonomic approaches have also begun to provide useful information on the effects of nutritional interventions,⁹⁶ lifestyle,⁹⁷ and interactions of mammalian with their complex gut microbiota.^{98, 99}

1.3.1 Analytical Techniques Used in Metabonomics

The concept of metabonomics has arisen from various analytical applications to study the metabolic composition of biofluids, cells, and tissues.⁸⁷ The very beginning of the global study of metabolites was dated back to the 1960s and 1970s, when Horning and Pauling separately applied gas chromatography coupled to mass spectrometry to acquire metabolite profiles of human blood and urine.^{86, 100} Today, the main analytical techniques that are employed for metabonomic studies are based on high resolution proton nuclear magnetic resonance (¹H NMR) spectroscopy as well as mass spectrometry (MS). MS requires a pre-separation of the metabolic components using either gas chromatography (GC) after chemical derivatization or liquid chromatography (LC), with the newer method of ultra-performance liquid chromatography (UPLC) being used increasingly.^{86, 101, 102} Metabolites are generally labile and chemically very diverse species and are often present in a wide dynamic range. Therefore, the technology platform of choice depends on the type of sample which will be investigated as well as on the metabolites that will be analyzed.¹⁰² The wide diversity of metabolites ensures that no single analytical platform is appropriate for all investigations.⁸⁶ In general, the application of metabonomic-based techniques results in complex multivariate

data sets where the understanding of the underlying biochemical information is limited by their sheer very complexity.⁸⁷ However, advances in visualization software and the development of powerful pattern recognition and bioinformatic methods for effective data interpretation have made it possible to measure and interpret complex metabolite profiles of cells, tissues, and biological fluids. Moreover the information recovery of metabolomic data sets has been maximized.^{103, 104} These techniques are also amenable in detecting combinations of variables, which might more accurately describe the monitored response than any of the variables considered individually.¹⁰⁴

1.3.1.1 Nuclear Magnetic Resonance Spectroscopy

Nuclear magnetic resonance (NMR) spectroscopy is a nondestructive technique widely used in analytical chemistry, which takes advantage of the magnetic properties of certain nuclei (e.g. ^1H , ^{13}C , ^{15}N , ^{31}P) and records the absorption of energy between quantized nuclear energy levels.^{105, 106} During metabolite profiling, NMR spectroscopy provides a rapid analysis of a wide range of metabolites with highly reduced sample preparation steps. Thereby, each detected resonance in an acquired spectra is specific to one particular compound due to differences in chemical shift, spin-spin coupling, and relaxation/diffusion parameters of the individual metabolites.^{105, 106} Moreover, NMR spectroscopy benefits from being nondestructive, as samples can be subsequently analyzed by other techniques, and is highly reproducible, and, unlike other profiling modalities, non-selective. But the technique suffers from a relatively low sensitivity, particularly when compared with MS.^{86, 107} Typically, the majority of metabolomic samples analyzed by NMR spectroscopy are in solution state, thus comprising either biofluids, such as urine or plasma, or metabolites extracted from tissue samples which were subsequently re-dissolved in deuteriated solvents. Plasma and urine are among the most useful and widely exploited biofluids as they can be obtained in a non- or minimally-invasive manner and are therefore ideal for disease diagnosis and clinical-trial monitoring.¹⁰⁴ In addition, it is also possible to analyze intact tissue samples in a non-destructive approach by avoiding tissue extractions using high resolution magic angle spinning (MAS) NMR.¹⁰⁸

Proton (^1H) NMR spectroscopy is a well-established and powerful tool in providing a snapshot of biological matrices, including plasma,¹⁰⁹ urine,¹¹⁰ feces,¹¹¹ and tissue extracts.¹¹² It provides structural and quantitative information on hundreds of endogenous metabolites within a biological matrix and a standard ^1H NMR spectra typically takes only a few minutes to acquire.¹¹³ In general, a simple and standardized one-dimensional (1D) solvent suppressed Noesy pulse sequence is used to acquire ^1H NMR spectroscopic data.^{113, 114} But biological fluids have their own distinct physicochemical properties. In plasma, the presence of proteins, lipids, and lipoproteins give rise to highly overlapped and broad ^1H NMR signals which are able to over shadow the resonances from low molecular weight metabolites. To

facilitate the observation of these smaller metabolites, a relaxation-edited one-dimensional ^1H Carr-Purcell-Meiboom-Gill (CPMG) pulse sequence can be applied.^{113, 115} In addition, ^1H diffusion-edited NMR spectra provide a complementary profile of protein and lipid resonances, the signals of low molecular weight metabolites being severely attenuated.^{113, 116} Moreover, the detection limit of ^1H NMR spectroscopy often suffers from a large number of co-resonances, as different metabolites are found to have resonances in the same NMR spectral region. Here, the application of two-dimensional (2D) NMR experiments in association with the use of nuclei such as ^{13}C can improve the resolution and identification efficacy of closely related signals.¹¹⁷

NMR fingerprinting is currently the method of choice for metabonomics, but many researchers, aware of its comparatively poor sensitivity, are complementing this approach with MS-based technologies.⁸⁵

1.3.1.2 Mass Spectrometry

Mass spectrometers are analytical tools that operate by the formation of positively or negatively charged molecules or molecule fragments (ions) from analytes of interest, separation of ions according to their mass-to-charge ratio (m/z), and detection of ions.^{86, 101, 118} Modern mass spectrometry (MS) offers an array of technologies that differ in operational principles and performances, including different ionization techniques (e.g. electrospray ionization (ESI), atmospheric pressure chemical ionization (APCI)), mass analyzer technologies (e.g. triple quadrupole, time of flight (TOF), quadrupole-time of flight (Q-TOF)), resolving power, and mass accuracy. In metabonomic studies, direct infusion MS (DIMS) is generally used to analyze crude mixtures without any prior chromatographic separation. This approach is the least informative but provides a high throughput screening tool that is often applied for large sample numbers.¹⁰¹ In addition, several hyphenated approaches are also incorporated in MS-based metabonomics, comprising GC-MS, LC-MS, and capillary electrophoresis MS (CE-MS). Chromatographic separation prior to MS analysis has several advantages, for example the reduction of matrix effects, separation of isomers, and proposition of additional data (i.e. retention time) valuable for metabolite annotation.^{86, 101, 118} As a result, the generic advantages of MS feature a high sensitivity, high resolution, wide dynamic detection range, coverage of a wide chemical diversity, robustness, and feasibility to elucidate the molecular weight and structure of unknown compounds.¹¹⁹ MS is inherently considerably more sensitive than NMR spectroscopy,¹²⁰ but samples cannot be reused after MS analysis and there is also a need to pre-select columns and elution conditions.¹²¹ Typically, MS is applied to the analysis of gaseous or liquid samples, though solid samples such as tissues can be evaluated either directly or after extraction processes.⁸⁶

LC-MS is an important tool in metabonomics and can be tailored for targeted and non-targeted analyses. It can be regarded as the separation of a component mixture based upon a metabolite equilibration between a liquid mobile phase and a solid (or liquid) stationary phase, where the metabolites elute from the separation column depending on their interaction with the mobile and stationary phase.^{102, 118, 122} The ionization technique of choice for LC-MS-based metabolic fingerprinting is ESI, whereas different applications of mass analyzers have been reported.¹¹⁸ LC-MS is most frequently used in pharmacokinetic studies of pharmaceuticals¹²³ and in plant secondary metabolism research,¹²⁴ but the application to metabonomic studies has tremendously increased during the last ten years.¹⁰¹ Moreover, the combination of high pressure pumps (6000–15000 psi) and smaller diameter column packings (< 2 μm) recently introduced a technique called ultra-performance LC-MS (UPLC-MS), which can grant chromatographic resolution equivalent to GC-MS and also provides a higher sensitivity than conventional LC-MS.¹¹⁹ This rise in performance is manifested in improved peak resolution, together with enhanced speed and sensitivity, and lower detection limits.¹¹⁸ As a result, this technology was very recently successfully applied to metabolic profiling of plasma,¹²⁵ urine,¹²⁶ and tissue extracts.¹²⁷

NMR and MS can be seen as complementary analytical platforms capable of producing complex metabolic profiles of living organisms in a relative short time.⁹⁶ Consequently, a combination of several analytical techniques should be used, for example, parallel LC separations can be coupled to MS- and/or NMR-based detection methods.⁸⁵

1.3.2 Chemometrics in Metabonomics

The rising use of “omic” technologies generates huge and complex data sets, which are difficult to summarize and overview without appropriate tools. This includes efficient and robust methods for modeling and analyzing complicated biological data tables to produce interpretable and reliable statistical models. Chemometrics is a general term applied to methods of data analysis used in metabonomic studies, including multivariate data analyses (MVDA), which are able to generate scientific hypotheses as well as testing hypotheses by reducing mathematically the numerous parameters. Therefore, MVDA provides an expert means of analyzing and maximizing information recovery from complex spectral data sets.^{88, 128, 129} Here, the most useful techniques are principal component analysis (PCA),¹³⁰ projection to latent structures (PLS)¹³¹ or orthogonal projections to latent structures (OPLS).¹³² PCA is a data overview tool, working by summarizing the variation in the data into a smaller number of latent components (principal components (PC)) *via* linear combinations of the starting variables with appropriate weighting coefficients. It is an unsupervised method, where no *a priori* knowledge of class membership is required. Moreover, it is used to give an overview of the data that will enable to reveal outliers, groups, and trends in the data set.⁸⁸ However,

metabonomic studies typically consist of a set of control and treated samples/individuals which implies additional knowledge of the samples, as for instance age, gender, disease state, and diet.¹²⁸ Therefore, data sets can be modeled by supervised methods, which require *prior* knowledge of the sample classes, to optimize the separation between two or more classes on the basis of a series of mathematical algorithms, including PLS and OPLS.¹²⁹ PLS-discriminant analysis (PLS-DA) is a regression extension of PCA. It relates a data matrix containing independent variables from samples, e.g. spectral values (variable X), to a matrix containing dependent variables, e.g. age (variable Y), by a linear multivariate model. Thereby, it can be used to identify the input variables X that are responsible for the changes in the output variables Y with the aim of maximizing the correlation between X and Y.¹³¹ The O-PLS algorithm extends the PLS regression by pre-filtering classification-irrelevant orthogonal variation from the data.^{129, 132} As a result, the application of O-PLS discriminant analysis (O-PLS-DA) improves the model predictability and interpretability of spectral variations between classes.¹²⁹

In summary, MVDAs can be adapted to a large variety of analysis procedures with respect to: (I) summarizing and visualizing data sets *via* reduction of the data dimensionality; (II) classification of samples and discriminant analysis; (III) identification of quantitative relationships among variables; and (IV) generation and testing of hypotheses.

1.4 Application of Metabonomics in Inflammatory Bowel Disease Research

Progression of the high-throughput “omic”-technologies, including, genomics, proteomics, and metabonomics, have provided an excellent means to enable better understanding and interpretation of biological functions at different levels of molecular organization. Application of these profiling techniques could potentially address the following key issues in the field of IBD research.^{133, 134} (I) expansion of the list of genes involved in disease pathogenesis and identification of disease-linked genetic mutations and allelic polymorphisms; (II) disentangling of the largely unknown disease etiology in connection to the improvement of the molecular understanding of the IBD pathogenesis and dissection of signaling pathways; (III) generation of new working hypothesis; (IV) allocation of new tools for improved clinical diagnosis and patient characterization including prognostic factors and specific disease biomarkers; (V) identification of potential new therapeutic targets and intervention strategies; and (VI) management of the disease treatment. So far, only a limited number of studies are available which have utilized metabonomic analysis to contribute to the current knowledge of the IBD disease pathogenesis (Table 1-2).

Our knowledge concerning the primary cause and etiology of IBD is still limited. Like in many other chronic diseases, IBD appears to be a complex, multifactorial disease, whereupon en-

environmental and dietary factors, the intestinal microbiota, and a genetic susceptibility of the host are discussed to collude during the initial phase of the disease.⁴⁻⁶ Each of these factors is individually able to alter the metabolite profile of an individual organism. Therefore, metabonomic techniques provide an efficient way to provide insights into the largely unknown disease pathogenesis and can be the basis for further hypothesis generation.

The genetic contribution to the development of IBD was early evident from concordance studies in monozygotic twins^{17, 18} and in recent years GWAS have led to the identification of nearly 100 susceptibility genes for IBD.^{19, 20} In general, genetic mutations can for instance modify enzymatic functions of proteins and will consequently alter the metabolite profile of the affected organism that can be detected by metabonomic analysis. Until today, the metabolic effects of the various genetic mutations in human IBD patients have not been investigated. But already a small number of studies started to monitor metabolic changes in genetically modified animal models, such as in IL-10^{-/-} mice.^{45, 126, 135, 136} Here, the immune-related functions of various IBD susceptibility genes are of special interest and should be therefore investigated in additional animal models with defective gastrointestinal immune response. This will contribute to further enhance the knowledge of the involvement of these genes in the overall disease processes.

In addition, there is growing interest in understanding the metabolic and physiological contribution of the gut microbiota co-metabolom to the host's metabolism, especially under IBD conditions. A crucial role of the intestinal microbiota in the IBD pathogenesis is indicated by the requirement of microbial exposure in animal models of IBD (e.g. IL-10^{-/-} 26) to develop intestinal inflammation, and by differences in the intestinal microbiota composition of UC and CD patients compared to healthy controls.²⁷ Profiling of urinary¹¹⁰ and fecal^{111, 137} levels of microbial metabolites demonstrated a clear dysbiosis and perturbations in bacterial species. This highlights that metabonomic tools may help to understand the influence of the intestinal microbial metabolism on the host in IBD.

In the last decade, several attempts have been made to assess the metabolic changes related to environmental factors, especially to diet and specific bioactive ingredients, with the help of metabonomic approaches. For example, Martin *et al.*¹³⁸ characterized whether the supplementation of the probiotic strain *Lactobacillus paracasei* could reverse the abnormalities of the metabolic signatures of a *Trichinella spiralis* infection in a mouse model of post-infective irritable bowel syndrome (IBS). Moreover, Lin *et al.*¹²⁶ investigated the potential of the addition of polyphenol-rich kiwi fruit extracts to the standard chow diet. This neither improved the histopathology injury scores, nor restored the metabolite profile of IL10^{-/-} to that of WT mice. Nevertheless, the application of metabonomic tools to nutritional research will offer a great opportunity to evaluate the metabolic response to specific dietary modulations at the individual level.⁹⁶

Although UC and CD strongly vary in their respective clinical manifestations, they share many similar etiological, clinical, and pathological features. As a result, distinguishing between the two types of disease can be difficult, especially for colonic CD or indeterminate colitis, as reliable tests that can discriminate these diseases do not exist so far.¹³³ Nevertheless, a correct diagnosis of the IBD phenotype could assist the disease management and following lead to the application of differentiated treatment strategies, including different surgery approaches and the distinct choice of immune-modulatory therapies. Thus, the search for biomarkers reflecting disease phenotype, disease state, and disease prognosis are required. The establishment of biomarkers measurable in easy accessible and non-invasive biofluids, such as blood and urine, would thus be beneficial. Until today, metabonomics was already successfully applied as a diagnostic tool to distinguish between UC and CD in human intestinal biopsies,^{112, 139-141} plasma¹²⁷ and urine¹¹⁰ samples, and fecal extracts.^{111, 137, 142} For example, Bezabeh *et al.*¹³⁹ was able to distinguish healthy control from IBD tissue, and differentiated UC from CD tissue samples with an accuracy of 97.9 % and 98.6 %, respectively. However, clinical biomarkers for disease diagnosis require extensive validation to ensure their accuracy and predictive value. In addition, IBD diagnosis via radiology or endoscopy with biopsies of pathological lesions is only possible at an advanced disease state when symptoms are clearly visible. *Via* application of metabonomic techniques it was possible to demonstrate that already biopsies from IBD patients that were not visibly inflamed on endoscopy or histopathology had abnormal spectral profiles.^{140, 141} This suggests that metabonomic-based approaches together with multivariate statistical analysis might be more sensitive than either endoscopy or histopathology at identifying preclinical markers of inflammation. This could help to define early biomarkers to be used for disease surveillance.¹⁴⁰

In addition, metabolite profiling was shown to be also an appropriate tool to monitor disease progression and the therapeutic response of individual patients to drug treatment.¹⁴³ The use of metabonomic analysis for monitoring IBD disease activity has already been demonstrated in the IL-10^{-/-} mouse model. Lin *et al.*⁴⁵ compared urinary metabolite profiles of IL-10^{-/-} and WT animals housed under either conventional or specific pathogen-free (SPF) conditions as inflammation in SPF IL-10^{-/-} mice is less severe than in conventional IL-10^{-/-} mice. Moreover, monitoring of the therapeutic response to drugs, thereby identifying responders and non-responders, and non-effectiveness or adverse effects of drugs, has been highlighted with a study of paracetamol administration to rats.¹⁴³ Translation of these results to the treatment of IBD patients would help to promote a substantial progress in personalized treatment strategies.

Table 1-2: Inflammatory bowel disease studies using metabonomic analysis (modified from Lin *et al.*¹³³)

Disease or animal model	Sample	Method	Metabolite differences between disease and control (alphabetically)		Studies	
			Up-regulated under disease	Down-regulated under disease		
Patient Samples	CD, UC	Urine	¹ H NMR	CD: formate, glycine, glycolate, guanidoacetate, methylhistidine. UC: citrate, glycine, glycolate, guanidoacetate, methylhistidine.	CD: 4-cresol sulfate, citrate, hippurate. UC: hippurate, trimethyllysine.	Williams <i>et al.</i> ¹¹⁰ (2009)
	CD, UC	Fecal extracts	¹ H NMR	CD: alanine, glycerol, isoleucine, leucine, lysine, valine. UC: glutamate, lysine.	CD: acetate, butyrate, methylamine, trimethylamine. UC: methylamine, trimethylamine.	Marchesi <i>et al.</i> ¹¹¹ (2007)
	CD	Fecal extracts	ICR-FT-MS	(Z)/4/hydroxyphenyl-acetaldehydeoxime, 3-(4-hydroxyphenyl)-lactate, 4- hydroxyphenyl-acetylglycine, arachidonic acid, chenodeoxyglycocholate, dopaquinone, glycocholate, linoleic acid, octadecatrienoic acid, oleic acid, palmitic acid, phenylalanine, stearic acid, taurocholate, trihydroxy-6-betacholanate, tryptophan, tyrosine.	2,3-dinor-8-iso-prostaglandin F2 α , prostaglandin E2 α , prostaglandin F1 α , prostaglandin F2 α .	Jansson <i>et al.</i> ¹⁴⁴ (2009)
	UC, IBS	Fecal extracts	¹ H NMR	UC: cadaverin, choline, glucose, taurine. IBS: choline, deoxycholate, glucose.	UC: 2-methylbutyrate. IBS: 2-methylbutyrate, isobutyrate, isovalerate.	Le Gall <i>et al.</i> ¹³⁷ (2011)
	CD, UC	Colonic mucosal tissue (intact)	¹ H MRS	CD & UC (direction of differences unspecified): amino acids (nonspecific), choline, creatine, lipids (non-specific), lysine.		Bezabeh <i>et al.</i> ¹³⁹ (2001)
	CD, UC	Colonic mucosal tissue extracts	¹ H MRS	CD: glucose, glycerophosphorylcholine. UC: arginine, glucose, glycerophosphorylcholine, lysine.	CD: alanine, choline, formate, glutamine/ glutamate, isoleucine/leucine/valine, lactate, myoinositol, succinate. UC: alanine, choline, formate, glutamine/ glutamate, isoleucine/leucine/valine, lactate, myoinositol, succinate.	Balasubramanian <i>et al.</i> ¹¹² (2009)
	CD, UC	Colonic mucosal tissue (un-involved, involved)	¹ H MRS	CD & UC: choline, formate, glutamate, glutamine, glycerophosphocholine, lactate, short chain fatty acids.	CD & UC: glucose.	Sharma <i>et al.</i> ¹⁴¹ (2010)

Disease or animal model	Sample	Method	Metabolite differences between disease and control (alphabetically)		Studies	
			Up-regulated under disease	Down-regulated under disease		
UC	Colonic mucosal tissue (intact), colonocyte extracts, urine, lymphocytes	¹ H NMR	Colon tissue: ascorbate, aspartate, glutamate, glutamine, glutathione, taurine.	Colon tissue: betaine, glycerophosphocholine, lipid, myoinositol.	Bjerrum <i>et al.</i> ¹⁴⁰ (2010)	
CD, UC	Serum, colonic mucosal tissue (only UC)	GC-MS	Serum: CD: alanine, aspartate, fumarate, glycine, malate, methionine, proline, succinate. UC: aspartate, fumarate, glycine. Colon tissue (UC): -	Serum: CD: glutamine, histidine, tryptophan. UC: asparagine, glutamine, histidine, tryptophan. Colon tissue (UC): alanine, asparagine, citrate, fumarate, glutamine, glycine, isocitrate, isoleucine, leucine, lysine, malate, methionine, N-acetylaspartate, phenylalanine, proline, serine, succinate, threonine, tyrosine, valine.	Ooi <i>et al.</i> ¹²⁷ (2011)	
Animal Models	IL10 ^{-/-} mice	Plasma	¹ H NMR	alanine, arginine, choline in phospholipids, citrate, fumarate, HDL, isoleucine, lactate, LDL, phenylalanine, polyunsaturated lipids, pyruvate.	creatinine, dimethylglycine, glucose, leucine, methionine, trimethylamine, tyrosine, VLDL.	Martin <i>et al.</i> ¹⁴⁵ (2009)
	IL10 ^{-/-} mice	Urine	¹ H NMR	3-indoxylsulfate, butyrate, dimethylamine, fucose, phenylacetylglycine, trimethylamine, trimethylamine-N-oxide, valine.	2-oxoglutarate, citrate, fumarate, N-isovaleroylglycine, succinate.	Murdoch <i>et al.</i> ^{135b} (2008)
	IL10 ^{-/-} mice	Urine	GC-MS	5-aminovaleric acid, fucose, uracil, xanthurenic acid.		Lin <i>et al.</i> ^{45, 126} (2010, 2011)
	IL10 ^{-/-} mice	Urine	Short column LC-MS	xanthurenic acid.	xanthurenic acid glucuronide, 2,5,7,8-tetramethyl-2-(2'-carboxyethyl)-6-hydroxychroman.	Otter <i>et al.</i> ¹³⁶ (2011)
	TNF ^{ΔARE/WT} mice	Intestinal tissue extracts	¹ H NMR LC-MS	¹H NMR: cholesterol (total, free, and esterified), choline in phospholipids, glycerophospholipids, plasmalogen, polyunsaturated fatty acids, sphingomyelin. LC-MS: choline glycerophospholipid with an ether bond (PCae C38:4, C38:5, C42:3) sphingomyelin (SM C16:0).	¹H NMR: diacylglycerides, fatty acids, triacylglycerides, unsaturated fatty acids. LC-MS: acyl-carnitine (C10:1, C12:1, C14:2-OH, C16:1-OH), choline glycerophospholipid with an ester bond (PCaa C16:0, C40:1).	Baur <i>et al.</i> ¹⁴⁶ (2011)

Disease or animal model	Sample	Method	Metabolite differences between disease and control (alphabetically)		Studies
			Up-regulated under disease	Down-regulated under disease	
Carrageenan-induced colitis, rats	Colonic mucosal tissue	¹ H NMR	creatine, lipids (non-specific), phosphocholine.		Varma <i>et al.</i> ¹⁴⁷ (2007)
DSS-induced colitis, mice	Serum	LC-MS	1-stearoyl-sn- glycero-3-phosphorylcholine.	1-oleoyl-sn-glycero-3-phosphorylcholine, 1-linoleoyl-sn-glycero-3-phosphorylcholine.	Chen <i>et al.</i> ¹⁴⁸ (2008)
DSS-induced colitis, mice	Serum, urine	¹ H NMR	Serum: acetoacetate, acetone, creatine, glycolate, 3-hydroxybutyrate, hypoxanthine, inosine, mannose, N-isovalerylglycine, tryptophan. Urine: alanine, allantoin, creatine, carnitine, dimethylamine, fucose, glycine, 3-indoxysulfate, lactate, 3-methyl-2-hydroxybutyrate, 3-methylxanthine, phenylalanine, trimethylamine, trimethylamine-N-oxide.	Serum: acetate, alanine, betaine, carnitine, citrate, fumarate, glucose, glutamine, glycine, histidine, lactate, methionine, 2-oxoglutarate, proline, tartrate, tyrosine. Urine: ascorbate, methionine, 1-methylnicotinamide, nicotinamide, 2-oxoisocaproate, urea.	Schicho <i>et al.</i> ¹⁰⁹ (2010)
DSS-induced colitis, mice	Serum, colon tissue	GC-MS	Only metabolites listed differing at the end point of treatment		Shiomi <i>et al.</i> ¹²⁵ (2011)
			Serum: decanoic acid, glyoxylic acid, 4-hydroxybenzoic acid, 3-hydroxybutyric acid, 3-hydroxypropionic acid, isovalerylglycine, L-isoleucine, L-leucine, L-phenylalanine, L-threonine, L-valine, 2-methyl-3-hydroxybutyric acid, octanoic acid, uracil. Colon tissues: α-aminobutyric acid, asparagine, citraconic acid, 3,4-dihydroxymandelic acid, ethylmalonic acid, glycolic acid, glyoxylic acid, hexanoylglycine, 4-hydroxybenzoic acid, 4-hydroxybutyric acid, 4-hydroxyproline, L-alanine, L-glutamic acid, L-isoleucine, L-leucine, L-methionine, L-phenyl-alanine, L-proline, L-serine, L-threonine, L-tyrosine, L-valine, maleic acid, malic acid, oxalic acid, 5-oxoproline, propionylglycine, succinic acid, thiodiglycolic acid, thymine, uracil, uric acid.	Serum: citric acid, 3,6 epoxydodecanedioic acid, L-glutamine, 2-hydroxyphenylacetic acid, indol-3-acetic acid, isocitric acid, L-tryptophan, L-tyrosine. Colon tissues: 3-hydroxydodecanedioic acid, 3-hydroxysebacic acid.	

Key: ICR-FT-MS: ion cyclotron resonance Fourier transformation mass spectrometry; MRS: magnetic resonance spectroscopy.

1.5 Aim of the Current Work

The aim of the present work is to illustrate and characterize metabolic variations during the development of chronic intestinal inflammation through the use of metabolic profiling of blood plasma and intestinal tissue extracts coupled to multivariate data analysis.

The consequences of inflammatory processes during the pathogenesis of IBD on the systemic and gastrointestinal metabolic fingerprints still remain largely unknown. But a better understanding of the complex etiology would help to effectively improve the disease management, including the expansion of the hypothesis generation and a non-invasive disease monitoring. Moreover, the current methods of assessing bowel inflammation are only applicable at an advanced disease state when symptoms are clearly visible and require the sampling of intestinal tissues for histopathological examination.

Therefore, the metabolite modifications during the development of intestinal inflammation are investigated in two different models of IBD, IL-10^{-/-} and TNF^{ΔARE/WT} mice, which exhibit intestinal compartment specific inflammation in the colon and the distal ileum, respectively. These animal models are relevant to the human UC- and CD-like IBD etiopathology and are consequently appropriate models to study metabolic changes associated with the IBD onset and progression. In the performed experiments, a dense and frequent spreading of time points for sample collection is also chosen to enable the complete monitoring of variations in the metabolite profiles over time. This will facilitate the detection of metabolic modifications that possibly occur already before the histopathological onset of inflammation. Moreover, WT and non-inflamed IL-10^{-/-} mice are used in a further study to characterize the physiological impact of a genetic predisposed but disease-free phenotype on the host's metabolism. The metabonomic approach includes a range of spectroscopic techniques, such as ¹H NMR spectroscopy and UPLC-MS of blood plasma and intestinal tissue extracts. These measurements are combined with histopathological analysis and measurements of body weight and composition as well as nutritional energy utilization and adipocyte size to characterize site specific and systemic metabolic phenotypes at different time points during the development of UC and CD-like ileitis. The integration of biofluid and multi-tissue ¹H NMR and LC-MS data together with the monitoring of body constitution and energy assimilation will provide a more complete understanding of intrinsic site-specific and systemic metabolic variations in relation to the development of IBD.

2 MATERIAL AND METHODS

The animal experiments presented in this work were conducted at the animal facility of the Technische Universität München (Freising/Weißenstephan; Germany) in accordance with the national German law for animal protection. All metabonomic analyses, including ^1H NMR spectroscopy and LC-MS analyses, were carried out at the Nestlé Research Center (Lausanne; Switzerland) within the department of Immunology and Metabonomics & Biomarkers.

2.1 General Work Flow for Metabonomic Analysis

The sequential strategy used in the current work to initially generate and subsequently analyze the acquired data sets is shown in Figure 2. First, blood plasma and intestinal samples were collected during the different animal experiments (Figure 2 A) and then analyzed by either ^1H NMR spectroscopy and/or LC-MS analysis (Figure 2 B). Following, the generated data sets were processed to transform them into suitable data for multivariate statistical analysis. Hereby, PCA was initially performed on each data matrix to obtain an overview on the relationships between the samples and to extract the variables contributing to these observed distributions without any *a priori* knowledge. Moreover, application of PCA enables to reveal outliers, clustering of groups, and trends in the spectral data sets. Then, O-PLS approaches were generally used to perform a discriminant analysis between two classes, according to the experimental design, with the aim of maximizing the separation of the two classes.

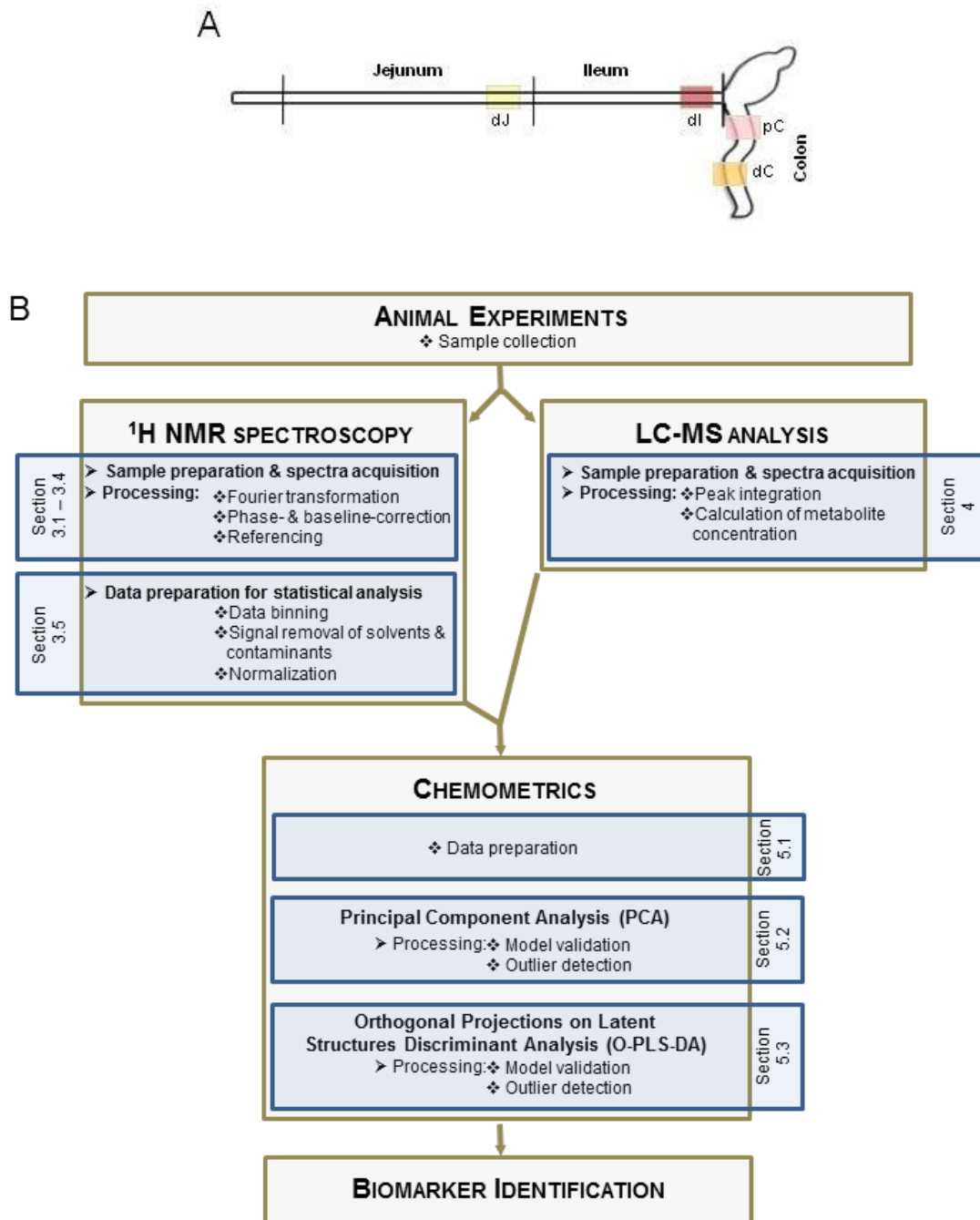


Figure 2: Metabonomic work flow

Experimental sampling scheme of the intestine (A). General pipeline for metabonomic analyses (B)

Abbreviations: dC: distal colon; dI: distal ileum; dJ: distal jejunum; pC: proximal colon.

2.2 Animal Experiments

2.2.1 IL-10^{-/-} Mouse Model

Experimental Design

A total of 20 WT and 20 IL-10^{-/-} mice on 129SvEv background were housed under conventional conditions (*Abbreviation: In the following called c-IL-10^{-/-}*). In addition, a total of 30 WT and 30 IL-10^{-/-} mice on 129SvEv background were housed under specific pathogen free (SPF) conditions (*Abbreviation: In the following called s-IL-10^{-/-}*). Both set of mice were raised at a constant room temperature (RT) (22 ± 2°C), air humidity (55 ± 5%), and a light/dark cycle of 12/12 h. Water and standard chow diet (Ssniff, Soest, Germany) were given *ad libitum*. WT and c-IL-10^{-/-} animals were sacrificed at the time points 1, 8, 16, and 24 weeks of age (n=5 at each time point). Blood from the retro-orbital plexus (200-500 µL; 1 week samples were < 200 µL) was collected under isoflurane anesthesia into tubes containing 10 µL of heparin (for metabonomic analysis) and ethylenediamine-tetraacetic acid (EDTA; for enzymatic assays). Plasma was obtained by centrifugation (8000g) and frozen at -80 °C prior to analysis. Animals were killed by cervical dislocation immediately after blood collection and intestinal sections (0.5 cm) were fixed in 4 % neutral buffered formalin for histopathological characterization.

WT and s-IL-10^{-/-} animals were sacrificed at the time points 4, 8, 12, 16, and 24 weeks of age (n=6 at each time point; 3 male/female). Blood (250 µL) was collected into tubes containing 10 µL of heparin and plasma was obtained after centrifugation (8000g) and frozen at -80 °C prior to analysis. For histopathological characterization, intestinal sections (0.5 cm) were fixed in 4 % neutral buffered formalin. For ¹H NMR and MS analysis, two times a 1 cm sample of the proximal colon (pC) were excised (Figure 2 A), flushed with 1 ml of phosphate buffered saline (PBS) and preserved at -80 °C prior to analysis.

Serum Amyloid A (SAA) Quantification

Protein levels of serum amyloid A (SAA) were determined using an enzyme linked immunosorbent assay (ELISA) kit (Biosource, Darmstadt, Germany) according to the manufacturer's instructions.

2.2.2 TNF^{ΔARE/WT} Mouse Model

Experimental Design

In total 48 heterozygous TNF^{ΔARE/WT} mice on C57BL/6 background (a generous gift from Kollias G., Institute for Immunology, Biomedical Sciences Research Center "Al. Fleming", Greece) as well as an equal number of corresponding WT C57BL/6 mice were conventionally housed at constant RT (22 ± 2°C), air humidity (55 ± 5%), and a light/dark cycle of 12/12 h.

Water and conventional chow diet (Ssniff, Soest, Germany) were given *ad libitum*. Groups of 8 animals per genotype (4 male and 4 female) were sacrificed at the age of 1, 4, 8, 12, 16, and 24 weeks.

One week before sacrifice, mice were separated into single cages and food uptake and water consumption was monitored during one week. Fecal samples were collected from individual mice every day, dried at 60 °C for 3 days, and stored air tight at RT until being assessed. Animals were sacrificed by cervical dislocation. For histopathological characterization, 0.5 cm sections of the distal jejunum (dJ) and ileum (dI) and proximal (pC) and distal colon (dC) (Figure 2 A) as well as samples of the subcutaneous, epididymal, and mesenteric fat tissue were fixed in 4 % neutral buffered formalin. For ¹H NMR and LC-MS analysis, two times a 1 cm sample of the different gut sections (dJ, dI, pC, dC) was excised and flushed with 1 ml of PBS using a sterile syringe and preserved at -80 °C prior to analysis.

Body Composition Assessment

For the assessment of body composition, 4 additional WT and TNF^{ΔARE/WT} mice were sacrificed at the time points 12, 16, and 24 weeks, fixed in a stretched position and stored at -80 °C until analysis. Computer tomographic (CT) measurements were performed using the CT-Scanner LaTheta LCT-100A (Aloka, Japan and Zinsser Analytic, Deutschland).

Gross Energy Content

Fecal pellets were manually ground and pressed into pellets and the gross energy content was determined in a 6300 Calorimeter (Parr Instrument Company, Moline, IL, USA).

Adipocyte Size Measurements

In formalin fixed tissue samples were embedded in paraffin, cut in 5 μm sections followed by hematoxylin and eosin staining. The mean adipocyte size (μm²) was determined in the stained fat sections at a magnification of 200 fold and the size of adipocytes was calculated with the software AxioVision 4.6 (Carl Zeiss AG, Jena, Germany).

Cytokine Quantification

Cytokines, including mouse IFN γ , IL-1 β , IL-6, IL-10, IL-12p70, TNF, and keratinocyte derived chemokine (KC), were analyzed using a mouse pro-inflammatory multiplex kit (Meso Scale Discoveries, Gaithersburg, Maryland, USA). Assay was carried out according to the manufacturer's manual.

2.2.3 Histopathological Scoring

In formalin fixed tissue samples were embedded in paraffin, cut in 5 μm sections followed by hematoxylin and eosin staining. Histopathological scoring was performed by blindly assessing the degree of lamina propria mononuclear cell infiltration, crypt hyperplasia, goblet cell depletion and architectural distortion in the different gut sections, resulting in a score from 0 (not inflamed) to 12 (inflamed), as previously described.¹⁴⁹

2.3 ^1H NMR Spectroscopy

2.3.1 NMR Spectroscopy Approaches: 1D and 2D Spectroscopy

In general, one-dimensional (1D) ^1H NMR spectra of complex biological matrices are characterized by a high number of overlapping signals which limit the assignment of a large number of metabolites. Consequently spectral-editing techniques, providing metabolic information on a selective class of metabolites without physical separation of samples, or methods like two-dimensional (2D) NMR spectroscopy, which disperses NMR signals in a second dimension, are applied.

The principle of spectral-editing is based on the spin properties of macromolecules and small molecules. Small molecules such as endogenous metabolites present in biofluids can be selectively observed by applying special magnetic-pulse sequences, like relaxation-edited NMR spectroscopy (Carr-Purcell-Meiboom-Gill (CPMG) spin-echo loops).¹¹⁵ Conversely, macromolecules tend to move slowly and can selectively be observed by diffusion-edited spectroscopy (Figure 3).¹¹⁶

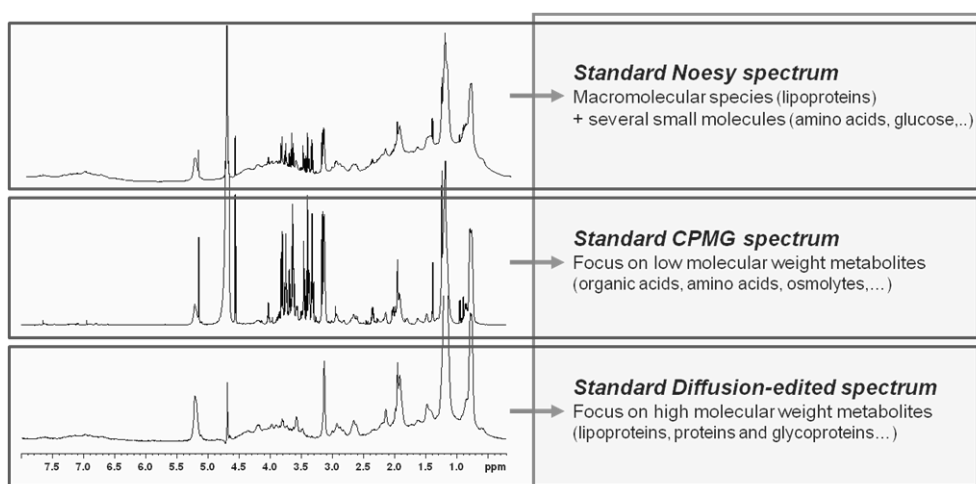
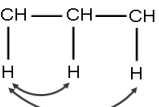


Figure 3: Plasma ^1H NMR pulse sequences and corresponding spectra used for spectral editing

Two-dimensional (2D) NMR spectroscopy separates relevant information by showing crossed peaks for coupled nuclei. For example, in a normal 1D ^1H NMR spectrum, overlap-

ping resonances on the chemical shift scale may obscure coupling information. J-resolved (JRES) ^1H NMR spectroscopy resolves chemical shifts from scalar couplings into orthogonal dimensions, allowing a direct measurement of homonuclear coupling constants.^{117, 150} A set of additional 2D NMR experiments commonly used in the analysis of biological fluids is reported in Table 2-1, where the resulting spectra show couplings existing between two protons (COSY, TOCSY) or one proton and one carbon atom (HSQC, HMBC).^{105, 117}

Table 2-1: Types of 2D experiments providing different structural information

Experiment	Type	Information
COSY <i>CORrelated SpectroscopY</i>	Homonuclear spin couplings of adjacent protons ($^1\text{H} - ^1\text{H}$ correlations)	
TOCSY <i>TOTal Correlation SpectroscopY</i>	Homonuclear long range spin couplings of protons ($^1\text{H} - ^1\text{H}$ correlations)	
HSQC <i>Heteronuclear Single Quantum Coherence</i>	Heteronuclear spin couplings between adjacent protons and carbon atoms ($^1\text{H} - ^{13}\text{C}$ correlations)	
HMBC <i>Heteronuclear Multiple Bond Coherence</i>	Heteronuclear long ranges spin couplings between non adjacent protons and carbons ($^1\text{H} - ^{13}\text{C}$ correlations)	

Key: Observed spin-spin couplings are indicated with bold lines.

2.3.2 Sample Preparation and ^1H NMR Spectroscopic Analysis

2.3.2.1 Plasma Samples

Plasma samples (30 μL) were prepared by dilution with 30 μL of PBS containing 90:10 $\text{D}_2\text{O}/\text{H}_2\text{O}$ (v/v) as a field frequency lock and transferred into 1.7 mm NMR tubes. ^1H NMR spectra were acquired at 600.13 MHz and ambient temperature (300 K) on a Bruker Avance III spectrometer (Bruker Biospin, Rheinstetten, Germany). For plasma samples three different pulse sequences were used as previously described (Figure 3):¹¹³

(I) A standard pulse sequence, using the first increment of the Noesy sequence ($\text{D1}-90^\circ-\text{t1}-90^\circ-\text{tm}-90^\circ$ - free induction decay (FID)) with solvent suppression.¹¹⁴ Spectra were obtained with a relaxation delay D1 of 2.5 s, during which the water resonance is selectively irradiated, and a fixed interval of t1 of 3 μs . The water resonance is irradiated for a second time during the mixing time tm of 100 ms.

(II) A Carr-Purcell-Meiboom-Gill (CPMG, D1-90°-(τ-180°-τ)-n-FID) spin-echo sequence with solvent suppression using a spin-echo loop time (2nτ) of 19.2 ms and a relaxation delay D1 of 2.5 s.¹¹⁵

(II) A diffusion-edited sequence (D1-90°-G1-180°-G1- 90°-G2-Δ-90°-G1-180°-G1-90°-G2-τ-90°-FID), where spectra are registered using a relaxation delay of 1 s, pulsed field gradients G1 and G2 set at 46.8 G*cm-1, and a diffusion delay of 120 ms during which the molecules are allowed to diffuse.¹¹⁶

For each single spectrum, 128 transients were collected into 64 k data points using a spectral width of 12 kHz corresponding to an acquisition time of 2.7 s.

Plasma Preparation and ¹H NMR Spectroscopic Analysis during c-IL-10^{-/-} Kinetic Study

Contrary to all other ¹H NMR plasma measurements, a modified protocol was used for the plasma of c-IL-10^{-/-} and corresponding WTs as the obtained plasma volume was sufficient to acquire the ¹H NMR spectra on a 5 mm inverse probe. Here, 320 μL were diluted with 40 μL of D₂O as locking substance. ¹H NMR spectra were acquired at 600.13 MHz and ambient temperature (300 K) on a Bruker Avance II spectrometer (Bruker Biospin, Rheinstetten, Germany) equipped with a 5 mm inverse probe. However, the same three different pulse sequences were used as previously described, including Noesy, CPMG, and diffusion-edited NMR spectra. For each sample, 32 FIDs were collected into 65 K data points using a spectral width of 12 KHz.

2.3.2.2 Intestinal Tissue Extracts

Around 5-10 mg of freeze dried and ground intestinal tissue were used to extract hydrophilic and lipophilic metabolites applying an adapted Folch procedure.^{113, 151} Briefly, samples were extracted three times with 0.5 mL of a chloroform-methanol solution (2:1, v:v). Combined extracts were washed first with 0.5 mL of water and second with 0.5 mL of a water-methanol solution (1:1, v:v). The upper hydrophilic phases were collected each time and combined together. Lipophilic and hydrophilic fractions were afterwards evaporated to dryness under nitrogen flow and freeze dried, respectively. Hydrophilic fractions were dissolved in 60 μL of a deuteriated PBS buffer (pH 7.4; 0.2 M NaH₂PO₄, Na₂HPO₄,) containing 0.05 % of trimethylsilylpropionic acid (TSP) as a standard reference (δ = 0.0) and transferred into 1.7 mm NMR tubes. The lipophilic phases were reconstituted in 60 μL of a deuteriated chloroform-methanol solution (2:1, v:v) and transferred into 1.7 mm NMR tubes using octamethylcyclotetrasiloxane (OMS) as standard reference (δ = 0.0). ¹H NMR spectra were registered at ambient temperature (300 K) on a Bruker Avance III spectrometer (Bruker Biospin, Rheinstetten, Germany) at 600.13 MHz. A standard 1D pulse sequence (zg) with

solvent suppression and a relaxation delay D1 of 4.0 s was used.¹¹³ For each sample, 128 transients were collected into 65 K data points using a spectral width of 12 kHz and an acquisition time of 2.7 s, resulting in a total recycling time of 6.7 s.

2.3.3 ¹H NMR Spectroscopic Assignment

The peak assignment to specific metabolites was achieved using an internal library of compounds and the literature,^{152, 153} and was confirmed by standard 2D NMR spectroscopy (JRES, COSY, TOCSY). Additionally, statistical correlation analysis STOCSY¹⁵⁴ (statistical total correlation spectroscopy) was also used on selected metabolites.

2.3.3.1 JRES ¹H NMR Spectroscopy

JRES NMR spectra provide information on chemical shifts and coupling constants separated into orthogonal axes in the 2D matrix.¹⁰⁵ 2K data points with 40 increments and 40 scans per increment were collected using spectral widths of 4.2 kHz in the F2 dimension and 50 Hz in the F1 dimension.

2.3.3.2 ¹H-¹H COSY and ¹H-¹H TOCSY

For 2D COSY and TOCSY^{117, 150} NMR spectra, 48 transients per increment and 256 increments were collected into 2K data points. The spectral width in both dimensions was 10 ppm. The TOCSY NMR spectra were acquired by using the MLEV-17 spin-lock scheme for ¹H-¹H transfers with a spin-lock power of 6 kHz. The COSY spectra were recorded with gradient selection. In both 2D NMR experiments, the water signal was irradiated with a weak pulse (≈ 50 Hz) during the recycle delay, and the data were zero-filled to 2K data points in the evolution dimension. Before Fourier transformation, an unshifted sine-bell and a shifted sine-bell apodization function were applied to the FIDs (in F1 and F2) of COSY and TOCSY spectra, respectively.

2.3.4 ¹H NMR Data Processing

¹H NMR spectra were processed using the software package Topspin (version 2.1, Bruker Biospin, Rheinstetten, Germany) and MATLAB (version 7.0; The MathWorks Inc., Natick, MA).

Prior to Fourier transformation, FIDs were multiplied by an exponential weighting function corresponding to a line broadening of 0.3 Hz for standard Noesy spectra of plasma and the

hydrophilic tissue extracts. A line broadening of 1 Hz was applied to CPMG spectra of plasma and lipophilic tissue extracts as well as to the diffusion-edited plasma spectra. The acquired NMR spectra were manually phase- and baseline-corrected and referenced to α -glucose at $\delta = 5.236$ for plasma spectra or the chemical shift of their respective standards at $\delta = 0.0$ (TSP for hydrophilic tissue extracts; OMS for lipophilic extracts).

2.3.5 ^1H NMR Data Preparation for Statistical Analysis

To prepare NMR spectra for statistical analysis, all spectra were binned into 22 K data points by spline cubic interpolation over the range of $\delta = 0.2 - 10.0$ and imported into the MATLAB software, thereby excluding the water residue (water $\delta = 4.50 - 5.19$), solvent signals (methanol $\delta = 3.24 - 3.27$ and $\delta = 4.25 - 4.60$; chloroform $\delta = 7.35 - 7.45$), and contaminant resonances (e.g. ethanol originating from the sacrifice of the animals). The spectra were normalized to a constant total sum of all intensities within the specified range. This resulted in a data matrix consisting of N rows (observations/samples) and K columns that represent variables, for example the spectral integrals of defined bins across the whole spectral width.

2.4 LC-MS Analysis

2.4.1 Sample Preparation and Biocrates Life Sciences AbsoluteIDQ™ kit Analysis

The Biocrates Life Sciences AbsoluteIDQ™ kit, originally designed for plasma samples, was adapted as previously published¹⁵⁵ to be also used for organ tissue. Therefore samples were prepared as follows: Intestinal tissue samples (20-30 mg wet weight) were homogenized in 300 μL of EDTA (0.292 mg/mL PBS) and 10 μL of BHT-buffer (butylated hydroxytoluene; 79.2 mg/mL PBS) using the FastPrep® 24 system (MP Biomedicals LLC; Illkirch, France). Plasma samples were used without former sample preparation steps. Well plate preparation and sample application was carried out according to the manufacturer's instructions. A final volume of 10 μL of plasma sample or tissue homogenate was loaded onto the provided 96-well plate. LC was realized on a Dionex Ultimate 3000 UPLC system (Dionex AG, Olten, Switzerland) coupled to a 3200 Q TRAP MS (AB Sciex; Foster City, CA, USA) fitted with a TurboV ion source operating in ESI mode. Sample extracts (20 μL) were injected two times (in + and - ESI modes) via direct infusion using a gradient flow rate of 0 - 2.4 min: 30 $\mu\text{L}/\text{min}$, 2.4 - 2.8 min: 200 $\mu\text{L}/\text{min}$, 2.9 - 3 min: 30 $\mu\text{L}/\text{min}$. MS source parameters were set at: Desolvation temperature (TEM): 200 °C, high voltage: -4500 V (ESI-), 5500 V (ESI+), curtain (CUR) and nebulizer (GS1 and GS2) gases: nitrogen; 20, 40, and 50 psi; respectively, nitrogen collision gas pressure: 5 mTorr. MS/MS acquisition was realized in scheduled reaction monitoring (SRM) mode with optimized declustering potential values for the 163 metabolites

screened in the assay. Raw data files (Analyst software, version 1.5.1; AB Sciex, Foster City, CA, USA) were imported into the provided analysis software MetIQ to calculate metabolite concentrations. List of all detectable metabolites is available online (<http://biocrates.com>; Biocrates Life Sciences, Austria).

2.4.2 Sample Preparation and Inflammation Marker Quantification by UPLC-ESI-MS/MS Using Isotope Dilution Technique

Internal standard (IS)

A mixture of the 22 deuteriated standards (5 ng each) was used as IS solution. Deuteriated 9 β -prostaglandin F2 α was chemically synthesized at the Nestlé Research Center (Lausanne, Switzerland). All other standards were purchased from Cayman Chemicals (Chemie Braunschweig AG, Basel, CH): arachidonic acid-d₈, (\pm)8,9-DiHETrE-d₁₁, (\pm)14,15-DiHETrE-d₁₁, (\pm)12,13-DiHOME-d₄, (\pm)9,10-DiHOME-d₄, (\pm)5,6-EpETrE-d₄, (\pm)14,15-EpETrE-d₁₁, 5-oxo-ETE-d₇, 5(s)-HETE-d₈, 12(s)-HETE-d₈, 15(s)-HETE-d₈, 20(s)-HETE-d₈, 13(s)-HODE-d₄, linoleic acid-d₄, leukotriene B4-d₄, prostaglandin B1-d₄, prostaglandin E1-d₄, prostaglandin E2-d₄, prostaglandin F2 α -d₄, 8-iso-prostaglandin F2 α -d₄.

Based on previously published work¹⁵⁶ a method to measure a panel of 63 inflammatory markers was developed at the Nestlé Research Center (Lausanne, Switzerland). Tissue samples (20-30 mg wet weight) were homogenized in 300 μ l of EDTA (0.292 mg/mL PBS) and 10 μ l of BHT-buffer (79.2 mg/mL PBS) using the FastPrep® 24 system. For each sample a total of 50 μ L of the tissue homogenates was mixed with 5 μ l of the IS solution (0.1 ng/ μ l). The mixture was acidified by adding 15 μ L of citric acid (1N). To precipitate proteins, a volume of 550 μ L of a methanol/ethanol solution (1:1, v:v) was added and samples were mixed during 15 min at 4° C before being centrifuged (3500 rpm, 10 min, 4 °C). The organic phase was evaporated to dryness under constant nitrogen flow and the residues were solubilised with 80 μ L water, followed by the addition of 20 μ L of acetonitrile, before being centrifuged at 3500 rpm for 1 min at 4 °C. LC was realized on a Dionex Ultimate 3000 UPLC system (Dionex AG, Olten, Switzerland). MS detection was realized on a 5500 Q TRAP MS (AB Sciex; Foster City, CA, USA) operating in ESI mode. Gradient chromatographic separation was performed on an Acquity BEH C18 column (2.1 x 150 mm, 1.7 μ m; Waters, Milford, USA). The injection volume was 5 μ L and the column was maintained at 50 °C. The mobile phase consisted of water containing 1% acetic acid (eluent A) and acetonitrile (eluent B) at a constant flow rate set at 450 μ L/min. Gradient elution started from 20 % B with a linear increase to 50 % B at 6 min, from 50 % to 95 % B at 13 min, hold for 3 min at 95 % B, before going back to 20 % B at 16.1 min and re-equilibration of the column for additional 11 min. Analytes were monitored in SRM mode provided within the Analyst software (version 1.5.1; AB Sciex, Fos-

ter City, CA, USA). The SRM detection window time was set at 120 sec with a target scan time of 0.5 sec. Nitrogen was used as curtain and desolvation gas at the respective pressure of CUR: 20, GS1: 70, GS2: 20 (arbitrary unit). Block source temperature was maintained at 600 °C, with the respective voltages: ISV: -4000 V, EP: -10 V, CXP: -5 V. A 15-points calibration curve was realized prior to sample analysis by measuring different dilutions of the standard solution (0-10 ng). Data processing was realized using Analyst software (version 1.5.1; AB Sciex, Foster City, CA, USA). Peak area ratio of each analyte versus its corresponding internal standard or surrogate marker was calculated. The obtained concentration values were then normalized to the tissue amount used.

2.5 Chemometrics

All MVDA was carried out with the Simca-P+ software (version 12.0; Umetrics AB, Umeå, Sweden) and the MATLAB software package (version 7.0; The Mathworks Inc., Natwick, MA).

2.5.1 Data Preparation

Prior to chemometric analysis, mean centering and scaling are essential pre-processing steps in the analysis of spectral data. By mean centering the data, the average value of each variable is calculated and subtracted from the data. This improves model interpretability, but the results lead to an overestimation of those metabolites that are present at high concentrations with corresponding high variances, since MVDA are maximum variance projection methods. Thus, to extract potentially influential metabolites that are present only at relatively low concentrations, a variety of scaling methods can be applied. Scaling addresses the substantially different concentration ranges of variables. For instance, with unit variance (UV) scaling, each variable range is divided by its standard deviation to give all the variables an equal variance (Figure 4). This will ensure that all variables are on a comparable footing and that no variable is allowed to dominate over another. However, unit variance scaling has the tendency to make analyses more susceptible to the influence of artefacts.

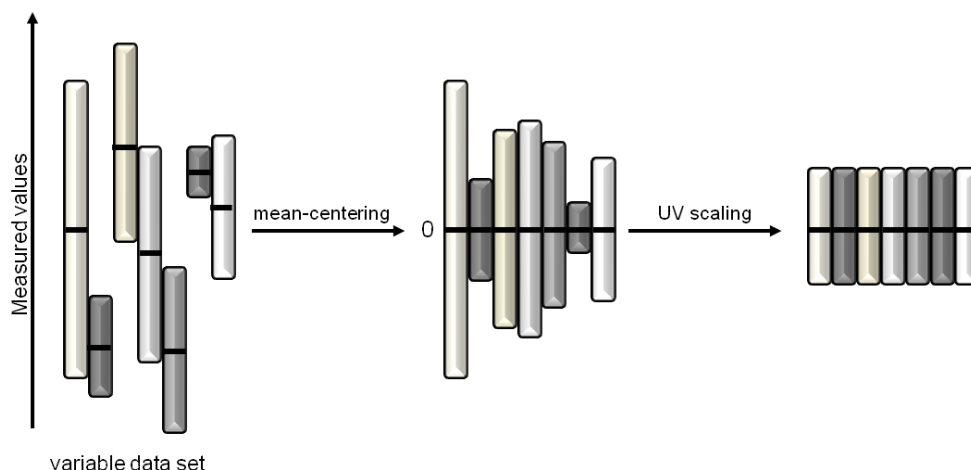


Figure 4: Data mean-centering and unit variance (UV) scaling

Each bar represents the intensity of the signal detected for each variable or metabolite and the short horizontal line inside each bar represents the mean value. After UV scaling, dividing each variable range by its standard deviation, the intensity of each variable is identical.

2.5.2 Principal Component Analysis

Principal component analysis (PCA) belongs to the unsupervised multivariate techniques in which no *a priori* knowledge of class membership is needed. PCA reduces the dimensionality of the initial data set according to its main variation so that a simplified overview of the data is obtained, dominant global metabolic variances are visualized, and outliers can be detected. Mathematically, PCA is defined as an orthogonal linear transformation that converts the initial data to a new coordinate system so that the variance is captured in Principal Components (PCs) ordered by their amplitude: The largest variance on PC1, second largest variance on PC2 etc. PCA is theoretically the optimum transformation for a given data set in least square terms.^{88, 128, 130}

Before PCA, the matrix X of a data set with N rows (observations: here samples) and k columns (variables: here spectral regions) has to be created as described in section 2.3.5 and Figure 5 A. From there, each variable represents one coordinate axis with a standardized length through scaling to unit variance and each observation of the X -matrix is placed in the k -dimensional variable space. All observations form a swarm of points projected in this space (Figure 5 B). According to the described effect of mean-centering, the origin of the coordinate system is moved so that the average point coincides now with the origin. The first PC (PC1) can then be calculated which accounts best for the shape of the point swarm and represents the maximum variance in the data (Figure 5 C). PC1 is the first latent variable in the new coordinate system that describes best the variation in the data. A second PC (PC2) is calculated to describe the largest variation in the data once contribution of PC1 to X is removed. It is orthogonal to PC1 by construction. PC2 is the second latent variable in the new coordinate system. PC1 and PC2 define together a plane window into the k -dimensional variable space

(Figure 5 D). For visualizing the structure of the investigated data, all observations have to be projected onto this reduced sub-space. The coordinate values of the observations on this plane are called scores and the plotting itself scores plot (Figure 5 E). Most influential variables behind each PC and also their correlation with each other (positively or negatively) can be revealed by the PC loadings (p). Geometrically, the loadings express the orientation of the original variables in the PC plane, therefore illustrating those variables contributing to the scores plots. When working with NMR spectra, the loadings plots, when generated on mean-centered data, have a shape similar to NMR spectra. The PC loadings can be interpreted to show which spectral regions have the greatest influence on the model.^{117, 174, 176}

In this PhD thesis, PCA models are created in a manner that 'how well the model fits the data' and the 'ability of the model to predict other samples' were maximized. The quantitative measure of how well a statistical model can fit the data is linked to the amount of variation within the data set that can be explained by the model. This is captured by the variable R^2X . Contrary, the Q^2Y value represents the predictability of the models and relates to its statistical validity. It measures how accurately the dataset X can be predicted either by using the existing data set or by using an independent validation set of observations. Consequently, the number of PCs selected for the models in this PhD thesis is aimed at maximizing both the R^2X and Q^2Y values. Plots of cumulative R^2X and Q^2Y values were calculated and the appropriate number of components was determined when cumulative R^2X was maximized whilst the cumulative Q^2 reached a plateau.

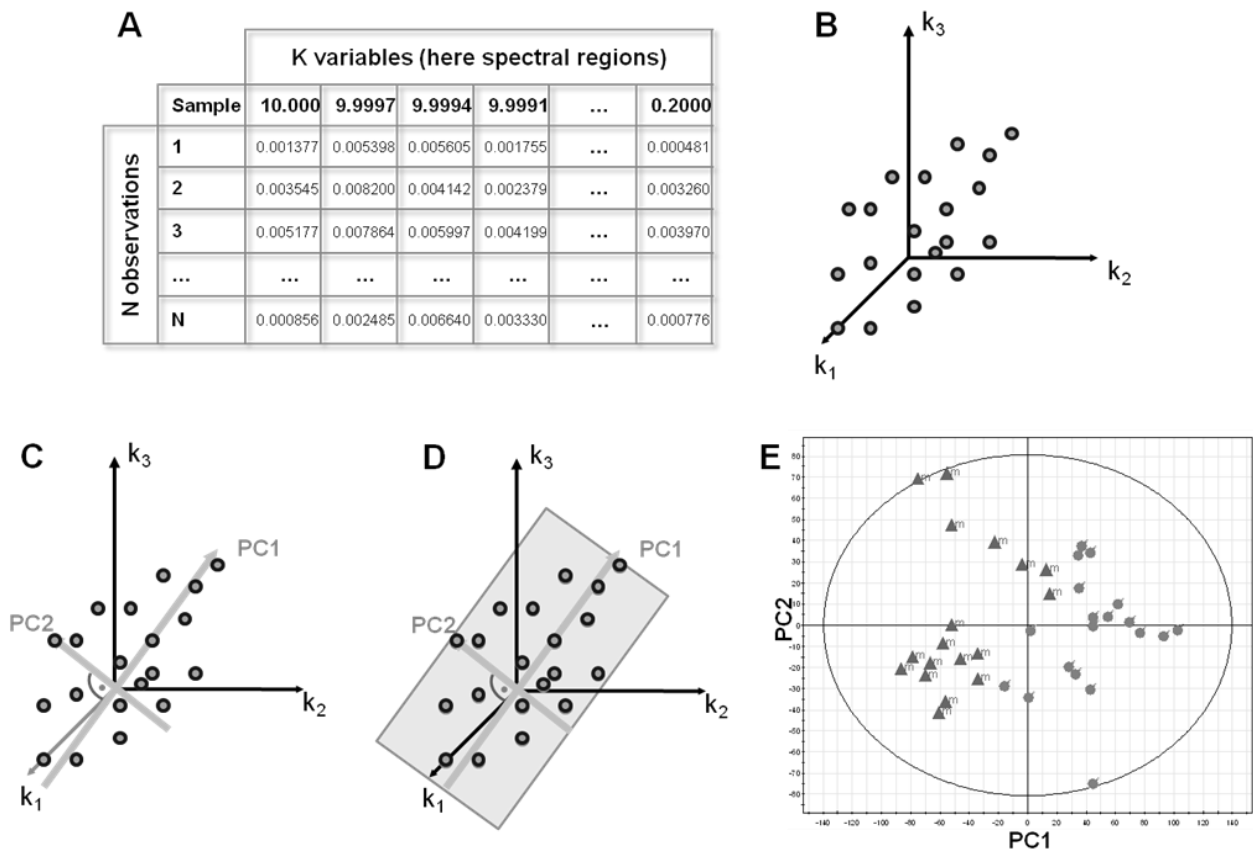


Figure 5: Principal Component Analysis (PCA)

A matrix X of a data set is created with N rows (observations: here samples) and K columns (variables: here spectral regions) (A). Each observation (sample) is placed in the K -dimensional variable space forming a swarm of points (for simplicity, only three variable axes are displayed) (B). The first (PC1) and the second (PC2) principal components are calculated (C). PC1 is the line that best accounts for the shape of the swarm of points in the least-square sense, and thus represents the maximum variance direction in the data set. PC2 reflects the second largest source of variation in the data set, and is orthogonal to PC1 by construction. PC1 and PC2 define together a plane window into the multidimensional space (D). All observations are projected onto a low-dimensional subspace, called scores plot (E).

2.5.3 Projections to Latent Structures (PLS) and Orthogonal-Projection to Latent Structures (O-PLS) Discriminant Analyses

Besides unsupervised multivariate techniques, like PCA, also supervised methods, namely partial least squares (PLS) methods by projections to latent structures and orthogonal-projection to latent structure (O-PLS) discriminant analysis (-DA), can be used to optimize the separation between two or more classes. These approaches are effective when it comes to filtering out metabolic information that is not correlated to the predefined classes, while the loading yields information on which spectral signals are associated with the observed clustering of samples.^{128, 132, 157, 158}

PLS is a regression extension of PCA and a method for relating two data matrices, an X matrix (e.g. NMR spectra) and a response matrix Y (descriptive variables or classes, e.g. age, gender, BMI), to each other by a linear multivariate model. The PLS technique provides a

means to identify input variables in \mathbf{X} that are responsible for the changes in the output variables \mathbf{Y} with the aim of maximizing the correlation between \mathbf{X} and \mathbf{Y} . These models attempt to approximate the best variation in the point swarms of the \mathbf{X} and \mathbf{Y} spaces thus giving a geometric interpretation similar to that of PCA. Briefly, the first PLS component is a line through the point swarms of the \mathbf{X} and \mathbf{Y} spaces. It is calculated such that it approximates as well as possible the point-swarms in \mathbf{X} and \mathbf{Y} , and provides a good correlation between the positions of points along these line in \mathbf{X} and \mathbf{Y} . Afterwards, successive components are orthogonal to preceding components. These lines improve the approximation and correlation of the positions of the \mathbf{X} and \mathbf{Y} planes.^{128, 131, 158}

PLS-discriminant analysis (PLS-DA) provides a class separation to ensure that maximal separation between pre-defined classes is achieved on the basis of their \mathbf{X} variables (Figure 6 A). Here, the \mathbf{Y} matrix of PLS-DA consists of a set of dummy variables, which are set up to describe the class membership of each observation in the \mathbf{X} matrix. A dummy variable is an artificial variable that assumes a discrete numerical value in the class description. The dummy variable matrix \mathbf{Y} has \mathbf{M} columns (for M classes) comprising a series of ones and zeros, such that the “ m ” column is one and the others zero for observations of class “ m ”. The quantitative measure of the discriminatory power for each chemical descriptor in a PLS-DA model can be obtained from a variable importance plot (VIP). The higher the numerical value for a variable in the VIP plot is, the stronger its discriminatory ability in the \mathbf{X} -matrix is. However, it is important to note that discriminative techniques like PLS-DA, have a tendency to overfit when variables out-number samples. An important feature of PLS-DA is that the validity of the models created using this technique must be determined by cross validation, which allows statistical evaluation as to whether the distinction between the classes is significant or not. The validity of the model against overfitting is tested by computing the cross-validation parameter Q^2 . The standard 7-fold crossvalidation method (repeatedly leaving out a seventh of the sample and predicting them back into the model) is generally applied to check the robustness of the model.^{157, 159}

The O-PLS algorithm is derived from the PLS regression. Here, the variation in the \mathbf{X} matrix and the \mathbf{Y} matrix is decomposed into three parts: The first part contains the variation common to \mathbf{X} and \mathbf{Y} , the second part contains the specific variation for \mathbf{X} , the so-called structured noise, and the last part contains the residual variance. Structured noise (e.g. baseline variability, drift and scattering effects in spectra but also biological factors such as age) in \mathbf{X} can be defined as the systematic variation of \mathbf{X} not linearly correlated with \mathbf{Y} . Because the variation in \mathbf{X} is unrelated to \mathbf{Y} this may weaken the predictive ability of the statistical model and makes it difficult to ascertain strong correlation between \mathbf{X} and \mathbf{Y} . So, the prediction of the model is improved compared to the PLS regression as the structured noise is modeled separately from the variation common to \mathbf{X} and \mathbf{Y} . This leads to a model with a minimal number of

predictive components defined by the number of degrees of freedom of the between-group variance. In this work, the O-PLS discriminant analysis (O-PLS-DA) mode is used. In the case of a comparison between two classes, the value of an O-PLS-DA loading for a variable corresponds to the correlation coefficient between the variable and the class descriptor, and loadings are described in the coefficients plots.^{128, 132, 158}

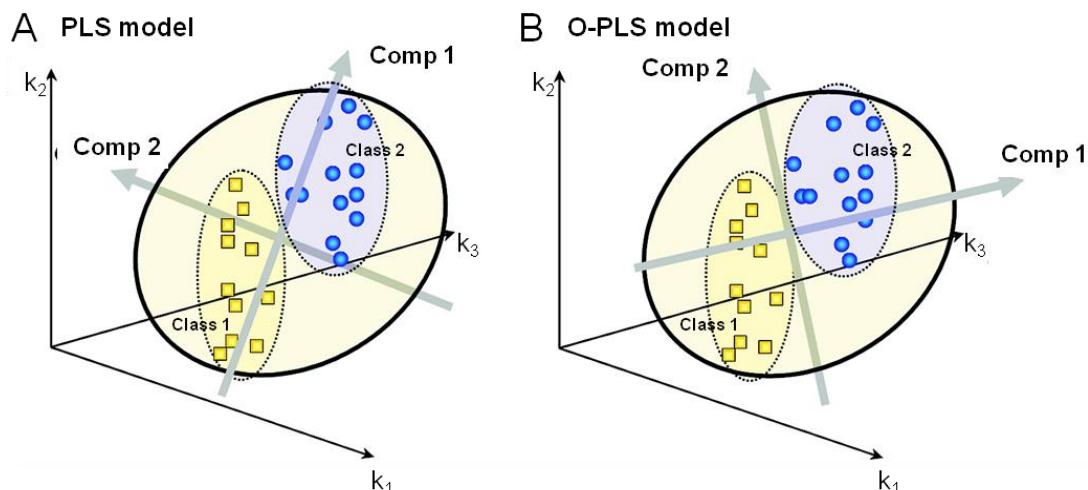


Figure 6: Geometrical illustration of the differences between the PLS-DA and O-PLS-DA models (modified from¹²⁸)

(A) PLS components are not able to separate between-class variations from within-class variations. The resulting PLS component loadings mix both types of variation. (B) O-PLS components are able to separate these two different variations. Component 1 is the predictive component and displays between-class variation of the samples and the corresponding loadings can be used to identify variables important for the class separation. Component 2 is the orthogonal component and models the within-group variation.

For NMR data, an O-PLS-DA coefficients plot, calculated according to the method described by Cloarec *et al.*¹⁶⁰, highlights the variables involved in the discrimination of the classes. The plots have the same shape as that of NMR spectra, the line shape corresponds to the mean-centered model representing the covariance of the variables. Additionally, each data variable is plotted with a color code which relates to the significance of class discrimination as calculated from the correlation matrix. Peaks colored in dark red show that the variation of these variables is highly correlated to the class separation, color codes in blue indicate a lower correlation or even no correlation in the discrimination of classes.

In this PhD thesis, O-PLS-DA models have been generated with one predictive component and one orthogonal component. Model statistical significance is based on the value of R^2X and Q^2Y .

3 RESULTS

3.1 Metabolic Characterization of the IL-10^{-/-} Mouse Model

3.1.1 Gradual Development of Body Weight and Inflammation Status in c-IL-10^{-/-} Mice

Histopathological scoring of colonic sections showed inflammation-related changes in all c-IL-10^{-/-} mice at the age of 8, 16, and 24 weeks, when compared to WT (Figure 7 A). The scores increased with age and were related to an elevated inflammatory cell infiltration into mucosa and submucosa. The architectural distortion of the epithelium was limited to hyperproliferation and irregular crypts. However, the changes were in a mild range with maximal scores of 3.20 ± 1.17 at 24 weeks in c-IL-10^{-/-} mice on a linear scale of 0-12 (Figure 7 B). Monitoring of animal body weight revealed a significantly reduced body weight in c-IL-10^{-/-} mice compared to WT controls only at 24 weeks (Figure 7 C). In addition, concentrations of serum amyloid A (SAA) were measured in the blood of WT and c-IL-10^{-/-} mice (Figure 7 D). Expression of SAA showed an upward trend in c-IL-10^{-/-} mice compared to WT animals at the age of 8, 16, and 24 weeks. The changes were more marked at 16 and 24 weeks, yet not significant. No age-dependent changes were observed in WT mice.

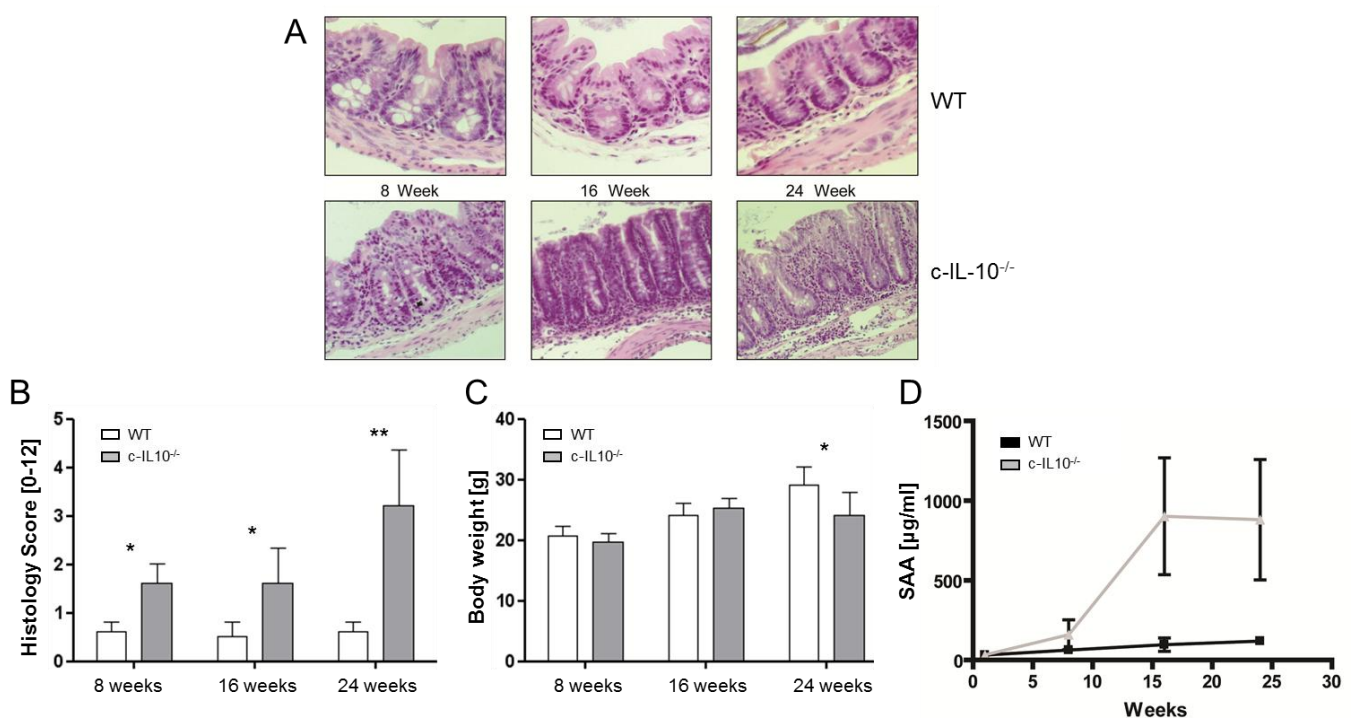


Figure 7: Histopathological changes, body weight development, and inflammatory marker changes during colitis in c-IL-10^{-/-} mice

Histopathological results (A) and scores [score: 0-12] (B) of the colon from WT and c-IL-10^{-/-} mice. Animal body weight development of WT and c-IL-10^{-/-} mice (C). Blood plasma concentrations of serum amyloid A (SAA) in WT and c-IL-10^{-/-} mice (D).

All scores are presented as mean values \pm SD from 5 animals per group. Significant differences were assessed by Mann-Whitney U test and marked as follows: * $p < 0.05$, ** $p < 0.01$.

3.1.2 Analysis of ^1H NMR Spectroscopic Profiles of Blood Plasma

Examples of typical ^1H CPMG and diffusion-edited NMR spectra of plasma samples obtained from WT and c-IL-10^{-/-} mice are shown in Figure 8. ^1H CPMG NMR data provide a clear profile of low molecular weight components through reduction of spectral contribution of broad signals from large molecules. In addition, ^1H diffusion-edited NMR spectra provide a complementary profile of the protein and lipid resonances, the signals of low molecular weight metabolites being severely attenuated. Overall, the ^1H NMR plasma profile exhibited a broad set of resonances arising from lipoproteins and lipids together with many sharper peaks arising from low molecular weight molecules, such as glucose, ketone bodies (3-D-hydroxybutyrate and acetoacetate), amino acids (alanine, glutamine, tyrosine, and valine) and other organic acids, such as acetate, lactate, succinate, pyruvate, and citrate (Table 3-1).

Visual inspection of the plasma ^1H NMR spectra revealed differences in the overall composition between WT and c-IL-10^{-/-} mice, as illustrated in Figure 8. For instance, c-IL-10^{-/-} mice showed a marked reduction in the global levels of lipoproteins and lipids, lower levels of choline, phosphocholine and glycerophosphocholine (GPC). These changes were associated with an increase in lactate, alanine, and glutamine. However, a more formal comparison of the metabolic profiles was carried out using MVDA to establish a global overview of the gradual development of colitis.

3.1.3 Time-Dependent Metabolic Changes in Blood Plasma Associated with Colitis

MVDA using first PCA was performed on the acquired spectra to provide an overview of metabolic features differentiating the plasma profiles of WT and IL-10^{-/-} mice by modeling the main sources of variation in the metabolic profiles. Generally, PCA scores plots can be used to display the relationships between the different plasma samples where each point in the scores plot corresponds to one full biochemical plasma profile. PCA was initially performed on the ^1H CPMG NMR metabolic profiles obtained from mice aged 1, 8, 16, and 24 weeks (data not shown). The distribution of the biochemical profiles along the first two PCs revealed a statistically significant separation of the samples obtained from 1 week old animals. This effect was directly related to the smaller volume of collected blood plasma and consequently to a dilution factor. Therefore, samples obtained from young mice were analyzed separately to avoid introducing any bias during chemometric analysis.

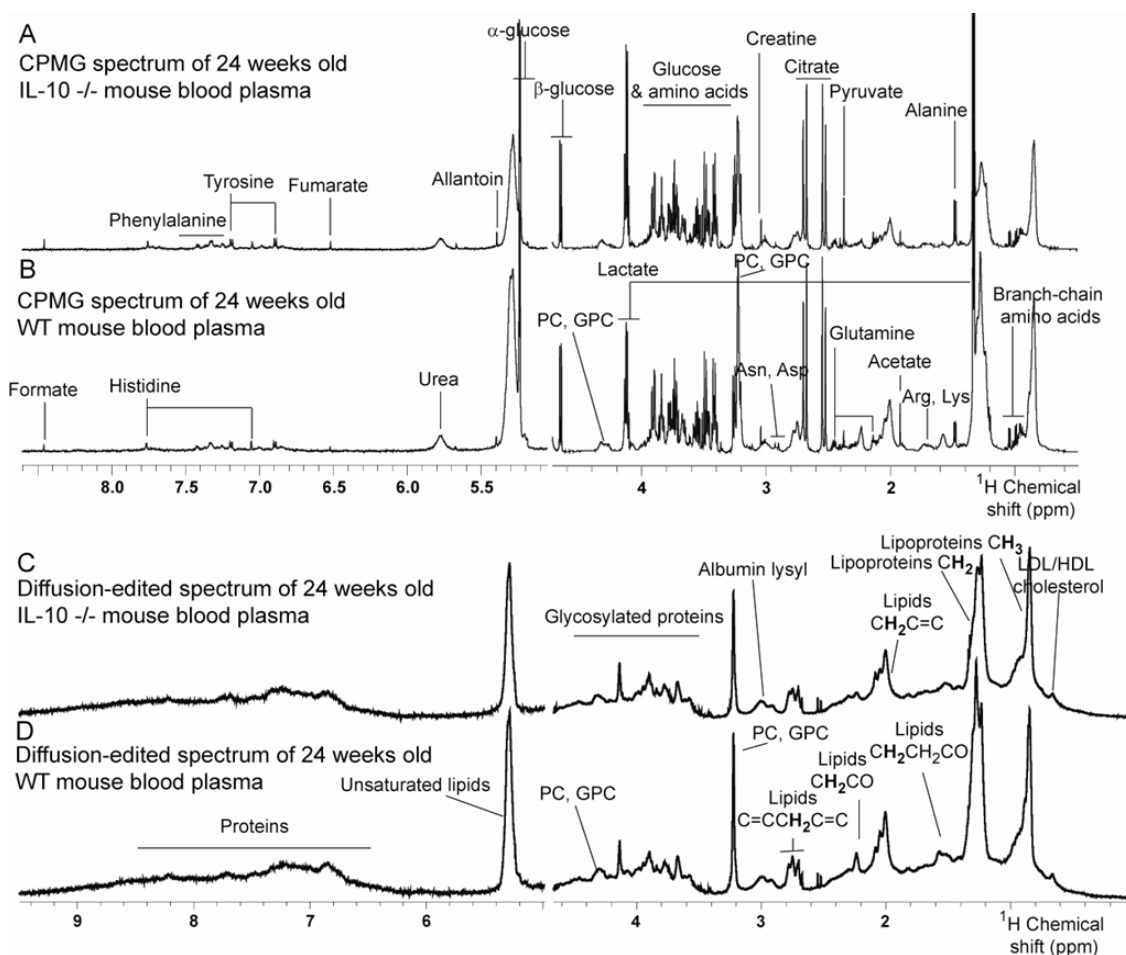


Figure 8: ¹H NMR-based metabolic profiling of blood plasma

Representative 600 MHz ¹H CPMG (A, B) and diffusion-edited (C, D) NMR spectra of blood plasma from c-IL-10^{-/-} (A, C) and WT mice (B, D) at 24 weeks. The spectra of the aromatic region (δ 5.2-8.5) were magnified compared to the aliphatic region (δ 0.7-4.5).

Abbreviations: GPC: glycerophosphocholine; HDL: high density lipoproteins; LDL: low density lipoproteins; PC: phosphocholine; VLDL: very low density lipoproteins.

PCA of ¹H CPMG NMR spectra of blood samples collected at 8, 16, and 24 weeks was generated using 4 PCs explaining 20, 9.5, 8, and 7 % of the total variance, respectively. The PCA scores plot revealed a co-mapping of samples according to their genetic background (WT and c-IL-10^{-/-}) along PC2 and PC3 (Figure 9 A), whilst PC1 described high inter-individual variability. Analysis of the sample distribution displayed that metabolic differences became more significant over time, the greatest variance being observed at the age of 24 weeks. PCA was also applied to ¹H diffusion-edited NMR metabolic profiles using a total of 4 PCs, which explained 43, 24, 12, and 7 % of the total variance. Intriguingly, metabolic variations modeled along PC1 and PC2 revealed high inter-individual variations in c-IL-10^{-/-} animals (data not shown), whilst PC3 and PC4 highlighted a clear time-dependent separation of WT and c-IL-10^{-/-} animals (Figure 9 B).

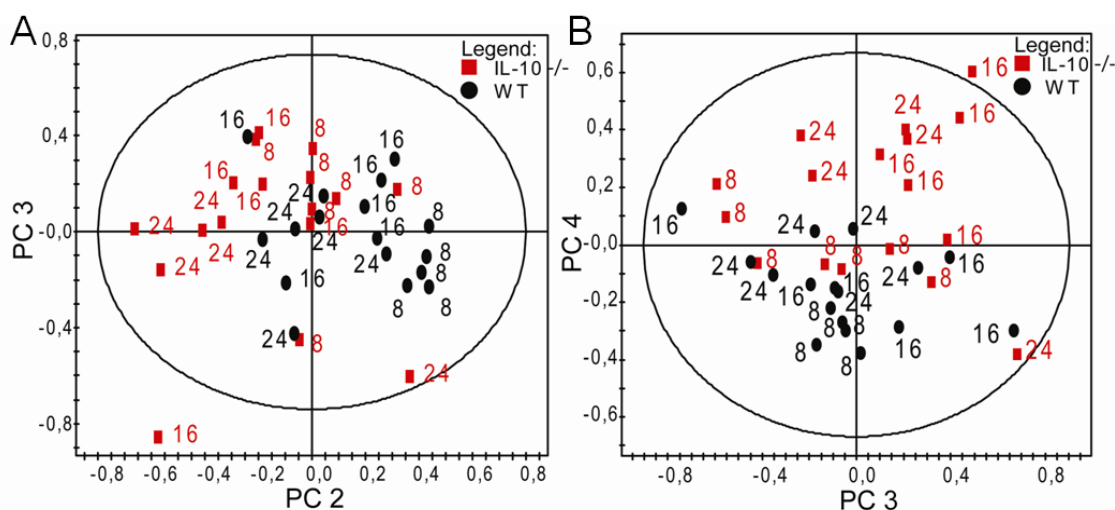


Figure 9: Blood plasma metabolic changes associated with colitis development by ^1H NMR spectroscopy PCA scores plot derived from ^1H CPMG (A) and diffusion-edited (B) NMR spectra of plasma indicating discrimination between WT (black) and c-IL-10 $^{-/-}$ (red) mice.

An O-PLS-DA method was further applied to maximize the separation of groups by a pairwise comparison of ^1H CPMG and diffusion-edited NMR spectra of blood plasma obtained from WT and c-IL-10 $^{-/-}$ animals. O-PLS-DA models were generated with 1 predictive and 1 orthogonal component to discriminate between the two mice groups/genotypes (Table 3-1). The R^2X value shows how much of the variation in the dataset X is explained by the model. The Q^2Y value represents the predictability of the models and relates to its statistical validity. Here, the metabolic profiles could be clearly clustered at the different ages as observed through the high and positive value of the model predictability parameter Q^2Y . Analysis of the corresponding coefficient plots allowed the identification of the NMR spectral regions that were responsible for the separation of plasma samples from WT and c-IL-10 $^{-/-}$ mice according to the method developed by Cloarec *et al.*¹⁶¹ (Figure 10). NMR spectral regions which are oriented in positive directions in the O-PLS-DA coefficients (Figure 10 A; e.g. lactate and pyruvate) refer to increased metabolic concentrations in the profiles projected in the positive plan of the scores plot (Figure 10 A; 16 weeks old c-IL-10 $^{-/-}$ mice). The signals are then positively correlated with the observations having positive scores in one of the PCs. Therefore, the metabolic profiles of these animals tend to have statistically higher levels of these variables when compared to other animals. To generate semi-quantitative data and following to calculate statistical significance of the observed differences, representative peak signals of these metabolites were integrated and are reported in Table 3-1.

At the age of 1 week, the plasma of c-IL-10 $^{-/-}$ mice was characterized by higher levels of citrate, glutamine, fumarate and lower levels of glucose and dimethylglycine (DMG) when compared to WT animals. These changes were associated with variations in the lipoprotein composition characterized by increased levels of polyunsaturated lipids (PUFAs), high and low

density lipoprotein (HDL and LDL), and decreased very low density lipoprotein (VLDL) concentrations when compared to WT mice. At the age of 8 weeks, the plasma of c-IL-10^{-/-} mice showed increased levels of alanine, arginine, glutamine, lactate, pyruvate, succinate, fumarate, creatine, DMG, choline in phospholipids (PL), GPC, and glycoproteins when compared to WT animals. In addition, c-IL-10^{-/-} mice had compositional changes in unsaturated fatty acids (UFAs), higher levels of certain PUFAs and decreased levels of VLDL when compared to WT mice. The plasma of 16 weeks old c-IL-10^{-/-} animals showed higher levels of isoleucine, citrate, pyruvate, lactate, phenylalanine, choline in PLs, glycoproteins, and lower levels of glutamine, leucine, tyrosine, methionine, creatine, DMG, trimethylamine (TMA), and glucose when compared to 16 weeks-old WT mice. These changes were associated with compositional variations of PUFAs, increase of HDL, LDL and certain UFAs, and decreased levels of VLDL when compared to WT animals. At the age of 24 weeks, the plasma of c-IL-10^{-/-} mice had increased levels of alanine, arginine, isoleucine, phenylalanine, and a decrease of TMA when compared to WT mice. This differential metabolite pattern was associated with an upward trend in HDL, LDL, higher levels of certain PUFAs, and lowered concentrations of VLDL when compared to WT animals.

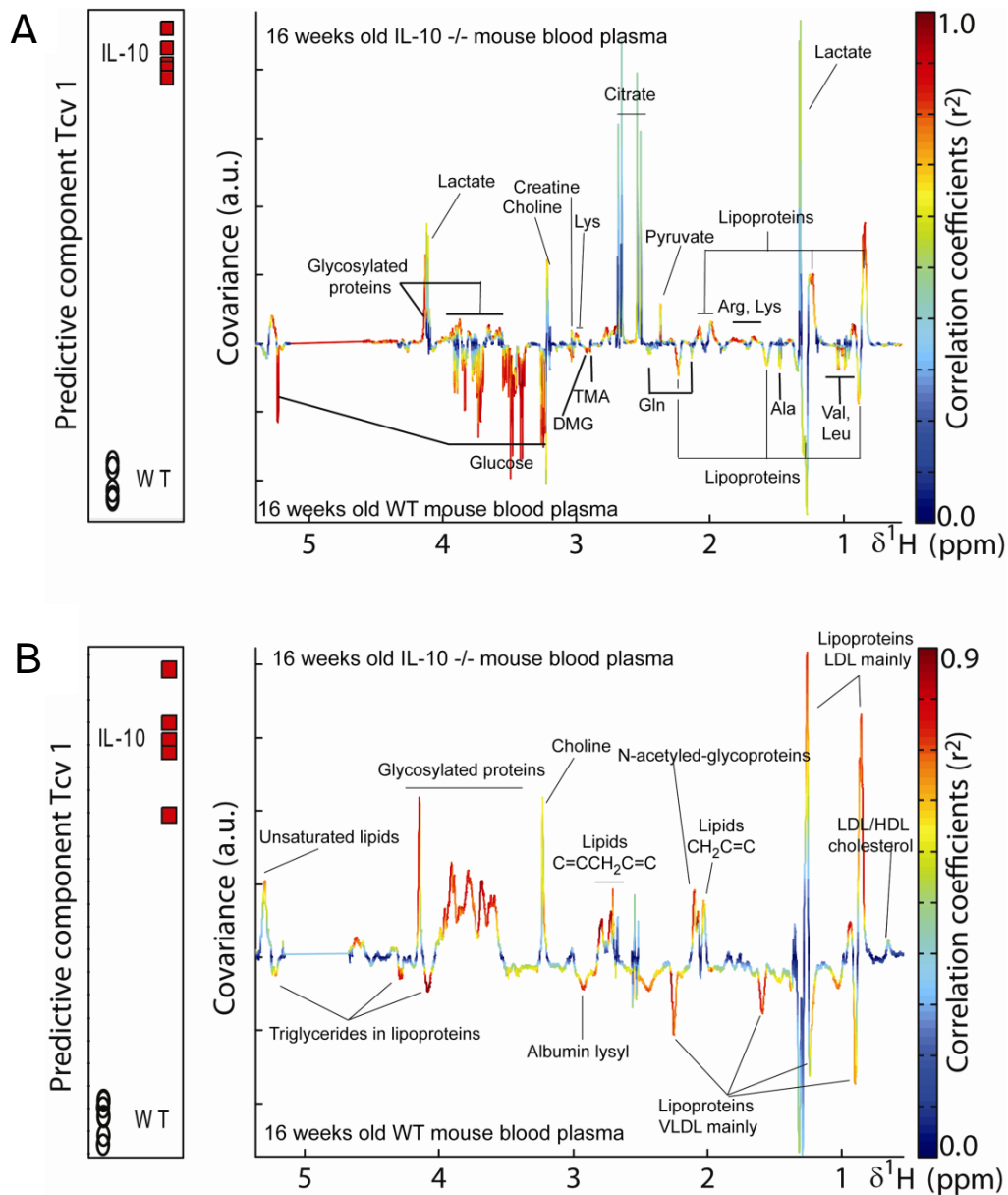


Figure 10: Chemometric analysis of plasma metabolic profiles

O-PLS-DA scores and coefficient plots derived from ^1H CPMG (A) and diffusion-edited (B) NMR spectra of blood plasma illustrating the discrimination between WT (black, $n=5$) and $c\text{-IL-10}^{-/-}$ (red, $n=5$) mice at the age of 16 weeks. The color code corresponds to the correlation coefficients of the variables.

Key: Ala: alanine; Arg: arginine; DMG: dimethylglycine; Glu: glutamine; HDL: high density lipoproteins; LDL: low density lipoproteins; Leu: leucine; Lys: lysine; TMA: trimethylamine; Val: valine; VLDL: very low density lipoproteins.

Table 3-1: Blood plasma metabolite differences between WT and c-IL-10^{-/-} mice at the age of 1, 8, 16, and 24 weeks detected by ¹H NMR spectroscopy.

		1 week		8 weeks		16 weeks		24 weeks	
O-PLS-DA parameters		CPMG		Q ² Y = 74% R ² X = 46%		Q ² Y = 76% R ² X = 36%		Q ² Y = 59% R ² X = 45%	
		Diffusion-edited		Q ² Y = 75% R ² X = 60%		Q ² Y = 58% R ² X = 47%		Q ² Y = 75% R ² X = 74%	
Metabolite peak integral (a.u.)	Chemical shift (δ)	WT Mean ± SD	c-IL-10 ^{-/-} Mean ± SD	WT Mean ± SD	c-IL-10 ^{-/-} Mean ± SD	WT Mean ± SD	c-IL-10 ^{-/-} Mean ± SD	WT Mean ± SD	c-IL-10 ^{-/-} Mean ± SD
Alanine	1.48	0.59±0.06	0.54±0.11	0.54±0.05	0.73±0.1**	0.61±0.09	0.59±0.07	0.55±0.04	0.70±0.12*
Arginine	1.68	1.00±0.19	0.97±0.25	0.86±0.08	1.11±0.17*	1.06±0.13	1.12±0.14	1.01±0.12	1.15±0.07^a
Choline in PL [§]	3.20-3.23	2.32±0.18	2.38±0.19	2.22±0.08	2.37±0.10*	2.29±0.13	2.44±0.12^a	2.31±0.12	2.41±0.17
Citrate	2.55	10.78±2.26	17.87±8.02*	4.46±1.06	4.52±0.88	3.44±1.10	4.37±0.69^a	4.18±1.18	4.56±1.16
Creatine	3.03	0.46±0.09	0.42±0.11	0.23±0.02	0.29±0.04*	0.28±0.04	0.23±0.01^a	0.26±0.03	0.27±0.05
Dimethylglycine	2.93	0.14±0.03	0.09±0.03^a	0.11±0.01	0.14±0.02*	0.15±0.03	0.09±0.01*	0.14±0.03	0.11±0.02
Fumarate	6.51	0.009±0.007	0.001±0.001*	0.007±0.001	0.01±0.003*	0.007±0.003	0.006±0.001	0.006±0.002	0.009±0.005
Glucose	4.64	0.67±0.05	0.47±0.14*	1.06±0.14	1.06±0.10	1.21±0.10	0.94±0.03*	1.09±0.11	0.98±0.11
Glutamine	2.45	0.42±0.06	0.53±0.05*	0.31±0.04	0.40±0.06*	0.41±0.10	0.32±0.02^a	0.38±0.05	0.41±0.11
GPC	4.35	0.57±0.05	0.52±0.15	0.44±0.10	0.58±0.11*	0.57±0.14	0.54±0.07	0.57±0.12	0.52±0.09
Glycoproteins [§]	4.16	6.87±0.59	6.85±0.62	8.54±0.16	9.11±0.23*	9.0±0.39	10.99±1.50*	9.43±0.42	10.15±0.84
Isoleucine	0.92	0.54±0.06	0.45±0.12	0.51±0.05	0.54±0.04	0.55±0.03	0.64±0.05*	0.54±0.05	0.62±0.04^a
Lactate	4.11	1.54±0.09	1.38±0.23	2.23±0.37	3.30±0.67*	2.80±0.41	3.33±0.44^a	2.74±0.36	3.31±0.82
Leucine	1.01	0.21±0.04	0.21±0.06	0.19±0.03	0.17±0.02	0.20±0.02	0.15±0.02*	0.18±0.02	0.16±0.01
Lipoproteins (HDL/LDL) [§]	0.81-0.88	43.23±3.21	52.34±3.94*	44.4±2.45	47.68±2.2	43.99±2.4	51.37±3.59*	46.39±1.71	49.03±3.52
Lipoproteins [§]	0.88	46.46±5.24	40.35±0.87^a	35.25±1.38	31.96±1.17*	33.46±2.2	32.01±0.61	32.96±1.10	32.84±3.93
Lipoproteins [§]	1.18-1.25	57.17±3.23	63.68±6.43^a	56.75±3.73	60.94±2.83	54.8±4.64	64.67±4.77*	58.89±3.37	60.95±4.51
Lipoproteins [§]	1.25-1.27	43.45±7.15	38.50±2.58	43.69±4.67	34.31±3.03*	36.89±8.20	34.31±2.12	36.74±4.60	33.73±13.90
Lipoproteins [§]	1.27-1.33	126.44±33.19	77.99±12.06*	69.55±3.91	55.41±4.76*	63.13±10.81	52.59±3.76	59.51±3.77	53.74±16.57
Lipoproteins (VLDL) [§]	1.56	22.47±1.89	18.70±2.33*	20.36±0.28	18.55±0.78*	19.59±1.08	17.32±0.63*	18.88±0.55	18.02±1.79
Lysine	1.72	0.30±0.05	0.27±0.08	0.31±0.03	0.39±0.03*	0.38±0.05	0.38±0.03	0.37±0.04	0.40±0.05
Methionine	2.14	0.17±0.03	0.15±0.03	0.14±0.02	0.18±0.02*	0.18±0.02	0.15±0.01*	0.15±0.02	0.17±0.03
Phenylalanine	7.44	0.09±0.03	0.06±0.03	0.08±0.01	0.1±0.01*	0.1±0.01	0.12±0.01*	0.09±0.01	0.11±0.02^a
PUFA [§]	2.73	3.07±0.19	3.57±0.26*	3.58±0.15	3.95±0.31*	3.72±0.22	4.41±0.14*	3.82±0.26	3.92±0.18
PUFA [§]	2.76	6.66±0.65	7.88±0.38*	7.41±0.32	7.51±0.22	7.58±0.43	8.09±0.29^a	7.57±0.32	8.41±1.02
PUFA [§]	2.78	9.50±0.48	8.75±1.65	6.79±0.14	7.07±0.26	7.02±0.56	7.78±0.42*	6.96±0.24	8.00±0.90^a
Pyruvate	2.41	0.26±0.07	0.22±0.01	0.19±0.01	0.28±0.05*	0.21±0.03	0.27±0.02*	0.23±0.02	0.29±0.07
Succinate	2.37	0.12±0.02	0.12±0.02	0.05±0.01	0.06±0.01*	0.05±0.02	0.05±0.01	0.06±0.01	0.06±0.01
Trimethylamine	2.87	0.05±0.02	0.02±0.02	0.08±0.01	0.07±0.02	0.09±0.02	0.06±0.02^a	0.09±0.01	0.07±0.01*
Tyrosine	6.90	0.05±0.05	0.05±0.01	0.06±0.01	0.07±0.01*	0.07±0.01	0.06±0.01*	0.06±0.01	0.06±0.01
UFA [§]	5.25	6.53±0.87	7.42±0.63	7.31±0.54	8.74±0.92*	7.69±0.46	9.31±0.73*	8.09±0.53	8.30±0.43

NB: All scores are presented as peak integral mean values ± standard deviation (SD) of area normalized NMR data from 5 animals per group. The values of the c-IL-10^{-/-} animals were compared at each time point with the WT mice. Significant differences were assessed by Mann-Whitney U test and marked as follows: ^ap<0.1, *p<0.05, **p<0.01.

§ designates spectral signals integrated from ¹H diffusion-edited NMR spectra, all other signals being integrated from ¹H CPMG NMR spectra.

Key: GPC: glycerophosphocholine; HDL: high density lipoprotein; LDL: low density lipoprotein; PL: phospholipids; PUFA: polyunsaturated fatty acids; UFA: unsaturated fatty acids; VLDL: very low density lipoprotein.

3.1.4 Gradual Development of Body Weight and Inflammation Status in s-IL-10^{-/-} Mice

Histopathological examination of the colon of WT and s-IL-10^{-/-} animals housed under specific pathogen free (SPF) conditions revealed no differences in the tissue morphology between the two genotypes as the scores of the s-IL-10^{-/-} mice were similar to the WT values at 24 weeks of age (Figure 11 A). Monitoring of body weight revealed significant differences at the time point of 4 weeks between WT and s-IL-10^{-/-} mice (Figure 11 B). Older s-IL-10^{-/-} animals (time points 8 – 24 weeks) did not significantly vary in their body weight from WT animals.

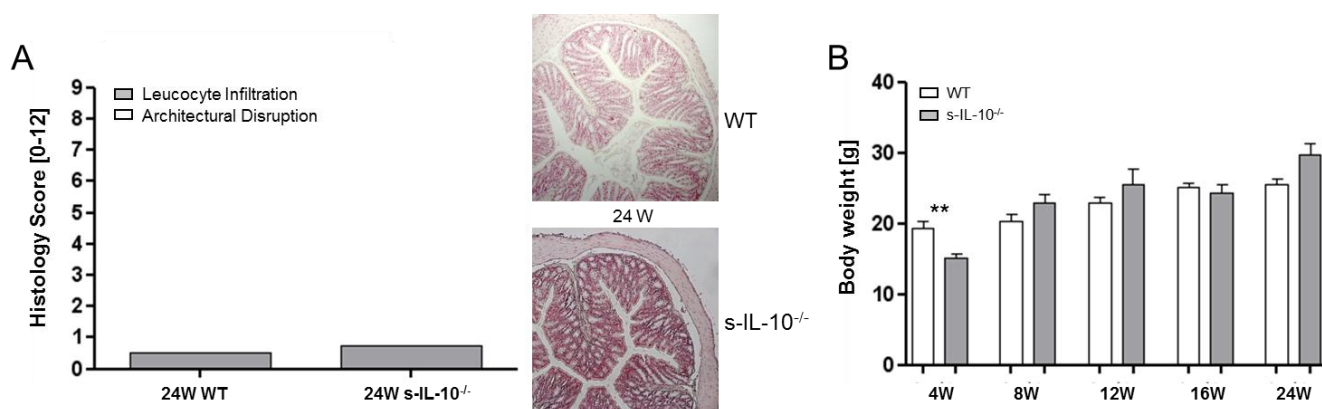


Figure 11: Histopathological score and body weight changes

Histopathological results and scores [score: 0-12] (A) of the proximal colon of WT and s-IL-10^{-/-} mice at 24 weeks of age. Animal body weight development of WT and s-IL-10^{-/-} mice (B).

All scores are presented as mean values \pm SD from 6 animals per group. Significant differences were assessed by Mann-Whitney U test and marked as follows: ** $p < 0.01$.

3.1.5 Time-Dependent Metabolic Changes in Blood Plasma Associated with Colitis Susceptibility

Examples of typical ¹H CPMG and diffusion-edited NMR spectra of plasma samples obtained from WT and IL-10^{-/-} mice are shown in Figure 8. PCA was initially applied to the acquired ¹H CPMG and diffusion-edited NMR plasma data to provide a general overview of metabolic pattern and to get a first insight into differences according to the genotype and age of WT and s-IL-10^{-/-} mice. For the ¹H CPMG NMR spectra, a PCA scores plot was generated using 5 PCs, explaining 10, 6, 6, 5, and 4 % of the total variance. For the ¹H diffusion-edited NMR spectra, a PCA scores plot with 4 PCs, explaining 25, 10, 6, and 3 % of the total variance, was generated. Inspection of the scores plots did not reveal any clustering according to time and genetic background in both, ¹H CPMG and diffusion-edited NMR spectral data sets (Figure 12).

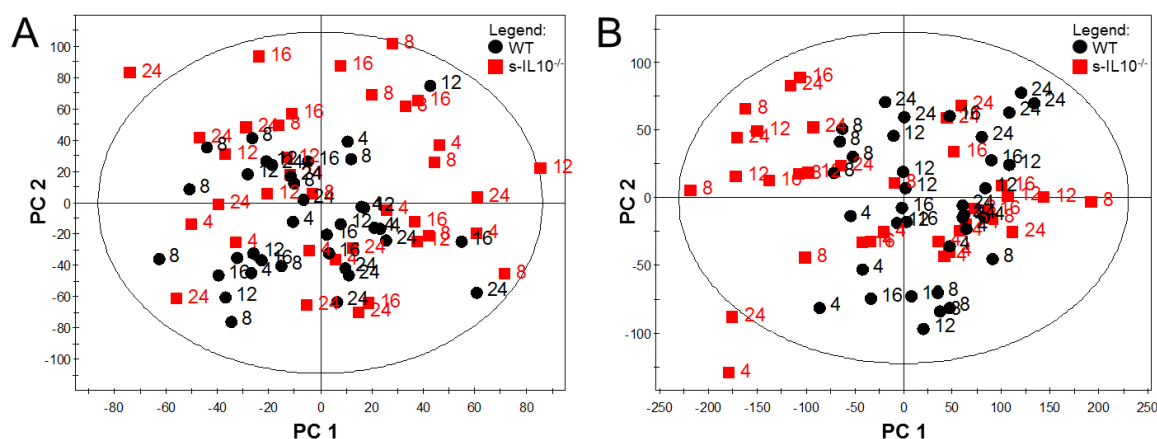


Figure 12: Blood plasma metabolic changes associated with colitis susceptibility by ^1H NMR spectroscopy PCA scores plot derived from ^1H CPMG (A) and diffusion-edited (B) NMR spectra of plasma indicating discrimination between WT (black) and s-IL-10 $^{-/-}$ (red) mice at the time points 4, 8, 12, 16, and 24 weeks.

Data were further investigated by using O-PLS-DA to maximize the separation of WT and s-IL-10 $^{-/-}$ mice at each single time point in a pairwise manner. O-PLS-DA models were generated using 1 predictive and 1 orthogonal component to discriminate between the two groups of mice. Interestingly, model predictability values (Q^2Y) were the highest for the models generated with samples from early time points (4 and 8 weeks) and decreased over time being the lowest at 24 weeks (Table 3-2). This was detected in both, ^1H CPMG and diffusion-edited NMR spectra. Statistical analyses on peak integrals from influential metabolites were conducted and are numerated in Table 3-2. Overall, only a small number of metabolites were detected to be significantly different between WT and s-IL-10 $^{-/-}$ animals. Here, similar to the Q^2Y value, also a higher number of significantly different metabolites were observable at the earlier time points, the number decreasing at the later time points.

At the age of 1 week, the plasma of s-IL-10 $^{-/-}$ mice was characterized by higher levels of DMG, glycoproteins, and tyrosine and a lower level of alanine when compared to WT animals. In addition, these changes were associated with variations in the lipoprotein composition. At the age of 8 weeks, the plasma of s-IL-10 $^{-/-}$ mice showed increased levels of the branch chain amino acids leucine and isoleucine and lower levels of citrate as well as VLDL when compared to WT animals. Plasma samples from 12 weeks old s-IL-10 $^{-/-}$ animals had decreased levels of citrate and creatine when compared to 12 weeks old WT controls. At the age of 16 weeks only elevated succinate levels were detected in the plasma of s-IL-10 $^{-/-}$ mice when compared to the respective WT controls. At the age of 24 weeks, the plasma of s-IL-10 $^{-/-}$ mice had increased levels of citrate and a decreased level of alanine when compared to WT mice.

Table 3-2: Blood plasma metabolite differences between WT and s-IL-10^{-/-} mice at the age of 4, 8, 12, 16, and 24 weeks detected by ¹H NMR spectroscopy.

		4 weeks		8 weeks		12 weeks		16 weeks		24 weeks	
O-PLS-DA parameters	CPMG	Q ² Y = 65% R ² X = 19% R ² Y = 99%		Q ² Y = 60% R ² X = 28% R ² Y = 96%		Q ² Y = 30% R ² X = 26% R ² Y = 99%		Q ² Y = 37% R ² X = 27% R ² Y = 99%		Q ² Y = 25% R ² X = 21% R ² Y = 97%	
	Diffusion-edited	Q ² Y = 55% R ² X = 30% R ² Y = 98%		Q ² Y = 21% R ² X = 42% R ² Y = 93%		Q ² Y = 28% R ² X = 34% R ² Y = 92%		Q ² Y = 22% R ² X = 34% R ² Y = 94%		Q ² Y = 8% R ² X = 37% R ² Y = 95%	
Metabolite peak integral (a.u.)	Chemical shift (δ)	WT Mean ± SD	s-IL-10 ^{-/-} Mean ± SD	WT Mean ± SD	s-IL-10 ^{-/-} Mean ± SD	WT Mean ± SD	s-IL-10 ^{-/-} Mean ± SD	WT Mean ± SD	s-IL-10 ^{-/-} Mean ± SD	WT Mean ± SD	s-IL-10 ^{-/-} Mean ± SD
Alanine	1.48	0.59±0.06	0.53±0.04*	0.55±0.06	0.56±0.60	0.60±0.04	0.52±0.05 ^a	0.63±0.07	0.59±0.09	0.58±0.04	0.53±0.07**
Choline in PL [§]	3.20-3.23	1.22±0.07	1.26±0.09	1.20±0.07	1.27±0.11	1.24±0.03	1.34±0.13	1.24±0.08	1.32±0.11	1.21±0.05	1.23±0.07
Citrate	2.55	0.24±0.02	0.28±0.05	0.26±0.02	0.21±0.04*	0.22±0.02	0.20±0.02*	0.25±0.03	0.24±0.03	0.24±0.02	0.28±0.04*
Creatine	3.03	0.21±0.03	0.20±0.03	0.18±0.02	0.17±0.03	0.19±0.01	0.16±0.03*	0.23±0.05	0.19±0.04	0.20±0.05	0.16±0.03 ^a
Dimethylglycine	2.93	0.07±0.01	0.08±0.01*	0.06±0.01	0.05±0.01	0.06±0.01	0.05±0.01	0.06±0.01	0.06±0.01	0.06±0.01	0.05±0.01 ^a
Fumarate	6.51	0.02±0.03	0.04±0.03	0.02±0.03	0.03±0.04	0.04±0.02	0.03±0.05	0.06±0.05	0.03±0.02	0.05±0.02	0.07±0.03
Glucose	4.64	1.62±0.13	1.76±0.16 ^a	1.63±0.15	1.57±0.16	1.50±0.18	1.72±0.15 ^a	1.62±0.13	1.60±0.17	1.61±0.08	1.76±0.22 ^a
Glutamine	2.45	0.19±0.01	0.18±0.02	0.19±0.02	0.17±0.02 ^a	0.19±0.01	0.17±0.03 ^a	0.19±0.10	0.17±0.02	0.19±0.02	0.17±0.02 ^a
GPC	4.35	0.89±0.15	0.78±0.09	0.87±0.14	0.89±0.06	0.88±0.15	0.89±0.13	0.88±0.14	0.75±0.14	0.90±0.11	0.85±0.16
Glycoproteins [§]	4.16	0.55±0.01	0.57±0.01**	0.56±0.01	0.56±0.02	0.57±0.02	0.55±0.02 ^a	0.56±0.03	0.55±0.03	0.57±0.04	0.56±0.02
Isoleucine	0.92	0.67±0.06	0.63±0.11	0.63±0.07	0.76±0.07**	0.71±0.03	0.70±0.06	0.67±0.09	0.64±0.05	0.79±0.09	0.71±0.09 ^a
Lactate	4.11	0.97±0.18	0.89±0.13	0.92±0.09	0.99±0.07	1.17±0.23	0.96±0.21	1.07±0.21	1.00±0.25	1.00±0.16	0.88±0.14 ^a
Leucine	1.01	0.20±0.02	0.19±0.03	0.17±0.02	0.22±0.03***	0.20±0.02	0.20±0.02	0.20±0.03	0.20±0.02	0.21±0.03	0.20±0.03
Lipoproteins (HDL/LDL) [§]	0.81-0.88	2.62±0.12	2.66±0.05	2.62±0.18	2.78±0.20 ^a	2.69±0.09	2.88±0.17	2.75±0.10	2.77±0.19	2.75±0.06	2.80±0.12
Lipoproteins [§]	0.88	0.71±0.03	0.66±0.02*	0.74±0.04	0.71±0.05	0.68±0.03	0.68±0.06	0.66±0.06	0.72±0.11	0.68±0.05	0.73±0.08
Lipoproteins [§]	1.18-1.25	2.71±0.13	2.67±0.10	2.68±0.22	2.80±0.23	2.74±0.15	2.96±0.25	2.80±0.16	2.81±0.20	2.75±0.07	2.78±0.13
Lipoproteins [§]	1.25-1.27	2.42±0.16	2.32±0.14	2.46±0.24	2.41±0.37	2.24±0.14	2.30±0.37	2.13±0.13	2.47±0.48	2.12±0.27	2.41±0.38
Lipoproteins [§]	1.27-1.33	2.16±0.09	2.03±0.09*	2.30±0.17	2.21±0.21	2.11±0.09	2.10±0.26	2.02±0.17	2.26±0.39	2.04±0.22	2.24±0.29 ^a
Lipoproteins (VLDL) [§]	1.56	0.91±0.02	0.90±0.01	0.94±0.02	0.91±0.01**	0.90±0.02	0.90±0.02	0.89±0.04	0.93±0.07	0.90±0.04	0.91±0.03
Lysine	1.72	0.19±0.03	0.19±0.02	0.21±0.03	0.20±0.03	0.21±0.02	0.20±0.02	0.20±0.02	0.19±0.03	0.21±0.03	0.19±0.03
Methionine	2.14	0.17±0.03	0.15±0.03	0.14±0.02	0.18±0.02	0.20±0.02	0.20±0.02	0.18±0.02	0.15±0.01	0.15±0.02	0.17±0.03
PUFA [§]	2.73	0.45±0.02	0.46±0.01	0.45±0.03	0.47±0.02	0.47±0.02	0.49±0.03	0.48±0.03	0.47±0.03	0.48±0.02	0.48±0.02
PUFA [§]	2.76	0.45±0.03	0.47±0.01	0.49±0.03	0.51±0.03	0.49±0.02	0.51±0.02 ^a	0.50±0.02	0.50±0.01	0.49±0.03	0.51±0.03
PUFA [§]	2.78	0.44±0.03	0.48±0.01*	0.45±0.02	0.47±0.03	0.44±0.01	0.46±0.03	0.45±0.02	0.47±0.01	0.45±0.03	0.46±0.02
Pyruvate	2.41	0.12±0.07	0.09±0.03	0.15±0.05	0.12±0.05	0.16±0.06	0.12±0.04	0.20±0.11	0.12±0.06	0.12±0.06	0.14±0.08
Succinate	2.37	0.11±0.02	0.13±0.02	0.13±0.01	0.13±0.01	0.14±0.03	0.15±0.03	0.13±0.02	0.17±0.01**	0.15±0.02	0.14±0.02
Tyrosine	6.90	0.05±0.01	0.07±0.01*	0.05±0.01	0.05±0.01	0.05±0.01	0.05±0.01	0.07±0.01	0.06±0.02	0.05±0.01	0.06±0.02

NB: All scores are presented as peak integral mean values ± SD of area normalized NMR data from 6 animals per group. The values from s-IL-10^{-/-} animals were compared at each time point with the WT mice. Significant differences were assessed by Mann-Whitney U test and marked as follows: ^ap<0.1, *p<0.05, **p<0.01, ***p<0.001.

§ designates spectral signals integrated from ¹H diffusion-edited NMR spectra, all other signals being integrated from ¹H CPMG NMR spectra.

Key: GPC: glycerophosphocholine, HDL: high density lipoprotein; LDL: low density lipoprotein; PL: phospholipid; PUFA: polyunsaturated fatty acids; UFA: unsaturated fatty acids; VLDL: very low density lipoprotein.

In a second experiment, a targeted LC-MS method was applied on plasma samples using the AbsoluteIDQ™ kit from Biocrates Life Sciences, Austria (<http://biocrates.com>) to improve the sensitivity and detection range of the metabolite analysis. With this technique it was possible to get qualitative concentration data on 163 metabolites, including amino acids, sugars, acyl-carnitines, sphingolipids, and GPL. To provide an initial overview and to detect possible outlier in the data set, PCA was applied, using 5 PCs explaining 28, 8, 7, 5, and 4 % of the total variance (data not shown). Inspection of the corresponding scores plot revealed no clear separation of the samples according to the different genetic background (WT and s-IL-10^{-/-}) and time. O-PLS-DA was further performed on the extracted concentrations of the measured metabolites to maximize the separation of WT and s-IL-10^{-/-} mice at each time point in a pairwise manner. Models were generated with 1 predictive and 1 orthogonal component to discriminate between the two groups of mice. As observed for the ¹H NMR data, models generated at 4 and 8 weeks time points displayed high and positive predictability (Q²Y) values, whereas the highest Q²Y was calculated for the 4 weeks samples (Table 3-3). This score decreased in older mice (12 and 16 weeks) and rose again at 24 weeks. Similarly, also the number of significantly regulated metabolites was highest for the comparison of the youngest WT and s-IL-10^{-/-} mice at 4 weeks and declined in the other models (Table 3-3). By using S-plots,¹⁶² variables correlating with the group separation of WT and s-IL-10^{-/-} animals in an O-PLS-DA model including all time points (4, 8, 12, 16, and 24 weeks) were identified. It visualizes the variable importance (VIP) score, representing the impact of a single metabolite to the group discrimination of the model. The ten most influential metabolites based on the computed VIP score for the discrimination between WT and s-IL-10^{-/-} mice are listed in Table 3-3 (all significantly regulated metabolites are listed in Appendix Table 6-1). The table comprises amino acids, acyl-carnitines as well as GPCs. Here, the concentration of the amino acids glycine, glutamine, and serine were reduced, whereas the concentration of the amino acid tyrosine was increased at all time points in the plasma of s-IL-10^{-/-} mice when compared to WT controls. Moreover, the plasma concentration of specific acyl-carnitines (C2, C3, C5-OH, C16:2) were decreased at the measured time points in s-IL-10^{-/-} animals compared to their respective WT controls. The concentration of the phosphatidylcholine PCaa C42:0 was elevated at all time points in the plasma of sIL10^{-/-} compared to WT mice. On the contrary, the PCae C44:6 did not show a distinct profile, being lower in 4-16 weeks old and higher in 24 weeks old s-IL-10^{-/-} animals compared to WT animals.

Table 3-3: Time-dependent metabolic differences in plasma of s-IL-10^{-/-} compared to WT mice detected by UPLC-ESI-MS/MS using the AbsoluteIDQ™ kit (Biocrates Life Sciences, Austria))

Metabolites [μM]		4 weeks		8 weeks		12 weeks		16 weeks		24 weeks	
		WT Mean ± SD	s-IL-10 ^{-/-} Mean ± SD	WT Mean ± SD	s-IL-10 ^{-/-} Mean ± SD	WT Mean ± SD	s-IL-10 ^{-/-} Mean ± SD	WT Mean ± SD	s-IL-10 ^{-/-} Mean ± SD	WT Mean ± SD	s-IL-10 ^{-/-} Mean ± SD
Plasma	O-PLS-DA parameters	Q ² Y = 75% R ² X = 35% R ² Y = 96%		Q ² Y = 54% R ² X = 46% R ² Y = 94%		Q ² Y = 7% R ² X = 40% R ² Y = 91%		Q ² Y = 6% R ² X = 41% R ² Y = 92%		Q ² Y = 31% R ² X = 38% R ² Y = 95%	
	Significantly regulated	41		14		6		8		13	
	Glycine	235.14 ± 31.05	210.43 ± 42.56*	218.75 ± 23.87	187.38 ± 38.95***	196.27 ± 28.18	160.67 ± 10.86	225.00 ± 56.34	152.00 ± 23.12	195.00 ± 48.53	167.60 ± 29.06
	Glutamine	1134.00 ± 113.60	975.29 ± 126.78*	1058.25 ± 123.21	856.75 ± 114.06***	926.71 ± 156.13	835.50 ± 75.87	896.83 ± 87.58	850.83 ± 206.01	839.25 ± 54.99	800.20 ± 71.88
	Serine	100.24 ± 20.46	90.66 ± 10.16	99.30 ± 8.35	91.71 ± 12.43	96.57 ± 19.33	88.92 ± 13.05	103.57 ± 6.65	94.20 ± 17.58	100.60 ± 14.44	80.80 ± 14.80**
	C2	28.34 ± 7.76	15.92 ± 3.31**	35.51 ± 4.08	30.58 ± 9.79	32.81 ± 5.34	34.70 ± 9.92	32.38 ± 8.64	31.48 ± 4.55	38.38 ± 5.46	28.90 ± 8.99**
	C3	0.658 ± 0.415	0.264 ± 0.085**	0.802 ± 0.147	0.564 ± 0.112**	0.745 ± 0.147	0.613 ± 0.315	0.800 ± 0.438	0.589 ± 0.235	0.545 ± 0.130	0.580 ± 0.279
	C5-OH	0.133 ± 0.035	0.082 ± 0.036*	0.138 ± 0.044	0.095 ± 0.028*	0.118 ± 0.032	0.116 ± 0.050	0.118 ± 0.045	0.118 ± 0.026	0.115 ± 0.038	0.101 ± 0.028
	PCaa C42:0	0.168 ± 0.066	0.183 ± 0.067	0.228 ± 0.064	0.299 ± 0.113	0.221 ± 0.052	0.367 ± 0.072**	0.250 ± 0.049	0.273 ± 0.065	0.226 ± 0.061	0.247 ± 0.071
	PCae C44:6	0.169 ± 0.045	0.144 ± 0.041*	0.194 ± 0.059	0.218 ± 0.075	0.173 ± 0.038	0.223 ± 0.039 ^a	0.166 ± 0.056	0.203 ± 0.059	0.184 ± 0.084	0.259 ± 0.074*
	Tyrosine	53.96 ± 14.15	72.10 ± 9.27*	63.54 ± 14.50	58.63 ± 13.29	62.43 ± 16.65	64.30 ± 11.73	71.43 ± 14.06	75.98 ± 29.03	49.55 ± 10.41	67.46 ± 17.76*
C16:2	0.019 ± 0.006	0.014 ± 0.006 ^a	0.021 ± 0.004	0.018 ± 0.005**	0.016 ± 0.006	0.021 ± 0.009	0.022 ± 0.006	0.013 ± 0.006	0.019 ± 0.009	0.014 ± 0.006 ^a	

NB: All metabolite concentrations are presented as mean values ± SD from 6 animals per group. The values from s-IL-10^{-/-} animals were compared at each time point with the WT mice. Significant differences were assessed by Mann-Whitney U test and marked as follows: ^ap<0.1, *p<0.05, **p<0.01, ***p<0.001.

Key: C: acyl-carnitine; PCaa: phosphatidylcholine; PCae: phosphatidylcholine with an ether bond.

3.1.6 Time-Dependent Metabolic Changes in the Colon Associated with Colitis Susceptibility

To monitor metabolic changes occurring at the expected site of inflammation, ^1H NMR spectra were acquired of the two fractions of colonic tissue extract from WT and $s\text{-IL-10}^{-/-}$ mice at 24 weeks. Examples of typical ^1H NMR spectra of hydrophilic and lipophilic fractions of the colon extract are shown in Figure 13 and Figure 14, respectively. The ^1H NMR spectra of the hydrophilic fractions were dominated by signals from amino acids (alanine, glutamine, leucine, isoleucine, methionine, phenylalanine, proline, tyrosine and valine), organic acids (3-D-hydroxybutyrate, acetate, lactate and succinate), nucleotide derivatives (cytidine, hypoxanthine, inosine, nicotinamide, uridine and uracil), osmolytes (betaine, carnitine, choline and creatine), D-glucose, and glycerol. The ^1H NMR spectral data of the lipophilic fractions contained a number of assignable resonances of the fatty acyl chain of saturated, unsaturated, polyunsaturated as well as ω -3 fatty acids (FA). Also different classes of membrane lipids like tri-, di-, and monoacylglycerides (TAGs, DAGs, MAGs) and GPL were identified together with free cholesterol and cholesterol esters. In addition, signals from other metabolites including plasmalogen, sphingomyelin (SM), choline, and retinol conjugated FAs were also observed in the spectra.

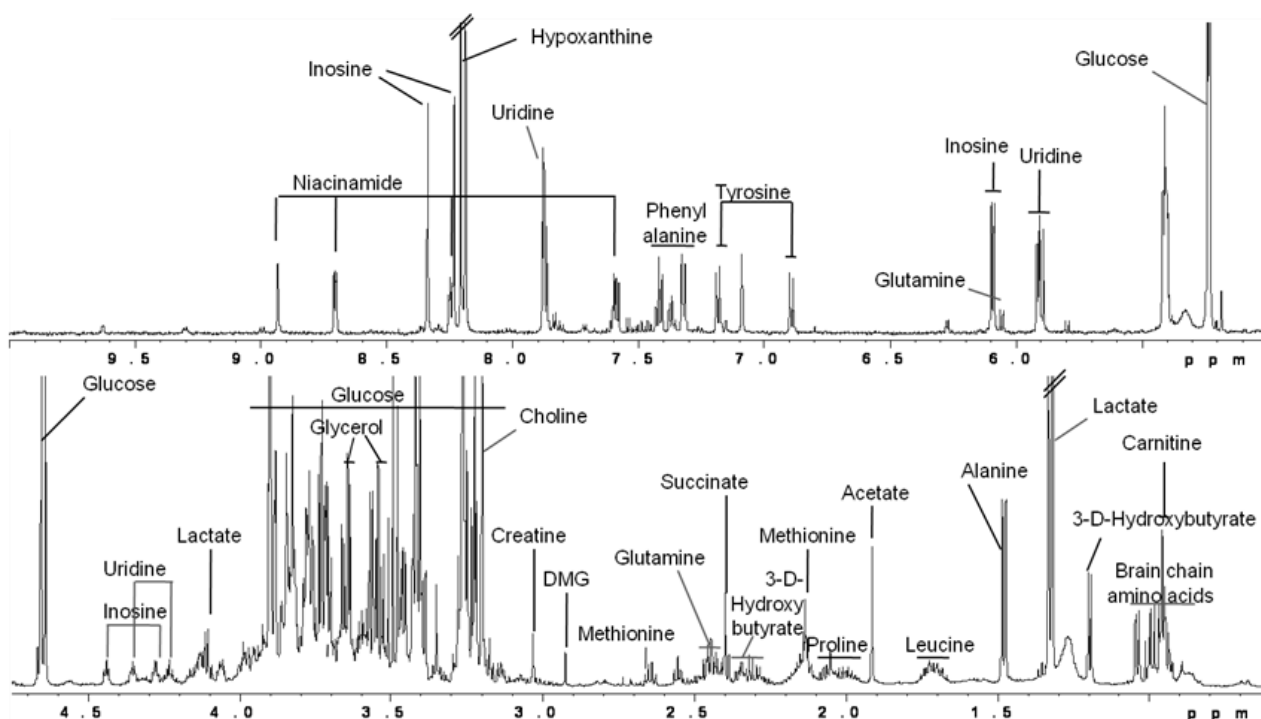


Figure 13: NMR-based metabolic profiling of the hydrophilic extract of colon tissue

Representative 600 MHz ^1H NMR spectra of the hydrophilic fraction of the colon extract of WT mice at 24 weeks of age. The aromatic region (δ 5.2-8.5) was magnified compared to the aliphatic region (δ 0.7-4.5).

Abbreviations: DMG: dimethylglycine.

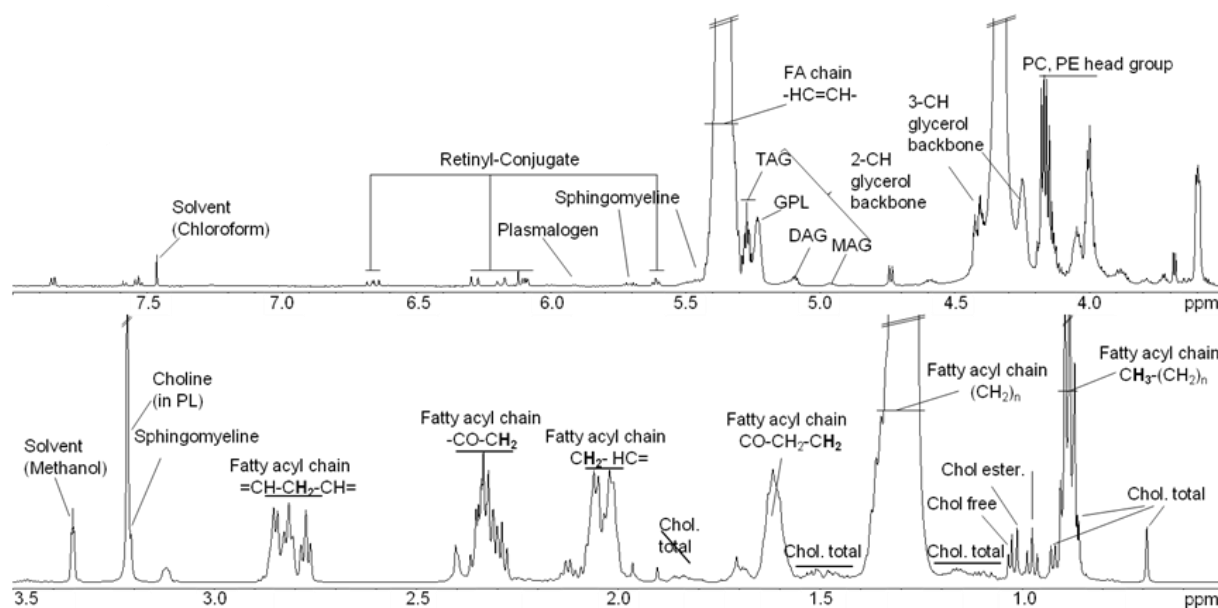


Figure 14: NMR-based metabolic profiling of the lipophilic extract of colon tissue

Representative 600 MHz ^1H NMR spectra of the lipophilic fraction of the colon extract of WT mice at 24 weeks of age. The region δ 3.5-8.0 of the spectrum was magnified.

Key: Chol: cholesterol, DAG: diacylglycerol, FA: fatty acid, GPL: glycerophospholipids, MAG: monoacylglycerol, PC: phosphocholine, PE: phosphoethanolamine, PL: phospholipids, TAG: triacylglycerol.

In order to generate a general overview of the metabolic variations in the colonic tissue extracts, PCA was performed on ^1H NMR spectra of the hydrophilic and lipophilic fractions from WT and $\text{IL}10^{-/-}$ colonic tissue samples at 24 weeks. PCA scores plot were generated using 4 PCs, explaining 12, 10, 9, and 7% of the total variance, for the ^1H NMR spectra of the hydrophilic fraction and 3 PCs, explaining 48, 6, and 6% of the total variance, for the ^1H NMR spectra of the lipophilic fraction. Inspection of the corresponding scores plots revealed no distinct separation between WT and $\text{s-IL-10}^{-/-}$ mice (Figure 15).

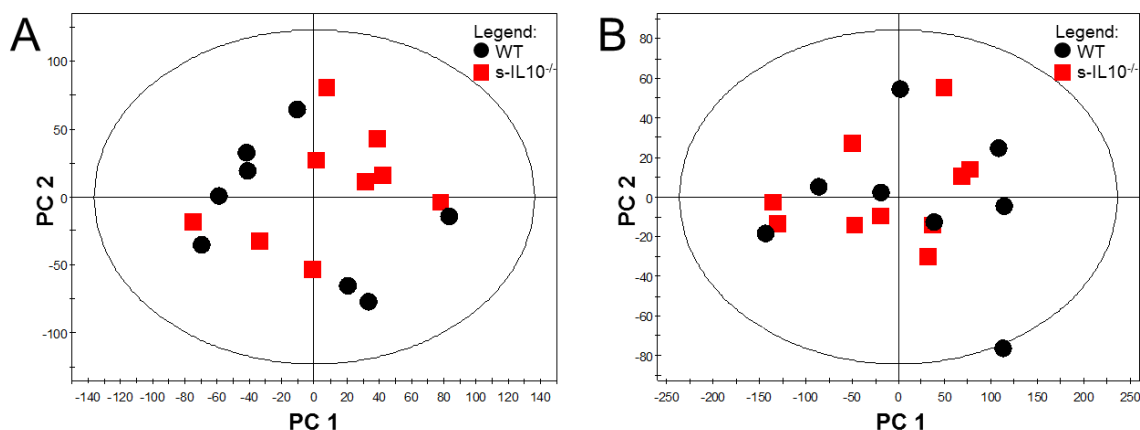


Figure 15: Colonic metabolic changes associated with colitis susceptibility by ^1H NMR spectroscopy

PCA scores plot derived from ^1H NMR spectra of the hydrophilic (A) and lipophilic (B) fraction of colonic tissue extracts indicating discrimination between WT (black) and $\text{s-IL-10}^{-/-}$ (red) mice.

In addition, the performance of O-PLS-DA on both data sets created models with negative Q^2Y values, therefore indicating a lack of statistical predictability and robustness (Table 3-4). PCA as well as O-PLS-DA therefore clearly indicated that there is no significant difference detectable by 1H NMR spectroscopy between WT and s-IL-10^{-/-} mice in the colonic tissue. These results were consistent with the absence of any significant difference in the histopathological scores of WT and s-IL-10^{-/-} animals at 24 weeks (Figure 11).

Table 3-4: O-PLS-DA model summary for the discrimination of 24 weeks old WT and s-IL-10^{-/-} mice by 1H NMR spectra of proximal colon extracts

WT vs. s-IL-10 ^{-/-}		24 weeks
O-PLS-DA parameters	Water fraction	$Q^2Y \leq 0\%$ $R^2X = 17\%$ $R^2Y = 99\%$
	Organic fraction	$Q^2Y \leq 0\%$ $R^2X = 52\%$ $R^2Y = 87\%$

NB: O-PLS-DA models were generated with 1 predictive component and 1 orthogonal component to discriminate between 2 groups of mice.

A second experiment was realized on the colonic tissue using a targeted LC-MS method implemented in the AbsoluteIDQ™ kit (Biocrates Life Science, Austria) to increase the sensitivity and detection range of the metabolites. Here, samples originating from the whole kinetic (4, 8, 12, 16, and 24 weeks) were used. Application of PCA analysis (4 PCs; explaining 26, 8, 7, and 4 % of total variance) was not able to demonstrate differences between WT and s-IL-10^{-/-} animals at the investigated time points. Moreover, no age-related differences were detectable in the metabolite profiles. Furthermore, O-PLS-DA was performed on the extracted concentrations of the measured metabolites to maximize the separation of WT and s-IL-10^{-/-} mice at each time point in a pairwise manner. Models were generated with 1 predictive and 1 orthogonal component to discriminate between the two groups of mice. The Q^2Y values of the generated models were low with maximal separation at 24 weeks (Table 3-5). Comparable to the plasma analysis, the highest number of significantly regulated metabolites was detected in the comparison of the youngest WT and s-IL-10^{-/-} mice at 4 weeks and the number of discriminating metabolites declined with age. The ten most influential metabolites based on the computed VIP score, correlating with the group separation of WT and s-IL-10^{-/-} animals in an O-PLS-DA model including all time points (4, 8, 12, 16, and 24 weeks), are listed in Table 3-5 (all significantly regulated metabolites are listed in Appendix Table 6-2). The table comprises the amino acids methionine and tryptophan, several acetyl-carnitines, sugars as well as GPCs. The concentration of the amino acids methionine and tryptophan and hexoses were higher in the colon of s-IL-10^{-/-} animals compared to their respective WT animals. The concentrations of the listed acyl-carnitines (C2, C3-DC, C4, C5, C16:2-OH) did

not show clear pattern of regulation. For example, the acyl-carnitine C5 a significantly reduced concentration was found in s-IL-10^{-/-} mice compared to WT mice at the age of 4 weeks, but increased levels were detected already at 8 weeks. Similarly, no clear pattern of regulation was observed for the GPCs PCaa C42:6 and PCae C40:0.

Table 3-5: Time-dependent metabolic differences in the colon of s-IL-10^{-/-} compared to WT mice detected by UPLC-ESI-MS/MS using the AbsoluteIDQ™ kit (Biocrates Life Sciences, Austria)

Metabolites [μM]		4 weeks		8 weeks		12 weeks		16 weeks		24 weeks	
		WT Mean ± SD	s-IL-10 ^{-/-} Mean ± SD	WT Mean ± SD	s-IL-10 ^{-/-} Mean ± SD	WT Mean ± SD	s-IL-10 ^{-/-} Mean ± SD	WT Mean ± SD	s-IL-10 ^{-/-} Mean ± SD	WT Mean ± SD	s-IL-10 ^{-/-} Mean ± SD
Colon distal	O-PLS-DA parameters	Q ² Y = 2% R ² X = 46% R ² Y = 88%		Q ² Y = 9% R ² X = 31% R ² Y = 88%		Q ² Y = 11% R ² X = 43% R ² Y = 94%		Q ² Y ≤ 0 R ² X = 30% R ² Y = 94%		Q ² Y = 20% R ² X = 36% R ² Y = 82%	
	Significantly regulated	18		7		5		2		5	
	C5	0.011 ± 0.003	0.007 ± 0.002*	0.010 ± 0.006	0.017 ± 0.005*	0.012 ± 0.004	0.013 ± 0.007	0.013 ± 0.004	0.017 ± 0.005	0.009 ± 0.005	0.017 ± 0.005***
	C3-DC (C4-OH)	0.012 ± 0.004	0.010 ± 0.002	0.009 ± 0.004	0.016 ± 0.004**	0.012 ± 0.004	0.017 ± 0.007	0.015 ± 0.008	0.018 ± 0.007	0.011 ± 0.006	0.015 ± 0.007
	C2	0.385 ± 0.053	0.490 ± 0.087*	0.444 ± 0.088	0.503 ± 0.071	0.479 ± 0.115	0.482 ± 0.118	0.474 ± 0.098	0.600 ± 0.136	0.526 ± 0.107	0.502 ± 0.061
	Tryptophan	0.537 ± 0.038	0.572 ± 0.097	0.570 ± 0.169	0.616 ± 0.154	0.607 ± 0.073	0.791 ± 0.192*	0.627 ± 0.080	0.662 ± 0.118	0.585 ± 0.129	0.639 ± 0.084
	PCaa C42:6	0.008 ± 0.001	0.011 ± 0.004**	0.009 ± 0.003	0.010 ± 0.004	0.008 ± 0.003	0.008 ± 0.003	0.009 ± 0.003	0.012 ± 0.002^a	0.009 ± 0.002	0.009 ± 0.004
	C16:2-OH	0.00031 ± 0.00014	0.00032 ± 0.00010	0.00034 ± 0.0001	0.00011 ± 0.0001*	0.00029 ± 0.00017	0.00030 ± 0.00007	0.00040 ± 0.00029	0.00026 ± 0.00012	0.00022 ± 0.00009	0.00021 ± 0.00013
	C4	0.090 ± 0.022	0.062 ± 0.041	0.039 ± 0.035	0.107 ± 0.034**	0.066 ± 0.042	0.067 ± 0.051	0.081 ± 0.049	0.113 ± 0.043	0.070 ± 0.061	0.102 ± 0.058
	H1	4.934 ± 1.142	5.468 ± 1.037	4.620 ± 0.762	5.882 ± 1.516*	4.088 ± 1.058	6.588 ± 3.087^a	5.179 ± 2.161	6.078 ± 1.632^a	6.516 ± 1.607	5.663 ± 2.143
	Methionine	0.903 ± 0.107	0.865 ± 0.306	1.054 ± 0.475	1.303 ± 0.437	1.114 ± 0.240	1.425 ± 0.194*	1.421 ± 0.196	1.270 ± 0.269	0.889 ± 0.272	1.177 ± 0.325^a
PCae C40:0	0.152 ± 0.010	0.178 ± 0.025*	0.153 ± 0.016	0.165 ± 0.013^a	0.160 ± 0.037	0.151 ± 0.027	0.152 ± 0.022	0.173 ± 0.035	0.157 ± 0.017	0.155 ± 0.023	

NB: All scores are presented as mean values ± SD from 6 animals per group. The values from s-IL-10^{-/-} animals were compared at each time point with the WT mice. Significant differences were assessed by Mann-Whitney U test and marked as follows: ^ap<0.1, *p<0.05, **p<0.01, ***p<0.001.

Key: C: acyl-carnitine; H: basic sugar structure; PCaa: phosphatidylcholine; PCae: phosphatidylcholine with an ether bond.

3.2 Metabolic Characterization of the TNF^{ΔARE/WT} Mouse Model

3.2.1 Gradual Development of Ileal Inflammation and Body Fat Composition in TNF^{ΔARE/WT} mice

Heterozygous TNF^{ΔARE/WT} mice develop two distinct pathologies called chronic inflammatory arthritis and CD-like ileitis.⁷⁸ Histopathological scoring of distal ileum (dl) sections from WT and TNF^{ΔARE/WT} animals aged 1, 4, 8, 12, 16, and 24 weeks revealed significant alterations in the tissue morphology of TNF^{ΔARE/WT} mice from 8 weeks onwards reaching a plateau at 12 weeks (Figure 16 A). The observed scores were associated with structural alterations and leukocyte infiltration into the mucosa, submucosa, and muscularis region. In addition, significant body weight differences were observed between WT and TNF^{ΔARE/WT} mice at the age of 12 weeks, which were maintained until the age of 24 weeks (Figure 16 B). In relation to the decreased body weight gain in TNF^{ΔARE/WT} mice, daily food intake and fecal energy loss were monitored. While food intake was significantly reduced in inflamed compared to non-inflamed mice only at 24 weeks (Figure 16 C), bomb calorimetric analysis highlighted a significant increased energy loss in the feces of TNF^{ΔARE/WT} mice compared to WT mice already from 8 weeks onwards (Figure 16 D). To gain further insights, body composition was assessed by using computerized tomography (CT) in mice aged 12, 16, and 24 weeks (Figure 16 E), since changes in body weight were observed from 12 weeks onwards. From this time point on, WT mice showed an increase in the percentage of their subcutaneous fat mass, whereas the overall visceral fat mass remained constant. TNF^{ΔARE/WT} mice displayed a very different body composition pattern, showing no significant relative increase of fat mass over time, and therefore having a significantly lower fat mass than WT mice at all three measured time points. These findings were in agreement with a reduced fat cell size in the subcutaneous and epididymal fat tissues from 24 weeks old TNF^{ΔARE/WT} animals (Figure 16 F). The mesenteric adipocytes were also of smaller proportions in different segments of the intestine (jejunum, ileum, and colon).

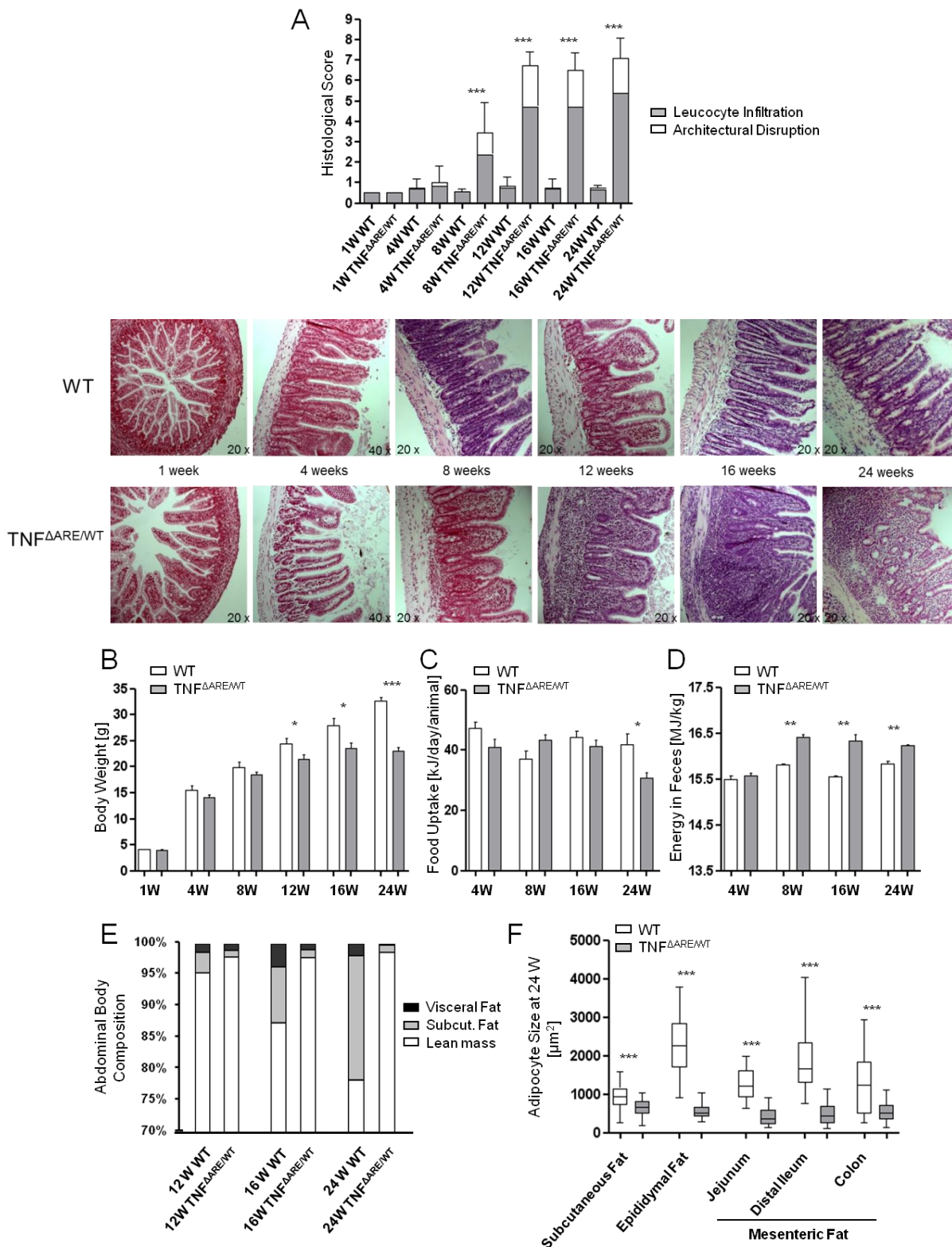


Figure 16: Histopathological scoring, body weight development, nutritional energy utilization, and adipose tissue morphology during CD-like ileitis in TNF Δ ARE/WT mice

Histopathological results and scores [score: 0-12] of the distal ileum in WT and TNF Δ ARE/WT mice (A). Body weight (B), daily food uptake (C), and energy content in feces (D) of WT and TNF Δ ARE/WT mice. Body composition (visceral and subcutaneous fat mass and lean mass) assessed by computerized tomography (CT) at 12, 16, and 24 weeks of age in WT and TNF Δ ARE/WT mice (E). Adipocyte size of the subcutaneous, epididymal, and mesenteric fat tissue of WT and TNF Δ ARE/WT mice (F).

All scores are presented as mean values \pm standard error mean (SEM) from 8 animals per group (exception: CT-measurements, n=4). Significant differences were assessed by Mann-Whitney U test and marked as follows: *p<0.05, **p<0.01, ***p<0.001.

3.2.2 Time-Dependent Metabolic Changes in Blood Plasma Associated with Ileitis

Examples of typical ^1H CPMG and diffusion-edited NMR spectra of plasma samples are shown in Figure 8. PCA was applied to the acquired ^1H CPMG and diffusion-edited NMR data to obtain a general overview of the metabolic pattern associated with the genotype and age of WT and $\text{TNF}^{\Delta\text{ARE}/\text{WT}}$ mice. PCA scores plot were generated using 4 PCs, explaining 10, 7, 6, and 5 % of the total variance, for the ^1H CPMG NMR spectra and 4 PCs, explaining 26, 8, 6, and 3 % of the total variance, for ^1H diffusion-edited NMR spectra. Inspection of the corresponding scores plots revealed no distinct separation according to the genotype of WT and $\text{TNF}^{\Delta\text{ARE}/\text{WT}}$ mice and with the time point of collection in the ^1H CPMG NMR spectral data (Figure 17 A). Intriguingly, PCA scores plot generated on ^1H diffusion-edited NMR data revealed a clear clustering of the $\text{TNF}^{\Delta\text{ARE}/\text{WT}}$ mice along PC1 and PC2 (Figure 17 B). Deeper analysis of the distribution of the samples showed that metabolic differences became more significant over time, modeled by PC3, the greatest variance being observed at the age of 24 weeks (data not shown).

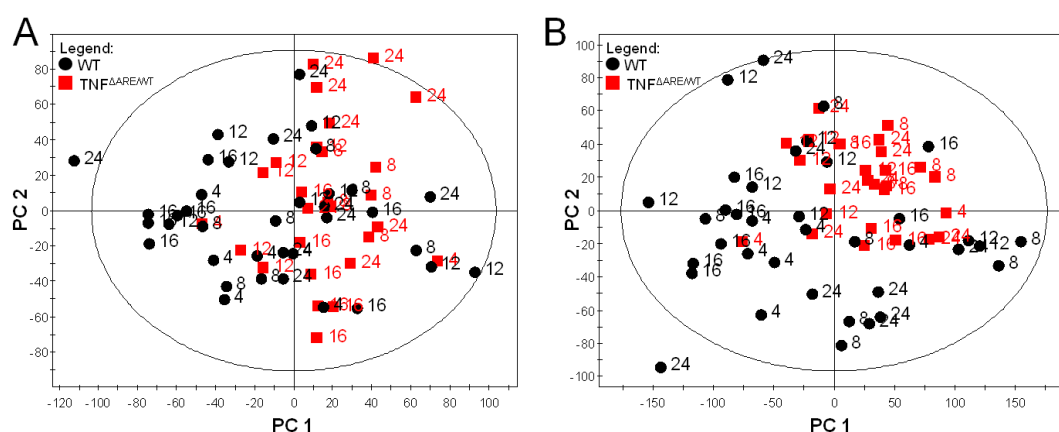


Figure 17: Blood plasma metabolic changes associated with CD-like ileitis development by ^1H NMR spectroscopy

PCA scores plot derived from ^1H CPMG (A) and diffusion-edited (B) NMR spectra of plasma indicating discrimination between WT (black) and $\text{TNF}^{\Delta\text{ARE}/\text{WT}}$ (red) mice.

In addition, maximal separation of the ^1H CPMG and diffusion-edited NMR spectra obtained from WT and $\text{TNF}^{\Delta\text{ARE}/\text{WT}}$ mice at the different time points was achieved using O-PLS-DA modeling. All O-PLS-DA models were generated using 1 predictive and 1 orthogonal component to discriminate between two groups of mice and the individual model characteristics are reported in Table 3-6. Samples of WT and $\text{TNF}^{\Delta\text{ARE}/\text{WT}}$ animals were distributed in clearly differentiated groups, as reflected by the high value of Q^2Y for each model of the ^1H CPMG as well as diffusion-edited NMR data. Peak integrals for all influential are reported in Table 3-6.

Table 3-6: Blood plasma metabolite differences between WT and TNF^{ΔARE/WT} at the age of 4, 8, 12, 16, and 24 weeks detected by ¹H NMR spectroscopy.

		4 weeks		8 weeks		12 weeks		16 weeks		24 weeks	
O-PLS-DA parameters	CPMG	Q ² Y = 45% R ² X = 37% R ² Y = 99%		Q ² Y = 60% R ² X = 25% R ² Y = 99%		Q ² Y = 22% R ² X = 28% R ² Y = 96%		Q ² Y = 49% R ² X = 27% R ² Y = 99%		Q ² Y = 27% R ² X = 18% R ² Y = 99%	
	Diffusion-edited	Q ² Y = 28% R ² X = 44% R ² Y = 99%		Q ² Y = 52% R ² X = 35% R ² Y = 97%		Q ² Y = 36% R ² X = 17% R ² Y = 99%		Q ² Y = 22% R ² X = 34% R ² Y = 94%		Q ² Y = 37% R ² X = 42% R ² Y = 97%	
Metabolite peak integral (a.u.)	Chemical shift (δ)	WT Mean ± SD	TNF ^{ΔARE/WT} Mean ± SD	WT Mean ± SD	TNF ^{ΔARE/WT} Mean ± SD	WT Mean ± SD	TNF ^{ΔARE/WT} Mean ± SD	WT Mean ± SD	TNF ^{ΔARE/WT} Mean ± SD	WT Mean ± SD	TNF ^{ΔARE/WT} Mean ± SD
Alanine	1.48	0.62±0.16	0.70±0.12	0.74±0.26	0.66±0.12	0.53±0.05	0.69±0.21*	0.45±0.01	0.50±0.10	0.65±0.11	0.63±0.12
Choline in PL [§]	3.20-3.23	2.12±0.20	1.86±0.08*	1.90±0.23	2.14±0.15*	2.22±0.25	1.93±0.11^a	2.07±0.16	1.88±0.21^a	2.17±0.18	2.14±0.14
Citrate	2.55	0.24±0.06	0.25±0.05	0.24±0.02	0.18±0.04	0.20±0.05	0.23±0.08**	0.20±0.04	0.24±0.05	0.20±0.06	0.20±0.04
Creatine	3.03	0.15±0.02	0.17±0.03	0.14±0.04	0.15±0.02	0.12±0.01	0.15±0.03*	0.10±0.02	0.11±0.01^a	0.13±0.03	0.15±0.03
Dimethylglycine	2.93	0.04±0.004	0.05±0.01^a	0.05±0.01	0.05±0.008	0.04±0.01	0.04±0.007	0.03±0.008	0.04±0.007	0.04±0.01	0.04±0.005
Glucose	4.64	2.16±0.20	2.28±0.34	2.22±0.18	2.27±0.19	2.32±0.42	2.24±0.18	2.03±0.26	2.54±0.26**	2.16±0.32	2.23±0.24
Glutamine	2.45	0.33±0.05	0.46±0.10**	0.42±0.13	0.37±0.04	0.32±0.07	0.42±0.13^a	0.28±0.09	0.32±0.07	0.38±0.08	0.45±0.12
GPC	4.35	0.42±0.12	0.33±0.11	0.32±0.16	0.38±0.17	0.34±0.08	0.40±0.15	0.31±0.09	0.34±0.18	0.31±0.09	0.31±0.08
Glycoproteins [§]	4.16	0.93±0.04	1.01±0.05*	1.04±0.08	1.15±0.03*	1.07±0.07	1.16±0.06	1.06±0.08	1.13±0.11	1.00±0.10	1.13±0.06*
Isoleucine	0.92	0.21±0.01	0.25±0.01**	0.29±0.02	0.29±0.02	0.29±0.03	0.29±0.03	0.26±0.02	0.24±0.03^a	0.32±0.05	0.32±0.05
Lactate	4.11	0.26±0.03	0.26±0.05	0.25±0.03	0.27±0.05	0.20±0.06	0.24±0.05	0.26±0.04	0.25±0.03	0.19±0.06	0.19±0.06
Leucine	1.01	0.39±0.04	0.48±0.05**	0.49±0.09	0.47±0.05	0.45±0.05	0.50±0.07^a	0.46±0.05	0.42±0.06	0.48±0.05	0.53±0.07
Lipoproteins (HDL/LDL) [§]	0.81-0.88	3.90±0.29	3.35±0.25**	3.50±0.40	3.87±0.90^a	4.14±0.37	3.43±0.54*	3.78±0.33	3.55±0.42	4.06±0.36	3.93±0.26
Lipoproteins [§]	0.88	2.08±0.19	1.95±0.22	1.93±0.26	1.65±0.07	1.87±0.30	1.95±0.17	2.19±0.29	1.89±0.11*	2.02±0.36	1.71±0.05*
Lipoproteins [§]	1.18-1.25	5.15±0.46	4.31±0.37**	4.61±0.60	4.94±0.27	5.29±0.60	4.27±0.90*	5.12±0.54	4.58±0.64	5.27±0.49	5.17±0.39
Lipoproteins [§]	1.25-1.27	4.95±0.82	4.02±0.96	4.13±1.16	3.20±0.36	4.17±1.40	3.91±0.75	5.31±1.26	3.73±2.36^a	4.49±1.42	3.44±0.31*
Lipoproteins [§]	1.27-1.33	5.15±0.71	4.53±0.76	4.65±0.94	3.61±0.22*	4.38±1.04	4.38±0.56	5.72±1.07	4.29±0.19*	4.94±1.37	3.91±0.23^a
Lipoproteins (VLDL) [§]	1.56	1.23±0.20	1.11±0.10	1.17±0.11	1.14±0.16	1.23±0.15	1.17±0.15	1.23±0.28	1.15±0.08	1.18±0.12	1.21±0.11
Lysine	1.72	0.38±0.06	0.46±0.09^a	0.45±0.15	0.41±0.08	0.36±0.04	0.45±0.01*	0.34±0.06	0.38±0.06	0.40±0.09	0.48±0.07
Methionine	2.14	0.62±0.21	0.73±0.16	0.50±0.13	0.50±0.17	0.52±0.12	0.63±0.17	0.54±0.08	0.48±0.26^a	0.45±0.12	0.42±0.05
PUFA [§]	2.73	0.70±0.03	0.68±0.03	0.74±0.02	0.78±0.02**	0.78±0.04	0.71±0.07^a	0.75±0.24	0.75±0.05	0.78±0.06	0.80±0.05
PUFA [§]	2.76	0.70±0.03	0.66±0.06	0.69±0.08	0.76±0.02^a	0.81±0.07	0.67±0.09**	0.73±0.06	0.72±0.06	0.75±0.06	0.75±0.03
PUFA [§]	2.78	0.70±0.04	0.70±0.04	0.69±0.07	0.79±0.05*	0.82±0.08	0.73±0.06^a	0.73±0.06	0.71±0.04	0.73±0.08	0.76±0.05
Pyruvate	2.41	0.14±0.10	0.11±0.04	0.26±0.16	0.15±0.22*	0.22±0.22	0.15±0.12	0.36±0.13	0.62±0.23*	0.18±0.13	0.21±0.16
Succinate	2.37	0.13±0.03	0.14±0.06	0.16±0.05	0.16±0.04	0.14±0.04	0.15±0.02	0.12±0.02	0.12±0.03	0.12±0.04	0.10±0.02
Trimethylamine	2.87	0.42±0.23	0.27±0.15	0.40±0.15	0.51±0.22	0.47±0.39	0.60±0.31	0.76±0.27	0.64±0.29	0.50±0.22	0.60±0.36
Tyrosine	6.90	0.06±0.01	0.07±0.03	0.09±0.03	0.06±0.01^a	0.06±0.01	0.08±0.03	0.05±0.02	0.06±0.02	0.07±0.01	0.06±0.01
UFA	5.25	2.56±0.22	2.19±0.35	2.17±0.54	2.25±0.17	2.66±0.45	2.28±0.30^a	2.61±0.45	2.22±0.14^a	2.52±0.28	2.25±0.21^a

NB: All scores are presented as peak integral mean values ± SD of area normalized NMR data from 8 animals per group. The values of the TNF^{ΔARE/WT} animals were compared at each time point with the WT mice. Significant differences were assessed by Mann-Whitney U test and marked as follows: ^ap<0.1, *p<0.05, **p<0.01.

§ designates spectral signals integrated from ¹H diffusion-edited NMR spectra, all other signals being integrated from ¹H CPMG NMR spectra.

Key: GPC: glycerophosphocholine; HDL: high density lipoprotein; LDL: low density lipoprotein; PL: phospholipids; PUFA: polyunsaturated fatty acids; UFA: unsaturated fatty acids; VLDL: very low density lipoprotein.

As it has been indicated by the PCA scores plot, the main differences between WT and TNF^{ΔARE/WT} mice were observed in the metabolites integrated from the diffusion-edited spectra. At the age of 4 weeks, the plasma of TNF^{ΔARE/WT} mice was characterized by higher levels of glutamine, isoleucine, leucine, and glycoproteins when compared to WT controls. These changes were associated with variations in lipoprotein composition characterized by increased levels of HDL and LDL concentrations in TNF^{ΔARE/WT} animals compared to WT mice. At the age of 8 weeks, the plasma of TNF^{ΔARE/WT} mice showed increased levels of choline in PL and glycoproteins when compared to WT animals. In addition, TNF^{ΔARE/WT} mice had higher levels of certain PUFAs and compositional changes of the lipoprotein VLDL when compared to WT mice. The plasma of 12 weeks old TNF^{ΔARE/WT} animals showed higher levels of alanine, citrate, creatine, and lysine and were associated with decreased levels of lipoproteins, mainly LDL and HDL, and compositional changes of PUFAs. The plasma of 16 weeks old TNF^{ΔARE/WT} mice showed higher levels of glucose as well as compositional variations in the lipoprotein profiles compared to WT mice. At the age of 24 weeks, the plasma of TNF^{ΔARE/WT} mice compositional variations in the lipoprotein profiles compared to WT animals.

In addition, a targeted LC-MS method using the AbsoluteIDQ™ kit (Biocrates Life Sciences, Austria) was applied on WT and TNF^{ΔARE/WT} plasma samples to get qualitative concentration data on the 163 available metabolites. To obtain a first overview, PCA was applied on the plasma spectra using 5 PCs, explaining 33, 8, 8, 6, and 4 % of the total variance. Inspection of the corresponding scores plot highlighted a clear separation of the WT samples from the TNF^{ΔARE/WT} samples by PC1 and PC2 (Figure 18). Here, no time-dependent differences in this discrimination were detectable. However, closer examination of the other PCs revealed a different behavior of the samples of WT and TNF^{ΔARE/WT} animals originating from 4 weeks. These spectra seem to differ from all other samples illustrated by PC5.

O-PLS-DA was performed on the extracted concentrations to maximize the separation of WT and TNF^{ΔARE/WT} mice at each time point in a pairwise manner. Models were generated using 1 predictive and 1 orthogonal component to discriminate between the two groups of mice. The ten most influential metabolites based on the computed VIP score from the O-PLS-DA model including all time points (4, 8, 12, 16, 24 weeks) discriminating WT and TNF^{ΔARE/WT} mice are listed in Table 3-7 together with the corresponding statistical significances calculated by Mann-Whitney U test (all significantly regulated metabolites are listed in Appendix Table 6-3). Inspection of the plasma data sets revealed high and positive model parameters (R^2X , R^2Y , and Q^2Y) already at the time point of 4 weeks, which remained constantly high over the other time points (Table 3-7). The highest Q^2Y was calculated for the 12 weeks samples. Similar to this, also the number of significantly regulated metabolites was highest (78) for the comparison of WT and TNF^{ΔARE/WT} mice at 12 weeks (Table 3-7). The table comprises primarily SM and GPCs. Overall decreased plasma concentrations of hydroxylated

SMs (SM(OH) 22:1, 22:2), lysophosphatidylcholines (lysoPCa 17:0, 18:2) and phosphatidylcholines with one ether bond (PCae 16:1, 16:2, 18:1, 18:2, 40:3, 40:4) were detectable in $\text{TNF}^{\Delta\text{ARE}/\text{WT}}$ mice when compared to WT mice.

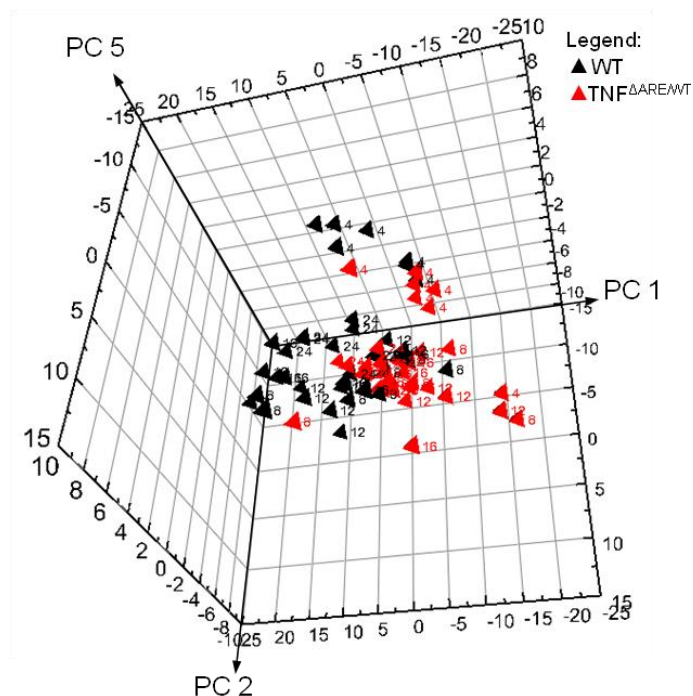


Figure 18: Blood plasma metabolic changes associated with CD-like ileitis development by LC-MS

Three-dimensional PCA scores plot derived from targeted LC-MS spectra of plasma indicating discrimination between WT (black) and $\text{TNF}^{\Delta\text{ARE}/\text{WT}}$ (red) mice.

Table 3-7: Most discriminating metabolites in the plasma of TNF^{ΔARE/WT} compared to WT mice at the age of 4, 8, 12, 16, and 24 weeks analyzed by UPLC-ESI-MS/MS using the AbsoluteIDQ™ Kit (Biocrates Life Sciences, Austria)

Time points		4 weeks		8 weeks		12 weeks		16 weeks		24 weeks	
		WT Mean ± SD	TNF ^{ΔARE/WT} Mean ± SD	WT Mean ± SD	TNF ^{ΔARE/WT} Mean ± SD	WT Mean ± SD	TNF ^{ΔARE/WT} Mean ± SD	WT Mean ± SD	TNF ^{ΔARE/WT} Mean ± SD	WT Mean ± SD	TNF ^{ΔARE/WT} Mean ± SD
Plasma metabolites (μmol/mg tissue)	O-PLS-DA Parameters	Q ² Y = 55% R ² X = 50% R ² Y = 99%		Q ² Y = 61% R ² X = 58% R ² Y = 96%		Q ² Y = 81% R ² X = 57% R ² Y = 98%		Q ² Y = 47% R ² X = 49% R ² Y = 82%		Q ² Y = 59% R ² X = 44% R ² Y = 97%	
	Significantly regulated	14		23		78		27		33	
	SM(OH) 22:1	7,22 ± 1,10	5,69 ± 0,93*	6,10 ± 1,69	2,82 ± 0,58***	6,98 ± 1,84	2,83 ± 0,68***	9,13 ± 2,87	4,17 ± 1,73**	7,56 ± 2,06	3,43 ± 0,83***
	PCae C38:1	1,31 ± 0,40	1,08 ± 0,23	1,51 ± 0,37	0,98 ± 0,28*	1,83 ± 0,36	0,83 ± 0,20***	2,07 ± 0,50	0,95 ± 0,25**	1,79 ± 0,45	0,96 ± 0,15***
	SM(OH) 22:2	3,56 ± 0,58	2,57 ± 0,70*	2,65 ± 0,54	1,57 ± 0,38***	0,74 ± 0,22	0,53 ± 0,11*	2,76 ± 0,58	2,13 ± 0,77*	3,42 ± 0,87	2,08 ± 0,41**
	PCae C38:2	3,05 ± 0,91	2,33 ± 0,67	4,55 ± 1,82	2,11 ± 0,57**	5,07 ± 1,93	2,08 ± 0,68**	6,81 ± 2,56	2,93 ± 1,57**	5,23 ± 2,10	2,53 ± 0,65**
	PCae C36:2	4,74 ± 1,09	3,51 ± 0,98*	6,32 ± 2,00	3,54 ± 0,82**	6,21 ± 1,86	3,50 ± 1,03*	7,43 ± 2,51	4,48 ± 1,39*	6,50 ± 1,94	4,36 ± 0,77*
	PCae C36:1	2,34 ± 0,75	1,74 ± 0,54*	2,48 ± 0,77	1,68 ± 0,43*	2,50 ± 0,63	1,44 ± 0,30**	2,83 ± 0,90	1,95 ± 0,80	2,73 ± 0,61	2,02 ± 0,26**
	lysoPCa C18:2	136,03 ± 46,28	90,65 ± 33,78**	200,75 ± 47,57	133,43 ± 43,82*	156,13 ± 16,90	122,39 ± 37,61*	193,38 ± 23,72	148,28 ± 46,90*	212,89 ± 33,90	155,43 ± 21,90**
	lysoPCa C17:0	2,57 ± 0,63	2,22 ± 0,63	4,80 ± 1,40	2,56 ± 0,78**	3,36 ± 0,67	2,07 ± 0,46**	3,78 ± 0,68	3,12 ± 1,25	4,10 ± 0,63	2,90 ± 0,81*
PCae C40:3	0,42 ± 0,10	0,34 ± 0,09	0,67 ± 0,26	0,36 ± 0,09**	0,71 ± 0,25	0,39 ± 0,11*	0,66 ± 0,24	0,47 ± 0,28 ^a	0,67 ± 0,15	0,50 ± 0,10*	
PCae C40:4	0,92 ± 0,18	0,78 ± 0,24	1,42 ± 0,54	0,93 ± 0,37*	1,80 ± 0,69	0,68 ± 0,24***	1,46 ± 0,33	1,12 ± 0,30 ^a	1,38 ± 0,23	0,90 ± 0,15**	

NB: All metabolite concentrations are presented as mean values ± SD from 8 animals per group. The values from TNF^{ΔARE/WT} animals were compared at each time point with the WT mice. Significant differences were assessed by Mann-Whitney U test and marked as follows: ^ap<0.1, *p<0.05, **p<0.01, ***p<0.001.

Key: lysoPCa: lysophosphatidylcholine; PCae: phosphatidylcholine with an ether bond; SM: sphingomyelin.

3.2.3 Time-Dependent Metabolic Changes in the Intestine Associated with Ileitis

Histopathological scoring of different parts of the intestine (distal jejunum (dJ) and ileum (dI), proximal (pC) and distal colon (dC)) was assessed at the age of 24 weeks to determine the predominant site of the gut associated inflammation. The most severe inflammatory changes were observed in the dI of the $TNF^{\Delta ARE/WT}$ mice (Figure 19 A). Investigation of the pC showed also a significant increase in the histopathology score in the $TNF^{\Delta ARE/WT}$ samples, which remained lower than in the dI. The dJ and dC scores were similar to WT scores. In addition, cytokine analysis in the dI of 24 weeks old animals using a multiplex biological assay highlighted significantly elevated concentrations of pro-inflammatory cytokines in the $TNF^{\Delta ARE/WT}$ animals, namely interferon gamma (IFN γ) and interleukin 6 (IL-6) (Figure 19 B). The detection of increased levels of TNF in the dI of $TNF^{\Delta ARE/WT}$ mice validated the impact of the genetic modification.

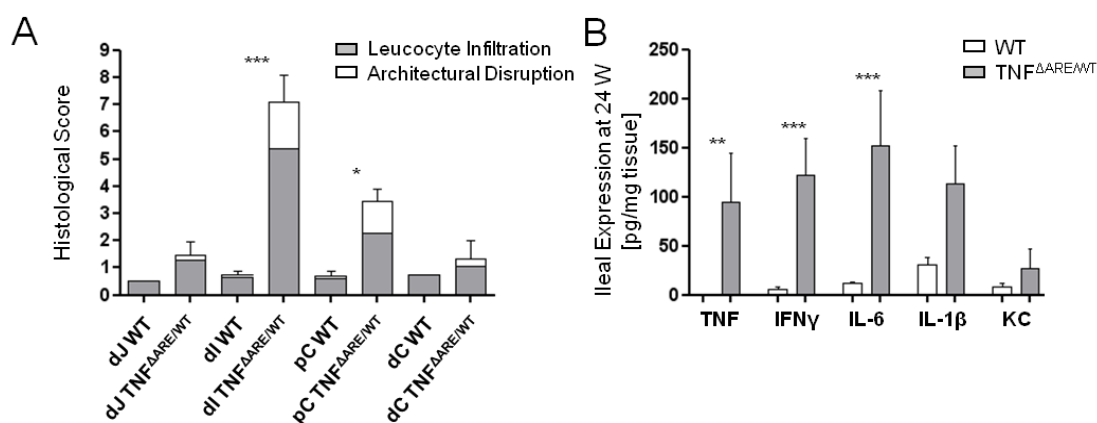


Figure 19: Topographical modeling of CD-like ileitis in the gastrointestinal tract of WT and $TNF^{\Delta ARE/WT}$ mice (A) Histopathological scores [score: 0-12] of different gut sections of WT and $TNF^{\Delta ARE/WT}$ mice at 24 weeks of age. (B) Cytokine expression level for IL-1 β , IFN γ , IL-6, KC, and TNF within the distal ileum of WT and $TNF^{\Delta ARE/WT}$ mice at 24 weeks of age.

All scores are presented as mean values \pm SEM from 8 animals per group. Significant differences were assessed by Mann-Whitney U test and marked as follows: * $p < 0.05$, ** $p < 0.01$, *** $p < 0.001$.

Abbreviations: IL: interleukin; KC: keratinocyte chemoattractant; IFN: interferon; TNF: tumor necrosis factor.

Metabonomic analysis of gut tissue extracts was conducted to provide additional insights into biochemical processes associated with structural and functional changes in the different intestinal compartments in relation to inflammation. Tissue extracts (hydrophilic and lipophilic fractions) of different intestinal parts (dJ, dI, pC and dC) obtained from 24 weeks old WT and $TNF^{\Delta ARE/WT}$ mice were therefore studied by 1H NMR spectroscopy. First, PCA analysis was applied to gain a general data overview and detect outliers in the data sets. PCA scores plot were generated using 4 PCs, explaining 21, 7, 6, and 5 % of the total variance, for the 1H NMR spectra of the hydrophilic fractions, and 5 PCs, explaining 59, 8, 5, 3, and 3 % of the total variance, for the 1H NMR spectra of the lipophilic fraction. Interestingly, the PCA scores plot generated on the 1H NMR data of the lipophilic fraction indicated clustering of WT and

TNF^{ΔARE/WT} animals by PC1 (Figure 20 A). Moreover, a clear separation of the different intestinal tissue segments was visible by PC2 in the same scores plot (Figure 20 B). Inspection of the PCA scores plots of the hydrophilic fraction of the intestinal tissue extracts revealed no clear separation between WT and TNF^{ΔARE/WT} mice (data not shown).

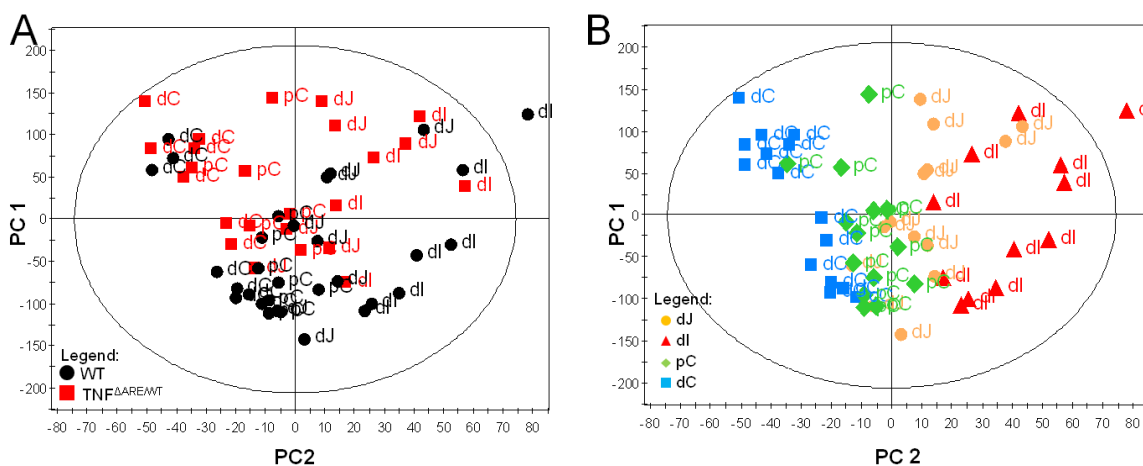


Figure 20: Intestinal metabolic diversity influenced by CD-like ileitis

PCA scores plot derived from the lipophilic extracts of intestinal tissues colored according to the different genotypes (A; WT (black) and TNF^{ΔARE/WT} (red) mice) and intestinal tissue sections (B; distal jejunum (dJ, yellow), distal ileum (dl, red), proximal colon (pC, green), distal colon (dC, blue)).

Supervised chemometric data analysis using O-PLS-DA was also employed on the hydrophilic and lipophilic fractions of the intestinal extracts to maximize the group separation and to model more subtle metabolic changes. The metabonomic analysis of the dJ and dC showed in agreement with the histopathological scoring no metabolic differences in the hydrophilic and lipophilic extracts. Interestingly, the analysis of the lipophilic extracts from the inflamed tissues, namely dl and pC, showed significant metabolic variations between WT and TNF^{ΔARE/WT} mice, but not in the hydrophilic extracts. Afterwards, influential metabolites were identified through the analysis of the corresponding coefficients plots. In addition, semi-quantitative information was generated by ¹H NMR peak integration in the original spectra and statistical significance was confirmed by Mann-Whitney U test (Table 3-8). These results described a significant modulation of cholesterol, triglycerides, GPL, saturated and unsaturated FAs as well as SM and plasmalogen metabolism in TNF^{ΔARE/WT} mice when compared to WT controls. Altogether, these data highlight the main inflammation location in dl and pC where most if not all significant metabolic changes were observed and mirror the histopathological findings.

Table 3-8: Metabolic differences in the lipophilic fraction of different intestinal compartments (distal jejunum, distal ileum, proximal colon and distal colon) in TNF^{ΔARE/WT} compared to WT mice at the age of 24 weeks detected by ¹H NMR spectroscopy

Intestinal compartment	Distal Jejunum		Distal Ileum		Proximal Colon		Distal Colon		
O-PLS-DA parameters	Q ² Y = 18% R ² X = 59% R ² Y = 82%		Q ² Y = 82% R ² X = 59% R ² Y = 97%		Q ² Y = 49% R ² X = 53% R ² Y = 96%		Q ² Y = 27% R ² X = 59% R ² Y = 90%		
	WT Mean ± SD	TNF^{ΔARE/WT} Mean ± SD							
Histopathological Score	0.50 ± 0.0	1.46 ± 1.37	0.67 ± 0.13	7.32 ± 1.03***	0.68 ± 0.37	4.08 ± 1.51*	0.75 ± 0.20	1.35 ± 1.22	
Peak Integral (a.u.)	Chemical shift								
Total Cholesterol	0.69 (s)	3.89 ± 2.54	5.98 ± 2.06	2.15 ± 0.86	4.95 ± 1.26**	2.84 ± 1.18	6.37 ± 2.36**	5.32 ± 3.01	7.19 ± 1.77
Free Cholesterol	1.01 (s)	4.13 ± 2.64	6.19 ± 2.14	2.38 ± 0.87	5.38 ± 1.07**	3.28 ± 1.28	7.29 ± 1.27**	6.16 ± 3.47	8.36 ± 2.05
Ester. Cholesterol	1.03 (s)	1.02 ± 0.75	1.63 ± 0.64	0.48 ± 0.20	1.32 ± 0.80*	0.60 ± 0.32	1.22 ± 0.49**	0.59 ± 0.32	0.76 ± 0.19
GPL	5.20 – 5.25 (m)	3.35 ± 2.10	4.77 ± 1.40	1.46 ± 0.53	3.57 ± 1.23**	2.03 ± 0.61	3.57 ± 0.95**	3.24 ± 1.58	4.49 ± 0.95
TG	5.25 – 5.30 (m)	4.32 ± 2.78	3.19 ± 2.13	4.92 ± 1.60	2.10 ± 1.17*	7.09 ± 1.30	3.72 ± 2.15**	5.18 ± 2.83	3.36 ± 1.64
DAG	5.07 – 5.11 (m)	3.07 ± 0.11	2.51 ± 0.09	5.20 ± 0.11	3.41 ± 0.25**	1.79 ± 0.08	1.92 ± 0.06^a	2.11 ± 0.12	2.51 ± 0.08
Cholin in PL	3.21 (s)	15.16 ± 11.00	22.04 ± 7.43	5.62 ± 2.39	17.45 ± 7.27**	9.27 ± 3.79	19.08 ± 6.56*	16.94 ± 9.81	24.58 ± 5.93
Methyl in FA	0.88 (t)	65.77 ± 4.11	61.25 ± 21.97	72.82 ± 1.43	67.15 ± 2.87**	71.59 ± 1.86	67.30 ± 1.96**	70.73 ± 3.92	67.78 ± 2.32
UFA	5.30 – 5.40 (m)	25.29 ± 9.48	25.95 ± 2.42	38.67 ± 1.77	33.89 ± 0.60 **	39.53 ± 1.67	34.36 ± 2.75***	28.48 ± 3.92	26.03 ± 2.15
PUFA I	2.74 – 2.79 (m)	9.55 ± 3.52	10.01 ± 1.46	9.57 ± 1.26	7.95 ± 2.19	11.39 ± 1.74	7.21 ± 2.49**	7.93 ± 2.72	6.34 ± 2.00
PUFA II	2.79 – 2.87 (m)	13.31 ± 7.77	19.43 ± 6.29	8.96 ± 2.21	16.98 ± 4.80*	10.92 ± 3.32	18.42 ± 5.39*	15.26 ± 6.89	19.32 ± 3.55
Sphingomyelin	5.70 (m)	0.27 ± 0.18	0.41 ± 0.15	0.17 ± 0.07	0.47 ± 0.10**	0.26 ± 0.13	0.54 ± 0.19*	0.42 ± 0.26	0.57 ± 0.15
Plasmalogen	5.90 (m)	0.17 ± 0.11	0.28 ± 0.09	0.10 ± 0.01	0.29 ± 0.09**	0.40 ± 0.17	0.75 ± 0.29*	0.79 ± 0.46	1.02 ± 0.29

NB: All scores are presented as peak integral mean values ± SD of normalized NMR data from 8 animals per group. The values from TNF^{ΔARE/WT} animals were compared at each time point with the WT mice. Significant differences were assessed by Mann-Whitney U test and marked as follows: ^ap<0.1, *p<0.05, **p<0.01, ***p<0.001.

KEY: DAG: diacylglycerides; FA: fatty acids; GPL: glycerophospholipids; PL: phospholipids; PUFA: polyunsaturated fatty acids; TG: triglycerides; UFA: unsaturated fatty acids.

Metabolic differences related to the development of inflammation in the dl were further monitored by applying a targeted LC-MS metabonomic method on dl tissues of WT and TNF^{ΔARE/WT} mice using the AbsoluteIDQ™ kit (Biocrates Life Sciences, Austria). O-PLS-DA was performed on quantitative information for 163 metabolites, including amino acids, sugars, acyl-carnitines, sphingolipids, and GPL, to maximize the separation of WT and TNF^{ΔARE/WT} mice at the age of 4, 8, 12, 16, and 24 weeks in a pairwise manner. Within this data set, models for the 12, 16, and 24 weeks time point displayed high and positive R²X, R²Y, and Q²Y parameters (Table 3-9), whereas the most robust model was obtained at 12 weeks. Also here, the ten most influential metabolites based on the computed VIP score are listed in Table 3-9. Statistical significances were assessed by Mann-Whitney U test (significantly regulated metabolites are listed in Appendix Table 6-4). The data show increased concentrations of SM (SM C16:0) as well as decreased levels of acyl-carnitines, especially of medium chain acyl-carnitines (C:10, C:12, C:14-OH, C:16-OH), at all measured time points in the dl of inflamed TNF^{ΔARE/WT} mice. Within the group of choline containing PCaa/ae a concentration rise was observed for the acyl ether lipids (PCae), whereas the level of PCs with ester bonds (PCaa) decreased in the dl of inflamed TNF^{ΔARE/WT} compared to WT mice at all time points. The listed metabolites showed a high variability over time due to variations during the normal aging process as well as inter-animal variability.

In addition, as metabolic changes were predominantly detected in the lipophilic fraction by ¹H NMR spectroscopy and targeted LC-MS, a second targeted LC-MS method was employed to investigate specific markers for fatty acids signalling within the dl over time (4, 8, 12, and 16 weeks). These measurements include arachidonic acid (AA), isomers of thromboxane, hydroxyeicosatetraenoic (HETE) acid, dihydroxyeicosatrienoic (DiHETrE) acid, hydroxyoctadecadienoic (HODE) acid, and prostaglandins (PG). Here, the pairwise application of O-PLS-DA revealed significant differences between WT and TNF^{ΔARE/WT} samples from 8 weeks onwards. Table 3-10 lists the O-PLS-DA model parameters as well as all fatty acid signaling markers changing in the dl of TNF^{ΔARE/WT} compared to WT mice. Significant differences were assessed by applying Mann-Whitney U tests. Some of the listed metabolites showed a high variability over time due to variations during the normal aging process as well as inter-animal variability. Metabolites generated from the precursor linoleic acid, namely 9- and 13- HODE, were decreased in the TNF^{ΔARE/WT} compared to WT mice at the time points 12 and 16 weeks. Also the levels of 9 HETE and DiHeTrE were lower at 12 weeks in the inflamed animals. In addition, TNF^{ΔARE/WT} mice showed significantly increased levels of the prostaglandins PGF1 alpha and PGF2 alpha as well as thromboxane B2 compared to WT mice.

Table 3-9: Most discriminating metabolites in the distal ileum of TNF^{ΔARE/WT} compared to WT mice at the age of 4, 8, 12, 16, and 24 weeks analyzed by UHPLC-ESI-MS/MS using the AbsoluteIDQ™ kit (Biocrates Life Sciences, Austria)

Time points		4 Weeks		8 Weeks		12 Weeks		16 Weeks		24 Weeks	
		WT Mean ± SD	TNF ^{ΔARE/WT} Mean ± SD	WT Mean ± SD	TNF ^{ΔARE/WT} Mean ± SD	WT Mean ± SD	TNF ^{ΔARE/WT} Mean ± SD	WT Mean ± SD	TNF ^{ΔARE/WT} Mean ± SD	WT Mean ± SD	TNF ^{ΔARE/WT} Mean ± SD
Distal ileum metabolites (μmol/mg tissue)	O-PLS-DA Parameters	Q ² Y < 0 R ² X = 36% R ² Y = 95%		Q ² Y < 0 R ² X = 49% R ² Y = 97%		Q ² Y = 75% R ² X = 58% R ² Y = 96%		Q ² Y = 38% R ² X = 40% R ² Y = 96%		Q ² Y = 22% R ² X = 51% R ² Y = 98%	
	Significantly regulated	4		2		33		25		12	
	PCae C38:5	0,023 ± 0,02	0,020 ± 0,01	0,013 ± 0,01	0,027 ± 0,03	0,017 ± 0,01	0,034 ± 0,02^a	0,008 ± 0,01	0,018 ± 0,01	0,013 ± 0,01	0,029 ± 0,01*
	C12:1	0,101 ± 0,06	0,080 ± 0,05	0,058 ± 0,04	0,058 ± 0,04	0,095 ± 0,02	0,039 ± 0,02**	0,122 ± 0,05	0,057 ± 0,02**	0,065 ± 0,03	0,047 ± 0,02
	C10:1	0,066 ± 0,03	0,051 ± 0,03	0,037 ± 0,02	0,035 ± 0,02	0,060 ± 0,02	0,025 ± 0,01**	0,072 ± 0,03	0,038 ± 0,0**	0,040 ± 0,01	0,035 ± 0,01
	SM C16:0	0,727 ± 0,26	0,664 ± 0,31	0,687 ± 0,49	0,817 ± 0,34	0,726 ± 0,43	0,792 ± 0,46	0,534 ± 0,21	1,078 ± 0,25**	0,429 ± 0,62	0,588 ± 0,22**
	C14:2-OH	0,0015 ± 0,001	0,0014 ± 0,001	0,0012 ± 0,001	0,0013 ± 0,001	0,0020 ± 0,001	0,0005 ± 0,001***	0,0035 ± 0,002	0,0011 ± 0,001*	0,0009 ± 0,001	0,0013 ± 0,001
	C16:1-OH	0,0038 ± 0,002	0,0240 ± 0,001	0,0027 ± 0,002	0,0022 ± 0,001	0,0045 ± 0,001	0,0015 ± 0,001***	0,0044 ± 0,003	0,0022 ± 0,002	0,0016 ± 0,001	0,0022 ± 0,001
	PCae C38:4	0,020 ± 0,02	0,019 ± 0,01	0,019 ± 0,02	0,022 ± 0,02	0,027 ± 0,02	0,021 ± 0,02	0,010 ± 0,01	0,014 ± 0,02	0,013 ± 0,01	0,027 ± 0,01*
	PCaa C26:0	0,202 ± 0,07	0,171 ± 0,06	0,120 ± 0,05	0,129 ± 0,06	0,189 ± 0,13	0,080 ± 0,04*	0,198 ± 0,07	0,089 ± 0,04**	0,118 ± 0,04	0,116 ± 0,03
	PCaa C40:1	0,098 ± 0,05	0,059 ± 0,02	0,059 ± 0,02	0,060 ± 0,03	0,076 ± 0,04	0,038 ± 0,01*	0,096 ± 0,07	0,051 ± 0,02	0,047 ± 0,02	0,046 ± 0,01
PCae C42:3	0,0050 ± 0,004	0,0056 ± 0,005	0,0054 ± 0,008	0,0042 ± 0,006	0,0032 ± 0,005	0,0040 ± 0,004	0,0015 ± 0,002	0,0038 ± 0,004	0,0019 ± 0,003	0,0058 ± 0,003*	

NB: All metabolite concentrations are presented as mean values ± SD from 8 animals per group. The values from TNF^{ΔARE/WT} animals were compared at each time point with the WT mice. Significant differences were assessed by Mann-Whitney U test and marked as follows: ^ap<0.1, *p<0.05, **p<0.01, ***p<0.001.

Key: C: acyl-carnitine; PCaa: phosphatidylcholine; PCae: phosphatidylcholine with an ether bond; SM: sphingomyelin.

Table 3-10: Concentration levels ($\mu\text{g/g}$ tissue) of fatty acid signaling markers in the distal ileum of $\text{TNF}^{\Delta\text{ARE}/\text{WT}}$ compared to WT mice at the age of 4, 8, 12, and 16 weeks analyzed by UPLC-ESI-MS/MS

Time points		4 Weeks		8 Weeks		12 Weeks		16 Weeks	
O-PLS-DA Parameters		$Q^2Y < 0$ $R^2X = 42\%$ $R^2Y = 67\%$		$Q^2Y = 63\%$ $R^2X = 46\%$ $R^2Y = 87\%$		$Q^2Y = 41\%$ $R^2X = 70\%$ $R^2Y = 74\%$		$Q^2Y = 66\%$ $R^2X = 54\%$ $R^2Y = 86\%$	
		WT Mean \pm SD	$\text{TNF}^{\Delta\text{ARE}/\text{WT}}$ Mean \pm SD	WT Mean \pm SD	$\text{TNF}^{\Delta\text{ARE}/\text{WT}}$ Mean \pm SD	WT Mean \pm SD	$\text{TNF}^{\Delta\text{ARE}/\text{WT}}$ Mean \pm SD	WT Mean \pm SD	$\text{TNF}^{\Delta\text{ARE}/\text{WT}}$ Mean \pm SD
Inflammatory marker ($\mu\text{g/g}$ tissue)	Arachidonic acid	342.19 \pm 142.94	230.53 \pm 71.91^a	209.33 \pm 58.07	189.85 \pm 50.41	225.71 \pm 85.58	123.74 \pm 18.92^{**}	119.03 \pm 22.81	320.76 \pm 134.24^{***}
	Thromboxane B2	3.493 \pm 2.44	3.087 \pm 1.66	1.990 \pm 0.85	4.309 \pm 2.29[*]	2.107 \pm 0.54	5.241 \pm 3.19[*]	0.900 \pm 0.32	7.167 \pm 4.32^{***}
	PGF1 alpha	1.130 \pm 0.49	0.989 \pm 0.43	0.689 \pm 0.19	0.935 \pm 0.19	1.257 \pm 0.80	0.624 \pm 0.20	0.571 \pm 0.10	1.663 \pm 0.88^{***}
	PGF2 alpha	5.542 \pm 1.70	7.125 \pm 2.88	6.146 \pm 2.88	8.100 \pm 2.90	8.982 \pm 6.87	5.471 \pm 2.50	2.975 \pm 1.77	15.163 \pm 0.74^{***}
	9 HODE	28.642 \pm 5.14	24.404 \pm 2.88	30.820 \pm 3.98	27.595 \pm 9.04	38.421 \pm 18.88	19.436 \pm 4.62^{**}	20.886 \pm 7.37	50.540 \pm 37.57^{**}
	13 HODE	42.729 \pm 9.55	35.338 \pm 55.87	38.952 \pm 12.26	43.058 \pm 18.64	52.598 \pm 25.79	27.568 \pm 8.51[*]	52.383 \pm 19.19	32.059 \pm 9.22[*]
	9 HETE	1.921 \pm 1.76	1.039 \pm 0.98	0.383 \pm 0.21	0.563 \pm 0.67	2.679 \pm 2.19	0.391 \pm 0.37[*]	0.357 \pm 0.11	1.722 \pm 2.46
	5,6 DiHeTrE	2.156 \pm 1.48	0.961 \pm 0.59	1.011 \pm 0.59	1.290 \pm 0.93	1.455 \pm 0.89	0.591 \pm 0.26^{**}	0.573 \pm 0.29	0.657 \pm 0.43
	8,9 DiHeTrE	0.396 \pm 0.09	0.340 \pm 0.20	0.236 \pm 0.14	0.220 \pm 0.13	0.284 \pm 0.10	0.162 \pm 0.03^{**}	0.183 \pm 0.10	0.218 \pm 0.19
	11,12 DiHeTrE	0.439 \pm 0.09	0.356 \pm 0.09	0.377 \pm 0.21	0.379 \pm 0.27	0.283 \pm 0.06	0.191 \pm 0.04^{**}	0.148 \pm 0.05	0.507 \pm 0.24^{**}
14,15 DiHeTrE	2.820 \pm 0.65	1.769 \pm 0.56	3.479 \pm 2.11	3.574 \pm 3.99	1.829 \pm 0.67	1.443 \pm 0.47	4.866 \pm 2.63	1.065 \pm 0.38^{***}	

NB: All metabolite concentrations are presented as mean values \pm SD from 8 animals per group. The values from $\text{TNF}^{\Delta\text{ARE}/\text{WT}}$ animals were compared at each time point with the WT mice. Significant differences were assessed by Mann-Whitney U test and marked as follows: ^a $p < 0.1$, $*p < 0.05$, $**p < 0.01$, $***p < 0.001$.

Key: DiHeTrE: dihydroxyicosatrienoic acid; HETE: hydroxyicosatetraenoic acid; HODE: hydroxyoctadecadienoic; PG: prostaglandin.

4 DISCUSSION

4.1 Effect of Inflammation on Plasma Lipids and Lipoprotein Metabolism

The intestine is responsible for absorption of nutrients provided by the diet and therefore represents an organ directly involved in lipid and lipoprotein metabolism. The impairment of lipoprotein particles is of particular significance as they efficiently transport and distribute large amounts of fat and lipid-soluble vitamins in the circulation, subsequently contributing to the maintenance of cellular membrane structure and function as well as energy and signaling metabolism.¹⁶³ Moreover, epidemiological studies suggest a link between chronic inflammatory diseases and atherosclerosis,¹⁶⁴ as the underlying pathogenesis involves an imbalanced lipid metabolism and a maladaptive immune response entailing a chronic inflammation of the arterial wall.¹⁶⁵ Specific alterations of plasma lipids and lipoproteins have been described in human IBD patients,^{163, 166} whereupon no difference in the lipid profile between UC and CD patients was observed.^{163, 167} Moreover, there was no evident correlation between the lipid changes and the disease index, the surgical history, or the current medication of the investigated patients.¹⁶³ Though, these alterations include an increase in TAGs due to an elevation in the concentration of VLDL, whereas the VLDL particles themselves are TAG depleted and enriched in apolipoproteins (apo). In addition, there is a decrease in HDL and apoA-I, LDL, and cholesterol levels during human IBD.^{163, 166, 167} Similar changes were also detected by ¹H NMR spectroscopy in the c-IL-10^{-/-} and the TNF^{ΔARE/WT} mouse model as well as in an additional colitis animal model, where inflammation was induced by the adoptive transfer of T cells into syngeneic RAG2^{-/-} lymphopenic mice (data not shown). However, these changes in structure and function of lipids and lipoproteins result from the initiation of the acute phase response, initially protecting the host from harmful effects of bacteria, viruses, and parasites.¹⁶⁸ Consequently, infection and inflammation seem to share common effector pathways which can be deleterious under chronic and prolonged activation and may contribute to the pathogenesis of atherosclerosis.¹⁶⁸ Similarities as well as discrepancies in the observed lipid changes during infection and inflammation in IBD patients and in the IL-10^{-/-} and TNF^{ΔARE/WT} mouse model will be discussed.

Inflammation leads to the induction of an early immune response by the host, the acute phase response, which is accompanied by specific changes in the concentration of plasma proteins, including C-reactive protein (CRP) and SAA.¹⁶⁸ Stimulation of the hepatic synthesis rate of these proteins are predominantly mediated by cytokines produced in response to a variety of stimuli in multiple cell types, including macrophages, monocytes, T-lymphocytes, and endothelial cells.¹⁶⁹ A dramatic increase in CRP and SAA can be observed in IBD patients¹⁷⁰ and in the IL-10^{-/-} mouse model.¹⁷¹ Elevated SAA levels were also found in the c-IL-10^{-/-} mice. Moreover, acute and chronic inflammations are generally associated with a profound change in the apo composition in HDL particles, the SAA protein family becoming

the major component. These observations suggest a role of SAA in lipoprotein function during inflammation.¹⁷² A decreased level of HDL was observed in IBD patients,^{163, 166} which might result from intestinal malabsorption, malnutrition, or other inflammation-related mechanisms.¹⁶⁶ Metabolic studies indicated that SAA-containing HDL is cleared more rapidly from the circulation than normal HDL,¹⁷³ and SAA also enhances HDL/SAA binding and uptake preferentially by macrophages.¹⁷⁴ In addition, in primates and humans, inflammation also leads to a decrease of total serum cholesterol levels *via* the action of LPS and pro-inflammatory cytokines. Contrary, inflammation in rodents increased serum total cholesterol and LDL levels *via* stimulating *de novo* cholesterol synthesis and decreasing lipoprotein clearance and the conversion of cholesterol into bile acids.¹⁶⁸ Increased plasma concentration of LDLs and/or of triglyceride-rich lipoproteins remnants are two major factors initiating inflammatory disorders *via* modification by oxidation or by aggregation.¹⁷⁵ In c-IL-10^{-/-} animals, elevated levels of LDL/HDL were detected even from 1 week onwards when compared to WT controls, whereas significantly decreased levels of both lipoprotein fractions were detected from 4 weeks in TNF^{ΔARE/WT} animals. Such species-specific responses to inflammation, including also the differences between primates and rodents, are common, but the underlying processes responsible for these mechanisms are not yet understood.¹⁶⁸ Moreover, data from subjects with active IBD show an increase in TAG levels, characterized also by an increase in VLDL levels,^{167, 168} a situation which has been widely described during inflammation.¹⁶⁸ The hypertriglyceridemia associated with infection and inflammation has been attributed to an increase in hepatic lipoprotein production and decreased lipoprotein clearance. These changes may be due to a decreased activity of lipoprotein lipase (LPL).¹⁷⁶ However, results in the literature are conflicting and only few studies failed to demonstrate any change in LPL activity.¹⁶⁷ Unfortunately, conclusions on changes in TAG levels are not feasible by acquisition of ¹H NMR spectra used in this study. The increased amounts of VLDL in IBD patients are most likely due to either increased VLDL production or decreased clearance.¹⁶⁸ Moreover, there are several studies indicating that subjects with IBD may synthesize VLDL with an abnormal composition of apo.^{163, 166} Investigation of VLDL particles in c-IL-10^{-/-} and TNF^{ΔARE/WT} mice, revealed significantly declined levels from very early time points onwards. It can be argued that this pattern was associated with a modification in the LPL activity in the capillary beds of adipose tissue and skeletal muscles to remove TAGs. Inflammation-related processes were indeed characterized by increased blood levels of secretory phospholipase A2 (PLA2), which promoted hydrolysis of PL in LDL and VLDL and generated PUFAs that can be oxidized and promote inflammation.¹⁷⁷ This is further supported by the observation of compositional changes of PUFAs within the plasma lipoprotein fraction of c-IL-10^{-/-} and TNF^{ΔARE/WT} mice.

Besides changes in the lipoprotein cycle, correlation analysis of the time-dependent increase in SAA against the full diffusion-edited metabolic plasma profile in the c-IL-10^{-/-} animal model

(data not shown) highlighted a marked correlation between glycosylated proteins and SAA over time which may reflect the overall inflammation-related shift in the plasma protein metabolism. Interestingly, this metabolic feature was also observed in the TNF^{ΔARE/WT} mouse model, an animal model of chemically induced colitis (data not shown) as well as in an adoptive T-cell colitis animal model (data not shown). Moreover, the described lipoprotein signatures of inflammation-related processes were strongly associated with changes in PL metabolism, such as increased levels of choline in PL and GPC, which promote formation of foam cells and inflammation.¹⁷⁷ This modification of the PL metabolism was the result of an alteration of the plasma PL transfer protein activity, a metabolic feature previously associated with plasma levels of SAA, CRP, glucose, and apo-I-HDL particles,¹⁷⁷ as presented here. These metabolic features were previously reported for acute colitis,¹⁷⁸ and were here observed at 1 week of age in c-IL-10^{-/-} and at 4 weeks of age in TNF^{ΔARE/WT} mice, prior to changes in body weight, inflammatory biomarkers, and epithelial damages.

4.2 Metabolic Assessment of Experimental Colitis in IL-10^{-/-} mice

The metabolic pattern associated with the gradual development of colitis in WT and c-IL-10^{-/-} mice were characterized using ¹H NMR-based metabolic profiles of blood plasma. This metabonomic approach provided a holistic inspection of metabolic homeostatic processes in relation to both genetic background and gradual development of inflammation. In a second study, WT and non-inflamed s-IL-10^{-/-} mice were used to investigate the physiological impact of a genetic predisposed but disease-free phenotype on the host's metabolism by ¹H NMR spectroscopy. Here, additionally a targeted LC-MS metabonomic approach was used to increase the detection range of specific lipids and to provide novel insights to extend the global understanding of the metabolic changes in this animal model. Furthermore, ¹H NMR-based as well as targeted LC-MS metabonomic techniques were also applied to the expected site of colonic inflammation to characterize the metabolic signature associated with genetic susceptibility.

4.2.1 Histopathological Scoring, Body Weight, and Inflammatory Biomarkers Describe the Gradual Development of Colitis

IL-10^{-/-} mice are described to be growth retarded, anemic, and to spontaneously develop chronic intestinal inflammation due to a loss of tolerance towards gut microbiota. The involved immune and inflammatory processes are characterized by an enhanced Th1 response in the early course of disease, and a high Th2 cytokine release at a later stage.³⁹ Conventionally housed c-IL-10^{-/-} mice developed moderate bowel inflammation from the age of 8 weeks on and reached a maximum of the inflammatory response at the age of 24 weeks, accompanied by important pathological changes in the colon. The intestinal tissues were characterized by increased inflammatory cell infiltrations into mucosa and submucosa, development of irregular crypts, abscesses, and hyperplasia, as previously reported.³⁹ Investigation of the intestinal tissues derived from s-IL-10^{-/-} animals housed under SPF conditions did only reveal attenuated structural changes and cell infiltrations that were restricted to the proximal colon. The intestinal microbiota is thought to play an important role in the initiation and perpetuation of IBD in the IL-10^{-/-} animal model³⁹ as well as in humans.¹⁷⁹ Differences in the pathological phenotypes due to the altered microbial environment confirmed that the development of colitis in IL-10^{-/-} mice is triggered by enteric microbiota, and that the composition determines the severity of symptoms.³⁹ In addition, growth retardation of IL-10^{-/-} mice, appearing in form of a reduced body weight, was only observed in the inflamed c-IL-10^{-/-} animals at 24 weeks. This result could be readily explained by disturbed nutrient absorption as a consequence of the intestinal alterations of these animals.³⁹ Moreover, the detected tissue destructive processes also induced a systemic reaction in the inflamed c-IL-10^{-/-} animals. The acute phase response arouses multiple physiologic adaptations, including the hepatic syn-

thesis of acute phase proteins, such as CRP and SAA.¹⁶⁸ SAA is clearly associated with colitis development in IBD patients¹⁷⁰ and in animal models of genetically induced colitis, such as the IL-10^{-/-} animal model.¹⁷¹ Monitoring of the circulating levels of SAA illustrated an increase of SAA levels at 16 and 24 weeks. This correlated with the histopathological development of inflammation from the age of 8 weeks onwards, as previously reported for acute colitis.¹⁸⁰

4.2.2 Association of Plasma Metabolic Changes with the Gradual Development of Colitis

The metabolism associated with the gradual development of colitis using plasma metabolite profiling *via* ¹H NMR spectroscopy in WT and c-IL-10^{-/-} mice provided a holistic inspection of metabolic homeostatic processes. Although the body weight of inflamed c-IL-10^{-/-} mice did not significantly differ from their WT controls, a consistent disruption of the plasma concentration of lipoproteins was evidenced (see 4.1).

Chronic intestinal inflammation has recently been linked to an energy deficiency state of the gut epithelium with alterations in the oxidative metabolism, which is maybe related to a loss of the energy homeostasis.¹⁸¹ Higher levels of free amino acids (arginine, lysine, phenylalanine, tyrosine, glutamine, and alanine) were observed in the plasma of c-IL-10^{-/-} mice, the differences being greatest at 8 weeks of age. These observations were in agreement with analyses of serum from DSS-treated mice¹²⁵ as well as UC and CD patients,¹²⁷ where elevated amounts of amino acids and trichloroacetic acid (TCA) intermediates were detected. IL-10^{-/-} animals are known to gradually develop diarrhea and muscle atrophy associated with increased protein catabolism.³⁹ Moreover, a higher energy demand during the disease state, as previously suggested,¹⁸¹ or decreased energy availability due to a decline in nutrient absorption through the impaired intestine may led to the increase of amino acid concentrations as observed in plasma of c-IL-10^{-/-} mice. In particular, glutamine represents the primary source of amino acids in the small intestinal mucosa, and plays besides butyrate a central role in colonocyte nutrition and integrity.¹⁸² Moreover, it has been demonstrated that glutamine can protect against intestinal inflammation evoked by TNBS¹⁸³ and DSS¹⁸⁴ in rodents. Additionally, the elevation of alanine and glutamine in plasma was associated with decreased levels of the branched-chain amino acids valine and leucine, which reflected both, breakdown of proteins and increased gluconeogenesis and carbon flux through the anapleurotic pathway, to support ATP production. In addition, the relative increased plasma concentration of arginine in c-IL-10^{-/-} mice could reflect alterations of the nitric oxide pathway, a key metabolic process involved in the pathogenesis of IBD.¹⁸⁵ Elevated levels of lactate, citrate, and pyruvate and decreased plasma glucose levels in the c-IL-10^{-/-} mice brought additional evidence of increased FA oxidation and suggested extensive glycolysis to accommodate a

higher energy demand or decreased energy availability due to decreased nutrient absorption through the impaired intestine. Our observations were supported by previous findings on differential expression of key enzymes of the citrate cycle associated with the development of inflammation.¹⁸⁶

4.2.3 Association of Plasma Metabolic Changes with Colitis Susceptibility

Modeling genetic IBD susceptibility in the non-inflamed s-IL-10^{-/-} animals via ¹H NMR- and LC-MS-based metabolic profiles of blood plasma revealed differences due to the genetic phenotype of the mice, irrespective of the presence of inflammation. Interestingly, the generated statistical models on data from both techniques had a higher model predictability values (Q²Y) at the early time points (4 and 8 weeks) which declined later (12 and 16 weeks). During the performance of the experiments, we realized that male and female IL-10^{-/-} animals displayed different plasma lipid profiles and lipoprotein compositions (data not shown). Sexual dimorphism of the lipid metabolism is already a well-recognized phenomenon in humans,¹⁸⁷ but not proven in IL-10^{-/-} mice. Nevertheless, this event may contribute to a higher intra-group variability within the samples belonging to the time points 12 and 16 weeks, when the animals were fully grown. As a result, subtle changes especially in the plasma lipid compartment were obscured.

Using ¹H NMR spectroscopy, compositional modifications of lipoproteins and glycosylated proteins were detected in this study. Decreased amounts of VLDL and elevated levels of LDL, HDL, as well as glycosylated proteins were discovered at 4 and 8 weeks, reflecting a similar pattern to the first kinetic study using c-IL-10^{-/-} mice. These early changes demonstrated that already a genetic susceptibility, here in form of the IL-10 gene knock-out, can lead to events detectable *via* ¹H NMR-based metabolic profiling. Taken together, such observations further suggest that silencing the IL-10 gene results in an alteration of the lipoprotein cycle which may increase the susceptibility towards inflammation of these animals. On the contrary, variations in the amount of several amino acids and citrate cycle intermediates did not reflect the previous results. This indicated that the postulated energy deficiency state in chronic intestinal inflammation is rather a consequence than a cause within the complex IBD pathogenesis.^{188, 189}

The use of a targeted LC-MS based metabolomic approach additionally verified individual observations, including for example the significant increase in tyrosine and decrease in glutamine, as shown by ¹H NMR spectroscopy. In addition, diminished concentrations of the short-chain acyl-carnitines acetyl-, propionyl-, and butyryl-carnitine were also identified. These changes suggest modified tissue absorption and/or production of these short-chain acyl-carnitines during IBD susceptibility in non-inflamed s-IL-10^{-/-} animals compared to their WT controls.

4.2.4 Association of Colonic Metabolic Changes with Colitis Susceptibility

Characterization of the metabolic pattern associated with colitis susceptibility in non-inflamed s-IL-10^{-/-} mice at the expected site of inflammation in the proximal colon *via* ¹H NMR-based metabolic profiling did not reveal any significant modifications. The application of the more sensitive LC-MS based metabonomic approach revealed subtle changes at least at 24 weeks. The detection of elevated levels of short-chain acyl-carnitines (hydroxybutyryl-carnitine, butyrylcarnitine, isovalerylcarnitine) and reduced concentrations of acetyl-carnitine in the colonic tissue of 24 weeks old s-IL-10^{-/-} animals pictured a very interesting aspect. In a healthy host, butyrate absorbed from the blood or lumen of the large intestine or resulting from β -oxidation of long chain fatty acids is largely metabolized by the colonic epithelial cells and is believed to be one of the major ATP sources for colonocytes.¹⁹⁰ As a result, reduced butyrate oxidation leads to a decreased energy supply to colonocytes which was already observed in biopsies of IBD patients.^{188, 189} These modifications were now detected in a pre-disposed but healthy phenotype and proof findings from biopsies collected from quiescent intestinal tissues of IBD patients.¹⁸⁹ This might indicate that the reduction of butyrate oxidation capacity is one of the starting points of the postulated energy deficiency state in the colon during IBD. In addition, there are indications for a reduced activity as well as a differentiated protein expression of enzymes involved in the metabolization of butyrate.¹⁹¹ These observations indicate that a genetic susceptibility through silencing the IL-10 gene leads to a disturbed oxidation of butyrate and other short-chain FAs, leading to increased concentrations of these short-chain acyl-carnitines in the non-inflamed s-IL-10^{-/-} animals. Moreover, this could be used to demonstrate that the energy deficiency state starts via a dysregulated oxidation capacity of colonocytes and is at first detectable in the colon, followed by metabolic changes in the plasma. Further analyses of colonic tissue extracts of inflamed and non-inflamed IL-10^{-/-} animals will be needed to verify this hypothesis.

4.3 Metabolic Phenotyping of Crohn's Disease-like IBD in TNF^{ΔARE/WT} Mice

In the TNF^{ΔARE/WT} study, a holistic metabonomic approach was applied to monitor systemic and local metabolic events associated with the gradual development of CD-like ileitis across age. Metabolic profiles of blood plasma and different intestinal compartments of WT and TNF^{ΔARE/WT} mice from the age of 4 up to 24 weeks were generated integrating holistic ¹H NMR spectroscopy and different targeted LC-MS techniques.

4.3.1 Body Compositional Changes Describe Ileal Inflammation in TNF^{ΔARE/WT} Mice

The heterozygous TNF^{ΔARE/WT} mouse model spontaneously developed a CD-like ileitis pathology, predominantly localized in the distal ileum and to a lower degree in the proximal colon, with mucosal and submucosal infiltration of inflammatory cells partially extending into the muscular layers of the bowel wall, as previously described.⁴⁰ Tissue pathology was associated with local expression of pro-inflammatory cytokines (e.g. TNF, IFN γ and IL-6), likely produced by infiltrated immune or epithelial cells, triggering inflammation-related processes. During CD large portions of the small intestinal mucosa are functionally impaired and patients subsequently suffer from malnutrition primarily explaining their modification of body composition and weight loss.¹⁹² In the current study, TNF^{ΔARE/WT} mice had a lower body weight from 12 weeks onwards when compared to WT animals. These observations were preceded by an increased fecal energy loss and an increased fecal fat excretion of TNF^{ΔARE/WT} mice as assessed by Fourier transform-infrared (FT-IR) spectroscopy of feces (data not shown). These findings suggest that TNF^{ΔARE/WT} mice also suffer from a malabsorption phenotype as observed in CD patients with ileal resection.¹⁹³ Huybers *et al.*¹⁹⁴ also reported calcium malabsorption and bone alteration in this animal model, providing therefore additional evidence of insufficient nutrient uptake in the intestine of TNF^{ΔARE/WT} mice. Besides, inflamed mice showed a significantly reduced food uptake at the age of 24 weeks. For CD patients a decreased caloric intake, correlating with disease severity, was reported and attributed to several factors, such as anorexia, abdominal pain, nausea, vomiting, and intestinal obstruction.¹⁹⁵ Anorexia could have applied in a similar manner for the reduced food uptake of the inflamed animals in the current study.

4.3.2 Association of Plasma Metabolic Changes with the Gradual Development of Ileitis

Modeling of the systemic metabolic pattern of CD-like ileitis in TNF^{ΔARE/WT} mice via ¹H NMR- and LC-MS-based metabonomic approaches revealed significant changes even before the histopathological onset of inflammation. Here only little metabolic changes linking to the de-

development of an energy deficiency state during inflammation were observed in the plasma of $\text{TNF}^{\Delta\text{ARE}/\text{WT}}$ mice. Still, higher amounts of the amino acids alanine and glutamine were detectable, which were previously related to increased energy supply to the colonocytes.^{125, 127} Using a targeted LC-MS metabolomic approach, the compositional changes of the circulating lipids during the development of CD-like ileitis were more closely examined in the plasma of WT and $\text{TNF}^{\Delta\text{ARE}/\text{WT}}$ mice. Plasma lipids are dissolved and dispersed through their association with specific groups of proteins. As a result, most free FAs and related structures with carboxyl groups associated with albumin, whereas the transport and distribution of more complex lipids are accomplished by means of plasma lipoproteins.¹⁹⁶ After a systemic initiation of inflammation, phospholipase A2 (PLA2) enzymes hydrolyze PL to produce free FAs and lysoPCs, initiating the production of inflammatory lipid mediators such as AA-derived eicosanoids and platelet-activating factors (PAF).¹⁹⁷ Reduced concentrations of PCs were detected in the plasma of $\text{TNF}^{\Delta\text{ARE}/\text{WT}}$ mice already from 4 weeks onwards, proofing the observed decrease of PL in the blood of IBD patients.^{167, 198} In addition, elevated plasma protein levels and increased enzyme activity of PLA2, either released from injured intestinal cells or activated inflammatory cells, were demonstrated in the sera of IBD patients.^{197, 199} Moreover, inhibition of PLA2 activity in an animal model of TNBS-induced colitis led to an amelioration of the intestinal inflammation,¹⁹⁷ demonstrating the importance of increased PLA2 activity and PL hydrolysis in IBD. Also, an elevated release of PUFAs, especially of precursors for pro-inflammatory eicosanoids, was demonstrated in plasma of IBD patients.²⁰⁰ In $\text{TNF}^{\Delta\text{ARE}/\text{WT}}$ mice, the increased release of PUFAs, shown by reduced levels of PCs, at a constant/not changing concentration of acyl-carnitines suggests that increased PUFA release might coexists with increased fatty acid consumption, as it was previously suggested.²⁰⁰ Besides reduced levels of PCs, also the concentration of lysoPCs decreased in the plasma of $\text{TNF}^{\Delta\text{ARE}/\text{WT}}$ mice over time. LysoPCs play an important role during inflammation. They act as chemoattractants, exert signaling functions, and can be further processed forming for example PAF, further supporting inflammation.¹⁹⁶ The concentration of lysoPCs was shown to be inversely correlated with CRP concentrations and to be reduced under inflammation, in colorectal cancer, and in rheumatoid arthritis, correlating with severity.^{198, 201} In addition to PCs, SMs are the second most abundant polar lipid class in plasma lipoproteins.²⁰² SMs are carried by serum albumin and are also present in blood cells and platelets.²⁰³ Cleavage of SMs by sphingomyelinase (SMase) generates active ceramides, which have important roles in the regulation of apoptosis, inflammation, angiogenesis, and intracellular trafficking.²⁰⁴ Increased levels of ceramides were found in plasma samples for example during acute inflammation.²⁰⁵ In the plasma of $\text{TNF}^{\Delta\text{ARE}/\text{WT}}$ mice, significantly reduced levels of specific SMs were already detectable from the time point of 4 weeks onwards and therefore even before histopathological onset of the ileitis. This indicated an elevated release of ceramides already during the initial stage of the disease. In addition, it has been

shown that lipopolysaccharides (LPS) and inflammatory cytokines, especially TNF, can cause activation of SMases and subsequently lead to the hydrolysis of SMs.²⁰⁶ Also the activity of the secretory SMase, which mediates the extracellular degradation of SM to ceramides, was shown to increase during monocyte-to-macrophage differentiation,²⁰⁷ and after stimulation of endothelial cells with inflammatory cytokines.²⁰⁸ In addition, dietary SMs and inhibitors of SM metabolism are discussed to play an important role in the prevention and intervention treatment during cancer and other diseases, including IBD.²⁰⁹ For example, positive effects of nutritional SM supplementation were proven for the treatment of colon carcinogenesis.²¹⁰ Here, contrary data is available for the management of IBD.^{211, 212} The possible mechanisms involve an altered rate in IEC apoptosis as well as LPS-induced cytokine release of macrophages.^{211, 213} Moreover, recent evidence indicates, that the presence of certain 2-hydroxy fatty acids in sphingolipids have specific roles in cell signaling, where the function is best described in the nervous system.²¹⁴ The acquired LC-MS data revealed a reduction of these hydroxylated SMs in the plasma of TNF^{ΔARE/WT} animals.

In conclusion, it was possible to detect metabolic changes in the plasma of TNF^{ΔARE/WT} animals even before the histopathological onset of CD-like ileitis. Unfortunately, it was not possible to identify if the described early changes are caused by rheumatoid arthritis or IBD, or results from an interplay between both diseases.

4.3.3 Association of Colonic Lipid Alterations with the Gradual Development of Ileitis

The applied metabolomic approach, integrating untargeted ¹H NMR spectroscopy and different targeted LC-MS techniques, highlighted modifications in the intestinal lipid metabolism of TNF^{ΔARE/WT} mice concomitant to the histopathological onset of inflammation in the ileum. The results describe different biological processes associated with the disease onset, including modifications of the general cell membrane composition, alterations of the energy homeostasis, and finally the generation of fatty acid signaling mediators. These three aspects work together to modify histopathological features and body composition in TNF^{ΔARE/WT} mice (Figure 21).

4.3.3.1 Inflammation-Related Changes in the Cell Membrane Composition

TNF^{ΔARE/WT} mice developed CD-like ileitis, predominantly localized in the distal ileum, with mucosal and submucosal infiltration of inflammatory cells partially extending into the muscular layers of the bowel wall. Several of the lipid metabolites detected by ¹H NMR spectroscopy, such as cholesterol, plasmalogen, SM, GPL, as well as PUFAs, are important cell membrane constituents. Their accumulation was maybe subsequent to a massive immune cell infiltration, as it was observed by histopathological scoring, leading to an alteration of the

overall lipid membrane composition in this tissue region. Moreover, it is known that inflammatory cells typically contain a high proportion of PUFAs, especially AA, to release them under inflammatory conditions.²¹⁵ Elevated concentrations of PUFAs were indeed detected in the inflamed intestinal tissues. In addition, generation and maintenance of the correct lipid composition of different cellular compartments is an important issue for proper cell function. Quantitative changes of any membrane lipid or micro-domain like lipid rafts during ileitis might have a strong impact on cellular fluidity, structure, and function. Modifications of the cholesterol²¹⁶ or PUFA²¹⁷ content in lipid rafts of IECs, known to stabilize the tight-junction assembly, can lead to an increased paracellular permeability, a well-known phenomenon in the pathophysiology of CD.²¹⁸ This mechanism seemed to be regulated by the action of TNF²¹⁹ and therefore could have been exacerbated in TNF^{ΔARE/WT} mice.

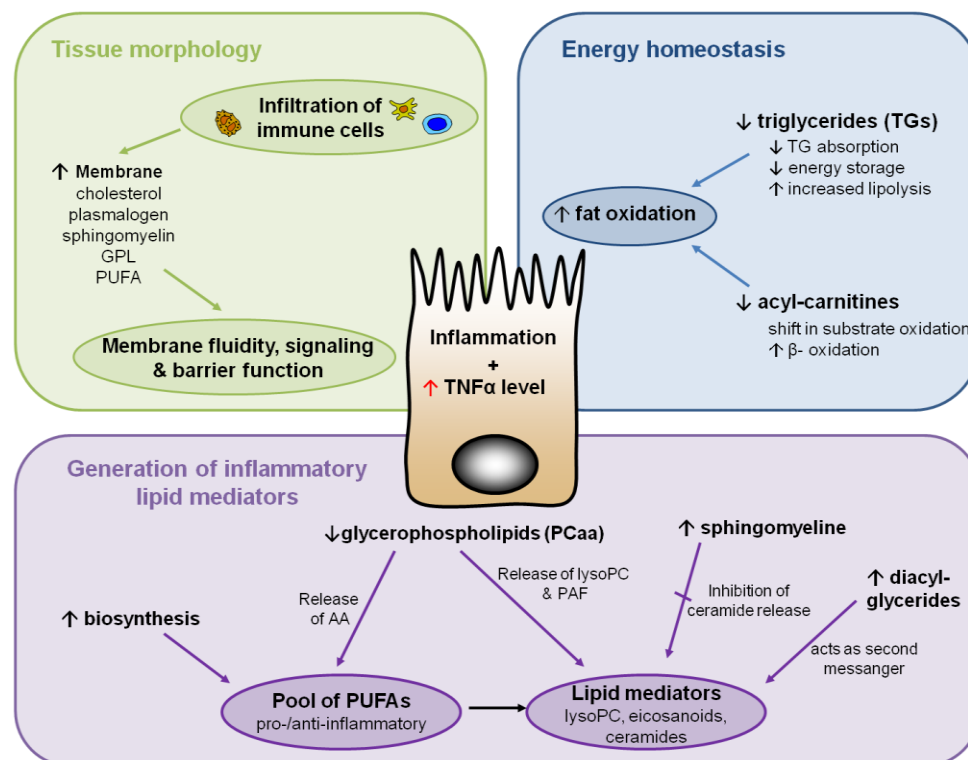


Figure 21: Schematic model of inflammation-driven alterations of lipid metabolism during CD-like ileitis in TNF^{ΔARE/WT} mice

4.3.3.2 Inflammation-Related Changes in the Energy Supply Machinery

Studies assessing body composition in CD patients previously described a reduction of body weight due to a depletion of fat but not the fat-free mass.²²⁰ In the current study, WT mice constantly increased the proportions of their adipose tissue from 12 weeks onwards, especially the subcutaneous fat fraction, whereas TNF^{ΔARE/WT} mice showed significant proportional reductions of subcutaneous and visceral fat depots over time. As previously suggested in CD

patients, these observations may indicate a shift towards lipolysis and fatty acid oxidation.²²¹ In addition, elevated TNF levels in the adipose tissue of TNF^{ΔARE/WT} mice (data not shown), whose induction of lipolytic actions is well reported, may promote increased lipolysis and fat oxidation in this animal model.²²² In contrast to the frequent finding of mesenteric fat hypertrophy in CD patients, called “creeping fat”,²²³ TNF^{ΔARE/WT} mice had smaller adipocytes when compared to WT cells in the mesenteric compartment, but also in the subcutaneous and epididymal fat.

Detection of low levels of TGs and modified levels of DAG, the degradation product of TAGs, in the intestine suggested that lipid malabsorption, leading to insufficient precursor availability, and increased TNF-driven lipolysis synergistically interact at the epithelial interface. In addition, studies in CD patients highlighted an elevated lipolysis and fatty acid oxidation, rather than the use of glucose as a metabolic fuel.^{221, 222} As alterations of other energy metabolites (amino acids, lactate, glucose as reported in other IBD models^{111, 125, 141}) were not observed, we hypothesized that under chronic intestinal inflammation IECs mainly rely on β -oxidation for their energy needs. A decrease of acyl-carnitines (C:10, C:12) was detected by LC-MS from the age of 12 weeks onwards, possibly indicating a higher use of these FAs for oxidation. As the decrease was mainly observed for medium chain acyl-carnitines, we further speculate that these FAs are now predominantly used for β -oxidation as the long chain FAs likely serve as substrate for the PUFA and lipid mediator synthesis.

4.3.3.3 Inflammation-Related Changes in Lipid Signaling

PUFAs are not only involved in the maintenance of cellular integrity by altering the fluidity and functional compartmentalization of cell membranes, but are also released as regulators of cell signaling, either by themselves or after conversion to other lipid mediators like eicosanoids. Elevated concentrations of the n-6 PUFA AA as well as Pro-inflammatory eicosanoids were found in the inflamed intestinal mucosa during the acute phase of human CD and are therefore thought to play a key role in the IBD pathogenesis.²¹⁵ In the current study, an increase of long chain polyunsaturated n-3 and n-6 FAs (C20:3 n-6, C20:4 n-6, C20:5 n-3, C22:6 n-3) was combined with a decrease of essential precursors (C18:2 n-6, C18:3 n-3) as detected by 2D-NMR spectroscopy (data not shown) in inflamed tissue regions of TNF^{ΔARE/WT} mice. Similar results were observed in earlier studies where chronic intestinal inflammation caused a similar shift in the mucosal fatty acid profile.²²⁴ It has been hypothesized that in active IBD the local PUFA biosynthesis is enhanced, coexisting with increased PUFA utilization related to the inflammatory process.²²⁴ Moreover, the hydrolysis of GPL is catalyzed by phospholipases liberating PUFAs, predominantly AA, to further initiate the production of eicosanoids to activate and/or resolve inflammation according to the nature and the timing of the formed eicosanoids.²²⁵ In our study, a decrease of GPL/PCaa was observed in TNF^{ΔARE/WT}

mice by ^1H NMR spectroscopy and LC-MS measurements, respectively. The expression and activity of the responsible enzyme, PLA2, seems to be increased under inflammation and has been shown to be elevated after TNF stimulation.²²⁶ We may hypothesize that increased biosynthesis in combination with elevated release sustain the pool of available PUFAs to fuel the generation of eicosanoids. In studies with human biopsies, leukotriene B4 and PGE2 are often reported to be elevated in the inflamed tissues of IBD patients.²²⁷ Unfortunately, we were not able to detect these two metabolites in our samples due to limited tissue availability. However, we observed significant changes of AA as well as other pro-inflammatory eicosanoids, such as PGF1 alpha and F2 alpha, which showed reduced concentration levels in $\text{TNF}^{\Delta\text{ARE}/\text{WT}}$ compared to WT mice at 12 weeks, followed by a significant increase by 16 weeks. It has been shown that the levels of these metabolites as well as of thromboxane B2 is also elevated during human IBD.²²⁷

During the release of PUFAs many other lipid mediators can be formed such as lysoPCas and DAGs. Diminished amounts of lysoPCas were observed under inflammation (see supplementary Appendix Table 6-4) in contrast to increased amounts of DAGs. DAG is a key metabolic intermediate in glycerolipid synthesis that also serves as a second messenger in regulating classical and novel protein kinase C enzymes. Besides, elevated levels of SMs, which can be hydrolyzed by SMases to release ceramides acting as pro- or anti-inflammatory mediators were detectable in the intestine of $\text{TNF}^{\Delta\text{ARE}/\text{WT}}$ mice. A reduction of the enzyme expression and activity, responsible for the sphingomyelin digestion in the intestine, was present in colorectal cancer as well as in patients with chronic colitis.²²⁸

5 CONCLUSION AND PERSPECTIVES

5.1 Comparison of the Results and Subsequent Implications

Understanding the metabolic fingerprint of IBD may be crucial for future IBD management, as this knowledge could facilitate the elucidation of the still unknown disease etiology and help to identify specific metabolic markers to improve IBD diagnosis and therapy. In the current study, metabolic variations during the development of chronic intestinal inflammation were investigated in two different animal models of IBD ($\text{TNF}^{\Delta\text{ARE}/\text{WT}}$, $\text{IL-10}^{-/-}$) through the application of holistic high-resolution ^1H NMR spectroscopy and targeted LC-MS analysis of blood plasma and intestinal tissue extracts at different time points. This integrated metabonomic approach, investigating the plasma profiles of each individual animal model at different time points, provided strong evidence for the loss of the energy homeostasis, an impaired metabolism of lipoproteins and glycosylated proteins, and the generation of pro-inflammatory signaling metabolites in the inflamed animals. But the comparison of both animal models with regard to their individual metabolic response during the development of IBD has been disregarded so far.

For a closer examination, spectral data originating from ^1H NMR spectroscopy of 24 weeks old s- $\text{IL-10}^{-/-}$ and $\text{TNF}^{\Delta\text{ARE}/\text{WT}}$ animals as well as from the respective WTs were combined into one single data set. Application of PCA initially highlighted the different genetic backgrounds of the animal models, the 129SvEv background in s- $\text{IL-10}^{-/-}$ and B6 background in $\text{TNF}^{\Delta\text{ARE}/\text{WT}}$ mice, respectively. Here only a slight grouping of samples according to their inflammation status was observed (Figure 22 A). *Via* the use of the O-PLS-DA technique, a clear separation between healthy (WT) and affected (s- $\text{IL-10}^{-/-}$ and $\text{TNF}^{\Delta\text{ARE}/\text{WT}}$) animals could be visualized. The resulting loadings plot is shown in Figure 22 B. It highlights a significant shift of the glycosylated protein metabolism, with a strong increase in these protein levels in the affected animals. Protein glycosylation and phosphorylation are very common post-translational modifications. Moreover, almost all of the key molecules involved in the innate and adaptive immune response are glycoproteins. For example, glycosylation processes are involved in the folding, quality control, and assembly of peptide-loaded MHC antigens and the T cell receptor complex. In addition, all immunoglobulins and most of the complement components are glycosylated.²²⁹ The alteration in protein glycosylation on the cell surface and in body fluids has been shown to correlate with the progression of cancer and other disease states.²³⁰ Consequently, the observed modification of plasma glycoproteins was probably either due to the induction of inflammatory-related processes or triggered by an altered lipoprotein metabolism with associated changes in the apolipoprotein fractions (described in section 4.1). In addition, these metabolic patterns were also reproduced by investigating another animal model of IBD, the $\text{RAG2}^{-/-}$ adoptive transfer model. Moreover, the feeding of a

high-fat diet, which increased the severity of the intestinal inflammation in the investigated animal model, was able to even augment this highlighted metabolic shift. As a result, the detected metabolic pattern within the glycoprotein metabolism could serve as a kind of surrogate marker in future ^1H NMR spectroscopic studies which generally occurs during chronic inflammation. However, it still needs to be clarified if this metabolic marker links to the general appearance of chronic inflammation or is implicitly specific for IBD.

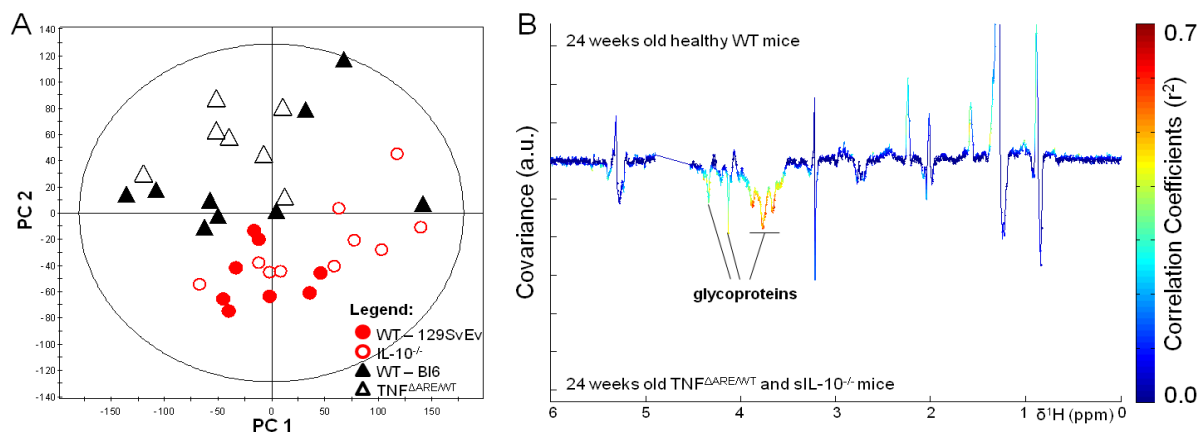


Figure 22: Analogy in the ^1H diffusion-edited NMR spectra of s-IL-10 $^{-/-}$ and TNF $^{\Delta\text{ARE/WT}}$ animals at 24 weeks of age

PCA scores (A) and O-PLS-DA coefficient (B) plots plot derived from ^1H diffusion-edited NMR spectra of plasma at 24 weeks of age indicating discrimination between the genotypes of the animal models: B16 (triangle, black), TNF $^{\Delta\text{ARE/WT}}$ (open triangle, black), 129SvEv (dot, red), and s-IL-10 $^{-/-}$ (circle, red) mice. The color code corresponds to the correlation coefficients of the variables.

In contrast to that, comparison of the different metabolite changes resulting from the targeted LC-MS analysis, using the AbsoluteIDQTM Kit, of plasma samples from 24 weeks old TNF $^{\Delta\text{ARE/WT}}$ and s-IL-10 $^{-/-}$ animals through using Venn diagrams, revealed that the detected metabolite differences were specific for each investigated animal model (Figure 23). Only the concentration changes of the amino acid tyrosine seemed to be consistently regulated, but the direction of these changes was the opposite in TNF $^{\Delta\text{ARE/WT}}$ and s-IL-10 $^{-/-}$ animals at this time point. Consequently, these investigations indicate that metabolite profiling using a targeted LC-MS technique is able to reveal unique metabolic fingerprints associated with the specific site of disease location in the intestine (ileum/colon). Therefore, further metabonomic studies in the context of IBD should be further implemented to establish a new diagnostic tool to distinguish between UC and CD in human patients based on the current findings.

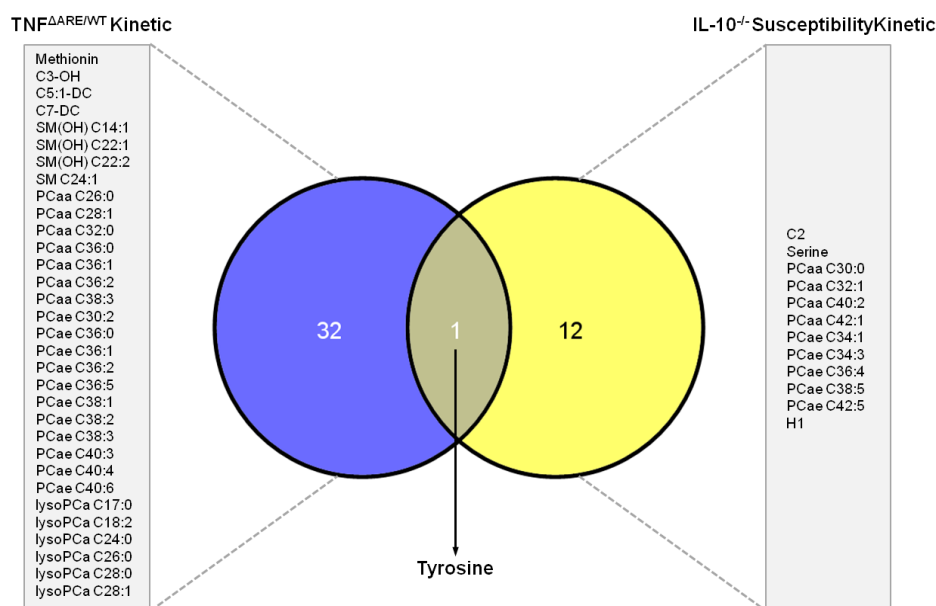


Figure 23: Parallels in the targeted LC-MS analysis of ileal tissue from TNF Δ ARE/WT animals and colonic tissue from s-IL-10 $^{-/-}$ animals at 24 weeks of age

Key: C: acyl-carnitine; lysoPCa: lysophosphatidylcholine; PCaa: phosphatidylcholine; PCae: phosphatidylcholine with an ether bond; SM: sphingomyelin.

* tyrosine is regulated oppositional in both data sets

5.2 Implications and Potential Future Studies

Although the application of metabonomics in the context of IBD is only in its infancy, first approaches have already depicted the potentialities of this technique as evidenced by the recent literature (Table 1-2). In the current study, the potential of metabonomic approaches to decipher UC- and CD-induced metabolic changes was demonstrated in plasma and intestinal tissue extracts of two IBD animal models. Moreover, it was highlighted that the metabolic profile of quiescent intestinal parts of inflamed mice tend to be already different from the control profiles, becoming significantly modified in the inflamed parts, as previously reported in IBD patients.^{111, 140} Furthermore, it was shown that early metabolite changes associated with the susceptibility for IBD can be detected *via* metabolite profiling. Taken together, this illustrates the enormous potential of metabonomic techniques, including ^1H NMR spectroscopy and LC-MS analyses, in terms of unraveling the unknown IBD disease etiology, hypothesis formation, biomarker identification, improvements to clinical diagnosis, and generation of prognostic information. The possibilities seem to be almost endless especially with regard to the ongoing developments of the analytical techniques and the advances in chemometric algorithms. Consequently, it should now be feasible to target specific metabolic pathways to get new insights into deregulated molecular mechanisms in future studies. In particular, the current metabonomic study could for example be completed by additional urine and fecal analysis to gain insights in time-averaged metabolic changes on the activity of the gut microbiota.

In the clinical situation, an easy accessible marker to uncover a human IBD predisposition or to diagnose very early stages of IBD in a non-invasive way is not available at the moment. Metabonomic tools are already successfully applied in small experimental set-ups to distinguish between UC and CD of human intestinal biopsies, plasma, urine, and fecal extract samples at an advanced disease state.^{110-112, 127, 137, 139-142} But so far, the validation of the identified markers and the translation to the clinical situation is still missing. Moreover, no single study investigated the metabolic effects of IBD susceptibility or metabolic changes associates with early stages of the disease in the human situation. Unfortunately, the translation of metabonomic data obtained from IBD animal models to humans is doubtful, but nevertheless they provide promising examples for the integration of the newly developed technological approaches. In addition, metabolite differences reported for IBD subjects and controls vary in between the studies, which may be attributed to differences in sample type, research approach (targeted or holistic analysis), and the lack of confirmation of metabolite identity with authentic standards.⁸⁹ Consequently, further research is required to validate these metabolite differences and improve the accuracy of metabolite markers for clinical IBD applications. Furthermore, the recent findings should also be confirmed with prospective and blinded analyses of IBD tissues. Besides all this, the generation of prognostic biomarkers with the help of metabonomic tools should be used to assess the likelihood for future illness. The ability to detect early inflammatory changes that are not apparent on endoscopy could have a significant impact on the treatment and management of IBD. The perspective of preventing IBD and normalizing their undesirable effects by specific nutritional interventions, such as probiotics or other functional ingredients, could benefit from the application of metabonomic for therapeutic surveillance, assessment of treatment efficacy, and therefore, it should have an impact on management of IBD. Moreover, defining the metabolic phenotype of human populations will offer a great opportunity to evaluate the metabolic response and the degree of this response to the development of IBD at the individual level. It is discussed as a promising approach towards personalized nutrition to provide health maintenance at individual level. In addition, the prospects of metabonomics is tremendously amplified when combined with other “omics” technologies, such as proteomics, genomics, and transcriptomics, becoming an important part of the global systems biology platform. However, so far these combination studies are a relatively new concept, and further investigation into their possible application in the context of IBD is still warranted.

6 APPENDIX

Appendix Table 6-1: All significantly regulated metabolites in the plasma of s-IL-10^{-/-} compared to WT mice at the age of 4, 8, 12, 16, and 24 weeks analyzed by UPLC-ESI-MS/MS using the AbsoluteIDQ™ kit (Biocrates Life Sciences, Austria)

		4 weeks		8 weeks		12 weeks		16 weeks		24 weeks	
Regulated metabolites		41		14		6		8		13	
Metabolites [μ M]		WT Mean \pm SD	s-IL10 ^{-/-} Mean \pm SD	WT Mean \pm SD	s-IL10 ^{-/-} Mean \pm SD	WT Mean \pm SD	s-IL10 ^{-/-} Mean \pm SD	WT Mean \pm SD	s-IL10 ^{-/-} Mean \pm SD	WT Mean \pm SD	s-IL10 ^{-/-} Mean \pm SD
Amino acids	Arg-PTC	119.26 \pm 21.20	93.40 \pm 22.57*	116.95 \pm 15.26	120.28 \pm 24.96	114.77 \pm 23.49	96.53 \pm 20.75	109.20 \pm 21.74	99.33 \pm 17.73	94.80 \pm 14.52	90.54 \pm 20.56
	Gln-PTC	1134.00 \pm 113.60	975.29 \pm 126.78*	1058.25 \pm 123.21	856.75 \pm 114.06**	926.71 \pm 156.13	835.50 \pm 75.87	896.83 \pm 87.58	850.83 \pm 206.01	839.25 \pm 54.99	800.20 \pm 71.88
	Gly-PTC	235.14 \pm 31.05	210.43 \pm 42.56	218.75 \pm 23.87	187.38 \pm 38.95	196.29 \pm 28.18	160.67 \pm 10.86*	225.00 \pm 56.34	152.00 \pm 23.12*	195.00 \pm 48.53	167.60 \pm 29.06
	His-PTC	90.87 \pm 13.42	68.19 \pm 11.30**	76.94 \pm 13.22	82.28 \pm 10.60	85.99 \pm 18.72	86.13 \pm 14.65	76.90 \pm 8.06	75.18 \pm 4.83	83.59 \pm 13.47	74.45 \pm 10.16
	Orn-PTC	47.60 \pm 9.64	38.01 \pm 16.10	35.33 \pm 8.16	47.26 \pm 10.35*	44.83 \pm 12.79	48.13 \pm 11.30	48.98 \pm 6.08	50.93 \pm 15.11	48.10 \pm 11.04	48.75 \pm 19.37
	Phe-PTC	54.01 \pm 6.88	53.09 \pm 9.80	51.81 \pm 5.77	62.06 \pm 7.53**	60.56 \pm 8.13	64.97 \pm 4.36	60.82 \pm 14.79	57.27 \pm 6.88	62.10 \pm 9.85	58.24 \pm 4.34
	Ser-PTC	100.24 \pm 20.45	90.66 \pm 10.16	99.30 \pm 8.35	91.71 \pm 12.43	96.57 \pm 19.33	88.92 \pm 13.05	103.57 \pm 6.65	94.20 \pm 17.58	100.60 \pm 14.44	80.80 \pm 14.80*
	Tyr-PTC	53.96 \pm 14.15	72.10 \pm 9.27*	63.54 \pm 14.49	58.63 \pm 13.29	62.43 \pm 16.65	64.30 \pm 11.73	71.43 \pm 14.06	75.98 \pm 29.03	49.55 \pm 10.41	67.46 \pm 17.76*
	Val-PTC	129.17 \pm 31.98	119.21 \pm 45.42	113.34 \pm 27.43	159.38 \pm 32.05**	141.14 \pm 17.80	132.33 \pm 16.07	131.47 \pm 46.03	122.37 \pm 15.41	147.38 \pm 32.54	133.34 \pm 20.94
xLeu-PTC	222.71 \pm 38.57	197.86 \pm 64.73	208.25 \pm 47.50	293.75 \pm 46.08**	252.29 \pm 23.29	272.67 \pm 46.04	242.50 \pm 89.02	204.67 \pm 37.09	252.13 \pm 55.65	225.20 \pm 27.23	
Acetylcarnitines	C2	28.34 \pm 7.75	15.92 \pm 3.31**	35.51 \pm 4.08	30.58 \pm 9.79	32.81 \pm 5.34	34.70 \pm 9.92	32.38 \pm 8.64	31.48 \pm 4.55	38.38 \pm 5.46	28.90 \pm 8.99*
	C3	0.66 \pm 0.42	0.26 \pm 0.08*	0.80 \pm 0.15	0.56 \pm 0.11**	0.75 \pm 0.15	0.61 \pm 0.32	0.80 \pm 0.44	0.59 \pm 0.24	0.55 \pm 0.13	0.58 \pm 0.28
	C4	0.98 \pm 0.49	0.47 \pm 0.13*	1.06 \pm 0.22	0.81 \pm 0.26	0.93 \pm 0.32	0.96 \pm 0.40	0.92 \pm 0.36	0.77 \pm 0.28	0.79 \pm 0.29	0.84 \pm 0.39
	C5	0.44 \pm 0.12	0.20 \pm 0.06***	0.29 \pm 0.15	0.32 \pm 0.06	0.23 \pm 0.07	0.28 \pm 0.15	0.30 \pm 0.11	0.29 \pm 0.10	0.26 \pm 0.07	0.24 \pm 0.08
	C5-OH (C3-DC-M)	0.13 \pm 0.03	0.08 \pm 0.04*	0.14 \pm 0.04	0.10 \pm 0.03*	0.12 \pm 0.03	0.12 \pm 0.05	0.12 \pm 0.05	0.12 \pm 0.03	0.12 \pm 0.04	0.10 \pm 0.03
	C6 (C4:1-DC)	0.13 \pm 0.04	0.12 \pm 0.03	0.17 \pm 0.02	0.11 \pm 0.04**	0.12 \pm 0.04	0.14 \pm 0.04	0.12 \pm 0.04	0.12 \pm 0.02	0.13 \pm 0.03	0.12 \pm 0.04
	C8	0.17 \pm 0.03	0.14 \pm 0.02*	0.15 \pm 0.03	0.16 \pm 0.03	0.17 \pm 0.02	0.15 \pm 0.02	0.14 \pm 0.03	0.14 \pm 0.02	0.14 \pm 0.02	0.14 \pm 0.03
	C12	0.16 \pm 0.03	0.17 \pm 0.02	0.17 \pm 0.03	0.13 \pm 0.03*	0.14 \pm 0.02	0.16 \pm 0.03	0.15 \pm 0.02	0.13 \pm 0.04	0.13 \pm 0.03	0.15 \pm 0.04
	C14:1	0.13 \pm 0.03	0.12 \pm 0.02	0.17 \pm 0.02	0.14 \pm 0.02*	0.13 \pm 0.02	0.14 \pm 0.03	0.12 \pm 0.02	0.15 \pm 0.03	0.13 \pm 0.02	0.14 \pm 0.03
	C14:1-OH	0.012 \pm 0.003	0.011 \pm 0.005	0.013 \pm 0.006	0.009 \pm 0.005	0.008 \pm 0.004	0.015 \pm 0.006*	0.011 \pm 0.002	0.008 \pm 0.006	0.011 \pm 0.006	0.012 \pm 0.004
	C14:2	0.016 \pm 0.005	0.023 \pm 0.006*	0.029 \pm 0.006	0.018 \pm 0.007**	0.021 \pm 0.008	0.020 \pm 0.007	0.027 \pm 0.007	0.014 \pm 0.008*	0.019 \pm 0.004	0.020 \pm 0.007
	C14:2-OH	0.014 \pm 0.004	0.011 \pm 0.004	0.010 \pm 0.004	0.013 \pm 0.004	0.008 \pm 0.002	0.013 \pm 0.003**	0.010 \pm 0.003	0.009 \pm 0.004	0.012 \pm 0.004	0.012 \pm 0.005
	C16	0.20 \pm 0.03	0.28 \pm 0.05**	0.23 \pm 0.02	0.22 \pm 0.05	0.17 \pm 0.02	0.19 \pm 0.03	0.15 \pm 0.02	0.16 \pm 0.02	0.20 \pm 0.02	0.18 \pm 0.03
	C16:2	0.02 \pm 0.01	0.01 \pm 0.01	0.02 \pm 0.01	0.02 \pm 0.01	0.02 \pm 0.01	0.02 \pm 0.01	0.02 \pm 0.01	0.02 \pm 0.01	0.01 \pm 0.01*	0.02 \pm 0.01
	C18	0.05 \pm 0.01	0.07 \pm 0.01*	0.06 \pm 0.02	0.05 \pm 0.01	0.05 \pm 0.01	0.06 \pm 0.02	0.04 \pm 0.01	0.04 \pm 0.01	0.05 \pm 0.02	0.05 \pm 0.01
C18:1	0.16 \pm 0.02	0.20 \pm 0.05	0.21 \pm 0.03	0.18 \pm 0.05	0.15 \pm 0.03	0.20 \pm 0.03*	0.18 \pm 0.04	0.18 \pm 0.05	0.18 \pm 0.02	0.18 \pm 0.04	
C18:1-OH	0.011 \pm 0.003	0.018 \pm 0.004**	0.019 \pm 0.004	0.019 \pm 0.006	0.016 \pm 0.005	0.016 \pm 0.001	0.013 \pm 0.004	0.015 \pm 0.007	0.016 \pm 0.004	0.016 \pm 0.004	
C18:2	0.07 \pm 0.02	0.10 \pm 0.02*	0.10 \pm 0.03	0.08 \pm 0.02	0.09 \pm 0.01	0.09 \pm 0.02	0.11 \pm 0.03	0.08 \pm 0.02	0.09 \pm 0.02	0.08 \pm 0.02	

		4 weeks		8 weeks		12 weeks		16 weeks		24 weeks		
Regulated metabolites		41		14		6		8		13		
Metabolites [μM]		WT Mean \pm SD	s-IL10 ^{-/-} Mean \pm SD	WT Mean \pm SD	s-IL10 ^{-/-} Mean \pm SD	WT Mean \pm SD	s-IL10 ^{-/-} Mean \pm SD	WT Mean \pm SD	s-IL10 ^{-/-} Mean \pm SD	WT Mean \pm SD	s-IL10 ^{-/-} Mean \pm SD	
Sugar	H1	5660.43 \pm 480.57	6100.00 \pm 843.01	6269.38 \pm 581.19	5647.63 \pm 842.07	5525.29 \pm 444.21	6904.33 \pm 1818.09	5841.67 \pm 698.21	5288.67 \pm 361.08	5617.13\pm767.37	7274.30\pm983.88**	
	Sphingolipids	SM C18:0	3.97\pm1.01	5.87\pm1.54*	4.52 \pm 1.41	4.77 \pm 1.79	4.34 \pm 1.65	4.70 \pm 2.32	4.47 \pm 1.92	6.80 \pm 2.84	4.68 \pm 2.20	5.07 \pm 2.89
		SM C24:0	13.83\pm2.05	11.56\pm1.05*	15.79 \pm 5.41	16.03 \pm 4.57	15.96 \pm 2.98	16.10 \pm 4.33	14.28 \pm 4.47	11.87 \pm 2.14	16.11 \pm 3.44	17.40 \pm 5.34
		SM (OH) C22:2	3.48\pm0.57	2.73\pm0.54*	4.42 \pm 1.06	4.51 \pm 0.53	5.36 \pm 1.02	5.21 \pm 0.95	4.63 \pm 1.21	3.87 \pm 1.05	5.61 \pm 1.24	4.65 \pm 0.94
SM (OH) C24:1		0.43 \pm 0.19	0.40 \pm 0.20	0.78\pm0.20	0.47\pm0.20**	0.70 \pm 0.24	0.51 \pm 0.26	0.52\pm0.08	0.71\pm0.16*	0.66 \pm 0.14	0.65 \pm 0.29	
Glycerophospholipids	PC aa C30:0	0.81 \pm 0.21	0.93 \pm 0.19	0.91 \pm 0.07	0.79 \pm 0.23	0.70 \pm 0.10	0.72 \pm 0.10	0.76 \pm 0.15	0.75 \pm 0.07	0.73\pm0.08	0.91\pm0.20*	
	PC aa C32:1	3.75\pm0.91	2.63\pm0.50*	2.69 \pm 0.51	3.36 \pm 0.98	2.87 \pm 0.45	3.43 \pm 1.33	2.24 \pm 0.39	2.36 \pm 0.52	2.30\pm0.32	3.36\pm1.07*	
	PC aa C34:1	138.57\pm23.73	99.87\pm11.98**	106.85 \pm 33.84	116.74 \pm 33.77	113.00 \pm 17.20	139.38 \pm 38.45	85.45 \pm 21.04	94.47 \pm 11.15	93.81 \pm 11.79	110.72 \pm 25.84	
	PC aa C34:3	8.06\pm0.59	7.14\pm0.44**	7.75 \pm 2.31	9.75 \pm 2.20	9.09 \pm 1.67	11.68 \pm 3.57	8.58 \pm 2.01	7.36 \pm 1.82	9.18 \pm 1.66	10.96 \pm 4.18	
	PC aa C36:1	23.69\pm3.27	19.93\pm2.42*	19.73 \pm 4.14	23.15 \pm 4.99	22.69 \pm 2.43	26.18 \pm 4.71	19.28 \pm 2.99	19.90 \pm 1.78	22.03 \pm 3.90	24.04 \pm 3.75	
	PC aa C36:3	54.30\pm7.57	35.96\pm3.77***	54.51 \pm 15.69	65.85 \pm 20.33	66.27 \pm 8.84	74.80 \pm 22.11	58.13 \pm 10.90	50.22 \pm 9.74	60.81 \pm 9.23	71.83 \pm 23.22	
	PC aa C36:5	4.43\pm1.15	3.24\pm0.44*	4.33 \pm 1.02	5.32 \pm 1.52	5.64 \pm 0.57	6.04 \pm 1.15	5.36 \pm 0.50	4.36 \pm 0.57	5.12 \pm 1.09	5.87 \pm 1.89	
	PC aa C36:6	0.29\pm0.10	0.18\pm0.04*	0.20 \pm 0.06	0.27 \pm 0.10	0.28 \pm 0.05	0.30 \pm 0.09	0.22 \pm 0.11	0.22 \pm 0.09	0.25 \pm 0.09	0.26 \pm 0.10	
	PC aa C38:3	20.41\pm2.65	15.74\pm1.59**	20.70 \pm 4.60	24.10 \pm 6.59	24.14 \pm 2.45	27.23 \pm 5.79	20.60 \pm 4.54	19.07 \pm 1.98	22.03 \pm 3.15	24.82 \pm 6.50	
	PC aa C38:4	93.21\pm4.85	107.61\pm14.65*	113.68\pm11.19	131.00\pm17.32*	126.29 \pm 24.96	129.50 \pm 12.24	122.17 \pm 11.20	115.50 \pm 16.56	114.40 \pm 24.05	122.80 \pm 23.00	
	PC aa C38:5	30.09\pm4.42	25.13\pm2.34*	31.61 \pm 7.05	38.81 \pm 10.80	41.23 \pm 3.19	43.73 \pm 7.75	34.68 \pm 4.89	30.03 \pm 5.15	36.40 \pm 8.42	38.92 \pm 9.40	
	PC aa C40:2	0.44 \pm 0.11	0.44 \pm 0.12	0.58 \pm 0.21	0.67 \pm 0.25	0.57 \pm 0.16	0.76 \pm 0.36	0.56 \pm 0.19	0.41 \pm 0.19	0.52\pm0.19	0.82\pm0.36*	
	PC aa C40:4	2.39\pm0.31	2.10\pm0.13*	3.08 \pm 1.33	3.69 \pm 1.81	3.35 \pm 0.70	4.13 \pm 1.59	2.88 \pm 0.96	2.42 \pm 0.75	2.76 \pm 0.78	3.85 \pm 1.61	
	PC aa C40:6	39.04\pm4.45	46.07\pm6.58*	44.59 \pm 5.57	47.24 \pm 6.88	46.39 \pm 3.94	50.93 \pm 5.12	47.98 \pm 7.97	48.53 \pm 8.89	44.89 \pm 6.59	47.83 \pm 8.23	
	PC aa C42:0	0.17 \pm 0.07	0.18 \pm 0.07	0.23 \pm 0.06	0.30 \pm 0.11	0.22\pm0.05	0.37\pm0.07**	0.25 \pm 0.05	0.27 \pm 0.06	0.23 \pm 0.06	0.25 \pm 0.07	
	PC aa C42:1	0.20 \pm 0.08	0.17 \pm 0.07	0.21 \pm 0.04	0.27 \pm 0.08	0.25 \pm 0.06	0.27 \pm 0.07	0.27 \pm 0.04	0.21 \pm 0.08	0.16\pm0.03	0.23\pm0.05**	
	PC ae C34:1	0.21 \pm 0.06	0.19 \pm 0.10	0.24 \pm 0.08	0.22 \pm 0.13	0.19 \pm 0.06	0.18 \pm 0.11	0.23 \pm 0.09	0.19 \pm 0.07	0.19\pm0.06	0.24\pm0.07*	
	PC ae C34:3	0.21\pm0.21	0.23\pm0.27**	0.16 \pm 0.16	0.22 \pm 0.25	0.13 \pm 0.16	0.24 \pm 0.23	0.15 \pm 0.20	0.16 \pm 0.22	0.13\pm0.11	0.23\pm0.21*	
	PC ae C36:1	0.10\pm0.04	0.12\pm0.07**	0.13 \pm 0.08	0.12 \pm 0.07	0.07 \pm 0.02	0.10 \pm 0.06	0.11 \pm 0.08	0.14 \pm 0.08	0.09 \pm 0.04	0.14 \pm 0.08	
	PC ae C36:4	0.64 \pm 0.19	0.48 \pm 0.15	0.66 \pm 0.20	0.69 \pm 0.23	0.58 \pm 0.08	0.71 \pm 0.19	0.66 \pm 0.15	0.75 \pm 0.21	0.71\pm0.09	0.86\pm0.20**	
	PC ae C36:5	2.97\pm0.42	2.53\pm0.38*	2.90 \pm 0.58	3.29 \pm 0.80	3.24 \pm 0.35	3.42 \pm 0.56	3.02 \pm 0.61	2.82 \pm 0.55	3.04 \pm 0.29	3.59 \pm 0.60	
	PC ae C38:0	0.86\pm0.14	0.69\pm0.02*	0.96 \pm 0.31	1.21 \pm 0.36	1.18 \pm 0.20	1.57 \pm 0.75	1.25 \pm 0.44	1.24 \pm 0.45	1.23 \pm 0.35	1.68 \pm 0.46	
	PC ae C38:3	2.68\pm0.48	1.99\pm0.22***	2.66 \pm 0.57	2.85 \pm 0.74	2.85 \pm 0.47	3.13 \pm 0.49	2.54 \pm 0.84	2.58 \pm 0.48	2.68 \pm 0.47	2.76 \pm 0.55	
	PC ae C38:5	2.42 \pm 0.19	2.40 \pm 0.35	3.10 \pm 0.78	3.98 \pm 1.04	3.75 \pm 0.44	3.72 \pm 0.74	3.36 \pm 0.77	3.09 \pm 0.77	3.11\pm0.70	4.05\pm0.62*	
PC ae C40:0	1.32\pm0.18	1.09\pm0.15**	1.70 \pm 0.35	2.06 \pm 0.46	2.01 \pm 0.36	2.18 \pm 0.43	2.17 \pm 0.44	2.25 \pm 0.76	2.05 \pm 0.45	2.36 \pm 0.34		
PC ae C40:1	2.26\pm0.39	1.81\pm0.27*	2.44 \pm 0.70	3.07 \pm 0.78	3.12 \pm 0.64	3.86 \pm 0.94	3.15\pm0.83	2.59\pm0.61*	3.06 \pm 0.56	3.39 \pm 1.20		

	4 weeks		8 weeks		12 weeks		16 weeks		24 weeks	
Regulated metabolites	41		14		6		8		13	
Metabolites [μ M]	WT Mean \pm SD	s-IL10 ^{-/-} Mean \pm SD	WT Mean \pm SD	s-IL10 ^{-/-} Mean \pm SD	WT Mean \pm SD	s-IL10 ^{-/-} Mean \pm SD	WT Mean \pm SD	s-IL10 ^{-/-} Mean \pm SD	WT Mean \pm SD	s-IL10 ^{-/-} Mean \pm SD
PC ae C40:3	1.49\pm0.16	1.10\pm0.10*	1.59\pm0.40	1.68\pm0.49**	1.83 \pm 0.15	1.77 \pm 0.31	1.63 \pm 0.31	1.43 \pm 0.26	1.72 \pm 0.29	1.76 \pm 0.54
PC ae C40:4	2.15\pm0.23	2.05\pm0.33*	2.55 \pm 0.59	3.19 \pm 0.65	3.21 \pm 0.41	3.00 \pm 0.38	3.04 \pm 0.60	2.85 \pm 0.62	2.86 \pm 0.42	3.29 \pm 0.41
PC ae C42:1	16.41 \pm 1.65	13.49 \pm 0.97	19.26 \pm 4.39	21.70 \pm 5.24	23.49 \pm 2.27	24.82 \pm 3.64	22.95\pm2.74	19.75\pm2.84*	22.81 \pm 3.46	23.69 \pm 5.46
PC ae C42:3	2.08 \pm 0.36	1.73 \pm 0.12	2.82 \pm 1.05	3.13 \pm 1.26	3.59 \pm 1.14	3.21 \pm 0.83	3.85\pm1.22	2.19\pm0.63*	3.29 \pm 1.00	3.50 \pm 1.52
PC ae C42:5	0.83 \pm 0.12	0.64 \pm 0.13	0.83 \pm 0.23	1.12 \pm 0.16	1.02 \pm 0.21	1.00 \pm 0.14	1.00 \pm 0.23	0.78 \pm 0.25	0.90\pm0.21	0.98\pm0.30**
PC ae C44:6	2.17 \pm 0.27	1.85 \pm 0.24	2.89 \pm 0.68	3.62 \pm 0.98	3.50\pm0.39	3.46\pm0.53*	3.45 \pm 0.58	2.84 \pm 0.81	3.19 \pm 0.43	3.58 \pm 0.85
lysoPC a C18:1	1.06\pm0.22	0.90\pm0.16*	1.60 \pm 0.59	1.80 \pm 0.84	1.56 \pm 0.46	1.99 \pm 0.76	1.56 \pm 0.51	1.16 \pm 0.44	1.45 \pm 0.36	1.94 \pm 0.79
lysoPC a C20:3	0.56\pm0.13	0.64\pm0.16**	0.89 \pm 0.20	0.91 \pm 0.37	0.97 \pm 0.22	1.01 \pm 0.21	1.02 \pm 0.24	0.68 \pm 0.19	0.84 \pm 0.15	0.93 \pm 0.30

NB: All metabolite concentrations are presented as mean values \pm SD from 6 animals per group. The values from s-IL-10^{-/-} animals were compared at each time point with the WT mice. Significant differences were assessed by Mann-Whitney U test and marked as follows: *p<0.05, **p<0.01, ***p<0.001.

Key: Arg: arginine; C: acyl-carnitine; Gln: glutamine; Gly: glycine; H: basic sugar structure; His: histidine; lysoPCa: lysophosphatidylcholine; Orn: ornithine; PCaa: phosphatidylcholine; PCae: phosphatidylcholine with an ether bond; Phe: phenylalanine; Ser: serine; SM: sphingomyelin; Tyr: tyrosine; Val: valine; xLeu: leucine.

Appendix Table 6-2: All significantly regulated metabolites in the proximal colon of s-IL-10^{-/-} compared to WT mice at the age of 4, 8, 12, 16, and 24 weeks analyzed by UPLC-ESI-MS/MS using the AbsoluteIDQ™ kit (Biocrates Life Sciences, Austria)

Comparisons		4 weeks		8 weeks		12 weeks		16 weeks		24 weeks	
Regulated metabolites		18		7		5		2		5	
Metabolites [μM]		WT Mean ± SD	s-IL10 ^{-/-} Mean ± SD	WT Mean ± SD	s-IL10 ^{-/-} Mean ± SD	WT Mean ± SD	s-IL10 ^{-/-} Mean ± SD	WT Mean ± SD	s-IL10 ^{-/-} Mean ± SD	WT Mean ± SD	s-IL10 ^{-/-} Mean ± SD
Amino acids	Arg-PTC	1.4452 ± 0.2268	1.3721 ± 0.4910	1.6451 ± 0.4617	2.0033 ± 0.7277	2.1230 ± 1.3107	2.5591 ± 0.3024	2.5549 ± 0.5065	1.8816 ± 0.5004*	1.6535 ± 0.5245	1.8444 ± 0.5234
	Met-PTC	0.9032 ± 0.1073	0.8653 ± 0.3055	1.0537 ± 0.4748	1.3035 ± 0.4370	1.1144 ± 0.2395	1.4253 ± 0.1935*	1.4211 ± 0.1958	1.2698 ± 0.2694	0.8894 ± 0.2718	1.1775 ± 0.3251
	Trp-PTC	0.5373 ± 0.0380	0.5719 ± 0.0966	0.5698 ± 0.1686	0.6158 ± 0.1535	0.6067 ± 0.0732	0.7912 ± 0.1918*	0.6269 ± 0.0798	0.6616 ± 0.1184	0.5852 ± 0.1288	0.6392 ± 0.0839
Acetylcarnitines	C2	0.3849 ± 0.0528	0.4896 ± 0.0874*	0.4440 ± 0.0877	0.5031 ± 0.0711	0.4792 ± 0.1145	0.4821 ± 0.1176	0.4740 ± 0.0975	0.5999 ± 0.1359	0.5261 ± 0.1070	0.5021 ± 0.0607
	C3-DC (C4-OH)	0.0122 ± 0.0039	0.0104 ± 0.0020*	0.0093 ± 0.0041	0.0162 ± 0.0042**	0.0116 ± 0.0043	0.0167 ± 0.0068	0.0154 ± 0.0085	0.0177 ± 0.0066	0.0112 ± 0.0058	0.0148 ± 0.0067
	C4	0.0898 ± 0.0220	0.0624 ± 0.0409	0.0392 ± 0.0349	0.1068 ± 0.0345**	0.0656 ± 0.0419	0.0666 ± 0.0513	0.0812 ± 0.0489	0.1126 ± 0.0426	0.0702 ± 0.0614	0.1015 ± 0.0577
	C4:1	0.0007 ± 0.0005	0.0002 ± 0.0005	0.0003 ± 0.0004	0.0010 ± 0.0006*	0.0003 ± 0.0003	0.0004 ± 0.0004	0.0004 ± 0.0004	0.0005 ± 0.0006	0.0005 ± 0.0005	0.0005 ± 0.0004
	C5	0.0109 ± 0.0034	0.0069 ± 0.0023*	0.0100 ± 0.0061	0.0171 ± 0.0054*	0.0123 ± 0.0040	0.0129 ± 0.0072	0.0133 ± 0.0044	0.0167 ± 0.0050	0.0094 ± 0.0052	0.0168 ± 0.0051**
	C5-M-DC	0.0022 ± 0.0009	0.0051 ± 0.0024**	0.0032 ± 0.0020	0.0022 ± 0.0012	0.0028 ± 0.0016	0.0021 ± 0.0010	0.0018 ± 0.0011	0.0022 ± 0.0011	0.0044 ± 0.0019	0.0020 ± 0.0010**
	C12:1	0.0113 ± 0.0050	0.0132 ± 0.0060	0.0122 ± 0.0028	0.0086 ± 0.0027*	0.0113 ± 0.0040	0.0110 ± 0.0034	0.0120 ± 0.0034	0.0117 ± 0.0041	0.0112 ± 0.0040	0.0108 ± 0.0033
	C16:1	0.0022 ± 0.0003	0.0028 ± 0.0006*	0.0024 ± 0.0005	0.0025 ± 0.0003	0.0024 ± 0.0003	0.0024 ± 0.0006	0.0026 ± 0.0005	0.0027 ± 0.0010	0.0027 ± 0.0004	0.0022 ± 0.0004*
C16:2-OH	0.0003 ± 0.0001	0.0003 ± 0.0001	0.0003 ± 0.0001	0.0001 ± 0.0001**	0.0003 ± 0.0002	0.0003 ± 0.0001	0.0004 ± 0.0003	0.0003 ± 0.0001	0.0003 ± 0.0001	0.0002 ± 0.0001	0.0002 ± 0.0001
	SM C18:1	0.0094 ± 0.0053	0.0161 ± 0.0053*	0.0140 ± 0.0063	0.0149 ± 0.0066	0.0143 ± 0.0087	0.0082 ± 0.0070	0.0165 ± 0.0085	0.0134 ± 0.0039	0.0159 ± 0.0063	0.0122 ± 0.0065
Glycerophospholipids	PC aa C28:1	0.0035 ± 0.0015	0.0057 ± 0.0050	0.0031 ± 0.0019	0.0030 ± 0.0012	0.0054 ± 0.0023	0.0011 ± 0.0011**	0.0057 ± 0.0035	0.0035 ± 0.0028	0.0061 ± 0.0040	0.0083 ± 0.0058
	PC aa C34:3	0.0146 ± 0.0073	0.0236 ± 0.0052*	0.0183 ± 0.0083	0.0199 ± 0.0042	0.0172 ± 0.0051	0.0169 ± 0.0117	0.0237 ± 0.0074	0.0214 ± 0.0081	0.0214 ± 0.0094	0.0192 ± 0.0069
	PC aa C36:2	0.0888 ± 0.0480	0.1415 ± 0.0333*	0.1218 ± 0.0569	0.1410 ± 0.0527	0.1280 ± 0.0430	0.0911 ± 0.0553	0.1638 ± 0.0685	0.1259 ± 0.0208	0.1240 ± 0.0481	0.1122 ± 0.0418
	PC aa C38:0	0.0058 ± 0.0024	0.0086 ± 0.0020*	0.0066 ± 0.0029	0.0067 ± 0.0020	0.0065 ± 0.0037	0.0069 ± 0.0024	0.0082 ± 0.0027	0.0089 ± 0.0021	0.0064 ± 0.0023	0.0064 ± 0.0021
	PC aa C42:1	0.0009 ± 0.0009	0.0016 ± 0.0011	0.0011 ± 0.0008	0.0022 ± 0.0012*	0.0015 ± 0.0015	0.0015 ± 0.0018	0.0015 ± 0.0012	0.0018 ± 0.0007	0.0013 ± 0.0009	0.0015 ± 0.0009
	PC ae C30:0	0.0140 ± 0.0076	0.0174 ± 0.0044	0.0136 ± 0.0066	0.0125 ± 0.0047	0.0133 ± 0.0062	0.0108 ± 0.0056	0.0123 ± 0.0040	0.0123 ± 0.0027	0.0175 ± 0.0044	0.0124 ± 0.0045*
	PC ae C30:1	0.0040 ± 0.0013	0.0068 ± 0.0033*	0.0038 ± 0.0030	0.0026 ± 0.0016	0.0041 ± 0.0021	0.0037 ± 0.0022	0.0059 ± 0.0009	0.0041 ± 0.0026	0.0069 ± 0.0025	0.0073 ± 0.0030
	PC ae C32:2	0.0075 ± 0.0059	0.0116 ± 0.0043	0.0060 ± 0.0040	0.0058 ± 0.0020	0.0076 ± 0.0043	0.0066 ± 0.0050	0.0088 ± 0.0045	0.0068 ± 0.0031	0.0106 ± 0.0033	0.0071 ± 0.0024*
	PC ae C34:3	0.0091 ± 0.0056	0.0167 ± 0.0048*	0.0112 ± 0.0043	0.0081 ± 0.0035	0.0131 ± 0.0043	0.0084 ± 0.0058	0.0136 ± 0.0040	0.0094 ± 0.0032	0.0134 ± 0.0059	0.0104 ± 0.0040
	PC ae C38:0	0.0048 ± 0.0023	0.0041 ± 0.0021	0.0051 ± 0.0018	0.0033 ± 0.0018	0.0038 ± 0.0024	0.0036 ± 0.0029	0.0055 ± 0.0019	0.0033 ± 0.0014*	0.0041 ± 0.0015	0.0059 ± 0.0036
	PC ae C38:4	0.0098 ± 0.0058	0.0192 ± 0.0058**	0.0129 ± 0.0057	0.0164 ± 0.0055	0.0171 ± 0.0075	0.0094 ± 0.0078	0.0159 ± 0.0055	0.0147 ± 0.0055	0.0172 ± 0.0080	0.0141 ± 0.0046
	PC ae C40:0	0.1516 ± 0.0102	0.1781 ± 0.0249*	0.1532 ± 0.0163	0.1650 ± 0.0127	0.1596 ± 0.0372	0.1512 ± 0.0268	0.1516 ± 0.0220	0.1734 ± 0.0355	0.1570 ± 0.0170	0.1551 ± 0.0230
	PC ae C40:6	0.0021 ± 0.0015	0.0036 ± 0.0015	0.0027 ± 0.0026	0.0013 ± 0.0012	0.0028 ± 0.0009	0.0011 ± 0.0009**	0.0026 ± 0.0014	0.0022 ± 0.0011	0.0033 ± 0.0022	0.0035 ± 0.0019
	PC ae C40:2	0.0106 ± 0.0024	0.0154 ± 0.0054*	0.0111 ± 0.0035	0.0127 ± 0.0029	0.0138 ± 0.0054	0.0103 ± 0.0011	0.0121 ± 0.0047	0.0122 ± 0.0019	0.0135 ± 0.0017	0.0116 ± 0.0031
	PC ae C42:0	0.0025 ± 0.0014	0.0051 ± 0.0027*	0.0033 ± 0.0013	0.0033 ± 0.0011	0.0030 ± 0.0024	0.0025 ± 0.0024	0.0048 ± 0.0035	0.0025 ± 0.0014	0.0044 ± 0.0013	0.0048 ± 0.0019
	PC ae C42:1	0.0005 ± 0.0005	0.0016 ± 0.0005*	0.0011 ± 0.0009	0.0015 ± 0.0016	0.0008 ± 0.0008	0.0021 ± 0.0032	0.0018 ± 0.0011	0.0010 ± 0.0007	0.0016 ± 0.0009	0.0017 ± 0.0013
	PC ae C42:3	0.0095 ± 0.0023	0.0141 ± 0.0037**	0.0113 ± 0.0019	0.0105 ± 0.0032	0.0106 ± 0.0035	0.0100 ± 0.0016	0.0105 ± 0.0015	0.0115 ± 0.0025	0.0118 ± 0.0024	0.0120 ± 0.0039
PC ae C42:5	0.0008 ± 0.0006	0.0008 ± 0.0007*	0.0007 ± 0.0007	0.0010 ± 0.0008	0.0017 ± 0.0011	0.0004 ± 0.0004	0.0010 ± 0.0011	0.0009 ± 0.0006	0.0010 ± 0.0004	0.0012 ± 0.0006	

Comparisons	4 weeks		8 weeks		12 weeks		16 weeks		24 weeks	
Regulated metabolites	18		7		5		2		5	
Metabolites [μM]	WT Mean ± SD	s-IL10 ^{-/-} Mean ± SD	WT Mean ± SD	s-IL10 ^{-/-} Mean ± SD	WT Mean ± SD	s-IL10 ^{-/-} Mean ± SD	WT Mean ± SD	s-IL10 ^{-/-} Mean ± SD	WT Mean ± SD	s-IL10 ^{-/-} Mean ± SD
PC ae C44:3	0.0161 ± 0.0119	0.0420 ± 0.0222	0.0257 ± 0.0142	0.0178 ± 0.0068	0.0349 ± 0.0167	0.0209 ± 0.0093*	0.0499 ± 0.0144	0.0339 ± 0.0289	0.0302 ± 0.0103	0.0369 ± 0.0159
lysoPC a C20:4	1.4452 ± 0.2268	1.3721 ± 0.4910*	1.6451 ± 0.4617	2.0033 ± 0.7277	2.1230 ± 1.3107	2.5591 ± 0.3024	2.5549 ± 0.5065	1.8816 ± 0.5004	1.6535 ± 0.5245	1.8444 ± 0.5234

NB: All metabolite concentrations are presented as mean values ± SD from 8 animals per group. The values from s-IL-10^{-/-} animals were compared at each time point with the WT mice. Significant differences were assessed by Mann-Whitney U test and marked as follows: *p<0.05, **p<0.01, ***p<0.001.

Key: Arg: arginine; C: acyl-carnitine; lysoPCa: lysophosphatidylcholine; Met: methionine; PCaa: phosphatidylcholine; PCae: phosphatidylcholine with an ether bond; SM: sphingomyelin; Trp: tryptophan.

Appendix Table 6-3: All significantly regulated metabolites in the plasma of TNF^{ΔARE/WT} compared to WT mice at the age of 4, 8, 12, 16, and 24 weeks analyzed by UPLC-ESI-MS/MS using the AbsoluteIDQ™ kit (Biocrates Life Sciences, Austria)

		4 weeks		8 weeks		12 weeks		16 weeks		24 weeks	
Regulated Metabolites		14		23		78		27		33	
Metabolites [μM]		WT Mean ± SD	TNF ^{ΔARE/WT} Mean ± SD	WT Mean ± SD	TNF ^{ΔARE/WT} Mean ± SD	WT Mean ± SD	TNF ^{ΔARE/WT} Mean ± SD	WT Mean ± SD	TNF ^{ΔARE/WT} Mean ± SD	WT Mean ± SD	TNF ^{ΔARE/WT} Mean ± SD
Amino acids	Arg-PTC	76.29±27.79	78.40±35.28	101.29±28.95	108.05±40.77	79.15±31.88	112.10±27.87*	73.90±36.95	123.55±52.76*	123.51±54.49	105.36±35.25
	Gln-PTC	1052.88±184.25	1021.88±165.26	1015.88±101.77	948.88±239.07	854.25±78.20	1056.25±203.67*	944.00±181.29	991.38±196.06	1126.33±232.91	1079.00±148.61
	Met-PTC	45.54±8.69	49.24±16.21	62.34±6.62	52.49±15.51	48.81±5.82	51.65±11.91	61.29±8.70	54.75±15.40	69.01±17.13	53.20±9.14*
	Phe-PTC	50.73±8.51	51.69±15.63	86.68±11.97	61.53±21.15*	58.90±13.11	69.59±22.21	82.54±19.25	79.78±18.99	76.17±17.75	66.31±11.87
	Pro-PTC	88.35±18.33	91.40±30.08	106.33±32.44	115.19±42.44	68.33±17.22	99.03±23.66*	104.78±50.24	83.95±21.56	94.06±24.03	88.94±9.89
	Tyr-PTC	76.14±15.94	88.84±35.56	121.01±27.37	76.00±25.36**	77.46±23.18	116.73±26.80**	112.11±36.49	98.40±25.73	104.37±22.26	79.27±18.75*
	Val-PTC	87.71±14.92	95.90±23.23	146.13±23.59	115.88±42.94	107.74±28.23	129.85±41.88	161.50±35.46	111.96±24.16**	160.73±60.11	125.93±26.67
Acetylcarnitines	C0	15.63±4.09	16.88±5.50	29.15±6.10	23.06±5.01*	21.36±7.65	21.59±2.48	30.73±5.24	19.21±6.76**	26.07±7.10	22.39±8.39
	C2	7.89±2.72	9.66±3.48	18.13±5.40	11.29±3.97*	15.28±3.84	11.35±2.63*	19.80±4.33	17.75±4.24	16.14±4.77	13.94±5.39
	C3	0.34±0.13	0.37±0.20	1.41±0.79	0.54±0.54*	0.52±0.40	0.54±0.28	1.19±0.44	1.20±0.32	0.78±0.37	0.75±0.67
	C3-OH	0.02±0.02	0.02±0.01	0.05±0.03	0.03±0.03	0.04±0.01	0.02±0.01*	0.04±0.03	0.03±0.01	0.03±0.01	0.02±0.01*
	C3:1	0.01±0.001	0.02±0.01	0.02±0.01	0.01±0.002*	0.02±0.01	0.02±0.003	0.03±0.01	0.02±0.01	0.01±0.003	0.02±0.01
	C4-OH (C3-DC)	0.13±0.05	0.19±0.09	0.20±0.06	0.15±0.03	0.18±0.08	0.11±0.03*	0.21±0.05	0.28±0.19	0.14±0.05	0.20±0.06
	C5-OH (C3-DC-M)	0.05±0.03	0.06±0.02	0.08±0.03	0.04±0.02**	0.08±0.03	0.05±0.03	0.08±0.05	0.06±0.03	0.07±0.03	0.05±0.02
	C5:1-DC	0.02±0.01	0.01±0.003	0.03±0.01	0.03±0.01	0.04±0.02	0.03±0.01	0.03±0.01	0.04±0.01	0.03±0.01	0.01±0.01*
	C7-DC	0.01 ± 0.005	0.01±0.00	0.02±0.01	0.02±0.004	0.02±0.01	0.02±0.01	0.02±0.01	0.01±0.01	0.01±0.003	0.01±0.002*
	C10:2	0.01±0.01	0.02±0.01	0.02±0.01	0.02±0.01	0.01±0.01	0.03±0.01*	0.01±0.01	0.02±0.01	0.02±0.01	0.01±0.01
	C12	0.11±0.03	0.14±0.03*	0.10±0.02	0.11±0.02	0.11±0.03	0.12±0.02	0.12±0.03	0.13±0.03	0.11±0.02	0.12±0.02
	C14:1	0.07±0.03	0.06±0.02	0.06±0.03	0.05±0.02	0.08±0.02	0.05±0.01**	0.06±0.01	0.06±0.02	0.08±0.02	0.07±0.01
	C16	0.09±0.04	0.10±0.03	0.12±0.04	0.11±0.05	0.15±0.07	0.08±0.02**	0.09±0.03	0.11±0.04	0.10±0.05	0.11±0.03
	C16:1	0.08±0.01	0.08±0.02	0.07±0.01	0.07±0.02	0.09±0.03	0.06±0.01*	0.06±0.01	0.08±0.02*	0.08±0.02	0.08±0.02
C18:1	0.09±0.03	0.08±0.02	0.12±0.05	0.10±0.03	0.13±0.06	0.09±0.02	0.07±0.02	0.12±0.05*	0.12±0.05	0.11±0.04	
C18:2	0.03±0.01	0.03±0.01	0.04±0.02	0.03±0.02	0.04±0.02	0.03±0.01*	0.03±0.01	0.04±0.02	0.03±0.01	0.04±0.02	
Sphingolipids	SM(OH) C14:1	1.40±0.47	1.19±0.39	1.26±0.36	0.76±0.34*	1.30±0.37	0.80±0.26**	1.30±0.12	0.99±0.33*	1.36±0.32	0.89±0.30*
	SM(OH) C22:1	7.22±1.10	5.69±0.93**	6.10±1.69	2.82±0.58***	6.98±1.84	2.83±0.68***	9.13±2.87	4.17±1.73***	7.56±2.06	3.43±0.83***
	SM(OH) C22:2	3.56±0.58	2.57±0.70**	2.65±0.54	1.57±0.38***	2.73±0.48	1.55±0.47***	2.76±0.58	2.13±0.77	3.42±0.87	2.08±0.41**
	SM(OH) C24:1	1.05±0.10	0.80±0.44	0.68±0.28	0.47±0.07	0.74±0.22	0.53±0.11*	0.68±0.16	0.59±0.17	0.75±0.16	0.63±0.26*
	SM C16:1	4.71±1.65	3.07±1.28*	2.56±1.05	2.74±1.13	3.71±1.07	2.23±0.91**	3.92±1.12	2.62±0.97*	3.58±0.93	3.30±0.50
	SM C18:1	1.41±0.42	0.95±0.44	0.81±0.31	0.76±0.31	0.95±0.20	0.52±0.24**	0.71±0.14	0.81±0.30	0.91±0.33	0.84±0.29

		4 weeks		8 weeks		12 weeks		16 weeks		24 weeks	
Regulated Metabolites		14		23		78		27		33	
Metabolites [μM]		WT Mean ± SD	TNF ^{AARE} /WT Mean ± SD	WT Mean ± SD	TNF ^{AARE} /WT Mean ± SD	WT Mean ± SD	TNF ^{AARE} /WT Mean ± SD	WT Mean ± SD	TNF ^{AARE} /WT Mean ± SD	WT Mean ± SD	TNF ^{AARE} /WT Mean ± SD
	SM C22:3	6.01±3.34	3.68±1.69	3.53±1.83	2.95±1.27	4.32±1.37	3.17±1.54	6.60±2.56	3.28±1.02**	5.32±2.03	4.60±1.12
	SM C24:0	12.67±3.26	9.51±2.79	8.87±2.80	7.81±2.50	13.51±3.40	6.99±2.82***	13.34±3.93	9.63±4.04	14.13±4.75	10.48±3.38
	SM C24:1	50.58±18.14	35.02±14.02	34.29±8.61	29.96±10.79	39.50±5.51	26.88±10.68*	35.66±7.13	34.08±10.85	47.58±8.81	36.91±4.22
	SM C26:0	0.52±0.32	0.56±0.43	0.34±0.10	0.29±0.09	0.41±0.20	0.27±0.08	0.62±0.16	0.38±0.24*	0.52±0.24	0.35±0.13
	SM C26:1	0.74±0.12	0.60±0.28	0.38±0.09	0.38±0.10	0.66±0.34	0.35±0.12*	0.79±0.23	0.56±0.34	0.69±0.32	0.62±0.21
Glycerophospholipids	PCaa C26:0	1.03±0.65	1.12±0.76	1.78±0.96	1.48±0.83	2.16±1.79	1.11±0.28	1.68±0.94	1.52±1.27	0.81±0.27	1.27±0.40*
	PCaa C28:1	0.31±0.19	0.28±0.19	0.61±0.30	0.41±0.34	0.60±0.54	0.35±0.12	0.41±0.25	0.41±0.29	0.22±0.06	0.37±0.18*
	PCaa C30:2	0.60±0.22	0.44±0.19	0.75±0.34	0.61±0.24	0.87±0.31	0.52±0.13*	0.80±0.14	0.63±0.32	0.77±0.23	0.72±0.13
	PCaa C32:0	7.28±2.09	6.30±2.09	8.24±2.04	8.54±3.23	8.85±2.07	7.07±2.44	9.01±1.83	8.52±1.79	8.38±1.45	9.89±1.29*
	PCaa C32:1	6.25±3.35	3.80±1.44	4.49±2.36	4.09±2.15	6.22±2.71	4.26±1.73	8.19±3.89	4.06±1.55*	6.67±3.91	6.46±2.56
	PCaa C32:2	0.99±0.36	0.67±0.26	0.86±0.32	0.79±0.43	1.13±0.37	0.74±0.37*	1.11±0.31	0.86±0.28	1.07±0.32	1.03±0.31
	PCaa C32:3	0.08±0.04	0.07±0.03	0.12±0.06	0.13±0.11	0.15±0.07	0.09±0.03*	0.11±0.06	0.11±0.05	0.09±0.04	0.11±0.05
	PCaa C34:1	135.16±64.30	76.70±30.53*	114.60±54.44	100.94±45.99	142.98±38.85	94.43±41.75*	170.75±67.95	108.96±46.10	152.49±59.30	145.71±36.63
	PCaa C34:2	219.51±84.59	138.31±55.48*	247.13±106.68	207.56±98.21	314.88±108.59	183.81±86.42*	372.88±133.92	212.13±58.61**	301.56±116.47	246.57±60.51
	PCaa C34:3	7.92±3.40	5.04±1.81	8.31±4.89	8.34±4.44	12.12±4.78	6.64±3.09*	12.67±4.41	7.70±2.86*	10.57±4.41	10.97±3.63
	PCaa C34:4	0.26±0.12	0.21±0.10	0.26±0.14	0.27±0.18	0.34±0.21	0.22±0.09	0.35±0.11	0.23±0.09*	0.33±0.06	0.33±0.08
	PCaa C36:0	2.87±0.87	2.03±0.75	2.84±0.99	2.29±0.72	3.69±0.54	1.93±0.51***	3.18±0.97	2.75±0.68	4.05±0.56	3.01±0.54**
	PCaa C36:1	28.44±9.01	18.66±6.49*	31.23±11.37	23.88±9.22	36.19±6.46	21.97±8.09**	36.64±11.62	29.40±9.64	43.67±8.66	33.36±5.64*
	PCaa C36:2	121.75±44.12	81.83±33.04	146.00±47.97	105.18±45.03	154.43±41.10	106.03±43.57*	172.99±50.83	130.23±34.87	182.44±40.32	134.86±26.80*
	PCaa C36:4	70.18±27.16	53.41±23.92	90.70±32.59	85.16±42.14	114.58±33.22	72.85±32.69*	105.34±30.85	80.88±14.32	97.36±18.57	101.51±14.25
	PCaa C36:5	4.25±2.34	2.34±0.99	3.85±2.24	3.13±1.71	4.81±1.57	3.35±1.65	6.59±2.80	3.44±1.11*	5.32±2.21	4.71±1.68
	PCaa C36:6	0.22±0.11	0.14±0.05	0.21±0.16	0.18±0.09	0.28±0.06	0.20±0.08*	0.26±0.09	0.18±0.06*	0.23±0.06	0.23±0.09
	PCaa C38:0	1.27±1.17	1.06±0.85	1.09±0.40	0.91±0.25	1.40±0.23	0.85±0.17***	1.16±0.30	1.03±0.25	1.15±0.27	0.93±0.10
	PCaa C38:1	2.32±1.49	1.94±1.22	2.22±1.15	1.92±0.55	3.36±1.03	1.72±0.44***	3.08±0.98	2.08±1.03	2.97±1.07	2.31±0.69
	PCaa C38:3	17.19±6.47	12.12±5.27	20.43±7.93	16.47±7.22	24.90±3.74	14.70±6.02**	22.11±6.77	19.34±6.58	29.12±4.09	21.41±3.32**
PCaa C38:4	41.32±15.94	35.98±18.22	57.95±19.03	56.56±25.91	76.00±19.07	42.25±17.53**	49.51±12.58	56.76±17.89	73.67±25.07	62.61±13.64	
PCaa C38:6	45.96±18.65	33.82±17.87	53.13±24.41	61.30±32.37	83.76±21.74	49.03±23.85**	66.71±21.25	55.28±14.05	64.07±15.97	71.94±9.14	
PCaa C40:1	0.34±0.20	0.37±0.13	0.37±0.11	0.28±0.05*	0.45±0.18	0.34±0.08	0.42±0.13	0.33±0.09	0.35±0.10	0.31±0.08	
PCaa C40:2	0.40±0.28	0.30±0.25	0.33±0.13	0.28±0.10	0.46±0.23	0.25±0.07*	0.52±0.16	0.35±0.18	0.39±0.19	0.35±0.10	
PCaa C40:3	0.38±0.12	0.35±0.16	0.58±0.38	0.37±0.14	0.93±0.33	0.46±0.17**	0.98±0.45	0.65±0.33	0.79±0.42	0.69±0.23	

	4 weeks		8 weeks		12 weeks		16 weeks		24 weeks	
Regulated Metabolites	14		23		78		27		33	
Metabolites [μM]	WT Mean ± SD	TNF ^{AARE} /WT Mean ± SD	WT Mean ± SD	TNF ^{AARE} /WT Mean ± SD	WT Mean ± SD	TNF ^{AARE} /WT Mean ± SD	WT Mean ± SD	TNF ^{AARE} /WT Mean ± SD	WT Mean ± SD	TNF ^{AARE} /WT Mean ± SD
PCaa C40:4	1.40±0.48	1.08±0.38	1.84±0.95	1.69±0.86	3.15±1.07	1.48±0.65**	2.64±0.97	2.02±0.61	2.54±0.76	2.38±0.58
PCaa C40:5	5.06±2.12	3.60±1.74	5.84±2.17	5.68±2.75	8.10±1.27	4.49±2.02***	6.27±1.71	6.06±1.70	7.79±1.10	7.19±1.11
PCaa C40:6	16.22±6.05	11.97±6.33	20.30±10.10	20.73±10.68	28.83±4.54	15.30±6.83***	20.55±5.92	19.92±6.23	27.19±8.38	22.84±4.92
PCaa C42:1	0.11±0.05	0.11±0.06	0.11±0.04	0.12±0.04	0.15±0.05	0.10±0.02*	0.12±0.06	0.11±0.04	0.13±0.05	0.12±0.06
PCaa C42:2	0.12±0.05	0.12±0.07	0.14±0.06	0.17±0.06	0.20±0.12	0.11±0.05	0.27±0.11	0.14±0.09*	0.19±0.07	0.15±0.05
PCaa C42:4	0.14±0.03	0.12±0.06	0.22±0.13	0.19±0.10	0.30±0.11	0.16±0.07**	0.31±0.13	0.22±0.08	0.25±0.11	0.23±0.07
PCaa C42:5	0.19±0.05	0.19±0.09	0.28±0.13	0.29±0.15	0.50±0.21	0.25±0.13*	0.41±0.15	0.30±0.13	0.39±0.23	0.36±0.16
PCaa C42:6	0.45±0.08	0.44±0.10	0.58±0.41	0.62±0.32	1.11±0.43	0.53±0.19**	1.22±0.43	0.79±0.35*	0.91±0.39	0.87±0.27
PCae C30:2	0.08±0.10	0.08±0.06	0.13±0.06	0.11±0.08	0.17±0.15	0.09±0.04	0.12±0.06	0.12±0.12	0.05±0.03	0.11±0.06*
PCae C32:1	0.42±0.14	0.35±0.15	0.62±0.24	0.51±0.27	0.68±0.31	0.39±0.10*	0.67±0.14	0.52±0.19	0.52±0.11	0.55±0.13
PCae C34:0	0.50±0.13	0.34±0.10*	0.59±0.25	0.45±0.20	0.56±0.13	0.40±0.15*	0.65±0.15	0.51±0.17	0.60±0.10	0.51±0.10
PCae C34:1	2.43±0.94	1.71±0.59	3.01±0.96	2.44±0.97	3.33±0.84	2.02±0.78**	3.51±1.07	2.58±0.86	3.15±0.75	2.97±0.48
PCae C34:2	1.68±0.68	1.16±0.47	2.45±0.83	1.73±0.82	2.67±0.95	1.57±0.65*	3.24±1.06	1.81±0.43**	2.42±0.85	2.03±0.42
PCae C34:3	0.48±0.20	0.33±0.17	0.69±0.31	0.46±0.25	0.76±0.25	0.49±0.21*	0.83±0.31	0.51±0.24*	0.80±0.24	0.61±0.20
PCae C36:0	0.53±0.23	0.42±0.15	0.54±0.21	0.48±0.11	0.57±0.14	0.32±0.06***	0.61±0.19	0.48±0.19	0.53±0.11	0.36±0.09**
PCae C36:1	2.34±0.74	1.74±0.54	2.48±0.77	1.68±0.43*	2.50±0.63	1.44±0.30***	2.83±0.90	1.95±0.80	2.73±0.61	2.02±0.26*
PCae C36:2	4.74±1.09	3.51±0.98*	6.32±2.00	3.54±0.82**	6.21±1.86	3.50±1.03**	7.43±2.51	4.48±1.39*	6.50±1.94	4.36±0.77*
PCae C36:3	1.12±0.32	0.76±0.28*	1.56±0.70	0.95±0.40*	1.60±0.51	0.90±0.40**	1.76±0.51	1.14±0.46*	1.53±0.39	1.29±0.33
PCae C36:4	1.63±0.65	1.07±0.51	2.54±0.83	1.76±0.78	2.96±0.85	1.43±0.59***	2.74±0.66	2.14±0.88	2.29±0.39	1.97±0.30
PCae C36:5	0.75±0.30	0.49±0.24	1.02±0.32	0.72±0.30	1.25±0.37	0.61±0.27**	1.07±0.35	0.93±0.44	1.17±0.26	0.93±0.09*
PCae C38:0	1.40±0.51	1.07±0.27	1.52±0.80	1.70±0.75	2.54±0.93	1.44±0.65*	2.06±0.75	1.63±0.43	2.00±0.64	2.33±0.68
PCae C38:1	1.31±0.40	1.08±0.23	1.51±0.37	0.98±0.28**	1.83±0.36	0.82±0.20***	2.07±0.50	1.15±0.62**	1.79±0.45	0.96±0.15***
PCae C38:2	3.05±0.91	2.33±0.67	4.55±1.82	2.11±0.57**	5.07±1.93	2.08±0.68**	6.81±2.56	2.93±1.57**	5.23±2.10	2.53±0.65**
PCae C38:3	1.11±0.27	0.90±0.26	1.42±0.39	0.95±0.35*	1.40±0.33	0.92±0.19**	1.53±0.42	1.24±0.60	1.61±0.33	1.24±0.18*
PCae C38:4	1.91±0.59	1.70±0.65	3.01±0.74	2.09±0.86*	3.53±1.24	1.81±0.65**	2.84±0.60	2.56±0.88	2.81±0.51	2.49±0.48
PCae C38:5	1.58±0.67	1.00±0.49	2.25±0.70	1.62±0.75	2.46±0.58	1.30±0.49***	2.22±0.66	1.89±0.75	2.09±0.34	1.86±0.29
PCae C38:6	0.84±0.20	0.60±0.19*	1.32±0.43	0.92±0.51	1.50±0.41	0.76±0.32**	1.33±0.40	1.04±0.37	1.21±0.24	1.07±0.26
PCae C40:1	1.23±0.21	0.86±0.30*	1.63±0.69	1.42±0.72	2.23±0.80	1.16±0.53**	2.03±0.57	1.58±0.58	1.92±0.41	1.87±0.40
PCae C40:2	0.42±0.22	0.40±0.25	0.46±0.20	0.37±0.08	0.57±0.13	0.29±0.08***	0.59±0.17	0.37±0.10**	0.46±0.07	0.41±0.09
PCae C40:3	0.42±0.10	0.34±0.09	0.67±0.26	0.36±0.09**	0.71±0.25	0.39±0.11**	0.66±0.24	0.47±0.28	0.67±0.15	0.50±0.09*

	4 weeks		8 weeks		12 weeks		16 weeks		24 weeks	
Regulated Metabolites	14		23		78		27		33	
Metabolites [μM]	WT Mean ± SD	TNF ^{ΔARE/WT} Mean ± SD	WT Mean ± SD	TNF ^{ΔARE/WT} Mean ± SD	WT Mean ± SD	TNF ^{ΔARE/WT} Mean ± SD	WT Mean ± SD	TNF ^{ΔARE/WT} Mean ± SD	WT Mean ± SD	TNF ^{ΔARE/WT} Mean ± SD
PCae C40:4	0.92±0.18	0.78±0.24	1.42±0.54	0.93±0.37	1.80±0.69	0.68±0.24***	1.46±0.33	1.12±0.30*	1.38±0.23	0.90±0.15***
PCae C40:5	0.62±0.19	0.53±0.19	0.90±0.30	0.64±0.31	0.93±0.23	0.58±0.20**	0.88±0.22	0.82±0.32	0.82±0.11	0.82±0.11
PCae C40:6	1.04±0.25	0.81±0.32	1.46±0.48	1.07±0.45	1.72±0.56	0.82±0.30**	1.51±0.37	1.19±0.36	1.48±0.29	1.02±0.31**
PCae C42:1	0.26±0.13	0.25±0.11	0.37±0.15	0.39±0.20	0.43±0.15	0.28±0.07*	0.37±0.09	0.38±0.13	0.43±0.11	0.46±0.05
PCae C42:5	0.41±0.07	0.42±0.09	0.51±0.14	0.51±0.12	0.54±0.13	0.40±0.06*	0.58±0.17	0.52±0.16	0.54±0.08	0.46±0.07
PCae C44:4	0.07±0.03	0.09±0.07	0.11±0.05	0.10±0.06	0.13±0.04	0.08±0.04*	0.11±0.06	0.12±0.09	0.13±0.04	0.10±0.02
lysoPCa C6:0	0.11±0.001	0.08±0.04	0.21±0.06	0.07±0.01**	0.11±0.06	0.11±0.06	0.07±0.01	0.08±0.01	0.07±0.01	0.11±0.06
lysoPCa C16:0	187.88±40.50	153.50±34.07	263.25±76.06	233.50±51.82	240.88±38.82	180.44±39.73**	269.13±58.31	246.50±106.95	249.11±31.42	260.57±28.18
lysoPCa C17:0	2.57±0.63	2.22±0.63	4.80±1.40	2.56±0.78**	3.36±0.67	2.07±0.46***	3.78±0.68	3.12±1.25	4.10±0.63	2.90±0.81**
lysoPCa C18:0	71.24±13.99	59.15±17.56	121.06±45.59	109.89±35.38	108.25±16.92	70.79±12.70***	91.51±18.98	112.78±43.84	129.64±37.92	105.30±20.55
lysoPCa C18:1	71.39±26.62	45.26±10.40*	85.01±24.00	64.08±12.95*	70.28±17.70	60.84±14.46	78.58±12.04	76.95±35.82	105.08±30.04	97.36±29.60
lysoPCa C18:2	136.03±46.28	90.65±33.78*	200.75±47.57	133.43±43.82*	156.13±16.90	122.39±37.61*	193.38±23.72	148.28±46.90*	212.89±33.90	155.43±21.90**
lysoPCa C24:0	0.67±0.17	0.80±0.29	1.36±0.79	0.94±0.48	1.49±0.84	0.75±0.18*	1.03±0.33	1.01±0.53	0.64±0.13	1.05±0.47*
lysoPCa C26:0	1.11±0.76	1.12±0.98	2.16±1.24	1.60±0.97	1.89±1.72	1.21±0.49	1.46±0.90	1.47±1.45	0.74±0.40	1.37±0.63*
lysoPCa C28:0	0.82±0.91	0.91±0.62	1.83±1.05	1.06±0.70	1.46±1.18	0.92±0.22	0.81±0.58	0.91±1.09	0.55±0.24	1.09±0.51*
lysoPCa C28:1	0.61±0.68	0.73±0.45	1.45±0.76	0.95±1.13	1.17±1.00	0.72±0.23	0.81±0.61	1.08±1.12	0.42±0.22	0.91±0.44*

NB: All metabolite concentrations are presented as mean values ± SD from 8 animals per group. The values from TNF^{ΔARE/WT} animals were compared at each time point with the WT mice. Significant differences were assessed by Mann-Whitney U test and marked as follows: *p<0.05, **p<0.01, ***p<0.001.

Key: Arg: arginine; C: acyl-carnitine; Gln: glutamine; lysoPCa: lysophosphatidylcholine; Met: methionine; PCaa: phosphatidylcholine; PCae: phosphatidylcholine with an ether bond; Phe: phenylalanine; Pro: proline; SM: sphingomyelin; Tyr: tyrosine; Val: valine.

Appendix Table 6-4: All significantly regulated metabolites in the distal ileum of TNF^{ΔARE/WT} compared to WT mice at the age of 4, 8, 12, 16, and 24 weeks analyzed by UPLC-ESI-MS/MS using the AbsoluteIDQ™ kit (Biocrates Life Sciences, Austria)

		4 weeks		8 weeks		12 weeks		16 weeks		24 weeks	
Regulated metabolites		4		2		33		25		12	
Metabolites [μM]		WT Mean ± SD	TNF ^{ΔARE/WT} Mean ± SD	WT Mean ± SD	TNF ^{ΔARE/WT} Mean ± SD	WT Mean ± SD	TNF ^{ΔARE/WT} Mean ± SD	WT Mean ± SD	TNF ^{ΔARE/WT} Mean ± SD	WT Mean ± SD	TNF ^{ΔARE/WT} Mean ± SD
Acetylcarnitines	C0	5.5643±1.415	6.5881±0.775	5.9291±1.740	5.4112±0.767	5.8746±1.342	7.0782±2.051	5.4313±0.864	6.0351±1.334	3.8822±1.313	5.4731±1.269*
	C2	1.2181±0.342	1.1444±0.691	1.1270±0.508	1.5221±0.494	1.7816±0.735	1.5209±0.350	1.3714±0.502	1.4929±0.365	0.6459±0.463	1.4031±0.855*
	C3-OH	0.0073±0.006	0.0044±0.004	0.0041±0.004	0.0020±0.002	0.0040±0.004	0.0020±0.001	0.0062±0.006	0.0009±0.002*	0.0021±0.002	0.0037±0.003
	C4-OH (C3-DC)	0.0484±0.018	0.0481±0.016	0.0473±0.020	0.0569±0.022	0.0648±0.022	0.0362±0.009**	0.0352±0.015	0.0402±0.016	0.0375±0.013	0.0384±0.013
	C5-M-DC	0.0512±0.031	0.0347±0.012	0.0210±0.010	0.0242±0.021	0.0410±0.041	0.0077±0.007*	0.0266±0.016	0.0135±0.006*	0.0124±0.005	0.0152±0.006
	C6 (C4:1-DC)	0.0297±0.006	0.0209±0.009*	0.0146±0.007	0.0184±0.009	0.0239±0.014	0.0119±0.005*	0.0200±0.008	0.0187±0.013	0.0181±0.006	0.0202±0.009
	C6:1	0.0076±0.005	0.0054±0.004	0.0133±0.008	0.0125±0.007	0.0106±0.005	0.0051±0.005*	0.0155±0.014	0.0126±0.008	0.0053±0.003	0.0099±0.004*
	C8	0.0689±0.037	0.0696±0.028	0.0517±0.020	0.0442±0.018	0.0573±0.021	0.0280±0.009**	0.0395±0.029	0.0260±0.011	0.0441±0.014	0.0493±0.014
	C8:1	0.0052±0.005	0.0032±0.002	0.0039±0.002	0.0034±0.002	0.0047±0.003	0.0022±0.001*	0.0063±0.003	0.0053±0.007	0.0030±0.001	0.0032±0.001
	C9	0.0049±0.004	0.0032±0.002	0.0032±0.002	0.0038±0.002	0.0068±0.006	0.0025±0.001	0.0068±0.006	0.0025±0.001*	0.0056±0.003	0.0043±0.002
	C10	0.0219±0.011	0.0234±0.013	0.0159±0.006	0.0148±0.007	0.0260±0.022	0.0082±0.002*	0.027±0.016	0.0075±0.004**	0.0192±0.009	0.0163±0.007
	C10:1	0.0661±0.027	0.0514±0.026	0.0366±0.019	0.0354±0.021	0.0601±0.017	0.0254±0.012***	0.0721±0.025	0.0383±0.016**	0.0411±0.014	0.0348±0.013
	C10:2	0.0044±0.002	0.0035±0.002	0.0034±0.001	0.0037±0.002	0.0027±0.002	0.0019±0.001	0.013±0.012	0.0013±0.001*	0.0035±0.002	0.0033±0.002
	C12	0.0452±0.017	0.0404±0.011	0.0312±0.011	0.0286±0.008	0.0497±0.026	0.0173±0.005**	0.0425±0.023	0.0276±0.016	0.0283±0.012	0.0286±0.008
	C12-DC	0.0275±0.010	0.0241±0.007	0.0185±0.006	0.0203±0.010	0.0296±0.015	0.0123±0.005**	0.0384±0.020	0.0188±0.008*	0.0198±0.007	0.0190±0.009
	C12:1	0.1014±0.059	0.0748±0.046	0.0577±0.037	0.0575±0.035	0.0952±0.019	0.0391±0.025***	0.1223±0.047	0.0573±0.024**	0.0624±0.024	0.0485±0.019
	C14	0.0292±0.008	0.0267±0.008	0.0200±0.008	0.0187±0.007	0.0275±0.012	0.0092±0.023**	0.0293±0.012	0.0173±0.007*	0.0160±0.006	0.0168±0.005
	C14:1	0.0027±0.002	0.0024±0.002	0.0017±0.001	0.0021±0.001	0.0027±0.001	0.0008±0.0001**	0.0031±0.001	0.0011±0.001**	0.0012±0.001	0.0016±0.001
C14:1-OH	0.0020±0.001	0.0012±0.001	0.0010±0.001	0.0014±0.001	0.0018±0.002	0.0011±0.001	0.0038±0.002	0.0016±0.001*	0.0011±0.001	0.0012±0.001	
C14:2-OH	0.0015±0.001	0.0014±0.001	0.0012±0.001	0.0013±0.001	0.0020±0.001	0.0005±0.001***	0.0035±0.002	0.0011±0.001*	0.0009±0.001	0.0013±0.001	
C16-OH	0.0011±0.001	0.0013±0.001	0.0012±0.001	0.0008±0.001	0.0015±0.001	0.0009±0.0002	0.0018±0.002	0.0013±0.001	0.0004±0.00001	0.0011±0.00007**	
C16:1	0.0206±0.008	0.0185±0.007	0.0117±0.004	0.0137±0.007	0.0198±0.012	0.0074±0.003*	0.0231±0.012	0.0097±0.004*	0.0122±0.005	0.0117±0.004	
C16:1-OH	0.0038±0.002	0.0240±0.001	0.0027±0.002	0.0022±0.001	0.0045±0.001	0.0015±0.001***	0.0044±0.003	0.0022±0.002	0.0016±0.001	0.0022±0.001	
C18	0.0054±0.004	0.0320±0.002	0.0039±0.003	0.0043±0.003	0.0050±0.005	0.0029±0.001	0.0038±0.002	0.0046±0.003	0.0017±0.001	0.0034±0.001*	
Sugars	H1	57.4480±12.639	53.3430±15.421	66.1890±43.379	57.1110±11.648	47.5700±13.790	69.3300±12.530**	51.9960±23.784	57.1950±9.515	42.8900±17.291	54.4500±27.546

		4 weeks		8 weeks		12 weeks		16 weeks		24 weeks	
Regulated metabolites		4		2		33		25		12	
Metabolites [μM]		WT Mean ± SD	TNF ^{ΔARE} /WT Mean ± SD	WT Mean ± SD	TNF ^{ΔARE} /WT Mean ± SD	WT Mean ± SD	TNF ^{ΔARE} /WT Mean ± SD	WT Mean ± SD	TNF ^{ΔARE} /WT Mean ± SD	WT Mean ± SD	TNF ^{ΔARE} /WT Mean ± SD
	SM(OH) C14:1	0.0177±0.016	0.0181±0.018	0.0230±0.024	0.0139±0.010	0.0300±0.017	0.0099±0.009*	0.0133±0.018	0.0099±0.013	0.0106±0.014	0.0132±0.080
	SM C16:0	0.7266±0.261	0.6643±0.310	0.6874±0.488	0.8169±0.337	0.7265±0.427	0.7918±0.456	0.5338±0.209	1.0782±0.247***	0.4182±0.541	0.5916±0.214
	SM C16:1	0.0389±0.023	0.0163±0.013*	0.0072±0.009	0.0224±0.017*	0.0165±0.030	0.0133±0.008	0.0064±0.010	0.0136±0.011	0.0151±0.010	0.0120±0.006
	SM C26:0	0.0054±0.008	0.0197±0.016*	0.0054±0.008	0.0197±0.016	0.0134±0.010	0.0181±0.014	0.0101±0.022	0.0044±0.008	0.0089±0.011	0.0099±0.007
Glycerophospholipids	PCaa C26:0	0.2019±0.066	0.1707±0.062	0.1203±0.047	0.1289±0.063	0.1899±0.127	0.0803±0.037*	0.1983±0.070	0.0885±0.035**	0.1180±0.041	0.1158±0.033
	PCaa C32:2	0.0145±0.014	0.0101±0.008	0.0033±0.004	0.0155±0.011*	0.0118±0.009	0.0157±0.012	0.0086±0.009	0.0103±0.006	0.0064±0.006	0.0056±0.004
	PCaa C36:5	0.0285±0.017	0.0257±0.015*	0.0190±0.023	0.0154±0.018	0.0389±0.045	0.0163±0.010	0.0064±0.007	0.0093±0.008	0.0202±0.015	0.0215±0.011
	PCaa C36:6	0.0065±0.006	0.0035±0.005	0.0043±0.004	0.0012±0.002	0.0072±0.004	0.0023±0.003*	0.0030±0.005	0.0034±0.004	0.0012±0.001	0.0037±0.001***
	PCaa C40:1	0.0979±0.052	0.0590±0.018	0.0587±0.024	0.0603±0.027	0.0755±0.038	0.0377±0.014*	0.0962±0.071	0.0514±0.020	0.0471±0.017	0.0456±0.013
	PCaa C40:6	0.2133±0.087	0.1905±0.071	0.1390±0.071	0.1469±0.069	0.1942±0.094	0.1090±0.038*	0.1963±0.090	0.0962±0.038*	0.1349±0.049	0.1508±0.028
	PCaa C42:5	0.0138±0.007	0.0110±0.010	0.0069±0.006	0.0117±0.006	0.0155±0.011	0.0090±0.005	0.0152±0.010	0.0043±0.004*	0.0079±0.005	0.0089±0.002
	PCaa C42:6	0.0962±0.039	0.0742±0.029	0.0586±0.023	0.0654±0.019	0.0776±0.028	0.0387±0.013**	0.0937±0.062	0.0446±0.017*	0.0462±0.015	0.0535±0.015
	PCae C36:0	0.0252±0.010	0.0247±0.014	0.0158±0.014	0.0168±0.008	0.0255±0.012	0.0101±0.005**	0.0256±0.024	0.0144±0.007	0.0179±0.009	0.0167±0.006
	PCae C38:3	0.0088±0.008	0.0098±0.007	0.0093±0.009	0.0078±0.008	0.0103±0.005	0.0097±0.008	0.0086±0.012	0.0058±0.004	0.0041±0.005	0.0098±0.005*
	PCae C38:4	0.0197±0.016	0.0194±0.011	0.0189±0.024	0.0218±0.022	0.0268±0.024	0.0210±0.017	0.0095±0.010	0.0136±0.015	0.0129±0.010	0.027±0.011*
	PCae C38:5	0.0229±0.021	0.0200±0.011	0.0133±0.014	0.0271±0.030	0.0165±0.011	0.0341±0.024	0.0080±0.009	0.0179±0.014	0.0129±0.010	0.0286±0.012*
	PCae C38:6	0.0099±0.011	0.0100±0.007	0.0085±0.006	0.0091±0.007	0.0124±0.011	0.0105±0.007	0.0042±0.005	0.0077±0.006	0.0057±0.004	0.013±0.005**
	PCae C40:0	1.5163±0.518	1.4087±0.371	0.9735±0.374	1.0538±0.413	1.4249±0.872	0.5468±0.147*	1.6245±0.622	0.7727±0.166**	1.0102±0.324	0.9784±0.295
	PCae C40:3	0.0063±0.005	0.0077±0.005	0.0033±0.004	0.0072±0.008	0.0091±0.006	0.0066±0.006	0.0043±0.007	0.0045±0.005	0.0041±0.002	0.0085±0.004*
	PCae C40:4	0.0223±0.013	0.0136±0.010	0.0161±0.010	0.0166±0.008	0.0253±0.012	0.0132±0.010*	0.0148±0.012	0.0111±0.008	0.0146±0.009	0.0193±0.004
	PCae C42:0	0.0832±0.041	0.0675±0.018	0.0570±0.026	0.0662±0.028	0.0887±0.066	0.0385±0.016	0.0831±0.031	0.0432±0.016**	0.0525±0.020	0.0524±0.021
	PCae C42:3	0.0050±0.004	0.0056±0.005	0.0054±0.008	0.0042±0.006	0.0032±0.005	0.0040±0.004	0.0015±0.002	0.0038±0.004	0.0019±0.003	0.0058±0.003*
	PCae C42:4	0.0024±0.003	0.0081±0.008	0.0075±0.011	0.0048±0.004	0.0054±0.004	0.0049±0.003	0.0057±0.006	0.0007±0.001*	0.0030±0.002	0.0035±0.004
	PCae C42:5	0.1224±0.054	0.0935±0.027	0.0633±0.018	0.0675±0.023	0.1135±0.089	0.0395±0.009*	0.0936±0.035	0.0526±0.026*	0.0636±0.021	0.0697±0.026
PCae C44:6	0.0151±0.010	0.0209±0.010	0.0112±0.006	0.0094±0.006	0.0149±0.010	0.0060±0.003*	0.0169±0.015	0.0083±0.017	0.0108±0.008	0.0080±0.003	
lysoPCa C6:0	0.0335±0.013	0.0412±0.042	0.0226±0.024	0.0256±0.023	0.0273±0.026	0.0046±0.005*	0.0490±0.082	0.0211±0.027	0.0521±0.040	0.0712±0.045	
lysoPCa C14:0	1.8300±0.533	1.9119±0.656	1.1207±0.396	1.3062±0.525	1.7733±1.014	0.7564±0.304*	1.7362±0.722	0.8449±0.233**	1.1183±0.310	1.1496±0.371	
lysoPCa C20:3	0.2013±0.070	0.2346±0.112	0.1281±0.087	0.2661±0.188	0.1935±0.117	0.0736±0.023*	0.2591±0.110	0.0669±0.043***	0.1285±0.067	0.1142±0.061	
lysoPCa C26:0	0.1676±0.089	0.1489±0.098	0.0943±0.078	0.0936±0.042	0.1571±0.075	0.0733±0.037*	0.1894±0.097	0.1540±0.077	0.0890±0.048	0.0707±0.037	

	4 weeks		8 weeks		12 weeks		16 weeks		24 weeks	
Regulated metabolites	4		2		33		25		12	
Metabolites [μ M]	WT Mean \pm SD	TNF ^{ΔAARE/WT} Mean \pm SD	WT Mean \pm SD	TNF ^{ΔAARE/WT} Mean \pm SD	WT Mean \pm SD	TNF ^{ΔAARE/WT} Mean \pm SD	WT Mean \pm SD	TNF ^{ΔAARE/WT} Mean \pm SD	WT Mean \pm SD	TNF ^{ΔAARE/WT} Mean \pm SD
lysoPCa C26:1	1.1318 \pm 0.336	0.9847 \pm 0.187	0.6734 \pm 0.233	0.8605 \pm 0.432	1.0357\pm0.727	0.4183\pm0.161*	1.2861\pm0.726	0.6109\pm0.226*	0.6399 \pm 0.222	0.6319 \pm 0.229

NB: All metabolite concentrations are presented as mean values \pm SD from 8 animals per group. The values from TNF ^{Δ AARE/WT} animals were compared at each time point with the WT mice. Significant differences were assessed by Mann-Whitney U test and marked as follows: * p <0.05, ** p <0.01, *** p <0.001.

Key: C: acyl-carnitine; H: basic sugar structure; lysoPCa: lysophosphatidylcholine; PCaa: phosphatidylcholine; PCae: phosphatidylcholine with an ether bond; SM: sphingomyelin.

LIST OF FIGURES

Figure 1: Loss of intestinal homeostasis results in chronic intestinal inflammation: Microbiota, intestinal epithelial cells, and lamina propria immune cells as targets, participants, and central organizers in intestinal immune responses (modified from ⁴)	10
Figure 2: Metabonomic work flow	29
Figure 3: Plasma ¹ H NMR pulse sequences and corresponding spectra used for spectral editing	32
Figure 4: Data mean-centering and unit variance (UV) scaling	39
Figure 5: Principal Component Analysis (PCA)	41
Figure 6: Geometrical illustration of the differences between the PLS-DA and O-PLS-DA models (modified from ¹²⁸)	43
Figure 7: Histopathological changes, body weight development, and inflammatory marker changes during colitis in c-IL-10 ^{-/-} mice	44
Figure 8: ¹ H NMR-based metabolic profiling of blood plasma	46
Figure 9: Blood plasma metabolic changes associated with colitis development by ¹ H NMR spectroscopy	47
Figure 10: Chemometric analysis of plasma metabolic profiles	49
Figure 11: Histopathological score and body weight changes	51
Figure 12: Blood plasma metabolic changes associated with colitis susceptibility by ¹ H NMR spectroscopy	52
Figure 13: NMR-based metabolic profiling of the hydrophilic extract of colon tissue	56
Figure 14: NMR-based metabolic profiling of the lipophilic extract of colon tissue	57
Figure 15: Colonic metabolic changes associated with colitis susceptibility by ¹ H NMR spectroscopy	57
Figure 16: Histopathological scoring, body weight development, nutritional energy utilization and adipose tissue morphology during CD-like ileitis in TNF ^{ΔARE/WT} mice	62
Figure 17: Blood plasma metabolic changes associated with CD-like ileitis development by ¹ H NMR spectroscopy	63
Figure 18: Blood plasma metabolic changes associated with CD-like ileitis development by LC-MS	66
Figure 19: Topographical modeling of CD-like ileitis in the gastrointestinal tract of WT and TNF ^{ΔARE/WT} mice	68
Figure 20: Intestinal metabolic diversity influenced by CD-like ileitis	69
Figure 21: Schematic model of inflammation-driven alterations of lipid metabolism during CD-like ileitis in TNF ^{ΔARE/WT} mice	84
Figure 22: Analogy in the ¹ H diffusion-edited NMR spectra of s-IL-10 ^{-/-} and TNF ^{ΔARE/WT} animals at 24 weeks of age	88
Figure 23: Parallels in the targeted LC-MS analysis of ileal tissue from TNF ^{ΔARE/WT} animals and colonic tissue from s-IL-10 ^{-/-} animals at 24 weeks of age	89

LIST OF TABLES

Table 1-1: Animal models of inflammatory bowel disease (modified from ³⁸).....	12
Table 1-2: Inflammatory bowel disease studies using metabonomic analysis (modified from Lin et al. ¹³³).....	24
Table 2-1: Types of 2D experiments providing different structural information.....	33
Table 3-1: Blood plasma metabolite differences between WT and c-IL-10 ^{-/-} mice at the age of 1, 8, 16, and 24 weeks detected by ¹ H NMR spectroscopy.....	50
Table 3-2: Blood plasma metabolite differences between WT and s-IL-10 ^{-/-} mice at the age of 4, 8, 12, 16, and 24 weeks detected by ¹ H NMR spectroscopy.....	53
Table 3-3: Time-dependent metabolic differences in plasma of s-IL-10 ^{-/-} compared to WT mice detected by UPLC-ESI-MS/MS using the AbsoluteIDQ TM Kit (Biocrates Life Sciences, Austria)	55
Table 3-4: O-PLS-DA model summary for the discrimination of 24 weeks old WT and s-IL-10 ^{-/-} mice by ¹ H NMR spectra of proximal colon extracts	58
Table 3-5: Time-dependent metabolic differences in the colon of s-IL-10 ^{-/-} compared to WT mice detected by UPLC-ESI-MS/MS using the AbsoluteIDQ TM Kit (Biocrates Life Sciences, Austria).....	60
Table 3-6: Blood plasma metabolite differences between WT and TNF ^{ΔARE/WT} at the age of 4, 8, 12, 16, and 24 weeks detected by ¹ H NMR spectroscopy.....	64
Table 3-7: Most discriminating metabolites in the plasma of TNF ^{ΔARE/WT} compared to WT mice at the age of 4, 8, 12, 16, and 24 weeks analyzed by UPLC-ESI-MS/MS using the AbsoluteIDQ TM Kit (Biocrates Life Sciences, Austria)	67
Table 3-8: Metabolic differences in the lipophilic fraction of different intestinal compartments (distal jejunum, distal ileum, proximal colon and distal colon) in TNF ^{ΔARE/WT} compared to WT mice at the age of 24 weeks detected by ¹ H NMR spectroscopy.....	70
Table 3-9: Most discriminating metabolites in the distal ileum of TNF ^{ΔARE/WT} compared to WT mice at the age of 4, 8, 12, 16, and 24 weeks analyzed by UHPLC-ESI-MS/MS using the AbsoluteIDQ TM Kit (Biocrates Life Sciences, Austria)	72
Table 3-10: Concentration levels (μg/g tissue) of fatty acid signaling markers in the distal ileum of TNF ^{ΔARE/WT} compared to WT mice at the age of 4, 8, 12, and 16 weeks analyzed by UPLC-ESI-MS/MS	73
Appendix Table 6-1: All significantly regulated metabolites in the plasma of s-IL-10 ^{-/-} compared to WT mice at the age of 4, 8, 12, 16, and 24 weeks analyzed by UPLC-ESI-MS/MS using the AbsoluteIDQ TM Kit (Biocrates Life Sciences, Austria).....	91
Appendix Table 6-2: All significantly regulated metabolites in the proximal colon of s-IL-10 ^{-/-} compared to WT mice at the age of 4, 8, 12, 16, and 24 weeks analyzed by UPLC-ESI-MS/MS using the AbsoluteIDQ TM Kit (Biocrates Life Sciences, Austria).....	94
Appendix Table 6-3: All significantly regulated metabolites in the plasma of TNF ^{ΔARE/WT} compared to WT mice at the age of 4, 8, 12, 16, and 24 weeks analyzed by UPLC-ESI-MS/MS using the AbsoluteIDQ TM Kit (Biocrates Life Sciences, Austria).....	96
Appendix Table 6-4: All significantly regulated metabolites in the distal ileum of TNF ^{ΔARE/WT} compared to WT mice at the age of 4, 8, 12, 16, and 24 weeks analyzed by UPLC-ESI-MS/MS using the AbsoluteIDQ TM Kit (Biocrates Life Sciences, Austria).....	100

ABBREVIATIONS

1D	One-Dimensional	FT-IR	Fourier transform-infrared spectroscopy
2D	Two-Dimensional	G1 / G2	Pulse field gradients
¹H	Hydrogen nucleus	Gai2	G protein ai2
¹³C	Carbon nucleus	GALT	Gut-associated immune system
¹⁵N	Nitrogen nucleus	GC	Gas chromatography
³¹P	Phosphor nucleus	GI	Gastrointestinal tract
A20	Tumor necrosis factor induced protein 3	Gln	Glutamine
AA	Arachidonic acid	Gly	Glycine
ABCB1	ATP-binding cassette subtype B1	GPC	Glycerophosphocholine
Ala	Alanine	GPL	Glycerophospholipids
APC	Antigen presenting cell	GS1/GS2	Nebulizer gas
APCI	atmospheric pressure chemical ionization	GTPase	Guanosine triphosphate hydrolase
		GWAS	Genome-wide association studies
apoA	Apolipoprotein A	H	Basic sugar structure
ARE	AU-rich elements	HDL	High density lipoprotein
Arg	Arginine	HETE	Hydroxyeicosatetraenoic acid
Atg	Autophagy gene	His	Histidine
ATG16L1	Autophagy-related protein 16 like 1	HLA-B27	Human β2 microglobulin
ATP	Adenosintriphosphat	HMBC	Heteronuclear multiple bond coherence
BHT	Butylated hydroxytoluene	HSQC	Heteronuclear single quantum coherence
C	Acyl-carnitine		
c-IL-10^{-/-}	IL-10 ^{-/-} mice housed under conventional conditions	HODE	Hydroxyoctadecadienoic acid
		IBD	Inflammatory bowel disease
CARD	Caspase recruitment domain-containing protein	IBS	Irritable bowel syndrome
		ICR-FT	Ion cyclotron resonance fourier transformation
CD	Crohn's disease		
CD4/8	Cluster of differentiation 4/8	IEC	Intestinal epithelial cell
CE	Capillary electrophoresis	IFN	Interferon
Chol	Cholesterol	Ig	Immunoglobulin
COSY	Correlated spectroscopy	IL	Interleukin
CPMG	Carr-Purcell-Meiboom-Gill	IRGM	Immunity-related GTPase family M
CRP	C-reactive protein	IS	Internal standard
CRFB	Interleukin 10 receptor β	ISV	Ion source voltage
CT	Computer tomography	JRES	J-resolved
CUR	Curtain gas	KC	Keratinocyte chemoattractant
CXP	Collision cell exit potential	LC	Liquid chromatography
δ	Chemical shift (in ppm from TSP)	LDL	Low density lipoprotein
D1	Relaxation delay	Leu	Leucine
D₂O	Deuterium oxide	LPL	Lipoprotein lipase
DA	Discriminant analysis	LPS	Lipopolysaccharide
DAG	Diacylglycerol	Lys	Lysine
dC	Distal colon	lysoPCa	Lysoohosphatidylcholine
DC	Dendritic cell	MAG	Monoacylglycerol
dI	Distalileum	MAS	Magic angle spinning
DiHETrE	Dihydroxyeicosatrienoic acid	Mdr	Multiple drug resistance
DiHOME	Dihydroxyoctadecenoic acid	Met	Methionine
DIMS	Direct infusion mass spectrometry	MHC	Major histocompatibility complex
dJ	Distal jejunum	mRNA	Messenger ribonucleic acid
DMA	Dimethylamine	MRS	Magnetic resonance spectroscopy
DMG	Dimethylglycine	MS	Mass spectrometry
DSS	Dextran sodium sulphate	Muc	Mucin
EDTA	Ethylenediaminetetraacetic acid	MVDA	Multivariate data analysis
ELISA	Enzyme linked immunosorbent assay	NaH₂PO₄	Sodium-dihydrogenphosphate
EpETrE	Epoxyeicosatrienoic acids	Na₂HPO₄	Disodium-hydrogenphosphate
ESI	Electrospray ionization	NCAD	N-cadherin
FA	Fatty acid	NEMO	NFκB Essential modulator
FID	Free induction decay	NFκB	Nuclear Factor κB
FT	Fourier transformation	NMR	Nuclear magnetic resonance

NOD	Nucleotide oligomerization domain	Trp	Tryptophan
NSAID	Non-steroidal anti-inflammatory drugs	Tyr	Tyrosine
OMS	Octamethylcyclotetrasiloxan	UC	Ulcerative colitis
O-PLS	Orthogonal projection to latent structure	UFA	Unsaturated fatty acids
Orn	Ornithine	UPLC	Ultra-performance liquid chromatography
PAF	Platelet-activating factor	UV	Unit variance
PBS	Phosphate buffered saline	v:v	Volume per volume
pC	Proximal colon	Val	Valine
PC(A)	Principal component (analysis)	VIP	Variable importance score
PCaa	Glycerophosphocholine	VLDL	Very low density lipoprotein
PCae	Glycerophosphocholine with an ether bond	WASP	Wiskott–Aldrich syndrome protein
PE	Phosphoethanolamine	WT	Wild type
PG	Prostaglandin	XBP	X-box bindingprotein
Phe	Phenylalanine	Δ	Diffusion delay
PL	Phospholipid		
PLA2	Phospholipase A2		
PLS	Projection to latent structures		
psi	Pound per square inch		
ppm	Parts per million		
Pro	Proline		
PRR	Pattern recognition receptor		
PUFA	Polyunsaturated fatty acids		
Q²Y	Cross-validation parameter		
QTOF	Quadrupole-time of flight		
QTRAP	Triple quadrupole- linear ion TRAP		
R₂X, R₂Y	Coefficient of determination		
RAG	Recombinase activating gene		
RT	Room temperature		
s-IL-10^{-/-}	IL-10 ^{-/-} mice housed under specific pathogen free conditions		
SAA	Serum amyloid A		
SCID	Severe combined immunodeficient		
SD	Standard deviation		
SEM	Standard error mean		
Ser	Serine		
SM	Sphingomyeline		
SMase	Sphingomyelinase		
SNP	Single nucleotide polymorphism		
SPF	Specific pathogen-free		
SRM	Scheduled reaction monitoring		
STAT	Signal transducer and activator of transcription		
STOCSY	Statistical total correlation spectroscopy		
TAC	Trichloroacetic acid		
TAG	Triacylglycerol		
T-bet	T-box transcription factor		
TCR	T Cell receptor		
TEM	Desolvation temperature		
tg	Transgene		
Tgε26	Transgenic epsilon		
TGF	Transforming growth factor		
Th	T helper cell		
TLR	Toll-like receptor		
tm	Mixing time		
TMA	Trimethylamine		
TNBS	Trinitrobenzene sulfonic acid		
TNF	Tumor necrosis factor		
TOCSY	Total correlation spectroscopy		
TOF	Time of flight		
TSP	Trimethylsilylpropionic acid		

REFERENCES

1. Gismera, C.S. and B.S. Aladren, *Inflammatory bowel diseases: a disease (s) of modern times? Is incidence still increasing?* World J Gastroenterol, 2008. **14**(36): p. 5491-8.
2. Hossain, P., B. Kavar, and M. El Nahas, *Obesity and diabetes in the developing world--a growing challenge.* N Engl J Med, 2007. **356**(3): p. 213-5.
3. Park, K.T. and D. Bass, *Inflammatory bowel disease-attributable costs and cost-effective strategies in the United States: a review.* Inflamm Bowel Dis, 2011. **17**(7): p. 1603-9.
4. Kaser, A., S. Zeissig, and R.S. Blumberg, *Inflammatory bowel disease.* Annu Rev Immunol, 2010. **28**: p. 573-621.
5. Abraham, C. and J.H. Cho, *Inflammatory bowel disease.* N Engl J Med, 2009. **361**(21): p. 2066-78.
6. Xavier, R.J. and D.K. Podolsky, *Unravelling the pathogenesis of inflammatory bowel disease.* Nature, 2007. **448**(7152): p. 427-34.
7. Lakatos, P.L., *Recent trends in the epidemiology of inflammatory bowel diseases: up or down?* World J Gastroenterol, 2006. **12**(38): p. 6102-8.
8. Monteleone, G., et al., *New mediators of immunity and inflammation in inflammatory bowel disease.* Curr Opin Gastroenterol, 2006. **22**(4): p. 361-4.
9. Monteleone, I., F. Pallone, and G. Monteleone, *Interleukin-23 and Th17 cells in the control of gut inflammation.* Mediators Inflamm, 2009. **2009**: p. 297645.
10. Liu, Z.J., et al., *Potential role of Th17 cells in the pathogenesis of inflammatory bowel disease.* World J Gastroenterol, 2009. **15**(46): p. 5784-8.
11. Brand, S., *Crohn's disease: Th1, Th17 or both? The change of a paradigm: new immunological and genetic insights implicate Th17 cells in the pathogenesis of Crohn's disease.* Gut, 2009. **58**(8): p. 1152-67.
12. Fujino, S., et al., *Increased expression of interleukin 17 in inflammatory bowel disease.* Gut, 2003. **52**(1): p. 65-70.
13. Lees, C.W., et al., *New IBD genetics: common pathways with other diseases.* Gut, 2011. **60**(12): p. 1739-53.
14. Noble, C.L., et al., *Characterization of intestinal gene expression profiles in Crohn's disease by genome-wide microarray analysis.* Inflamm Bowel Dis, 2010. **16**(10): p. 1717-28.
15. Strober, W., I. Fuss, and P. Mannon, *The fundamental basis of inflammatory bowel disease.* J Clin Invest, 2007. **117**(3): p. 514-21.
16. Clavel, T. and D. Haller, *Bacteria- and host-derived mechanisms to control intestinal epithelial cell homeostasis: implications for chronic inflammation.* Inflamm Bowel Dis, 2007. **13**(9): p. 1153-64.
17. Halfvarson, J., et al., *Inflammatory bowel disease in a Swedish twin cohort: a long-term follow-up of concordance and clinical characteristics.* Gastroenterology, 2003. **124**(7): p. 1767-73.
18. Tysk, C., et al., *Ulcerative colitis and Crohn's disease in an unselected population of monozygotic and dizygotic twins. A study of heritability and the influence of smoking.* Gut, 1988. **29**(7): p. 990-6.
19. Anderson, C.A., et al., *Meta-analysis identifies 29 additional ulcerative colitis risk loci, increasing the number of confirmed associations to 47.* Nat Genet, 2011. **43**(3): p. 246-52.
20. Umeno, J., et al., *Meta-analysis of published studies identified eight additional common susceptibility loci for Crohn's disease and ulcerative colitis.* Inflamm Bowel Dis, 2011. **17**(12): p. 2407-15.
21. Korzenik, J.R., *Past and current theories of etiology of IBD: toothpaste, worms, and refrigerators.* J Clin Gastroenterol, 2005. **39**(4 Suppl 2): p. S59-65.
22. Sartor, R.B., *Microbial influences in inflammatory bowel diseases.* Gastroenterology, 2008. **134**(2): p. 577-94.
23. Round, J.L. and S.K. Mazmanian, *The gut microbiota shapes intestinal immune responses during health and disease.* Nat Rev Immunol, 2009. **9**(5): p. 313-23.
24. Khan, K.J., et al., *Antibiotic therapy in inflammatory bowel disease: a systematic review and meta-analysis.* Am J Gastroenterol, 2011. **106**(4): p. 661-73.

25. Contractor, N.V., et al., *Lymphoid hyperplasia, autoimmunity, and compromised intestinal intraepithelial lymphocyte development in colitis-free gnotobiotic IL-2-deficient mice*. J Immunol, 1998. **160**(1): p. 385-94.
26. Sellon, R.K., et al., *Resident enteric bacteria are necessary for development of spontaneous colitis and immune system activation in interleukin-10-deficient mice*. Infect Immun, 1998. **66**(11): p. 5224-31.
27. Kaur, N., et al., *Intestinal dysbiosis in inflammatory bowel disease*. Gut Microbes, 2011. **2**(4): p. 211-6.
28. Walker, A.W., et al., *High-throughput clone library analysis of the mucosa-associated microbiota reveals dysbiosis and differences between inflamed and non-inflamed regions of the intestine in inflammatory bowel disease*. BMC Microbiol, 2011. **11**: p. 7.
29. Strober, W., *Adherent-invasive E. coli in Crohn disease: bacterial "agent provocateur"*. J Clin Invest, 2011. **121**(3): p. 841-4.
30. Haller, D., *Intestinal epithelial cell signalling and host-derived negative regulators under chronic inflammation: to be or not to be activated determines the balance towards commensal bacteria*. Neurogastroenterol Motil, 2006. **18**(3): p. 184-99.
31. Moehle, C., et al., *Aberrant intestinal expression and allelic variants of mucin genes associated with inflammatory bowel disease*. J Mol Med (Berl), 2006. **84**(12): p. 1055-66.
32. Schulzke, J.D., et al., *Epithelial tight junctions in intestinal inflammation*. Ann N Y Acad Sci, 2009. **1165**: p. 294-300.
33. Turner, J.R., *Intestinal mucosal barrier function in health and disease*. Nat Rev Immunol, 2009. **9**(11): p. 799-809.
34. Wehkamp, J., M. Schmid, and E.F. Stange, *Defensins and other antimicrobial peptides in inflammatory bowel disease*. Curr Opin Gastroenterol, 2007. **23**(4): p. 370-8.
35. Roda, G., et al., *Intestinal epithelial cells in inflammatory bowel diseases*. World J Gastroenterol, 2010. **16**(34): p. 4264-71.
36. Sartor, R.B., *Review article: How relevant to human inflammatory bowel disease are current animal models of intestinal inflammation?* Aliment Pharmacol Ther, 1997. **11 Suppl 3**: p. 89-96; discussion 96-7.
37. Mizoguchi, A. and E. Mizoguchi, *Animal models of IBD: linkage to human disease*. Curr Opin Pharmacol, 2010. **10**(5): p. 578-87.
38. Blumberg, R.S., L.J. Saubermann, and W. Strober, *Animal models of mucosal inflammation and their relation to human inflammatory bowel disease*. Curr Opin Immunol, 1999. **11**(6): p. 648-56.
39. Kuhn, R., et al., *Interleukin-10-deficient mice develop chronic enterocolitis*. Cell, 1993. **75**(2): p. 263-74.
40. Kontoyiannis, D., et al., *Impaired on/off regulation of TNF biosynthesis in mice lacking TNF AU-rich elements: implications for joint and gut-associated immunopathologies*. Immunity, 1999. **10**(3): p. 387-98.
41. Fiorentino, D.F., M.W. Bond, and T.R. Mosmann, *Two types of mouse T helper cell. IV. Th2 clones secrete a factor that inhibits cytokine production by Th1 clones*. J Exp Med, 1989. **170**(6): p. 2081-95.
42. Commins, S., J.W. Steinke, and L. Borish, *The extended IL-10 superfamily: IL-10, IL-19, IL-20, IL-22, IL-24, IL-26, IL-28, and IL-29*. J Allergy Clin Immunol, 2008. **121**(5): p. 1108-11.
43. Paul, G., V. Khare, and C. Gasche, *Inflamed gut mucosa: downstream of interleukin-10*. Eur J Clin Invest, 2012. **42**(1): p. 95-109.
44. Maynard, C.L. and C.T. Weaver, *Diversity in the contribution of interleukin-10 to T-cell-mediated immune regulation*. Immunol Rev, 2008. **226**: p. 219-33.
45. Lin, H.M., et al., *Metabolomic analysis identifies inflammatory and noninflammatory metabolic effects of genetic modification in a mouse model of Crohn's disease*. J Proteome Res, 2010. **9**(4): p. 1965-75.
46. Franke, A., et al., *Sequence variants in IL10, ARPC2 and multiple other loci contribute to ulcerative colitis susceptibility*. Nat Genet, 2008. **40**(11): p. 1319-23.
47. Correa, I., et al., *Defective IL-10 production in severe phenotypes of Crohn's disease*. J Leukoc Biol, 2009. **85**(5): p. 896-903.
48. Noguchi, E., et al., *A Crohn's disease-associated NOD2 mutation suppresses transcription of human IL10 by inhibiting activity of the nuclear ribonucleoprotein hnRNP-A1*. Nat Immunol, 2009. **10**(5): p. 471-9.
49. Glocker, E.O., et al., *Inflammatory bowel disease and mutations affecting the interleukin-10 receptor*. N Engl J Med, 2009. **361**(21): p. 2033-45.

50. Barrett, J.C., et al., *Genome-wide association defines more than 30 distinct susceptibility loci for Crohn's disease*. Nat Genet, 2008. **40**(8): p. 955-62.
51. Lindsay, J., et al., *IL-10 gene therapy prevents TNBS-induced colitis*. Gene Ther, 2002. **9**(24): p. 1715-21.
52. Colombel, J.F., et al., *Interleukin 10 (Tenovil) in the prevention of postoperative recurrence of Crohn's disease*. Gut, 2001. **49**(1): p. 42-6.
53. Tilg, H., et al., *Treatment of Crohn's disease with recombinant human interleukin 10 induces the proinflammatory cytokine interferon gamma*. Gut, 2002. **50**(2): p. 191-5.
54. Wirtz, S. and M.F. Neurath, *Mouse models of inflammatory bowel disease*. Adv Drug Deliv Rev, 2007. **59**(11): p. 1073-83.
55. Berg, D.J., et al., *Enterocolitis and colon cancer in interleukin-10-deficient mice are associated with aberrant cytokine production and CD4(+) TH1-like responses*. J Clin Invest, 1996. **98**(4): p. 1010-20.
56. Lindsay, J.O., et al., *Local delivery of adenoviral vectors encoding murine interleukin 10 induces colonic interleukin 10 production and is therapeutic for murine colitis*. Gut, 2003. **52**(7): p. 981-7.
57. Spencer, S.D., et al., *The orphan receptor CRF2-4 is an essential subunit of the interleukin 10 receptor*. J Exp Med, 1998. **187**(4): p. 571-8.
58. Madsen, K.L., et al., *Interleukin-10 gene-deficient mice develop a primary intestinal permeability defect in response to enteric microflora*. Inflamm Bowel Dis, 1999. **5**(4): p. 262-70.
59. Old, L.J., *Tumor necrosis factor (TNF)*. Science, 1985. **230**(4726): p. 630-2.
60. Locksley, R.M., N. Killeen, and M.J. Lenardo, *The TNF and TNF receptor superfamilies: integrating mammalian biology*. Cell, 2001. **104**(4): p. 487-501.
61. Vassalli, P., *The pathophysiology of tumor necrosis factors*. Annu Rev Immunol, 1992. **10**: p. 411-52.
62. Black, R.A., et al., *A metalloproteinase disintegrin that releases tumour-necrosis factor-alpha from cells*. Nature, 1997. **385**(6618): p. 729-33.
63. Pinckard, J.K., et al., *Constitutive shedding of both p55 and p75 murine TNF receptors in vivo*. J Immunol, 1997. **158**(8): p. 3869-73.
64. Wajant, H., K. Pfizenmaier, and P. Scheurich, *Tumor necrosis factor signaling*. Cell Death Differ, 2003. **10**(1): p. 45-65.
65. Apostolaki, M., et al., *Cellular mechanisms of TNF function in models of inflammation and autoimmunity*. Curr Dir Autoimmun, 2010. **11**: p. 1-26.
66. Murch, S.H., et al., *Location of tumour necrosis factor alpha by immunohistochemistry in chronic inflammatory bowel disease*. Gut, 1993. **34**(12): p. 1705-9.
67. Breese, E.J., et al., *Tumor necrosis factor alpha-producing cells in the intestinal mucosa of children with inflammatory bowel disease*. Gastroenterology, 1994. **106**(6): p. 1455-66.
68. Van Deventer, S.J., *Tumour necrosis factor and Crohn's disease*. Gut, 1997. **40**(4): p. 443-8.
69. Ferguson, L.R., et al., *Single nucleotide polymorphism in the tumor necrosis factor-alpha gene affects inflammatory bowel diseases risk*. World J Gastroenterol, 2008. **14**(29): p. 4652-61.
70. Fan, W., et al., *Relationship between the polymorphism of tumor necrosis factor-alpha-308 G>A and susceptibility to inflammatory bowel diseases and colorectal cancer: a meta-analysis*. Eur J Hum Genet, 2011. **19**(4): p. 432-7.
71. Koss, K., et al., *Cytokine (TNF alpha, LT alpha and IL-10) polymorphisms in inflammatory bowel diseases and normal controls: differential effects on production and allele frequencies*. Genes Immun, 2000. **1**(3): p. 185-90.
72. Gratz, R., et al., *Murine monoclonal anti-tNF antibody administration has a beneficial effect on inflammatory bowel disease that develops in IL-10 knockout mice*. Dig Dis Sci, 2002. **47**(8): p. 1723-7.
73. Marini, M., et al., *TNF-alpha neutralization ameliorates the severity of murine Crohn's-like ileitis by abrogation of intestinal epithelial cell apoptosis*. Proc Natl Acad Sci U S A, 2003. **100**(14): p. 8366-71.
74. van Dullemen, H.M., et al., *Treatment of Crohn's disease with anti-tumor necrosis factor chimeric monoclonal antibody (cA2)*. Gastroenterology, 1995. **109**(1): p. 129-35.
75. Peyrin-Biroulet, L., *Anti-TNF therapy in inflammatory bowel diseases: a huge review*. Minerva Gastroenterol Dietol, 2010. **56**(2): p. 233-43.

76. Magro, F. and F. Portela, *Management of inflammatory bowel disease with infliximab and other anti-tumor necrosis factor alpha therapies*. *BioDrugs*, 2010. **24 Suppl 1**: p. 3-14.
77. Sandborn, W.J. and S.B. Hanauer, *Antitumor necrosis factor therapy for inflammatory bowel disease: a review of agents, pharmacology, clinical results, and safety*. *Inflamm Bowel Dis*, 1999. **5**(2): p. 119-33.
78. Apostolaki, M., et al., *Role of beta7 integrin and the chemokine/chemokine receptor pair CCL25/CCR9 in modeled TNF-dependent Crohn's disease*. *Gastroenterology*, 2008. **134**(7): p. 2025-35.
79. Kontoyiannis, D., et al., *Genetic dissection of the cellular pathways and signaling mechanisms in modeled tumor necrosis factor-induced Crohn's-like inflammatory bowel disease*. *J Exp Med*, 2002. **196**(12): p. 1563-74.
80. Bamias, G., et al., *Role of TL1A and its receptor DR3 in two models of chronic murine ileitis*. *Proc Natl Acad Sci U S A*, 2006. **103**(22): p. 8441-6.
81. Jacques, P., et al., *Invariant natural killer T cells are natural regulators of murine spondylarthritis*. *Arthritis Rheum*, 2010. **62**(4): p. 988-99.
82. Roulis, M., et al., *Intestinal epithelial cells as producers but not targets of chronic TNF suffice to cause murine Crohn-like pathology*. *Proc Natl Acad Sci U S A*, 2011. **108**(13): p. 5396-401.
83. Fiehn, O., *Metabolomics--the link between genotypes and phenotypes*. *Plant Mol Biol*, 2002. **48**(1-2): p. 155-71.
84. Nicholson, J.K. and I.D. Wilson, *Opinion: understanding 'global' systems biology: metabolomics and the continuum of metabolism*. *Nat Rev Drug Discov*, 2003. **2**(8): p. 668-76.
85. Goodacre, R., et al., *Metabolomics by numbers: acquiring and understanding global metabolite data*. *Trends Biotechnol*, 2004. **22**(5): p. 245-52.
86. Dunn, W.B., et al., *Systems level studies of mammalian metabolomes: the roles of mass spectrometry and nuclear magnetic resonance spectroscopy*. *Chem Soc Rev*, 2011. **40**(1): p. 387-426.
87. Nicholson, J.K., J.C. Lindon, and E. Holmes, *'Metabolomics': understanding the metabolic responses of living systems to pathophysiological stimuli via multivariate statistical analysis of biological NMR spectroscopic data*. *Xenobiotica*, 1999. **29**(11): p. 1181-9.
88. Madsen, R., T. Lundstedt, and J. Trygg, *Chemometrics in metabolomics--a review in human disease diagnosis*. *Anal Chim Acta*, 2010. **659**(1-2): p. 23-33.
89. Bjerrum, J.T., et al., *Technology insight: metabolomics in gastroenterology--basic principles and potential clinical applications*. *Nat Clin Pract Gastroenterol Hepatol*, 2008. **5**(6): p. 332-43.
90. Nicholson, J.K. and J.C. Lindon, *Systems biology: Metabolomics*. *Nature*, 2008. **455**(7216): p. 1054-6.
91. Lindon, J.C., et al., *Contemporary issues in toxicology the role of metabolomics in toxicology and its evaluation by the COMET project*. *Toxicol Appl Pharmacol*, 2003. **187**(3): p. 137-46.
92. Nicholson, J.K., et al., *Metabolomics: a platform for studying drug toxicity and gene function*. *Nat Rev Drug Discov*, 2002. **1**(2): p. 153-61.
93. Lauridsen, M.B., et al., *¹H NMR spectroscopy-based interventional metabolic phenotyping: a cohort study of rheumatoid arthritis patients*. *J Proteome Res*, 2010. **9**(9): p. 4545-53.
94. Kim, S.H., et al., *¹H-nuclear magnetic resonance spectroscopy-based metabolic assessment in a rat model of obesity induced by a high-fat diet*. *Anal Bioanal Chem*, 2009. **395**(4): p. 1117-24.
95. Zhang, S., et al., *Correlative and quantitative ¹H NMR-based metabolomics reveals specific metabolic pathway disturbances in diabetic rats*. *Anal Biochem*, 2008. **383**(1): p. 76-84.
96. Rezzi, S., et al., *Nutritional metabolomics: applications and perspectives*. *J Proteome Res*, 2007. **6**(2): p. 513-25.
97. Martin, F.P., et al., *Metabolic effects of dark chocolate consumption on energy, gut microbiota, and stress-related metabolism in free-living subjects*. *J Proteome Res*, 2009. **8**(12): p. 5568-79.
98. Martin, F.P., et al., *A top-down systems biology view of microbiome-mammalian metabolic interactions in a mouse model*. *Mol Syst Biol*, 2007. **3**: p. 112.
99. Martin, F.P., et al., *Top-down systems biology integration of conditional prebiotic modulated transgenomic interactions in a humanized microbiome mouse model*. *Mol Syst Biol*, 2008. **4**: p. 205.
100. Pauling, L., et al., *Quantitative analysis of urine vapor and breath by gas-liquid partition chromatography*. *Proc Natl Acad Sci U S A*, 1971. **68**(10): p. 2374-6.

101. Lei, Z., D.V. Huhman, and L.W. Sumner, *Mass spectrometry strategies in metabolomics*. J Biol Chem, 2011. **286**(29): p. 25435-42.
102. Hollywood, K., D.R. Brison, and R. Goodacre, *Metabolomics: current technologies and future trends*. Proteomics, 2006. **6**(17): p. 4716-23.
103. Nicholson, J.K. and I.D. Wilson, *High resolution proton magnetic resonance spectroscopy of biological fluids*. Prog NMR Spectr, 1989. **21**: p. 449-501.
104. Bollard, M.E., et al., *NMR-based metabonomic approaches for evaluating physiological influences on biofluid composition*. NMR Biomed, 2005. **18**(3): p. 143-62.
105. Claridge, T., *High-Resolution NMR Techniques in Organic Chemistry*. Pergamon 1999.
106. Hore, P.J., J.A. Jones, and S. Wipieris, *NMR: The toolkit*. Oxford Science Publications 2000.
107. Lindon, J.C., E. Holmes, and J.K. Nicholson, *Metabonomics techniques and applications to pharmaceutical research & development*. Pharm Res, 2006. **23**(6): p. 1075-88.
108. Wang, Y., et al., *Biochemical characterization of rat intestine development using high-resolution magic-angle-spinning ¹H NMR spectroscopy and multivariate data analysis*. J Proteome Res, 2005. **4**(4): p. 1324-9.
109. Schicho, R., et al., *Quantitative metabolomic profiling of serum and urine in DSS-induced ulcerative colitis of mice by (¹H) NMR spectroscopy*. J Proteome Res, 2010. **9**(12): p. 6265-73.
110. Williams, H.R., et al., *Characterization of inflammatory bowel disease with urinary metabolic profiling*. Am J Gastroenterol, 2009. **104**(6): p. 1435-44.
111. Marchesi, J.R., et al., *Rapid and noninvasive metabonomic characterization of inflammatory bowel disease*. J Proteome Res, 2007. **6**(2): p. 546-51.
112. Balasubramanian, K., et al., *Metabolism of the colonic mucosa in patients with inflammatory bowel diseases: an in vitro proton magnetic resonance spectroscopy study*. Magn Reson Imaging, 2009. **27**(1): p. 79-86.
113. Beckonert, O., et al., *Metabolic profiling, metabolomic and metabonomic procedures for NMR spectroscopy of urine, plasma, serum and tissue extracts*. Nat Protoc, 2007. **2**(11): p. 2692-703.
114. Jeener, J., et al., *Investigation of exchange processes by twodimensional NMR spectroscopy*. J Chem Phys, 1979. **71**: p. 4546-4553.
115. Meiboom, S. and D. Gill, *Modified Spin-Echo Method for Measuring Nuclear Relaxation Times*. Rev Sci Instrum, 1958. **29**(8): p. 688 - 691.
116. Wu, D.H., A.D. Chen, and C.S. Johnson, *An Improved Diffusion-ordered Spectroscopy Experiment Incorporating Bipolar-Gradient Pulses*. J Magn Reson, Ser A, 1995. **115**: p. 260-264.
117. Nagayama, K., *Experimental Techniques of two-dimensional correlated spectroscopy*. J Magn Reson, Ser A, 1980. **40**(2): p. 321-334.
118. Dettmer, K., P.A. Aronov, and B.D. Hammock, *Mass spectrometry-based metabolomics*. Mass Spectrom Rev, 2007. **26**(1): p. 51-78.
119. Lu, X., et al., *LC-MS-based metabonomics analysis*. J Chromatogr B Analyt Technol Biomed Life Sci, 2008. **866**(1-2): p. 64-76.
120. Dunn, W.B., N.J. Bailey, and H.E. Johnson, *Measuring the metabolome: current analytical technologies*. Analyst, 2005. **130**(5): p. 606-25.
121. Wilson, I.D., et al., *HPLC-MS-based methods for the study of metabonomics*. J Chromatogr B Analyt Technol Biomed Life Sci, 2005. **817**(1): p. 67-76.
122. Villas-Boas, S.G., et al., *Mass spectrometry in metabolome analysis*. Mass Spectrom Rev, 2005. **24**(5): p. 613-46.
123. Hsieh, Y. and W. Korfmacher, *The role of hyphenated chromatography-mass spectrometry techniques in exploratory drug metabolism and pharmacokinetics*. Curr Pharm Des, 2009. **15**(19): p. 2251-61.
124. Glinski, M. and W. Weckwerth, *The role of mass spectrometry in plant systems biology*. Mass Spectrom Rev, 2006. **25**(2): p. 173-214.
125. Shiomi, Y., et al., *GCMS-based metabolomic study in mice with colitis induced by dextran sulfate sodium*. Inflamm Bowel Dis, 2011.

126. Lin, H.M., et al., *Metabolomic analysis reveals differences in urinary excretion of kiwifruit-derived metabolites in a mouse model of inflammatory bowel disease*. *Mol Nutr Food Res*, 2011. **55**(12): p. 1900-4.
127. Ooi, M., et al., *GC/MS-based profiling of amino acids and TCA cycle-related molecules in ulcerative colitis*. *Inflamm Res*, 2011. **60**(9): p. 831-40.
128. Trygg, J., E. Holmes, and T. Lundstedt, *Chemometrics in metabonomics*. *J Proteome Res*, 2007. **6**(2): p. 469-79.
129. Coen, M., et al., *NMR-based metabolic profiling and metabonomic approaches to problems in molecular toxicology*. *Chem Res Toxicol*, 2008. **21**(1): p. 9-27.
130. Eriksson, L., et al., *Multivariate and Megavariate Data Analysis Basic Principles and Applications (Part I)*. 2 ed2006: Umetrics. 425.
131. Wold, S., M. Sjöström, and L. Eriksson, *PLS-regression: a basic tool of chemometrics*. *Chemometrics and Intelligent Laboratory Systems*, 2001. **58**(2): p. 109-130.
132. Trygg, J. and S. Wold, *Orthogonal projections to latent structures, OPLS*. *Chemom*, 2002. **16**(3): p. 119-128.
133. Lin, H.M., et al., *Using metabolomic analysis to understand inflammatory bowel diseases*. *Inflamm Bowel Dis*, 2011. **17**(4): p. 1021-9.
134. Warner, E.E. and B.K. Dieckgraefe, *Application of genome-wide gene expression profiling by high-density DNA arrays to the treatment and study of inflammatory bowel disease*. *Inflamm Bowel Dis*, 2002. **8**(2): p. 140-57.
135. Murdoch, T.B., et al., *Urinary metabolic profiles of inflammatory bowel disease in interleukin-10 gene-deficient mice*. *Anal Chem*, 2008. **80**(14): p. 5524-31.
136. Otter, D., et al., *Identification of urinary biomarkers of colon inflammation in IL10^{-/-} mice using Short-Column LCMS metabolomics*. *J Biomed Biotechnol*, 2011. **2011**: p. 974701.
137. Le Gall, G., et al., *Metabolomics of fecal extracts detects altered metabolic activity of gut microbiota in ulcerative colitis and irritable bowel syndrome*. *J Proteome Res*, 2011. **10**(9): p. 4208-18.
138. Martin, F.P., et al., *Transgenomic metabolic interactions in a mouse disease model: interactions of Trichinella spiralis infection with dietary Lactobacillus paracasei supplementation*. *J Proteome Res*, 2006. **5**(9): p. 2185-93.
139. Bezabeh, T., et al., *The use of 1H magnetic resonance spectroscopy in inflammatory bowel diseases: distinguishing ulcerative colitis from Crohn's disease*. *Am J Gastroenterol*, 2001. **96**(2): p. 442-8.
140. Bjerrum, J.T., et al., *Metabonomics in ulcerative colitis: diagnostics, biomarker identification, and insight into the pathophysiology*. *J Proteome Res*, 2010. **9**(2): p. 954-62.
141. Sharma, U., et al., *Similarity in the metabolic profile in macroscopically involved and un-involved colonic mucosa in patients with inflammatory bowel disease: an in vitro proton ((1)H) MR spectroscopy study*. *Magn Reson Imaging*, 2010. **28**(7): p. 1022-9.
142. Bezabeh, T., R.L. Somorjai, and I.C. Smith, *MR metabolomics of fecal extracts: applications in the study of bowel diseases*. *Magn Reson Chem*, 2009. **47 Suppl 1**: p. S54-61.
143. Clayton, T.A., et al., *Pharmaco-metabonomic phenotyping and personalized drug treatment*. *Nature*, 2006. **440**(7087): p. 1073-7.
144. Jansson, J., et al., *Metabolomics reveals metabolic biomarkers of Crohn's disease*. *PLoS One*, 2009. **4**(7): p. e6386.
145. Martin, F.P., et al., *Metabolic assessment of gradual development of moderate experimental colitis in IL-10 deficient mice*. *J Proteome Res*, 2009. **8**(5): p. 2376-87.
146. Baur, P., et al., *Metabolic Phenotyping of the Crohn's Disease-like IBD Etiopathology in the TNF(DeltaAREW/T) Mouse Model*. *J Proteome Res*, 2011.
147. Varma, S., et al., *Detection of inflammatory bowel disease by proton magnetic resonance spectroscopy (1H MRS) using an animal model*. *J Inflamm (Lond)*, 2007. **4**: p. 24.
148. Chen, C., et al., *Metabolomics reveals that hepatic stearoyl-CoA desaturase 1 downregulation exacerbates inflammation and acute colitis*. *Cell Metab*, 2008. **7**(2): p. 135-47.
149. Katakura, K., et al., *Toll-like receptor 9-induced type I IFN protects mice from experimental colitis*. *J Clin Invest*, 2005. **115**(3): p. 695-702.

150. Nagayama, K., *Spin decoupling in 2-dimensional J-resolved NMR-spectroscopy*. J Chem Phys, 1979. **71**(11): p. 4404-4415.
151. Folch, J., M. Lees, and G.H. Sloane Stanley, *A simple method for the isolation and purification of total lipides from animal tissues*. J Biol Chem, 1957. **226**(1): p. 497-509.
152. Siddiqui, N., et al., *Multicomponent analysis of encapsulated marine oil supplements using high-resolution ¹H and ¹³C NMR techniques*. J Lipid Res, 2003. **44**(12): p. 2406-27.
153. Oostendorp, M., et al., *Diagnosing inborn errors of lipid metabolism with proton nuclear magnetic resonance spectroscopy*. Clin Chem, 2006. **52**(7): p. 1395-405.
154. Cloarec, O., et al., *Statistical total correlation spectroscopy: an exploratory approach for latent biomarker identification from metabolic ¹H NMR data sets*. Anal Chem, 2005. **77**(5): p. 1282-1289.
155. Römisch-Margl, W., et al., *Procedure for tissue sample preparation and metabolite extraction for high-throughput targeted metabolomics*. Metabolomics, 11th March 2011. (doi:10.1007/s11306-011-0293-4).
156. Deems, R., et al., *Detection and quantitation of eicosanoids via high performance liquid chromatography-electrospray ionization-mass spectrometry*. Methods Enzymol, 2007. **432**: p. 59-82.
157. Eriksson, L., et al., *Multi- and megavariable data analysis. Part 1: Basic principles and applications*, ed. U. AB2006.
158. Trygg, J., *O2-PLS for qualitative and quantitative analysis in multivariate calibration*. J Chemom, 2002. **17**: p. 53-64.
159. Trygg, J. and S. Wold, *Orthogonal projections to latent structures, OPLS*. J Chemom, 2002. **16**(3): p. 119-128.
160. Cloarec, O., et al., *Evaluation of the orthogonal projection on latent structure model limitations caused by chemical shift variability and improved visualization of biomarker changes in ¹H NMR spectroscopic metabolomic studies*. Anal Chem, 2005. **77**(2): p. 517-526.
161. Cloarec, O., et al., *Evaluation of the orthogonal projection on latent structure model limitations caused by chemical shift variability and improved visualization of biomarker changes in ¹H NMR spectroscopic metabolomic studies*. Anal Chem, 2005. **77**(2): p. 517-26.
162. Wiklund, S., et al., *Visualization of GC/TOF-MS-based metabolomics data for identification of biochemically interesting compounds using OPLS class models*. Anal Chem, 2008. **80**(1): p. 115-22.
163. Levy, E., et al., *Altered lipid profile, lipoprotein composition, and oxidant and antioxidant status in pediatric Crohn disease*. Am J Clin Nutr, 2000. **71**(3): p. 807-15.
164. Ross, R., *Atherosclerosis is an inflammatory disease*. Am Heart J, 1999. **138**(5 Pt 2): p. S419-20.
165. Weber, C. and H. Noels, *Atherosclerosis: current pathogenesis and therapeutic options*. Nat Med, 2011. **17**(11): p. 1410-22.
166. Romanato, G., et al., *Plasma lipids and inflammation in active inflammatory bowel diseases*. Aliment Pharmacol Ther, 2009. **29**(3): p. 298-307.
167. Ripolles Piquer, B., et al., *Altered lipid, apolipoprotein, and lipoprotein profiles in inflammatory bowel disease: consequences on the cholesterol efflux capacity of serum using Fu5AH cell system*. Metabolism, 2006. **55**(7): p. 980-8.
168. Khovidhunkit, W., et al., *Effects of infection and inflammation on lipid and lipoprotein metabolism: mechanisms and consequences to the host*. J Lipid Res, 2004. **45**(7): p. 1169-96.
169. Gabay, C. and I. Kushner, *Acute-phase proteins and other systemic responses to inflammation*. N Engl J Med, 1999. **340**(6): p. 448-54.
170. Niederau, C., F. Backmerhoff, and B. Schumacher, *Inflammatory mediators and acute phase proteins in patients with Crohn's disease and ulcerative colitis*. Hepatogastroenterology, 1997. **44**(13): p. 90-107.
171. Singh, U.P., et al., *CXCL10-producing mucosal CD4+ T cells, NK cells, and NKT cells are associated with chronic colitis in IL-10(-/-) mice, which can be abrogated by anti-CXCL10 antibody inhibition*. J Interferon Cytokine Res, 2008. **28**(1): p. 31-43.
172. Getz, G.S. and C.A. Reardon, *SAA, HDL biogenesis, and inflammation*. J Lipid Res, 2008. **49**(2): p. 269-70.
173. Hoffman, J.S. and E.P. Benditt, *Plasma clearance kinetics of the amyloid-related high density lipoprotein apoprotein, serum amyloid protein (apoSAA), in the mouse. Evidence for rapid apoSAA clearance*. J Clin Invest, 1983. **71**(4): p. 926-34.

174. Banka, C.L., et al., *Serum amyloid A (SAA): influence on HDL-mediated cellular cholesterol efflux*. J Lipid Res, 1995. **36**(5): p. 1058-65.
175. Barter, P., *The inflammation: lipoprotein cycle*. Atheroscler Suppl, 2005. **6**(2): p. 15-20.
176. Gouni, I., et al., *Endotoxin-induced hypertriglyceridemia is mediated by suppression of lipoprotein lipase at a post-transcriptional level*. J Lipid Res, 1993. **34**(1): p. 139-46.
177. Cheung, M.C., et al., *Phospholipid transfer protein activity is associated with inflammatory markers in patients with cardiovascular disease*. Biochim Biophys Acta, 2006. **1762**(1): p. 131-7.
178. Caligiuri, G., et al., *Interleukin-10 deficiency increases atherosclerosis, thrombosis, and low-density lipoproteins in apolipoprotein E knockout mice*. Mol Med, 2003. **9**(1-2): p. 10-7.
179. Sartor, R.B., *Review article: Role of the enteric microflora in the pathogenesis of intestinal inflammation and arthritis*. Aliment Pharmacol Ther, 1997. **11 Suppl 3**: p. 17-22; discussion 22-3.
180. Chambers, R.E., et al., *Serum amyloid A protein compared with C-reactive protein, alpha 1-antichymotrypsin and alpha 1-acid glycoprotein as a monitor of inflammatory bowel disease*. Eur J Clin Invest, 1987. **17**(5): p. 460-7.
181. Shkoda, A., et al., *Interleukin-10 blocked endoplasmic reticulum stress in intestinal epithelial cells: impact on chronic inflammation*. Gastroenterology, 2007. **132**(1): p. 190-207.
182. Newsholme, P., et al., *Glutamine and glutamate--their central role in cell metabolism and function*. Cell Biochem Funct, 2003. **21**(1): p. 1-9.
183. Israeli, E., et al., *Prophylactic administration of topical glutamine enhances the capability of the rat colon to resist inflammatory damage*. Dig Dis Sci, 2004. **49**(10): p. 1705-12.
184. Vicario, M., et al., *Dietary glutamine affects mucosal functions in rats with mild DSS-induced colitis*. J Nutr, 2007. **137**(8): p. 1931-7.
185. Cross, R.K. and K.T. Wilson, *Nitric oxide in inflammatory bowel disease*. Inflamm Bowel Dis, 2003. **9**(3): p. 179-89.
186. Werner, T., A. Shkoda, and D. Haller, *Intestinal epithelial cell proteome in IL-10 deficient mice and IL-10 receptor reconstituted epithelial cells: impact on chronic inflammation*. J Proteome Res, 2007. **6**(9): p. 3691-704.
187. Mittendorfer, B., *Sexual dimorphism in human lipid metabolism*. J Nutr, 2005. **135**(4): p. 681-6.
188. Ahmad, M.S., et al., *Butyrate and glucose metabolism by colonocytes in experimental colitis in mice*. Gut, 2000. **46**(4): p. 493-9.
189. Chapman, M.A., et al., *Butyrate oxidation is impaired in the colonic mucosa of sufferers of quiescent ulcerative colitis*. Gut, 1994. **35**(1): p. 73-6.
190. Thibault, R., et al., *Butyrate utilization by the colonic mucosa in inflammatory bowel diseases: a transport deficiency*. Inflamm Bowel Dis, 2010. **16**(4): p. 684-95.
191. Cooney, J.M., et al., *Proteomic Analysis of Colon Tissue from Interleukin-10 Gene-Deficient Mice Fed Polyunsaturated Fatty Acids with Comparison to Transcriptomic Analysis*. J Proteome Res, 2012.
192. Fisher, R.L., *Wasting in chronic gastrointestinal diseases*. J Nutr, 1999. **129**(1S Suppl): p. 252S-255S.
193. Filipsson, S., L. Hulten, and G. Lindstedt, *Malabsorption of fat and vitamin B12 before and after intestinal resection for Crohn's disease*. Scand J Gastroenterol, 1978. **13**(5): p. 529-36.
194. Huybers, S., et al., *Murine TNF(DeltaARE) Crohn's disease model displays diminished expression of intestinal Ca²⁺ transporters*. Inflamm Bowel Dis, 2008. **14**(6): p. 803-11.
195. Bannerman, E., et al., *Altered subjective appetite parameters in Crohn's disease patients*. Clin Nutr, 2001. **20**(5): p. 399-405.
196. Wymann, M.P. and R. Schneider, *Lipid signalling in disease*. Nat Rev Mol Cell Biol, 2008. **9**(2): p. 162-76.
197. Krinsky, M., et al., *Amelioration of TNBS-induced colon inflammation in rats by phospholipase A2 inhibitor*. Am J Physiol Gastrointest Liver Physiol, 2003. **285**(3): p. G586-92.
198. Taylor, L.A., et al., *Plasma lyso-phosphatidylcholine concentration is decreased in cancer patients with weight loss and activated inflammatory status*. Lipids Health Dis, 2007. **6**: p. 17.
199. Minami, T., et al., *Elevation of phospholipase A2 protein in sera of patients with Crohn's disease and ulcerative colitis*. Am J Gastroenterol, 1993. **88**(7): p. 1076-80.

200. Esteve-Comas, M., et al., *Plasma polyunsaturated fatty acid pattern in active inflammatory bowel disease*. Gut, 1992. **33**(10): p. 1365-9.
201. Zhao, Z., et al., *Plasma lysophosphatidylcholine levels: potential biomarkers for colorectal cancer*. J Clin Oncol, 2007. **25**(19): p. 2696-701.
202. Nilsson, A. and R.D. Duan, *Absorption and lipoprotein transport of sphingomyelin*. J Lipid Res, 2006. **47**(1): p. 154-71.
203. Hammad, S.M., *Blood sphingolipids in homeostasis and pathobiology*. Adv Exp Med Biol, 2011. **721**: p. 57-66.
204. Hannun, Y.A. and L.M. Obeid, *Principles of bioactive lipid signalling: lessons from sphingolipids*. Nat Rev Mol Cell Biol, 2008. **9**(2): p. 139-50.
205. Lightle, S., et al., *Elevation of ceramide in serum lipoproteins during acute phase response in humans and mice: role of serine-palmitoyl transferase*. Arch Biochem Biophys, 2003. **419**(2): p. 120-8.
206. Wong, M.L., et al., *Acute systemic inflammation up-regulates secretory sphingomyelinase in vivo: a possible link between inflammatory cytokines and atherogenesis*. Proc Natl Acad Sci U S A, 2000. **97**(15): p. 8681-6.
207. Langmann, T., et al., *Transcription factors Sp1 and AP-2 mediate induction of acid sphingomyelinase during monocytic differentiation*. J Lipid Res, 1999. **40**(5): p. 870-80.
208. Barsacchi, R., et al., *Activation of endothelial nitric-oxide synthase by tumor necrosis factor-alpha: a novel pathway involving sequential activation of neutral sphingomyelinase, phosphatidylinositol-3' kinase, and Akt*. Mol Pharmacol, 2003. **63**(4): p. 886-95.
209. Merrill, A.H., Jr., et al., *Role of dietary sphingolipids and inhibitors of sphingolipid metabolism in cancer and other diseases*. J Nutr, 1995. **125**(6 Suppl): p. 1677S-1682S.
210. Zhang, P., et al., *Dietary sphingomyelin inhibits colonic tumorigenesis with an up-regulation of alkaline sphingomyelinase expression in ICR mice*. Anticancer Res, 2008. **28**(6A): p. 3631-5.
211. Fischbeck, A., et al., *Sphingomyelin induces cathepsin D-mediated apoptosis in intestinal epithelial cells and increases inflammation in DSS colitis*. Gut, 2011. **60**(1): p. 55-65.
212. Furuya, H., et al., *Dietary sphingomyelin alleviates experimental inflammatory bowel disease in mice*. Int J Vitam Nutr Res, 2008. **78**(1): p. 41-9.
213. Sakata, A., et al., *Acid sphingomyelinase inhibition suppresses lipopolysaccharide-mediated release of inflammatory cytokines from macrophages and protects against disease pathology in dextran sulphate sodium-induced colitis in mice*. Immunology, 2007. **122**(1): p. 54-64.
214. Hama, H., *Fatty acid 2-Hydroxylation in mammalian sphingolipid biology*. Biochim Biophys Acta, 2010. **1801**(4): p. 405-14.
215. Calder, P.C., *Polyunsaturated fatty acids, inflammatory processes and inflammatory bowel diseases*. Mol Nutr Food Res, 2008. **52**(8): p. 885-97.
216. Lambert, D., C.A. O'Neill, and P.J. Padfield, *Depletion of Caco-2 cell cholesterol disrupts barrier function by altering the detergent solubility and distribution of specific tight-junction proteins*. Biochem J, 2005. **387**(Pt 2): p. 553-60.
217. Innis, S.M., et al., *Perinatal lipid nutrition alters early intestinal development and programs the response to experimental colitis in young adult rats*. Am J Physiol Gastrointest Liver Physiol, 2010. **299**(6): p. G1376-85.
218. McGuckin, M.A., et al., *Intestinal barrier dysfunction in inflammatory bowel diseases*. Inflamm Bowel Dis, 2009. **15**(1): p. 100-13.
219. Li, Q., et al., *Interferon-gamma and tumor necrosis factor-alpha disrupt epithelial barrier function by altering lipid composition in membrane microdomains of tight junction*. Clin Immunol, 2008. **126**(1): p. 67-80.
220. Rocha, R., et al., *Analysis of fat and muscle mass in patients with inflammatory bowel disease during remission and active phase*. Br J Nutr, 2009. **101**(5): p. 676-9.
221. Al-Jaouni, R., et al., *Energy metabolism and substrate oxidation in patients with Crohn's disease*. Nutrition, 2000. **16**(3): p. 173-8.
222. Mingrone, G., et al., *Increased resting lipid oxidation in Crohn's disease*. Dig Dis Sci, 1996. **41**(1): p. 72-6.
223. Peyrin-Biroulet, L., et al., *Mesenteric fat in Crohn's disease: a pathogenetic hallmark or an innocent bystander?* Gut, 2007. **56**(4): p. 577-83.

-
224. Buhner, S., et al., *Ileal and colonic fatty acid profiles in patients with active Crohn's disease*. Gut, 1994. **35**(10): p. 1424-8.
 225. Morita, H., et al., *Phospholipid turnover in the inflamed intestinal mucosa: arachidonic acid-rich phosphatidyl/plasmenyl-ethanolamine in the mucosa in inflammatory bowel disease*. J Gastroenterol, 1999. **34**(1): p. 46-53.
 226. Lee, C.W., et al., *Activation and induction of cytosolic phospholipase a(2) by TNF-alpha mediated through Nox2, MAPKs, NF-kappa B, and p300 in human tracheal smooth muscle cells*. J Cell Physiol, 2010.
 227. Hawkey, C.J., F. Karmeli, and D. Rachmilewitz, *Imbalance of prostacyclin and thromboxane synthesis in Crohn's disease*. Gut, 1983. **24**(10): p. 881-5.
 228. Sjoqvist, U., et al., *Chronic colitis is associated with a reduction of mucosal alkaline sphingomyelinase activity*. Inflamm Bowel Dis, 2002. **8**(4): p. 258-63.
 229. Rudd, P.M., et al., *Glycosylation and the immune system*. Science, 2001. **291**(5512): p. 2370-6.
 230. Zhao, J., et al., *Analysis of protein glycosylation and phosphorylation using liquid phase separation, protein microarray technology, and mass spectrometry*. Methods Mol Biol, 2009. **492**: p. 321-51.

EIDESSTATTLICHE ERKLÄRUNG

Hiermit erkläre ich, dass ich die vorliegende Doktorarbeit selbständig angefertigt habe. Es wurden nur die in der Arbeit ausdrücklich benannten Quellen und Hilfsmittel benutzt. Wörtlich oder sinngemäß übernommenes Gedankengut habe ich als solches kenntlich gemacht.

Ort, Datum

Pia Lichti